

**THERMO-MECHANICAL BEHAVIOUR OF
INSULATED FRP-CONCRETE COMPOSITES AT
ELEVATED TEMPERATURE**

Aaruga Selvaratnam

198039A

Degree of Master of Science

Department of Civil Engineering

University of Moratuwa

Sri Lanka

November 2020

**THERMO-MECHANICAL BEHAVIOUR OF
INSULATED FRP-CONCRETE COMPOSITES AT
ELEVATED TEMPERATURE**

Aaruga Selvaratnam

198039A

Thesis submitted in partial fulfillment of the requirements for the degree Master of
Science in Civil Engineering

Department of Civil Engineering

University of Moratuwa


Sri Lanka

November 2020

DECLARATION

I declare that this is my own work and this thesis does not incorporate without acknowledgement any material previously submitted for a Degree or Diploma in any other university or institute of higher learning and to the best of my knowledge and belief it does not contain any material previously published or written by another person except where the acknowledgement is made in the text.


Also, I hereby grant to University of Moratuwa the non-exclusive right to reproduce and distribute the thesis, in whole or in part in print, electronic or other medium. I retain the right to use this content in whole or part in future works (such as articles or books).

Signature: 

Date: 04.11.2020

The above candidate has carried out research for the Masters under my supervision

Name of the supervisor: Dr. (Mrs.) J.C.P.H. Gamage

Signature of the supervisor: 

Date: 04.11.2020

ACKNOWLEDGEMENT

Under the Research Project, I had the opportunity of gaining very valuable experience of how to apply the theoretical knowledge gathered throughout the four years as an undergraduate to produce important findings for the well-being and development of the community. There are a number of persons whom I must pay my gratitude for their help towards the successful completion of the research project and report.

First, I am very grateful for the valuable guidance and encouragement given by my research supervisor, **Dr. (Mrs.) J.C.P.H. Gamage**, Senior lecturer in the Department of Civil Engineering, University of Moratuwa. Without her support and guidance none of this would be possible. And I would like to thank my research chairperson Dr. **G.I.P. De Silva**, Senior Lecturer in the Department of Materials Science Engineering, University of Moratuwa.

Further, I am thankful to Senior professor, **Prof. A.A.D.J. Perera**, Senior Professor in Department of Civil Engineering, University of Moratuwa, the research coordinator for evaluating and giving us valuable instructions regarding the research findings we presented during the research progress presentations.

I would like to appreciate the National Research Council, Sri Lanka, and Airow Solutions (Pvt.) Ltd. for the financial support of the project (Grant No. PPP18-01). Especially, **Mrs. Naduni Wanniarachchi**, Scientific Officer, National Research Council, Sri Lanka, and **Mr. Vajira Attanayake**, General Manager, Airow Solutions (Pvt.) Ltd., Sri Lanka for their support.

Next, I would like to express my gratitude to **Mr. D.M.N.L. Dissanayaka**, technical officer in Structural Testing Laboratory, **Mr. H.T.R.M. Thanthirage**, technical officer in Building Materials Laboratory and the non-academic staff of Structural Testing Laboratory, Building Materials Laboratory, Rock mechanics Laboratory, Computational mechanics laboratory and Computer Laboratory of Department of Civil Engineering and EPM Laboratory of Department of Material Science engineering as well.

Moreover, I would like to thank EPCI Homes (Pvt) Ltd, Ja-Ela, Sri Lanka, and RPC Polymers (Pvt) Ltd, Horana, Sri Lanka to providing EPS materials for my research. And I would like to appreciate my colleagues and all the staff in the Department of Civil Engineering for their kind support throughout this period. At last but not least, I would like to thank my Family and Friends for believing me and supporting me throughout these years.

S.Aaruga.

Department of Civil Engineering

University of Moratuwa

10.07.2020

ABSTRACT

The Fiber-reinforced polymer (FRP) retrofitting technique has become an efficient method for retrofitting the concrete structures, especially in buildings and bridges. Though FRP has superior mechanical properties, the fire performance remains an obstacle for practical applications. Degradation of mechanical and bond properties of FRP composites was found when it was subjected to elevated temperatures since the glass transition temperature of the adhesive component is around 70°C. At high temperatures, the epoxy resins will soften and eventually ignite, which causes the polymer matrix weaker, and hence a potential concern raises on the structural integrity of FRP bonded concrete composite structures.

When designing the buildings, adequate fire resistance between 2 h and 4 h should be provided depending on the type of building. Though several techniques have been investigated to control the temperature of the CFRP composite structures, controlling the temperature is impossible in large scale civil engineering applications. Therefore, using insulation materials for CFRP-Concrete composites have become an effective solution. However, to achieve 2 hours of fire endurance, 40-50 mm thickness of insulation is required. Though there are many fireproofing materials for CFRP composites, the available Insulation materials in the market are very high cost which is not affordable in countries like Sri Lanka. Hence, a cost-effective insulation system for CFRP composites is required.

In this study, two types of solutions are proposed to make the CFRP retrofitting projects economical without affecting structural integrity. In such a way as the first solution, and alternative CFRP bond arrangement was investigated by bonding the CFRP laminates in a groove within the nominal cover of the member. A test program was carried out to compare the thermal and structural performance of grooved and external bonding techniques. A total of 15 CFRP-Concrete specimens were exposed to different fire scenarios with and without insulation. A numerical model was also developed to predict the effects of sensitive parameters on thermo-mechanical

performance under standard fire. A reduction of up to 36% of Insulation requirement was observed by using this method with less than 4% flexural capacity reduction.

In phase 2, a cement-based Insulated plaster was developed using EPS particles as the base material. An experimental program was conducted, and ten different trial mixes were prepared to study the mechanical and thermal behaviour of the EPS-cement mortar with different mix proportions. Replacement of fine aggregates by EPS particles from 0% to 200% was examined in this study. It was noted that the mechanical properties of the mortar reduce with increasing EPS particles and the thermal properties increases with increasing EPS particles. A reduction up to 69% and 53% were noted in thermal conductivity and density, respectively due to the replacement of aggregates with EPS in the conventional mortar. Two types of mix proportions were selected for further study and the effect of particle size and water/cement ratio was studied. Finally, the mix with 200% replacement of fine aggregates by EPS was selected as the ideal mix to provide an insulation for CFRP composites. And it was discovered that 125% replacement plaster can be used as a external wall plaster to improve the thermal comfort within buildings.

In the next phase of this research, the developed plaster was applied to the masonry walls. A heat transfer model was developed to assess the performance of the developed mortar using EPS blend to enhance the thermal comfort within the buildings. The internal wall temperature with different plasters was compared with the conventional cement-sand plaster. A reduction of 18% and an increment of 20% were noted in the decrement factor and time lag, respectively in the wall panels with the developed EPS-Cement plaster.

LIST OF PUBLICATIONS

Journals

1. Selvaratnam, A., Kahandawa Arachchi, K.A.T.Y. and Gamage, J.C.P.H. 'Investigation on an economical and effective bond arrangement of CFRP strengthened concrete members for fire safety' *submitted to Fire Safety Journal*.

Book Chapters

1. Selvaratnam, A., Gamage, J.C.P.H. (2020) 'A Review on Thermo-mechanical behaviour of CFRP-Concrete composites at elevated temperature and available insulation systems', *Lecture Notes in Civil Engineering*, Volume 94. pp. 9. http://doi.org/10.1107/978-981-15-7222-7_43.

International Conferences

1. Aaruga, S., Chandrathilaka, E.R.K. and Gamage, J.C.P.H. (2019), 'Finite element Modelling on Flexural Performance of CFRP strengthened reinforced concrete curved beams', *5th International multidisciplinary engineering research conference*, Moratuwa, Sri Lanka. <http://doi.org/10.1109/MERCon.2019.8818797>.
2. Selvaratnam, A. and Gamage, J.C.P.H. (2019), 'Effect of steel reinforcement ratio on flexural enhancement in CFRP-strengthened concrete curved beams', *10th International Conference on Sustainable Built Environment*, Kandy, Sri Lanka, 12-14 December 2019.
3. Aaruga, S. and Gamage, J.C.P.H. (2019), 'Numerical modelling of effect of anchorages on flexural behaviour of CFRP-strengthened reinforced concrete curved beams', *75th Annual session of Sri Lanka Association for the advancement of Science*, Sri Lanka, 2 – 6 December.
4. Selvaratnam, A., Gamage, J.C.P.H. and De Silva, G.I.P. (2020) 'EPS blended cementitious plaster for improved thermal comfort in buildings' *11th*

International Conference on Sustainable Built Environment, Kandy, Sri Lanka, 10-12 December 2020. (Submitted)

Journals in-preparation

1. Selvaratnam, A., Kahandawa Arachchi, K.A.D.Y.T., Selvaranjan, K. and Gamage, J.C.P.H. 'Behaviour of CFRP-strengthened concrete curved beams subjected to out-of-plane bending'
2. Selvaratnam, A., Kahandawa Arachchi, K.A.D.Y.T., Gamage, J.C.P.H. and De Silva, G.I.P. 'Development of a cost-effective insulation system for CFRP/Concrete composites using recycled EPS-Cement blend'.
3. Selvaratnam, A., Kahandawa Arachchi, K.A.D.Y.T., Gamage, J.C.P.H. and Attanayake, V. 'Development of a thermal insulation wall plaster using recycled EPS to improve the thermal comfort in buildings.'
4. Kahandawa Arachchi, K.A.D.Y.T., Selvaratnam, A., Gamage, J.C.P.H. and De Silva, G.I.P. 'Development of an innovative insulated plaster using Bottom Ash to enhance thermal comfort in buildings.'
5. Kahandawa Arachchi, K.A.D.Y.T., Selvaratnam, A., Gamage, J.C.P.H. and Attanayake, V. 'Investigating on developing a cementitious insulation using Bottom ash for CFRP/Concrete composites'

TABLE OF CONTENTS

DECLARATION.....	i
ACKNOWLEDGEMENT.....	ii
ABSTRACT	iv
LIST OF PUBLICATIONS.....	vi
LIST OF FIGURES	xiii
LIST OF TABLES	xix
CHAPTER 1: INTRODUCTION.....	1
1.1 Background.....	1
1.2 Research Objective	2
1.3. Methodology.....	2
1.3.1. Development of an alternative CFRP bond arrangement.....	3
1.3.2. Development of a low-cost cement-based Insulation material.....	4
1.4. Significance of the Research	5
1.5. Thesis Arrangement.....	5
CHAPTER 2: LITERATURE REVIEW.....	7
2.1. FRP Composites	7
2.2 FRP Material behaviour.....	8
2.2.1. Properties at Elevated temperature	9
2.2.2. FRP at fire.....	9
2.3. FRP materials in Civil Engineering.....	10
2.3.1 Applications of CFRP strengthening.....	10
2.4. CFRP retrofitting patterns	12
2.5. CFRP-Concrete members under Elevated Temperatures.....	15
2.6. Thermal Insulation materials	18

2.7. Cementitious Insulation materials	22
2.7.1. Replacement using Fly ash.....	22
2.7.2. Replacement using bottom ash.....	23
2.7.3. Replacement using Rice husk-ash.....	23
2.7.4. Replacement using fiber.....	24
2.7.5. Replacement using Expanded Polystyrene (EPS).....	25
2.8. Insulation system for CFRP-Concrete Members.....	26
2.9. An analytical method for heat transfer analysis	31
CHAPTER 3: THERMAL PERFORMANCE OF ALTERNATIVE	
ARRANGEMENTS OF CFRP-CONCRETE MEMBERS	33
3.1 Introduction to the proposed Plan.....	33
3.2. Experimental Program.....	33
3.2.1. Materials	33
3.2.2. Specimen preparation	34
3.2.3. Testing of material properties.....	38
3.2.3. Testing	41
3.2.4. Results	42
3.3. Theoretical Analysis of flexural performance prediction.....	44
3.4. Numerical Modelling.....	46
3.4.1. Thermal properties.....	46
3.4.1.1. Concrete.....	46
3.4.1.1. CFRP	47
3.4.2. Finite element mesh and interactions	49
3.4.3. Transient Heat transfer Analysis	50
3.4.6. Results & Validation	52
3.5. Heat transient analysis under ISO standard fire	55

3.5 Parametric study	57
3.5.1. Effect of the geometry of the concrete specimen	57
3.5.3. Effect of groove depth	59
3.5.4. Effect of thermal conductivity	61
3.6. Design Recommendations	62
3.7. Summary.....	64
CHAPTER 4: DEVELOPMENT OF A COST-EFFECTIVE CEMENTITIOUS INSULATION MATERIAL USING LOCALLY AVAILABLE MATERIALS.....	66
4.1. Test Program	66
4.1.1. Overview	66
4.2. Development of EPS-cement blend mortar (Stage 1)	67
4.2.1. Materials	67
4.2.2. Sample preparation & testing (Phase 1)	67
4.2.3. Test results (Phase 1).....	69
4.2.4. Sample preparation & results (Phase 2)	72
4.2.4. Sample preparation & results (Phase 3)	74
4.2.6. Sample preparation & results (Phase 4)	76
4.2.7. Testing thermal conductivity	79
4.2.7. Modification of insulated plaster for masonry walls (Phase 5).....	82
4.2.8. Modification of insulated plaster for CFRP composites (Phase 6)	83
4.3. Applications of the selected mortar mixes.....	85
4.4. Exposure to the Fire	86
4.5. Summary	87
CHAPTER 5: PREDICTING THE THERMAL PERFORMANCE OF CFRP/CONCRETE COMPOSITES WITH EPS-CEMENT INSULATION.....	90
5.1 Overview	90

5.2. Morphology	90
5.3. Experimental program	91
5.3.1. Material properties and specimen preparation.....	91
5.3.2. Testing & results.....	92
5.4. Finite Element Modelling to understand the heat transfer behaviour of CFRP/Concrete composites with developed insulation	94
5.5 Model results & validation	95
5.6. Heat transfer Analysis of CFRP/Concrete composites under ISO Standard fire	96
5.7 Summary.....	97
CHAPTER 6: NUMERICAL MODELLING TO PREDICT THE THERMAL COMFORT OF BUILDINGS WITH EPS-BASED INSULATIVE PLASTER	98
6.1. Heat transfer modeling	98
6.1.1. Wall Panel specification	99
6.1.2. Material properties.....	100
6.2. Theoretical prediction & Validation.....	100
6.2.1. Steady-state analysis.....	100
6.2.2. Transient Analysis	101
6.3. Model results & experimental validation	102
6.4. Parametric study	106
6.4.1. Effect of thickness of plaster	106
6.4.2. Effect of thermal conductivity of the plaster	107
6.4.3. Effect of specific heat of the plaster	109
6.6. Summary.....	110
CHAPTER 7: COST ANALYSIS.....	111
7.1. Bill of Quantities	111

7.2. Summary.....	114
CHAPTER 8: CONCLUSIONS	115
CHAPTER 9: RECOMMENDATIONS	117
9.1 Groove bonding technique.....	117
9.2 Application of Insulation material on CFRP composites	117
9.3. Application of Insulation material on wall panels.....	117
REFERNCES	118
ANNEXES	i
ANNEX A	ii
A1. Sample Calculation of flexural performances	ii
A2. FEM results for Bond line temperature	v
ANNEX B	vi
B1. Heating and cooling curves obtained during thermal conductivity test.....	vi
ANNEX C	viii
C1. Theoretical analysis for transient heat transfer	viii
ANNEX D	ix
D1. Copy of Publications	ix

LIST OF FIGURES

Figure 1: Methodology – Phase 1.....	3
Figure 2: Methodology – Phase 2.....	4
Figure 3: Temperature variation within bond line of non-insulated CFRP-concrete specimen.....	10
Figure 4: Slab strengthening using CFRP laminates.....	11
Figure 5: Strengthening of Beam-Column joint using CFRP.....	11
Figure 6: Steel bridge retrofitted using CFRP strips	11
Figure 7: Concrete bridge retrofitted using CFRP sheets.....	11
Figure 8: Load vs. deflection behaviour of the beam specimens.....	13
Figure 9: Section details of the CFRP strengthened beams.....	14
Figure 10: (a) Groove Cutting (b) Filling Grooves with Epoxy and Fixing CFRP Sheets.....	15
Figure 11: Relative strength vs temperature of CFRP/epoxy/concrete bond.....	16
Figure 12: Variation of bond strength with temperature.....	17
Figure 13: Effect on normalized tensile strength vs temperature of FRP composites	18
Figure 14: Relationship between thermal conductivity, apparent density and temperature of Insulation materials	19
Figure 15: Thermal resistance of common building insulation materials.....	20
Figure 16: Thermal insulation material selection procedure.....	20
Figure 17: Insulation and thermocouple details for specimens.....	27
Figure 18: Finite element model of insulated CFRP-concrete specimen.....	28
Figure 19: EBR-CFRP-strengthened RC beams with CS boards.....	29

Figure 20: NSM-CFRP-strengthened beams with Calcium Silicate boards	29
Figure 21: Comparison between the fire performance of EBR and NSM strengthening systems.....	30
Figure 22: Insulation system for CFRP-concrete beams	31
Figure 23. Specimen configurations.....	33
Figure 24. Materials used.....	34
Figure 25. Preparation of concrete blocks.....	34
Figure 26. Testing of concrete cube strength using compressive test machine.....	35
Figure 27. Grooving the concrete blocks.....	36
Figure 28. (a) Grinding the surface of specimen without grooves; (b) After grinding the surface of specimen with grooves.....	36
Figure 29. (a) Fixing the thermo couples; (b) Applying the adhesive layer.....	37
Figure 30. (a)Prepared B0_0 samples; (b) Prepared B20_0 samples.....	37
Figure 31. (a) Mixing the vermiculite-cement mortar; (b) Applying insulation for B0_20 specimen; (c) Applying insulation for B20_0 specimen.....	36
Figure 32. (a) B_20 specimen after applying the insulation; (b) B20_0 specimen after applying.....	36
Figure 33. (a) Specimen preparation; (b) Testing of thermal conductivity.....	39
Figure 34. (a) Specimen preparation; (b) Testing of specific heat.....	40
Figure 35. Test set-up.....	41
Figure 36. Temperature profile of the oven.....	42
Figure 37. Average temperature variation with time within the adhesive layer.....	42
Figure 38. Comparison of the specimens.....	44

Figure 39. Bond arrangements.....	45
Figure 40. Thermal properties of CFRP.....	47
Figure 41. Thermal conductivity variations of Epoxy resin	48
Figure 42. Specific heat variations of Epoxy resin	46
Figure 43. Finite element mesh of (a) B20-0; (b) B20-20; (c) B20-40.....	50
Figure 44. (a) Experiment sample; (b) Finite element model.....	51
Figure 45. CFRP concrete-member simulated using ABAQUS with 50 mm thick vermiculite layer.....	51
Figure 46. Temperature variation within the adhesive layer.....	52
Figure 47. Comparison of experimental results (Exp) and numerically predicted results.....	53
Figure 48 Standard fire curve – ISO 834.....	55
Figure 49. Bond line Temperature under ISO 834 fire curve.....	56
Figure 50. Effect of concrete geometry on Bond line Temperature.....	57
Figure 51. Schematic diagram of Insulation application.....	58
Figure 52. Effect of Insulation thickness on bond line temperature.....	57
Figure 53. Effect of groove depth on bond line temperature.....	60
Figure 54. Effect of thermal conductivity on bond line temperature.....	61
Figure 55. Design Fire resistances for different bond types and different exposure conditions.....	63
Figure 56. Materials.....	67
Figure 57. Sample preparation for thermal conductivity testing.....	68
Figure 58. Sample preparation for compressive strength testing.....	68
Figure 59. Testing apparatus.....	69

Figure 60. Variation of the flow – phase 1.....	70
Figure 61. Compressive strength variation – Phase 1.....	70
Figure 62. Density variation – Phase 1.....	71
Figure 63. Mix samples – Phase 1.....	71
Figure 64. Effect of aggregates/cement ratio in the Density.....	73
Figure 65. Effect of aggregates/cement ratio in the flow.....	73
Figure 66. Effect of aggregates/cement ratio in the Compressive strength.....	74
Figure 67. Mix samples – Phase 3.....	74
Figure 68. Variation of the flow – Phase 3.....	75
Figure 69. Compressive strength variation – Phase 3.....	76
Figure 70. Density variation – Phase 3.....	76
Figure 71. EPS resin particles.....	77
Figure 72. Mix using EPS resin.....	77
Figure 73. Variation of the flow – Phase 3.....	78
Figure 74. Effect of particle size in compressive strength.....	78
Figure 75. Effect of particle size in density.....	78
Figure 76. Temperature of Lee’s disk (T1) vs time for EPS-0.....	80
Figure 77. Thermal conductivity variation.....	81
Figure 78. Effect of water/cement ratio in EPS-125-F.....	83
Figure 79. Effect of water/cement ratio in EPS-200.....	84
Figure 80. Effect of water/cement ratio in EPS-200-F.....	85
Figure 81. Application of EPS plaster as external wall plaster.....	85
Figure 82. Application of EPS plaster as insulation for CFRP composites.....	86

Figure 83. Testing for fire.....	86
Figure 84. Effect of fire.....	87
Figure 85. SEM images of (a)HIP; (b) MIP; (c) Vermiculite cement mix.....	90
Figure 86. (a) CFRP application; (b) Prepared specimens.....	92
Figure 87. Testing under elevated temperature.....	93
Figure 88. Test results.....	93
Figure 89. Finite element model.....	94
Figure 90. Mesh sensitivity analysis results.....	95
Figure 91. Model results and validation.....	96
Figure 92 . Model results under standard fire.....	97
Figure 93. Finite element mesh of the wall panel with plaster.....	98
Figure 94. Temperature profile across the wall panel.....	100
Figure 95. Heat conduction through the wall.....	101
Figure 96. Temperate contours though the wall cross section (WP_0).....	102
Figure 97. Comparison of theoretical results and FE model predicted results.....	102
Figure 98. Building prototype.....	103
Figure 99 . Comparison of measured temperature and predicted temperature.....	103
Figure 100. Temperature variation in the outside surface and inside surface for 6 days period in model WP_CS.....	104
Figure 101. Temperature variation in the outside surface and inside surface for 24 hours period.....	105
Figure 102. Effect of plaster thickness on thermal performance of developed composite wall.....	106
Figure 103. Effect of plaster thickness on decrement factor and time lag.....	106

Figure 104. Effect of thermal conductivity on thermal performance of developed composite wall.....	108
Figure 105. Effect of thermal conductivity on decrement factor and time lag.....	108
Figure 106. Effect of specific heat on thermal performance of developed composite wall.....	109
Figure 107. Effect of specific heat on decrement factor and time lag.....	110
Figure 108. Cost comparison for wall plasters.....	113
Figure 109. Cost comparison for CFRP insulation materials.....	113
Figure 110. Bond line temperature for different nodes of B20_40 specimen when one side is exposed to ISO standard fire.....	V
Figure 111. Bond line temperature for different nodes of B20_40 specimen when four sides are exposed to ISO standard fire.....	V
Figure 112. Heating & cooling curve of Vermiculite sample.....	VI
Figure 113. Heating & cooling curve of EPS-0-3 sample.....	VI
Figure 114. Heating & cooling curve of EPS-200 sample.....	VII
Figure 115. Heating & cooling curve of EPS-200-F sample.....	VII
Figure 116. Heating & cooling curve of EPS-125-F sample.....	VII

LIST OF TABLES

Table 1: Summary of results on CFRP-concrete composites at elevated temperature.....	17
Table 2: Summary of thermal properties of insulation materials.....	21
Table 3: Summary of the beam specimens.....	27
Table 4: Comparison of thermal conductivity.....	39
Table 5: Measurements for specific heat calculations.....	40
Table 6: Measurements and density calculations.....	41
Table 7. Mechanical properties.....	44
Table 8. Beam configurations.....	45
Table 9. Moment capacity results.....	46
Table 10. Temperature variations predicted using FE model.....	54
Table 11. Comparison of temperatures at $t = 10$ min.....	54
Table 12. Fire resistance durations under ISO 834 standard fire curve.....	56
Table 13. Required insulation thicknesses to achieve 2 hours of fire resistance (t_f)...	60
Table 14: Mix proportions for phase 1.....	67
Table 15: Test results - phase 1.....	69
Table 16: Mix proportions for phase 2.....	72
Table 17: Test results – phase 2.....	72
Table 18: Mix proportions for phase 3.....	74
Table 19: Test results - phase 3.....	75
Table 20: Mix proportions for phase 4.....	77
Table 21: Test results – phase 4.....	77

Table 22: Measured thermal conductivities.....	81
Table 23: Mix proportions for phase 5.....	82
Table 24: Test results – phase 5.....	82
Table 25: Mix proportions for phase 6.....	83
Table 26: Test results – phase 6.....	84
Table 27: Selected Products.....	87
Table 28: Product specification of LIP-F.....	88
Table 29: Product specification of MIP-F.....	88
Table 30: Product specification of HIP-C.....	89
Table 31: Thermal and mechanical properties at ambient temperature.....	91
Table 32: Specimen Configurations.....	92
Table 33: Wall panel specifications.....	99
Table 34: Thermal properties.....	100
Table 35: Numerical model results.....	105
Table 36: Thermal conductivities of the control materials selected for this study...	107
Table 37: Specific heats of the control materials selected for this study.....	109
Table 38: Market prices of materials.....	111
Table 39: Bill of Quantities.....	112
Table 40: Moment Capacity- Sample calculation.....	II
Table 41: Finite difference method for temperature prediction.....	VII

CHAPTER 1: INTRODUCTION

1.1 Background

In the last few decades, Fiber reinforced polymer (FRP) application in Construction industry has been drastically increased due to their superior mechanical properties. FRP strengthening technique has become an efficient method for retrofitting of Concrete structures especially in buildings. Fire resistance is a key property of construction materials which can delay the flame to affect the structures. Though FRPs have superior properties, the fire remains an obstacle to practical applications (Chowdhury et al., 2007).

In the case of CFRP-Concrete composite structures will be directly exposed to the environment. A degradation of mechanical and bond properties of CFRP composites was found when it is subjected to elevated temperatures since its glass transition temperature is only 70°C. At high temperatures, the epoxy resins will soften and eventually ignite, which will cause the polymer matrix weaker and hence raise a potential concern on the structural integrity of CFRP-concrete composite structures. It results in the reduction of bond strength, tensile strength, and Elastic modulus etc. Several conclusions on the Bond behaviour at elevated temperature had been made from the results obtained from single-lap shear test (J. Gamage et al., 2005) , Double-lap shear tests (Chandrathilaka et al., 2018), and Beam test (Dong et al., 2018).

When designing the buildings, a minimum fire resistance period from 60-120 minutes should be provided depending on the types of buildings, the height of the building, and story levels. Several techniques have been investigated to control the temperature of the CFRP composite structures (Chandrathilaka et al., 2018). However, civil engineering applications are large, and hence controlling the temperature is impossible. Therefore, using insulation materials for CFRP composites will be an effective solution.

The suitability of several insulation materials for FRP composites has been already widely investigated using Calcium silicate board, thick coating, ultrathin coating, Vermitex-TH, Perlite, and Vermiculite and fire endurance of more than 2 hours were

achieved (J. C. P. H. Gamage et al., 2006)(Dong et al., 2018)(Salama, Ghanem, & S.F, 2012). From several past studies, it has been found that the higher the insulation thickness, the higher the fire resistance period. And all of these fire endurances more than 2 hours have been achieved using a large thickness of the insulation layer (J. C. P. H. Gamage et al., 2006). However, increasing the insulation thickness will change the appearance of the existing structure, increase the dead load, and cost.

Since the adhesive based FRP composite is exposed to the environment in both the External bonding technique (EBT) and near-surface mounted technique (NSMT), the degradation of properties will be extremely high, and the need of surface area of insulation material is also high. Hence, the resistance to fire of FRP composites remains unsolved. In such a case, the possible solutions for this problem can be as follows.

- i. Developing a low-cost Insulation material
- ii. Improving the CFRP bond arrangements
- iii. Improving the adhesive properties

1.2 Research Objectives

- Study the available Insulation systems for CFRP-concrete composites and reveal the drawbacks in the existing systems
- Develop a feasible insulation system using waste material as a cost-effective solution for CFRP/concrete composites
- Determine an effective bonding system to enhance the thermo-mechanical behaviour of CFRP/concrete composites
- Provide guidelines to improve thermal performance of CFRP/concrete systems

1.3. Methodology

A complete literature survey was conducted and thermo mechanical behaviour of different CFRP-Concrete composites and the effectiveness of existing insulation

systems were identified. From this, this research was divided into two different paths to provide two different solutions. And they are described below.

1.3.1. Development of an alternative CFRP bond arrangement

The methodology followed is described in Figure 1.

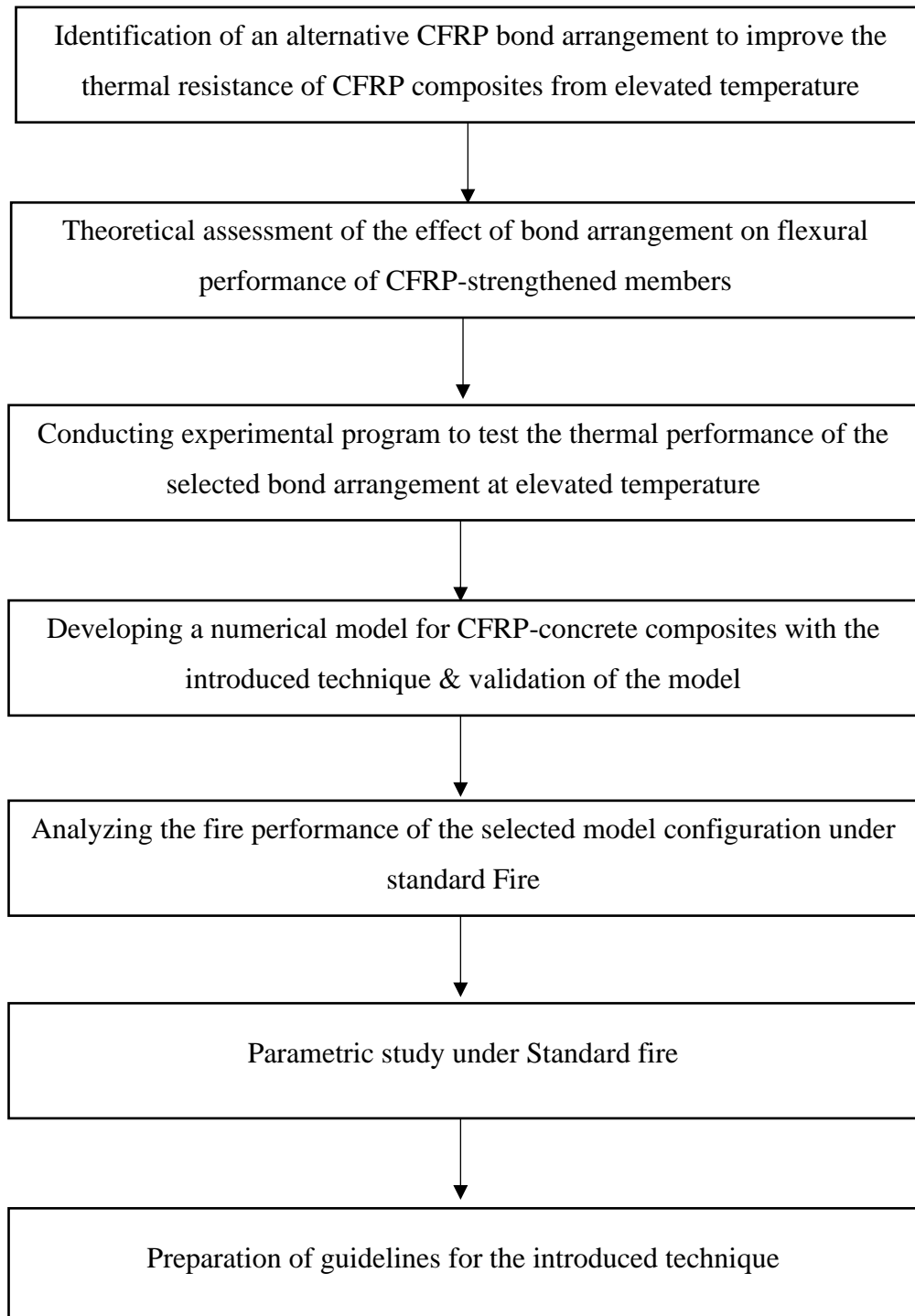


Figure 1: Methodology – Phase 1

1.3.2. Development of a low-cost cement-based Insulation material

The methodology followed is described Figure 2.

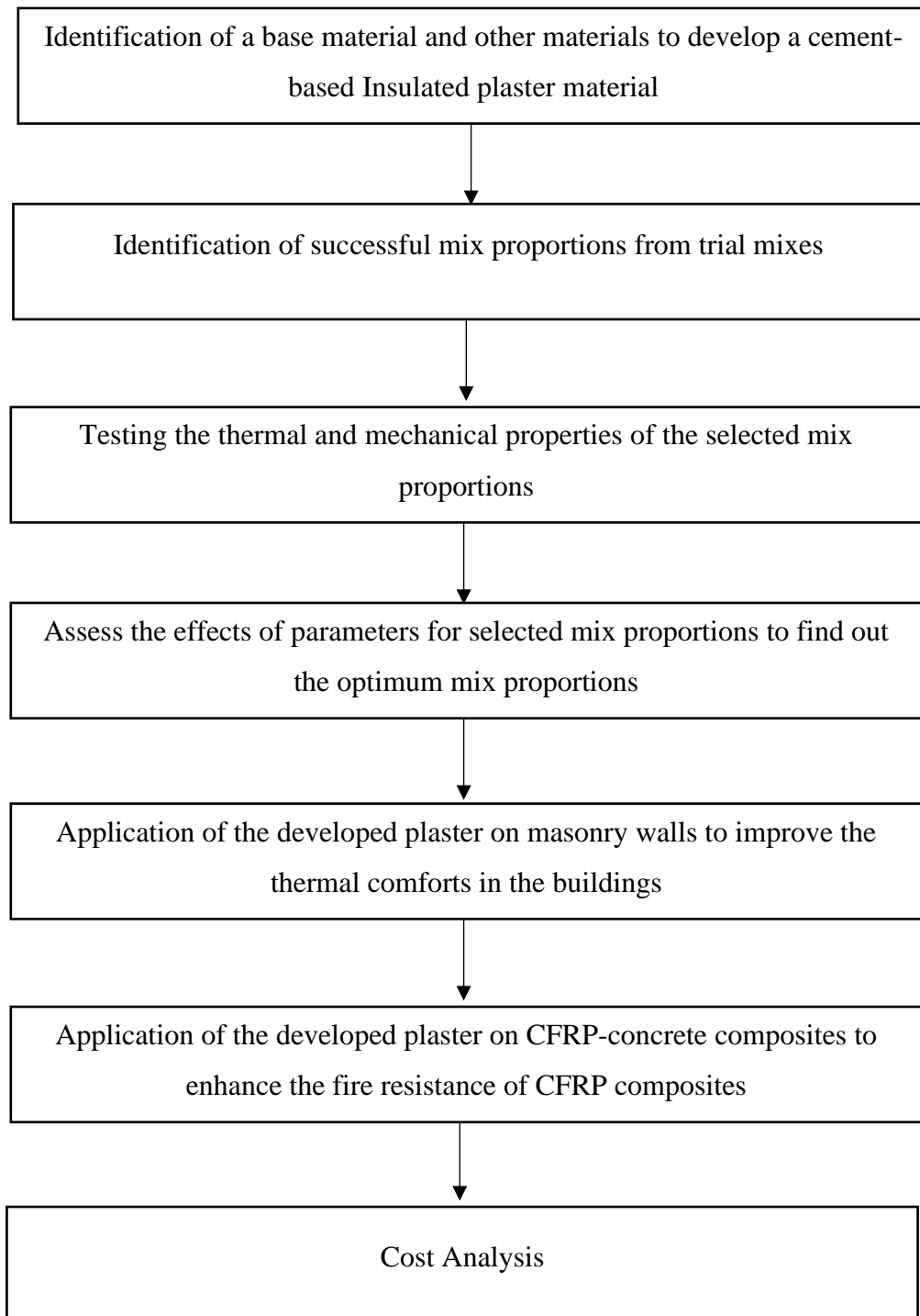


Figure 2: Methodology – Phase 2

1.4. Significance of the Research

The fire resistance of CFRP/Concrete composites still remains unsolved. Though insulation layers can be applied on top of the CFRP composites, the cost for current insulation systems are not affordable since the required thickness are relatively high. Moreover, addition of high thick insulations increases the dead load of the structures and unlikely changes in the appearance of the structure. Thereby, developing an insulation system for better thermo-mechanical behaviour of CFRP/Concrete composites is necessary.

1.5. Thesis Arrangement

In this thesis, the research work has been divided into seven chapters and they are described as follows.

Chapter 1. The Introduction to the research project including the research objectives and methodology are described in this chapter

Chapter 2. The detailed literature review which explains the background of this topic. The behaviour of CFRP/concrete composites and the drawbacks with the existing systems are described with evidence. The research gaps in developing an insulation system for CFRP/concrete was also clearly described.

Chapter 3. This chapter presents a bond arrangements for CFRP/concrete composites which can improve the thermal-mechanical behaviour of the composite with less insulation material. The possible fire ratings for the selected bond types were also recommended in this chapter.

Chapter 4. Development of cement-based insulation material with addition of waste materials is described in this chapter. Assessment of thermo-mechanical properties of the selected mix proportions is also presented. Further, multi-purpose of the developed plaster is recommended at the end of the chapter.

Chapter 5. The application of the developed plaster as an insulation for CFRP/Concrete composites is explored. An experimental program and numerical analysis under standard fire is presented in this chapter.

Chapter 6. The application of the developed insulated plaster as an external wall plaster was assessed in this chapter to enhance the thermal comforts in the buildings. A numerical model has been developed to evaluate the performance and compared with the conventional cement-sand plaster.

Chapter 7. A preliminary cost estimation for the developed plasters were carried out and compared with the conventional materials.

Chapter 8. Research conclusions

Chapter 9. Recommendations

CHAPTER 2: LITERATURE REVIEW

Fibre reinforced polymer (FRP) composites were initially introduced in the aerospace applications and automobile industries because of their superior strength and lightweight behaviour. Later, due to the drawbacks in Construction industry and its superior material behaviour, it has been developed in the construction industry. Due to the increasing concern with the deterioration of concrete, steel, and timber, FRPs were found as an excellent solution worldwide. FRPs have been mainly used for rehabilitation & strengthening of existing infrastructures and as internal reinforcements in the forms of bars, rods, and prestressing tendons. Though FRP has superior mechanical properties, its thermal performance for elevated temperature is low.

2.1. FRP Composites

Polymer composites are generated by combining reinforcing fibers polymer matrix, and fillers to develop a composite material with better properties than the individual materials (Das & Enamul, 2014). When embedding the fibers in a polymeric matrix, the composite will get excellent properties such as high tensile strength, lightweight, stiffness, flexibility, and resistance to chemical harm. Here, the purpose of using fibers is to strengthen the polymer matrix and improve its mechanical properties such as strength and stiffness (Das & Enamul, 2014). Generally, fibers have high resistance and brittle behaviour. The most widely used fiber types are Carbon fibers, Glass fibers, Aramid fibers, and Basalt fibers.

The role of this matrix is to disperse and separate the individual fibers, to prevent the fibers from damage, and environmental degradation, to transfer externally applied stresses to the fibers through shear stresses that creates at the fiber-matrix interface, and to provide adequate lateral support to the fibers against buckling when it is subjected to compression (Stoner, 2015). The matrices used for structural applications can be categorized as thermoplastic polymers and thermosetting polymers. Thermoplastics resins generally consist of long-chain molecules with weak secondary forces. This molecular structure allows the material to be softened in cyclic procedure and hardened without any degradation of the mechanical properties of the material (Stoner, 2015).

Thermosetting resins are also long-chain molecules where these chains are highly cross-linked by major chemical bonds. Therefore, thermosets are unable to soften in the cycle and will deteriorate at high temperatures (Chandra Das & Haque Nizam, 2014). Commonly these polymers have high thermal resistance at service temperatures, excellent resistant to chemicals and show very low creep and relaxation properties. The specific types of thermosetting matrixes in construction technology are Polyester Resin, epoxy resin, and vinyl ester resin. Polyester resins are comparatively cost-effective and easy to process. Epoxy resins are commonly used in FRP plates and sheets due to their curing ability at room temperature and excellent adhesion characteristics. The mechanical and in-service properties of Vinyl ester resins are like epoxy resins and the processing techniques are equivalent to unsaturated polyesters.

Fillers are inorganic components which are mixed to the polymer matrix to reduce the cost of the product by diluting the expensive resin materials. Further, it reduces the organic content of the composite, which helps to improve the fire resistance of FRP composites (Stoner, 2015). Additives are also added to resin materials and serve to facilitate the processing of materials, improve the performance of the product, and to modify specific mechanical properties of the composites. This can be also used to prevent the degradation of the FRP due to ultraviolet exposure, to ease the removal of the FRP from the molds, increase toughness, or to reduce flammability and smoke production (Stoner, 2015).

2.2 FRP Material behaviour

Fibers are the components that provide the strength and stiffness in a Fiber Reinforced Polymer because they are continuous and oriented in a specific direction in structural applications. FRPs are orthotropic, and they are stiffer and stronger in the direction of fiber.

The highest performance of stiffness and strength in one particular direction comes from unidirectional fiber composites, when all fibers are in parallel and produce their ultimate performance in this particular direction (Chandra Das & Haque Nizam, 2014). Though the strength limit is low when the fibers are arranged in a weave form in the way the strength can be gained in many directions, (Chandra Das & Haque

Nizam, 2014). By trimming the fibers in its small pieces and locating them randomly, similar strength can be achieved in all directions This is the most cost-effective method which is generally used for the fewer demand structures.

The mechanical properties of FRPs depend on relative fractions of fiber and matrix, mechanical properties of constituent materials, the orientation of the fiber particles, and the method used for manufacturing (Chandra Das & Haque Nizam, 2014).

2.2.1. Properties at Elevated temperature

When FRP composites are exposed to the elevated temperatures, the epoxy resin will lose its properties beyond its glass transient temperature (T_g) (J. C. P. H. Gamage et al., 2006). However, FRP materials have comparatively low thermal conductivities in both longitudinal and transverse directions. When the FRP composites are exposed to high temperature, the consistency of resin will change from hard and brittle to rubbery or viscous, which process is referred as “Glass transitioning” (Firmo et al., 2015). Generally, the glass transition will occur within 50-120°C.

Beyond the Glass transient temperature, the epoxy resins will soften and gradually ignite, which will cause the polymer resin weaker. Therefore, reduction in the bond strength, tensile strength, elastic modulus will occur (Maraveas et al., 2014). Hence, a potential concern regarding the structural integrity of the CFRP composite structure will arise.

2.2.2. FRP at fire

Fire resistance is a key property for all construction materials. 60 – 240 minutes Fire endurance is required for Building construction materials depending on various factors including the type of building. Several researches have been focused to explore the behaviour of FRP composites under fire. It was revealed that the epoxy layer reaches the glass transient temperature within 5-6 minutes (Figure 3) when subjected to the standard fire (J. C. P. H. Gamage et al., 2006). This shows the epoxy layer reaches the failure temperature within a very short time comparing to the fire rating duration. Therefore, it is required to provide adequate fire protection for CFRP

retrofitted elements to maintain its integrity between CFRP and structural members at elevated temperatures.

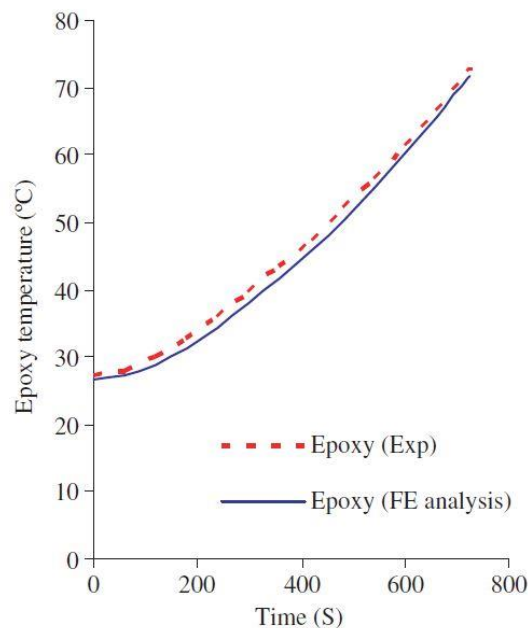


Figure 3: Temperature variation within bondline of non-insulated CFRP-concrete specimen (J.C.P.C.H.Gamage et al., 2006)

2.3. FRP materials in Civil Engineering

2.3.1 Applications of CFRP strengthening

Strengthening the concrete structures using FRPs was found as a successive solution through many research and laboratory testing in the last two decades. This technology will be needed when it required to carry additional loads, enhancing the capacity loss due to deterioration, imperfect initial design, new standards, accidents as fire or seismic events, aging of materials, and construction deficiencies due to lack of maintenance (Islam, 2014).

In the concept of rehabilitation of concrete infrastructures, it is important that there is a different between repairing, strengthening, and retrofitting terms which are often mistakenly used interchangeably (Islam, 2014). In this scenario, “Repairing” the structure is referred to fixing a structure or functional deficiency such as cracks or severely degraded structural components using FRP composites. And the

“strengthening” of the structure refers specifically to the cases where the addition or application of FRP composites could improve the existing design performance capacity level (Das & Enamul, 2014). Figures 4-7 show different FRP retrofitting arrangements for Concrete and steel structural elements.



Figure 4: Slab strengthening using CFRP laminates (Chowdru & Islam, 2014)



Figure 5: Strengthening of Beam-Column joint using CFRP (Chowdru & Islam, 2014)

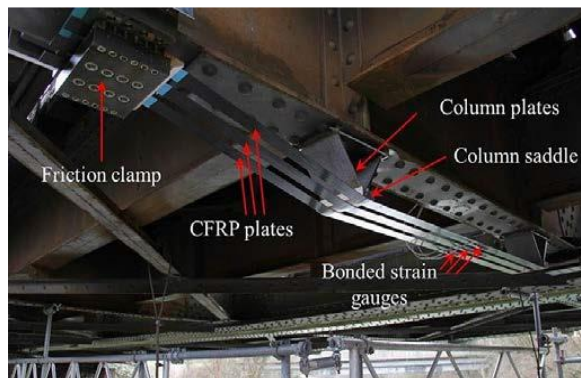


Figure 6: Steel bridge retrofitted using CFRP strips (Sonnenschein, Gajdosova, & Holly, 2016)



Figure 7: Concrete bridge retrofitted using CFRP sheets (Sonnenschein, Gajdosova, & Holly, 2016)

The problems encountered in structural deficiencies of existing infrastructures are high especially in seismic regions, though the seismic design structures are comparatively newly built. The use of confinement in structurally deficient concrete columns in seismically active regions around the world has proven to be one of the most essential applications of FRP composites in civil engineering industry (FIB Bulletin 35, 2006). More than providing confinement without increasing the stiffness,

the FRP retrofitting in this application also contributes to the rapid fabrication of cost-effective and durable jackets without the interference of traffic (Das & Enamul, 2014).

The ductility and energy dissipation capacity of a column can be improved by strengthening the column using a single layer of CFRP sheet. But, insufficient lap length can cause breaking of the bond during seismic activity and lead to lap splice failure where shear failure, plastic hinge formation, lap splice failure is the failure ways during an earthquake (Islam, 2014).

2.4. CFRP retrofitting patterns

Generally, the field applications of FRP materials are being used as internal reinforcement bars in Reinforced Concrete infrastructures, and external retrofitting of RC, Hybrid, and Fully composite structures as well. The external strengthening of concrete structures was initially introduced with steel plate bonding. Later, Fibre reinforced polymer (FRP) composites were introduced as an alternative to the steel plate. Different types of external bonding using FRPs have been adapted over the past 10 years considering the structural member. Flexural strengthening of concrete beams can be achieved by attaching the FRP composites externally using unidirectional laminates. However, comparing to the Externally bonded reinforcement technique (EBR), the near-surface-mounted (NSM) technique has many advantages including larger bond surface, higher tensile strength, and higher resistance to peeling-off (Aaruga, 2019).

FRP composites can be also utilized for strengthening the aged bridges. As many bridges are being deteriorated by time due to corrosion and other sequences, it is required to undergo reconstruction. Rather than the rehabilitation, strengthening the parts using FRPs will be cost-effective and time-saving.

Karuppiyah et al. (2016) carried out an investigation to discuss the effect of flexural and shear strengthening of reinforced concrete beams using CFRP laminates on the stress distribution, ultimate strength, initial crack, and crack propagation. A total number of five beams were cast where three beams with CFRP and two beams without CFRP. The two beams without CFRP were control beam and strengthened beam. The CFRP strengthened beams are (a) semi-wrapped beam, (b) U-wrapped beam, and (c) flexural-wrapped beam.

1.2 mm thickness with 160 GPa elastic modulus CFRP fabrics were used to retrofit the beams. From the results obtained from the load vs. deflection graph (Figure 8), it was found that the retrofitted beam can carry more loads than the others. The capacity enhancement at the retrofitted beam was noted as 10%. Of the control beam. However, the delay in the initial crack was more effective in the U-wrapped beam which was also noted as 10% of the control beam.

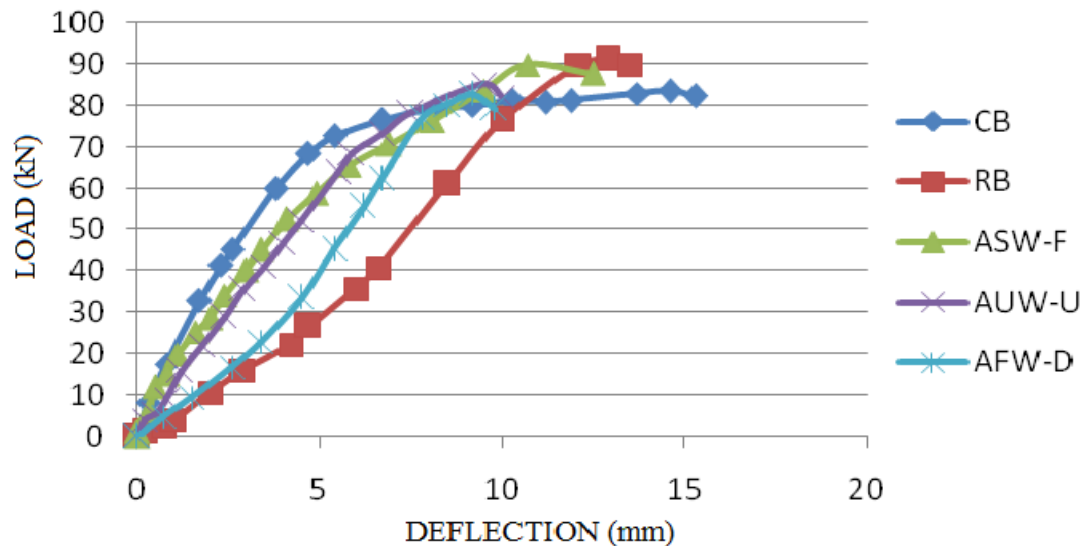


Figure 8: Load vs. deflection behaviour of the beam specimens (Karuppiah et al.,2016)

The maximum deflection was noted less in the U-wrapped beam compared to all others. It was found that the ductility property of the beams decreases with CFRP strengthening. A higher ductility ratio was also observed in the U-wrapped beam which is also an important factor in earthquake sensitive areas.

Morssy and Mahmoud conducted a study on an alternative method for bonding the FRP composites to reinforced concrete beams by connecting steel rivets through FRP laminates and concrete beams (Morsy & Mahmoud, 2013). This technique has less installation time and improves the ductility of CFRP strengthened beams. The aim of this investigation was to explore the mechanical bonding of the CFRP-concrete substrate to enhance the flexural capacity using steel plates bonded with 10 mm steel rivets to avoid de-bonding failures.

Total no of five full-scale RC beams were cast and retrofitted using CFRP laminates (B1, B2, B3, B4, and B5). B1 was a non-strengthened control beam and B2 was a CFRP flexural strengthened beam without steel rivets. B3 and B4 were CFRP flexural strengthened beams with two rivets on each end in B3 and 10 rivets in B4. B5 was strengthened in both shear and flexure with an additional three 5 mm width CFRP laminate at both sides and both ends for B4. The longitudinal and cross-section view of the shear and flexural strengthened beams with steel rivets is shown in Figure 9.

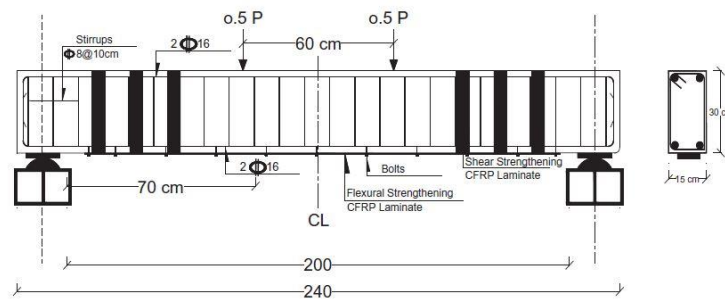


Figure 9: Section details of the CFRP strengthened beams

The results have shown that the externally bonded CFRP laminate is an excellent technique to enhance the load-carrying capacity of the RC beams. When comparing the CFRP strengthened beams, the beams with rivets (18.75% capacity increment) gives a better result than the conventional method (12% capacity increment). However, both flexural and shear strengthened beam gave a high load capacity enhancement which was 37%.

Beam B2 failed due to the peeling of the CFRP where the complete strength of the CFRP was not able to utilize. But, in the beams with steel rivets, concrete failed. Hence, it can be concluded that using the fastening method is more efficient in improving the flexural capacity of RC beams.

Antony et al. conducted another study on an alternative method to bond the CFRP laminates over the conventional EBR technique. In this study, the grooving method (GM) has been invented as an alternative bonding method. GM is a special technique as an alternative method to the conventional EBR technique by altering the surface preparation for bonding. Five beams were bonded with CFRP using the EBR

technique, eight beams using GM technique and one was a control beam. The length and number of plies of CFRP have been varied in both techniques. 600 mm, 650 mm, and 700 mm CFRP laminates were used as 1, 2, and 3 plies. The number of groves and directions of groves varied in the GM technique. In the GM method, the groves were cut in the tension zone using a saw and the groves were filled using epoxy. Then, the CFRP sheets were fixed on the top of the epoxy-filled groves. The experimental procedure of the GM method is shown in Figure 10.



Figure 10: (a) Groove Cutting (b) Filling Grooves with Epoxy and Fixing CFRP Sheets

The reference beam failed due to concrete crushing, and the beams strengthened using the EBR technique failed due to the debonding of CFRP laminates. The beams strengthened using the GM method failed due to the FRP rupture. It was also noted, that the increase in the ultimate load was 15% to 27% in the beams strengthened using the EBR technique. And 29% to 78% load increment was noted in the beams strengthened using the GM method.

Further, the effect of strengthening methods, the effect of the number of CFRP layers, bond length, and groove pattern were studied. It was noted that the decrease in bond length decreases the load-carrying capacity of the CFRP strengthened beams in both techniques.

2.5. CFRP-Concrete members under Elevated Temperatures

The bond performance of FRP-concrete interfaces at high temperatures was investigated by many researchers. Both specimens strengthened using the External bonding technique and NSM technique have been investigated experimentally and numerically. Blontrock et al. conducted a double shear-lap test on CFRP strengthened

Concrete member strengthened using EBR technique and they observed that the bond strength at 40°C, 55°C, and 70°C temperature were 141%, 124%, and 82%, respectively (Blontrock, 2003). It was also noted that concrete cohesive failure occurred at ambient temperature and concrete-adhesive interface failure occurred at elevated temperature.

Klamer et al. also performed double lap shear tests on CFRP-Concrete specimens within 10°C to 75°C temperature and observed strength increment until T_g and strength reduction after T_g similar to Blontrock's results (Klamer, E et al., 2015). Gamage et al. performed a single lap shear test on CFRP sheet bonded concrete blocks and she has also observed strength reduction with increasing temperature (Figure 11). A combined failure of bond and concrete rupture was observed in low temperatures less than 50°C. Peeling off of the CFRP sheet was noted as the failure pattern for the samples tested in high temperatures greater than 60°C (J. Gamage et al., 2005).

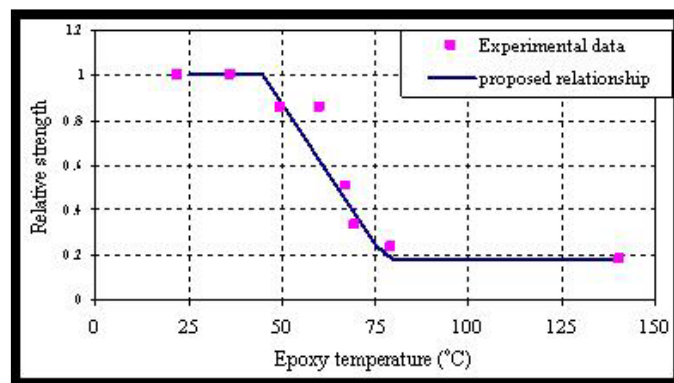


Figure 11: Relative strength vs temperature of CFRP/epoxy/concrete bond (Gamage et al., 2005)

Palmieri et al. have investigated the concrete members bonded with CFRP strips and rods using the NSM technique at a temperature between 20°C and 100°C. He also noted that the bond strength increases below the adhesive T_g and decreases above T_g . The failure mode changed from splitting of resin (debonding) to combined failure of debonding at CFRP-epoxy interface and pull-out of the strips/bars (Palmieri et al., 2011). Maraveas et al. (2014) has reviewed the CFRP-Concrete structures exposed to fire and mentioned that the temperature can compromise the bond between the concrete and FRP. The reduction in bond strength is shown in Figure 12. Bond tests summarized from the literature are tabulated in Table 1.

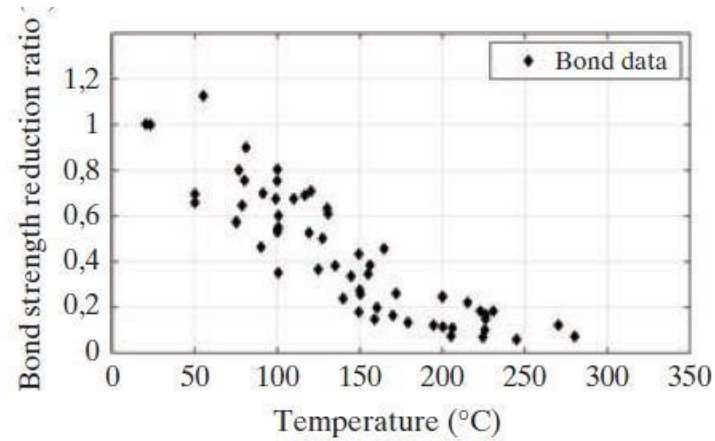


Figure 12: Variation of bond strength with temperature (Maraveas C, 2012)

The tensile behaviour of FRP composites is also important when predicting the load-carrying capacity of FRP bonded concrete members. The effect of temperature in the tensile strength has studied by several researchers and it is shown in Figure 13. It can be observed that the tensile strength of FRP materials reduces similarly with increasing temperature except for the GFRP sheets (Chowdhury et al., 2011). However, the tensile strength of epoxy reduces suddenly when the temperature reaches the T_g .

Table 1: Summary of results on CFRP-concrete composites at elevated temperature

Authors	Strengthening technique	CFRP shape	Test setup	Glass transition		Temperature range [°C]
				T_g [°C]	Method	
Blontrock [21]	EBR	strips	Double lap	62	n.a.	20 to 70
Klamer et al. [22]	EBR	strips	Double lap	62	n.a.	10 to 75
Klamer [23]	EBR	strips	Double lap	62	n.a.	-20 to 90
Wu et al. [24]	EBR	sheets	Double lap	34 to 38	n.a.	26 to 50
Gamage et al. [25]	EBR	sheets	Single lap	n.a.	n.a.	20 to -140
Leone et al. [26]	EBR	strips and sheets	Double lap	55	DSC	20 to 80
Firmo et al. [27]	EBR	strips ^a	Double lap	47	DMA (onset E')	20 to 120
Palmieri et al. [28]	NSM	strips and rods	Double lap	65	n.a.	20 to 100
Burke et al. [29]	NSM and EBR	strips and sheets	Beam tests ^b	59 and 69	DMA ($\tan \delta$)	21 to 200
Yu and Kodur [30]	NSM	strips and rods	Pull-out	82 and 120	n.a.	100 to 400 ^c
Firmo et al. [31]	NSM	strips	Double lap	44 and 47	DMA (onset E')	20 to 150

The modulus of elasticity also plays an important role in the design of retrofitting the structures using FRP composites as it affects the stiffness and deflection characteristics of members. Test results of the effect of temperature on GFRP, CFRP, and epoxy materials are shown below in Figure 13. Similar to the tensile strength

behaviour, all FRP materials show nearly the same behaviour except the GFRP sheets. And the elastic modulus of epoxy suddenly drops when it reaches the T_g .

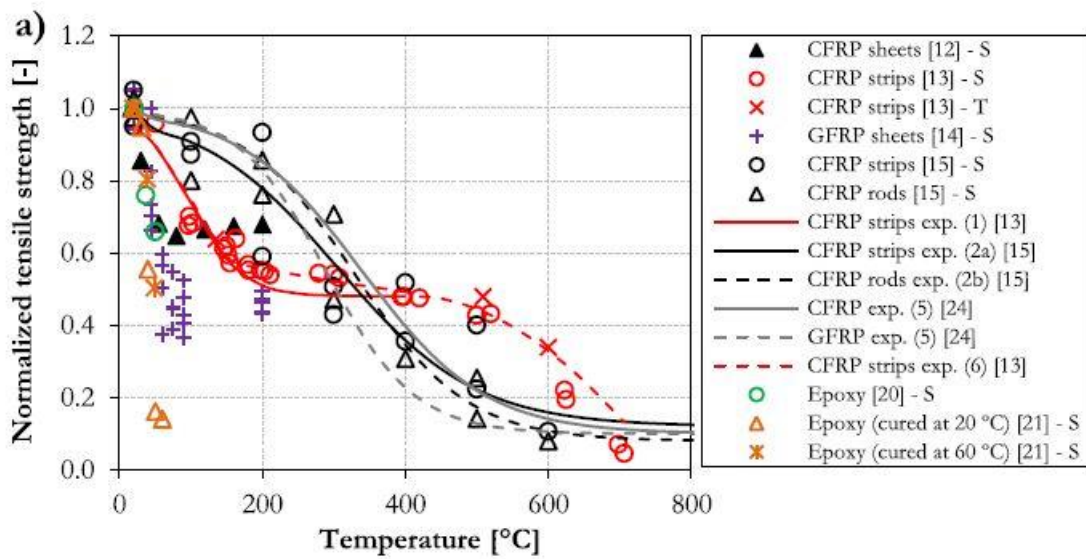


Figure 13: Effect on normalized tensile strength vs temperature of FRP composites (Firmo, J.P, 2015)

2.6. Thermal Insulation materials

Insulation materials should have properties which make them good insulation. The major properties affecting the performance of insulation materials are thermal conductivity, temperature difference, specific heat, thermal resistance, density, open joints, convection, moisture, aging, and permeability. The thermal conductivity of a material does not have a constant value. The conductivity depends on the temperature and the apparent density, and for the suitable design, it should be known (Zeitler & Munchen, 2010). It is a multi-dimensional function of density and temperature. Generally, the thermal conductivity approximately increases with increasing temperature. Figure 14 shows the interdependence of the conductivity on temperature and apparent density. The effect of thickness on thermal conductivity is less important compared to the effect of temperature.

Several types of thermal insulation materials are available for the construction projects such as inorganic materials, organic materials, and metallic or metalized reflective membranes. The available forms of insulation materials are produced in various forms

such as loose fills, blankets, rolls, batts, rigid boards, sprayed in-place, and blocks (Al-homoud, 2005). Figure 15 shows the graphical comparison of thermal resistance of some available insulation materials reference to the concrete blocks per 5 cm thickness.

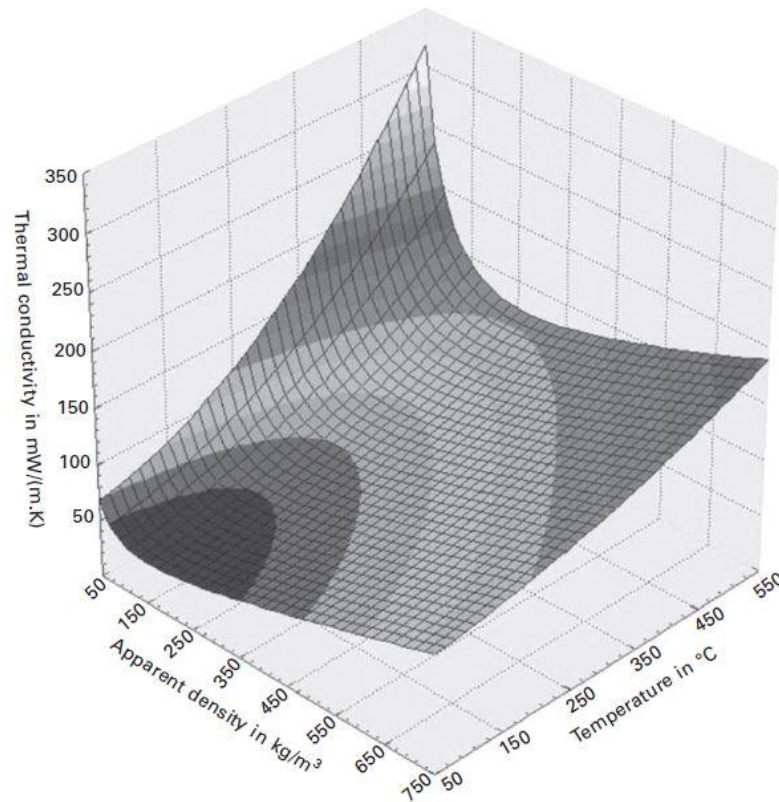


Figure 14: Relationship between thermal conductivity, apparent density and temperature of Insulation materials (Zeitler & Munchen, 2010)

Several parameters need to be considered in the selection of a thermal insulation material such as cost, durability, strength, fire resistance, airtightness, availability, and environmental impact, ease of application, thermal conductivity, and water vapor absorption. However, the thermal resistance of the insulating material is the key property when focusing the thermal performance and energy conversion problems. The process of selecting a thermal insulation material is presented in Figure 16.

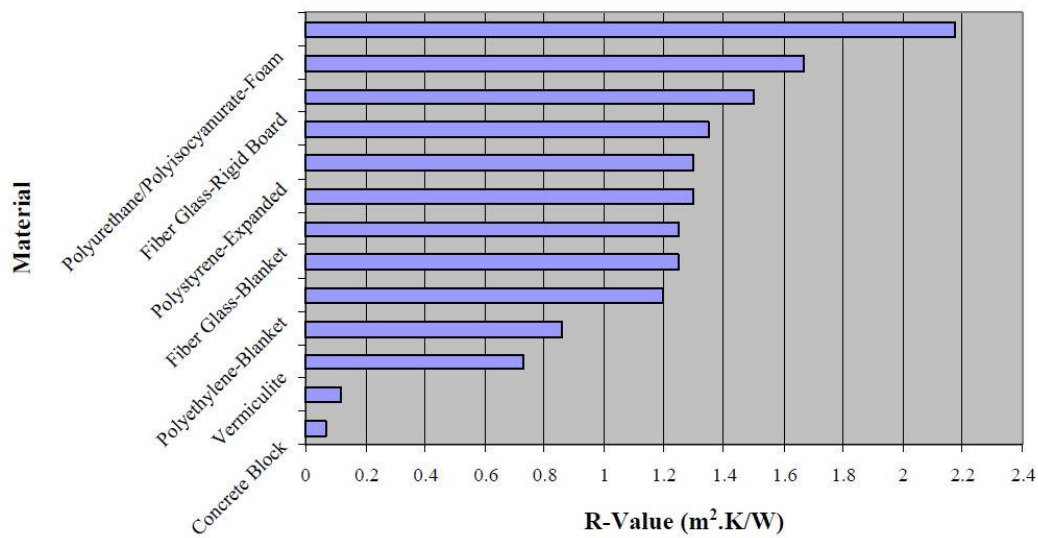


Figure 15: Thermal resistance of common building insulation materials (Al-homoud, 2005)

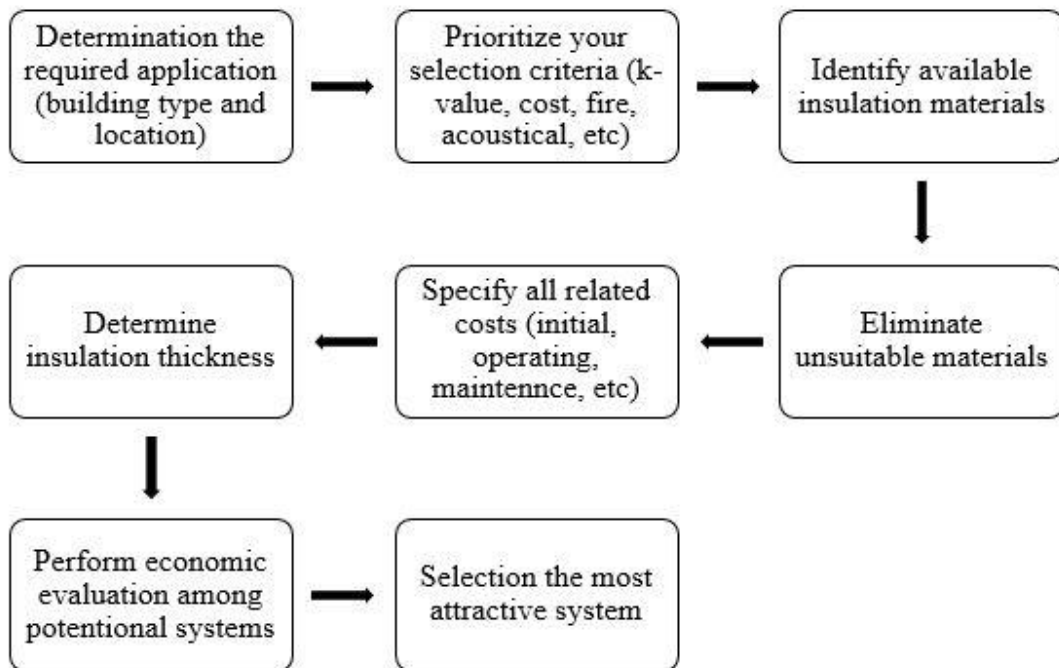


Figure 16: Thermal insulation material selection procedure (Al-homoud, 2005)

Commonly used construction insulation materials and their thermal properties are listed in Table 2.

Table 2: Summary of thermal properties of insulation materials

Insulation material	Thermal conductivity (W/m.K)	Thermal resistance (K.m²/W) [thickness(mm)]	Specific heat (J/(kg.K))	Density kg/m³
Wood fibre (board)	0.038	2.5 [100]	2100	160
Cellulose	0.035	2.632 [100]	2020	27-65
Wool (batts)	0.038	2.63 [100]	1800	23
Hemp (batts)	0.039-0.040	2.5 [100]	1800-2300	25-38
hempcrete	0.06	1.429 [100]	1500-1700	275
Cellular glass (boards)	0.041	n/a	1000	115
Straw	0.08	4.37 [350]	-	110-130
Glass mineral wool	0.035	2.85	1030	
Rock mineral	0.032-0.044	2.7-2.85	n/a	n/a
Icynene H2Foamlite	0.039	n/a	n/a	7.5-8.3
Phenolic foam	0.02	5 [100]	n/a	35
Polurethene foams	0.023-0.026	4.5 [100]	n/a	30-40

Expanded polystyrene (EPS)	0.034-0.038	3.52 [100]	1300	15-30
Extruded polystyrene (XPS)	0.033-0.035	3 [100]	n/a	20-40
Aerogel	0.014	3.8 [50]	1000	150
Vermiculite	0.06		840-1080	130
Perlite	0.04-0.05		840	400

2.7. Cementitious Insulation materials

The addition of cement is always a great solution in order to achieve high strength and workability in insulation materials. In such a case, replacement of fine aggregates by insulative materials such as fly ash in cement-sand mortar is a common practice nowadays. However, several investigations have been carried out on the replacement of other insulative materials such as bottom ash, natural fibers, foam glass, fibers, polystyrene, aluminum filling, and rice husk ash (Borhan & Janna, 2016; Kami et al., 2019).

2.7.1. Replacement using Fly ash

Fly ash (FA) is being used as a replacement material for cement and fine aggregates as well in cement-based materials. An experimental program was carried by Liang Li et al. to study the influence of FA on cement-FA mortar, several mixes with different FA proportions such as 30%, 50%, and 60% have been prepared. It was found that the introduction of fly ash delays the initial and final setting time of the mortar and at the same time it reduces the compressive strength as well. It was also revealed that the addition of fly ash can reduce the heat of hydration as well (Li et al., n.d.).

Bentz and Pletz have investigated the thermal behaviour of fly ash mixed cement mortar and it was found that the introduction of fly ash can significantly reduce the

thermal conductivity and density as well. And it was noted that the density has an effect on thermal conductivity of cement-fly ash mortars (Bentz et al., 2009).

Ghosh et al. have also studied the reuse of fly ash in mortars for improved thermal comforts in buildings. Two grades of mortars were used with 1:6 and 1:4 cement: sand ratio and the sand were replaced with an increasing percentage of fly ash from 10% to 100% (Ghosh et al., 2018). In both grades, it was noticed that with the increasing amount of fly ash, the thermal conductivity of mortar will increase. However, the compressive strength reduces with increasing fly ash replacement.

2.7.2. Replacement using bottom ash

Disposal of bottom ash which is a by-product of coal combustion has also become a reason for the rise of global crises (Piyarathne & Udamulla, 2016). Piyarathne & Udamulla. (2016). have investigated the effect of river sand replacement using bottom ash in cement mortar by replacing 0% to 40% of river sand(Piyarathne & Udamulla, 2016). It was noted that the compressive strength of the mortar increases with increasing bottom ash content to 30% and it reduces for 40% replacement. The density kept reducing with an increment of bottom ash and the water absorption kept increasing with increasing bottom ash content.

Ghosh et al. (2018) Ghost et al. have studied the reuse of bottom ash in cement mortar for better thermal performance for buildings. It was shown that the increment of bottom ash will reduce the thermal conductivity and compressive strength as well. In the comparison of fly ash and bottom ash, the thermal performance was better in the bottom ash mixed mortar and the mechanical properties were better in fly ash mixed mortar. It was revealed that replacing the river sand by fly ash and bottom ash can reduce the thermal conductivity up to 0.29, and 0.28, respectively. This was due to the increased porosity in the bottom ash mixed cement mortar.

2.7.3. Replacement using Rice husk-ash

Rice husk-ash is a by-product generated in the burning process of rice husk. Putra Jaya et al. (2013) have investigated the properties of mortar containing rice husk ash by replacing cement as rice husk ash from 10% to 30%. It was clearly seen that 10%-

15% is the optimum amount of bottom ash to be mixed with cement for greater performance. Ahmad et al. (2015) have also studied the behavior of cement mortar mixed with raw rice husk from different mixes. It was observed that with an increment of rice husk proportion from 0% to 20% the porosity of the mortar increases from 8% to 36%. Since porosity decreases the thermal conductivity of materials, increasing rice husk will decrease the thermal conductivity of cement mortar. Johnson et al. (2017) have also investigated the thermal properties of rice husk ash mixed cement and found that with the addition of rice husk the thermal conductivity reduces and at the same time the compressive strength also reduces which can lead to catastrophes in load-bearing structures.

Further, Habeeb & Mahmud. (2010) have researched on replacement of cement using rice husk ash in concrete with varying proportions of rice husk ash. He found that using rice husk ash up to a certain level can provide increased strength in the concrete and superplasticizers should be used to maintain the desired workability. Anantha Lekshmi et al. have conducted an experimental program to improve the thermal performance of concrete using locally available biomass wastes (L et al., 2020). In such a case, jute, coir, and rice husk were selected for this study and it was revealed that coir and rice husk can significantly reduce the thermal conductivity compared to jute.

2.7.4. Replacement using fiber

Shon et al. (2019) have focused on the studies of physical, mechanical, and thermal properties of common reed fibres (CRF) and steel fibres (SF) added cement mixtures. Six different mixes were prepared with different proportions of fibres and the physical, mechanical, and thermal properties were tested. It was noticed that the porosity increases with the addition of CRF up to 6% and there is less effect of SF compared to CRF. And the flow generally reduces more than 1% of CRF but it increases with the addition of 0.5% SF again. The compressive strength gradually reduces with an increment of CRF and it increases with the addition of SF. The thermal conductivity affected by both fibres and it gradually reduces with the addition of fibres, but it slightly increases when both fibres are present together.

Benmansour et al. have investigated the mechanical and thermal behaviour of cement mortar mixed with date pal fibers (DPF) with different sizes of DPF particles. They noted the thermal conductivity reduces from 0.8 W/m.K to 0.1 W/m.K with the addition of DPF from 0% to 30%. Further, they noted that DPF of 3 mm can reduce the thermal conductivity more effectively than 6 mm particles. Leung & Lin. (2012) have carried out an investigation on cement-based materials with a high thermal performance by adding Polypropylene (PP) fibre and Sica fume (SF) into foam concrete. It was noted that the thermal conductivity effectively reduces with an increasing amount of foam volume which shows the effect of using foaming agents for insulation materials. Further, they found that the effect of silica fume is high in the reduction of thermal conductivity while there is no significant effect from PP fibre.

2.7.5. Replacement using Expanded Polystyrene (EPS)

The use of EPS as insulation materials has become very popular due to its low thermal conductivity and light weight behaviour as well. Several studies have been conducted on adding EPS particles in cementitious materials which is expected to have better mechanical and thermal behaviour as well. Petrella et al. (2020) have conducted studies on EPS mixed cement mortar as partial and full replacement for sand. Different mixes were prepared with different cement-sand ratio and different EPS proportions and their properties were tested. It was noticed that complete replacement with EPS has more flow compared to others and it increases with finer EPS. However, the compressive strength reduces with the replacement of EPS. It was also noted that, the thermal conductivity reduces with increasing proportions of EPS, and the mix with finer EPS achieved very less thermal conductivity and which was noted as 0.25 W/m.K.

González et al. (2014) have investigated the properties of lightweight plasters with EPS foams with different proportions of EPS and some further additions of fibers, plasticizers, and bonding agent. It was found that the maximum allowable ratio of EPS is 2% in order to achieve the required workability. And it was further noted that by the addition of bonding agents the mechanical properties can be improved by improving the cohesion between particles.

Zhang et al. (2019) have conducted investigations on EPS based cement mortar on improving the thermal and mechanical properties. The percentage of EPS was varied from 79.3% to 84.5% of total volume and both mechanical and thermal properties were noticed. It was observed that the thermal conductivity reduces from 0.1192 W/m.K from 0.0838 W/m.K for the corresponding EPS fraction and the compressive strength 1.06 MPa to 0.64 MPa, respectively. In order to increase the affinity between the particles polymer emulsion adhesive (POEA) was used. Two types of POEA were used in this study which is polyvinyl formaldehyde adhesive (PFA) and polyvinyl acetate emulsion (PAE). It was noticed that the addition of both POEA in an appropriate proportion can increase the compressive strength to a certain level. The samples were also tested with the addition of air-entraining agents from 0.05% to 0.15% and it was noticed that thermal conductivity can be reduced from 0.0982 to 0.626 W/m.K.

Another investigation has been conducted on the performance of normalized cement mortar with EPS (Ferrández et al., 2014). Different shape and size of EPS particles were used in this study and the noted porosities were high in EPS mixed mortar especially using spherical larger particles than 3 mm. Further, three types of additives were also used which were air-entraining agent, water retainer agent, and superplasticizer. It was noticed that the porosity increases with the addition of additives and the effect were more in the mix using a water retainer agent.

2.8. Insulation system for CFRP-Concrete Members

Several insulation materials have been investigated to provide protection for the CFRP composite in the fire. Dong et al. (2018) have investigated the fire performance of insulated CFRP-bonded reinforced concrete beams. Four CFRP-bonded Reinforced Concrete beams were insulated using a thick coating system, calcium silicate board system, and ultrathin coating system, respectively. All the specimens were tested under exposure of ISO834 standard fire. The main role of the fire protection materials is to delay the adhesive failure and hence reduce the degradation of concrete and internal reinforcements. The details of the specimens in fire tests are listed in Table 3. The insulated CFRP-strengthened beams with thermocouples are shown in Figure 17.

Table 3: Summary of the beam specimens

Specimen	Length in Fire (m)	Insulation Material	Insulation Configuration	Thickness (mm)	Anchorage Zone	Load Ratio
L1	4.0	Thick Coating	Completely Protected	50	Out of Fire	0.435
L2	4.0	Thick Coating	Partly Protected	50 (20)	Out of Fire	0.435
L3	4.5	Calcium Silicate Board	Completely Protected	40	In Fire	0.630
L4	4.5	Ultrathin Coating	Completely Protected	1.5	In Fire	0.630

The thermal conductivities of Calcium silicate board system, thick coating system, and Ultrathin coating system are 0.06, 0.12, and 0.06, respectively. Adequate fire resistance of 2 hours was obtained for CFRP bonded reinforced concrete beams with insulating with calcium silicate board, thick coating, and ultrathin fireproof coating for the entire span (Dong et al., 2018). Further, it was noted that U-shaped insulation for CFRP-retrofitted Concrete beams is a successive technique. And it was also found that, insulating the anchorage zone have an essential effect on ensuring the fire resistance capacity.

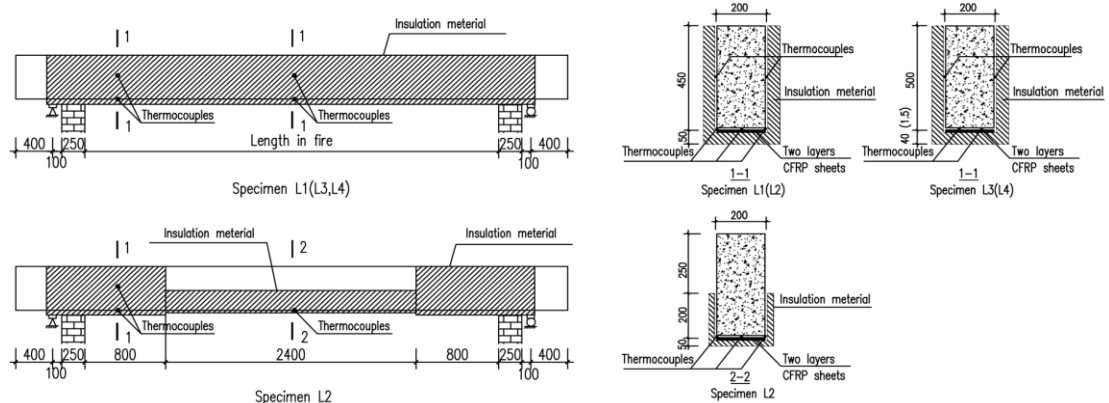


Figure 17: Insulation and thermocouple details for specimens

Gamage et al. (2006) investigated the bond performance of CFRP-concrete composites at high temperatures. A three-dimensional numerical model has been simulated to investigate the heat effects and it was validated using available experimental studies. After knowing the need for insulation, two series of single lap-shear tests were conducted (without insulation and with insulation). Concrete with compressive strength 55 MPa was used for this study. 0.176 mm thickness CFRP

laminates were bonded to the external surface of the concrete member with the use of epoxy adhesive (J. C. P. H. Gamage et al., 2006).

Vermitek-TX was used as an insulation material for fire protection which thermal conductivity is 0.127 W/m K. Strand7, finite element software was used to develop the model and it is shown in Figure 18. The model was tested under AS1530.4 standard fire curve. It was revealed that the thickness and the thermal conductivity of the insulation layer affect the fire rating of the insulated concrete specimen. And it was observed that the bond length does not have effects on the fire resistance of the insulated specimen. Fire rating of 1.76 h was able to achieve using a 50 mm thick insulation layer.

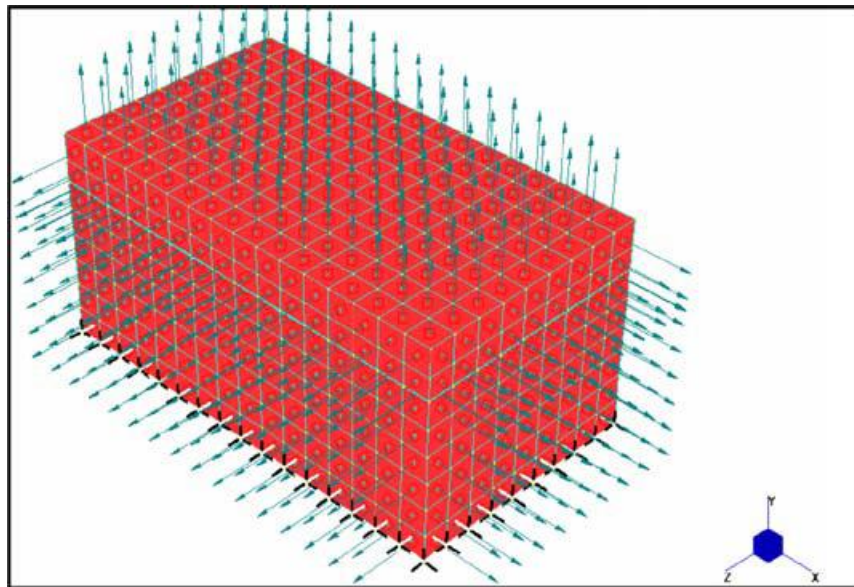


Figure 18: Finite element model of insulated CFRP-concrete specimen (J. C. P. H. Gamage et al., 2006)

Firno & Correia have also focused on the performance of reinforced concrete (RC) beams retrofitted using EBR-CFRP strips and NSM-CFRP strips in flexure. The focus of this study was understanding the structural effectiveness of CFRP strengthening systems during the fire, evaluating the efficiency of the fire protection method, providing mechanical anchorages at the end of the CFRP strips, and using an epoxy with a high glass transition temperature.

Calcium silicate boards were used at the bottom surface of the CFRP-concrete beam to provide fire protection to the area. The insulated beams with EBR-CFRP and NSM-CFRP are shown in Figure 19 & 20. The thickness of the insulation varied along the beams in the range of 0 to 50 mm. A numerical model was also simulated to study the performance of the beams using ABAQUS. The beams were subjected to ISO 834 fire. A two-point loading was applied to investigate the structural performance of the beams during the fire.

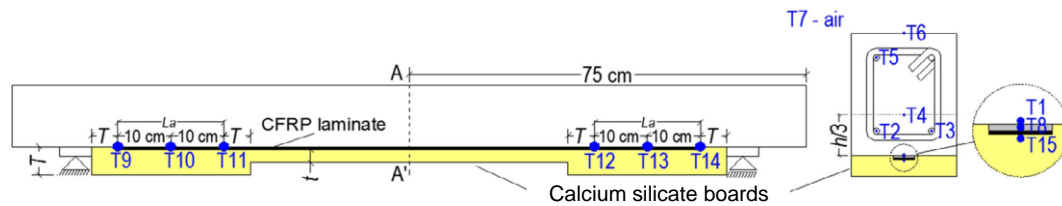


Figure 19: EBR-CFRP-strengthened RC beams with CS boards

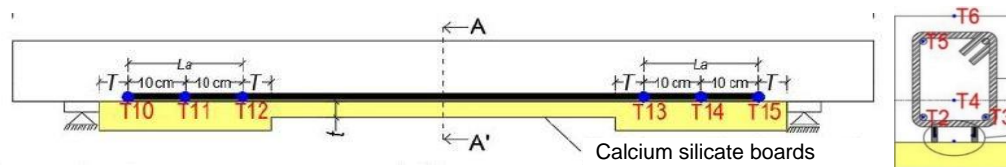


Figure 20: NSM-CFRP-strengthened beams with Calcium Silicate boards

The results provided evidence that the NSM technique has much better fire resistance compared to EBR technique which is shown in Figure 21. Regarding the numerical investigations, the results obtained provided further insights about the stress transfer mechanism in NSM-CFRP strengthening systems during the fire, confirming that the application of a thicker insulation layer in the CFRP anchorage zones allows making use of the cable behaviour and hence extend the fire rating of the strengthening system. It was also noted with a higher thickness of the insulation layer; higher fire resistance can be obtained.

Salama et al. studied the performance of CFRP-retrofitted concrete beams subjected to elevated temperature and four-point bending (Salama, Ghanem, Abd-Elnaby, et al., 2012). At phase 1, six different cement-based mixes were prepared with the addition of Perlite, and vermiculite and the thermal properties were tested. The most appropriate mix which resulted in both low thermal conductivity and high strength. In phase 2, the obtained mortar mix was applied to CFRP strengthened reinforced

concrete beams as cement rendering to protect against elevated temperature. 5 cm of Perlite mortar was overlaid to protect the RC beams.

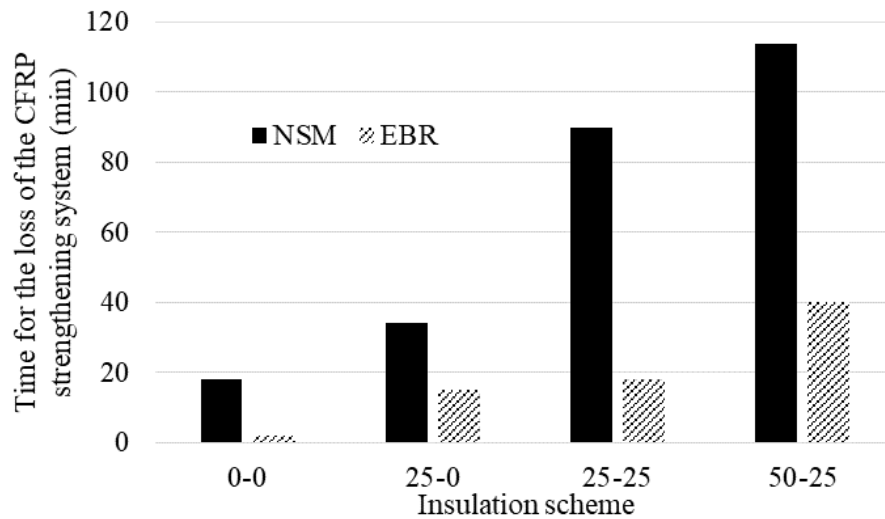


Figure 21: Comparison between the fire performance of EBR and NSM strengthening systems

Thermal conductivity ranges of Perlite mortar and Vermiculite mortar are 0.15-0.28, and 0.32-0.40, respectively. Perlite mortar has shown 2.5 times lower thermal conductivity compared to Vermiculite mortar and has required compressive strength. No capacity loss was noted in the beams protected with thermal insulation layer when it was loaded at 500°C for 3 hours and cooled, then loaded to failure.

An experimental program was conducted by Hu et al. (2007) on reinforced concrete beams bonded using CFRP laminates and insulated with thick-painted fire resistance. The well-known fire resistance methods for steel structure are cover fireproofing plates and paint fire-resistant coating. These methods were found as applicable techniques for CFRP protection.

Two CFRP strengthened reinforced concrete beams (L1, L2) were cast and different insulation technique was applied. Beam L1 was completely insulated using 50 mm fire-resistant coating in the bottom face and side faces. Beam L2 was half protected where 50 mm thickness coating was used in the anchorage region and 20 mm thickness insulation was applied in the non-anchorage region. All the beams were

tested according to the standard fire curve ISO834-1975. The beam specimens are shown in Figure 22.

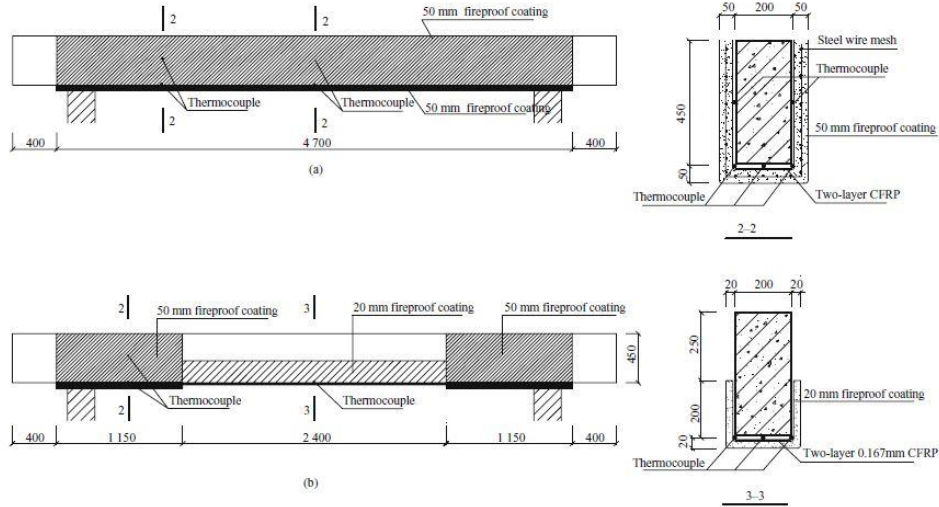


Figure 22: Insulation system for CFRP-concrete beams (a) L1 and (b) L2

Because of the layered installation of the insulation layer, by time layers started to drop from the beam. In the beam L1, at 28 min two-layer coating dropped from the bottom at the midspan. And the complete failure of the beam was noted at 150 min. In the beam specimen L2, after 27 min, the thickness of the coating started to change, and horizontal cracks started to propagate. And the beam collapsed at 117 min.

Further, steel wire mesh was placed into the insulation layer which was able to protect the layer from cracking and eroding under fire. This method was also suggested to use in the reinforced concrete slabs and columns. But it was mentioned to use the appropriate thickness of coating according to the fire protection requirements.

2.9. An analytical method for heat transfer analysis

Heat transfer at fire is based on three ways which are conduction, convection, and radiation. The governing heat transfer equation for a three dimensional element (3D) in steady state is given below (Rafi, 2010; Rafi & Nadjai, 2014)

$$\frac{\partial}{\partial x} \left(k \frac{\partial T}{\partial x} \right) + \frac{\partial}{\partial y} \left(k \frac{\partial T}{\partial y} \right) + \frac{\partial}{\partial z} \left(k \frac{\partial T}{\partial z} \right) + Q - \rho c \frac{\partial T}{\partial t} = 0 \quad (1)$$

Where k is the thermal conductivity, p is the density; c is the specific heat; Q is the internally generated heat; T is the temperature, and t is the time. By applying the

Neumann boundary condition for the above equation, the combined heat transfer equation through conduction, convection, and radiation can be written as follows,

$$-k \frac{\partial T}{\partial x} = q + h_c(T_s - T_f) + h_f(T_s - T_f) \quad (2)$$

Where T_s is solid surface temperature; T_f is fluid temperature, h_c convection heat transfer coefficient, and h_r is radiative heat transfer coefficient.

Since the standard fire is a transient heat transfer, the effect of time in the temperature should be included. Therefore, Eq 3 for transient analysis can be determined if the initial condition (temperature distribution with time) and the boundary condition of the part is given. The heat transfer equation for the transient state can be written based on Galerkin weighted residual method with a combination coefficient h which is given in Eq 3.

$$[K]\{T\} + [C]\{\dot{T}\} = \{F\} \quad (3)$$

$$T = [L]\{T_n\} \quad (4)$$

$$[K] = \int_{V_n} [B]^T [k] [B] dV + \int_{A_n} [L]^T h [L] dA \quad (5)$$

$$[C] = \int_{V_n} [L]^T c \rho [L] dV \quad (6)$$

$$\{F\} = \int_{A_n} [L]^T h T_f dA \quad (7)$$

Where $[K]$, $[C]$, $\{T\}$, $\{F\}$, $[L]$, $[B]$, A , V and dot represents the element heat conduction matrix, the element heat capacity matrix, the element nodal temperature, element nodal heat input vector which is defined at the boundary nodes, shape function matrix, derivative of $[L]$, Element area, Element Volume, and the partial differentiation respect to time, respectively.

CHAPTER 3: THERMAL PERFORMANCE OF ALTERNATIVE ARRANGEMENTS OF CFRP-CONCRETE MEMBERS

3.1 Introduction to the proposed Plan

An alternative CFRP bonding pattern has been introduced in order to increase the fire endurance of the CFRP-concrete member. In this method, a modified NSM bonding technique has been considered which will be referred as the Groove bonding technique (GBT) in this study. Five different models were simulated to predict the heat transfer behaviour of CFRP-concrete member and they are a non-insulated specimen without grooves (B0-0); an insulated specimen with 20 mm insulation layer without grooves (B0-20); a non-insulated specimen with 20 mm grooves (B20-0); an insulated specimen with 20 mm groove filling (B20-20); an insulated specimen with 20 mm insulation layer and 20 mm grooves (B20-40). The model configurations are shown in Figure 23.

3.2. Experimental Program

Total numbers of 15 CFRP-concrete specimens were cast with three identical samples. 100 mm x 100 mm x 200 mm size of concrete blocks were cast and 30 mm width CFRP laminates were attached to the concrete members according to the beam specimen shown in Figure 23. Vermiculite has been used as an insulation material in this program.

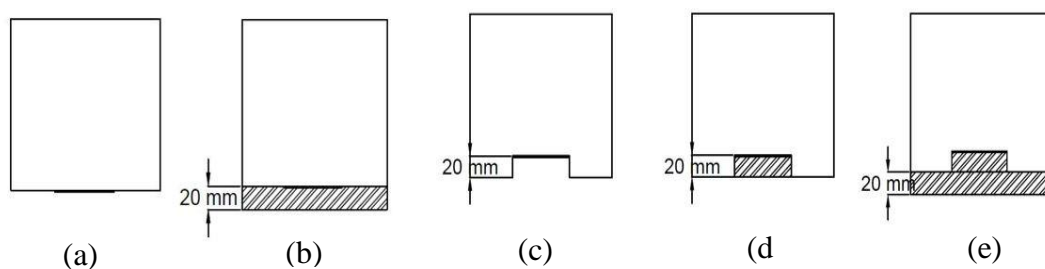


Figure 23. Specimen configurations (a) B0-0; (b) B0-20; (c) B20-0; (d) B20-20; (e) B20-40

3.2.1. Materials

A ready-mix concrete with a 28 days average compressive strength of 24.7 MPa was used to prepare the concrete blocks. 3 mm width and 1.2 mm thick CFRP laminates

(*Technical Data Sheet (CFRP)*, n.d.) was used to retrofit the concrete members using Resin 220 (*Technical data sheet, S & P Resin 220 HP, High performance epoxy adhesive, 2004*) as a bonding agent. Part A (hardener) and the Part B (primer) were mixed in 4:1 ratio as mentioned in manufacturer guidelines. Monokote (Vermiculite), a commercially available fireproofing material was used to provide thermal insulation for CFRP strengthened concrete members at elevated temperature. K-type high-temperature thermocouples were used to measure the temperature. All the materials are shown in Figure 24.

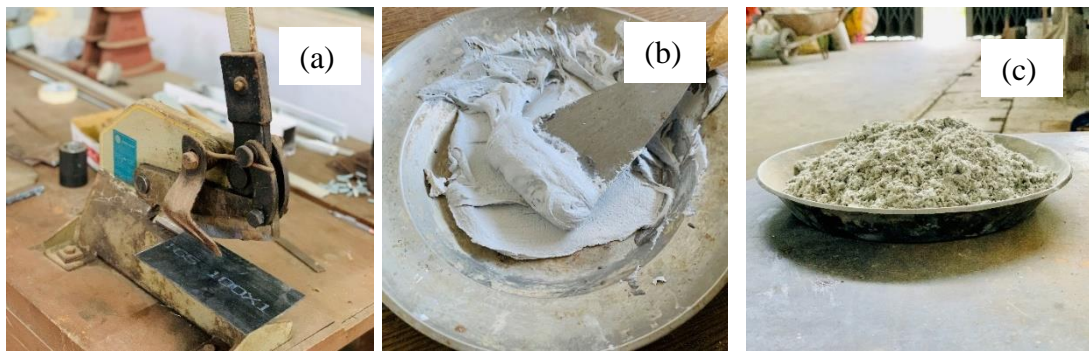


Figure 24. Materials used (a) CFRP; (b) Adhesive (c) Vermiculite-cement

3.2.2. Specimen preparation

3.2.2.1. Casting Concrete blocks

Steel formworks have been used to cast the concrete blocks as shown in Figure 25(a). Mould oil has been applied before pouring the concrete. The concrete mix design was prepared for the strength of 25 N/mm² at 28 days. And the calculated mass of the materials for 1 m³ concrete was 345 kg, 205 kg, 900 kg, and 936 kg for cement, water, fine aggregate, and coarse aggregate, respectively. A concrete mixer was used to prepare the concrete. Three concrete cubes were cast from each concrete batch to test

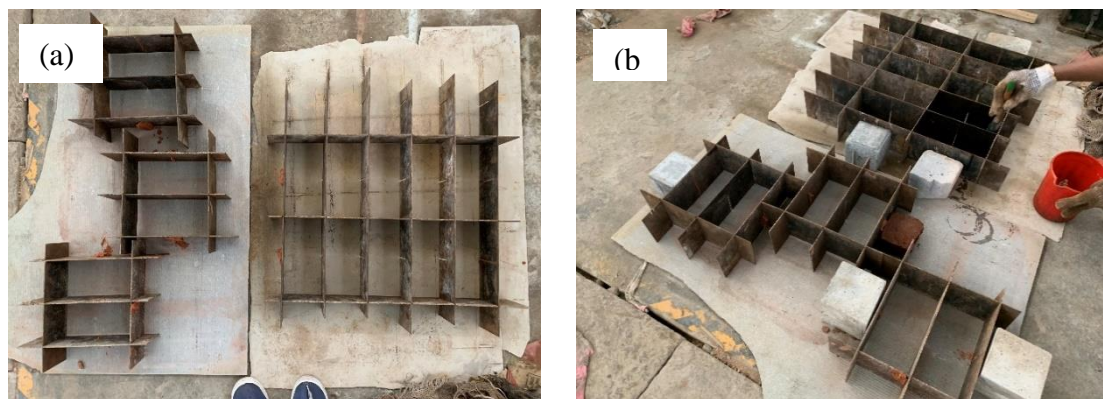




Figure 25. Preparation of concrete blocks (a) Steel formworks; (b) Applying mould oil; (c) Casting concrete blocks; (d) Mechanical compaction of concrete cubes (e) Concrete blocks after formwork removal (f) Concrete blocks during curing process

the compressive strength of the concrete. The formworks were removed after 24 hours and the concrete blocks were kept for curing for 28 days to absorb adequate moisture for further hydration and strength development. The cube test was carried out after 28 days as shown in Figure 25(f).



Figure 26. Testing of concrete cube strength using compressive test machine

3.2.2.2. Grooving Concrete blocks

A grinder was used to make cuts in the concrete blocks as shown in Figure 27. After taking out the concrete particles using chisels the grooved surface was leveled again using a grinder in order to prepare the concrete surface for better bondage.



Figure 27. Grooving the concrete blocks

3.2.2.3. CFRP fabrication

Since the surface preparation has a major impact on the bond performance of the CFRP-concrete composites, it was carried out by grinding the concrete surface (Figure 28). After the completion of the grinding, the dust and debris on the concrete surface were cleaned out. K-type thermocouples were placed on the concrete surface before the application of adhesive to measure the temperature variation within the adhesive layer (Figure 29). Then the two-part adhesive layer was applied for 2-3 mm thickness according to the manufacturer guidelines. The CFRP laminates were cut into appropriate dimensions (20 cm x 3 cm) and bonded on top of the adhesive layer. The



Figure 28. (a) Grinding the surface of specimen without grooves; (b) After grinding the surface of specimen with grooves

CFRP fabricated concrete composite samples were let to cure for 7 – 14 days (Figure 30).

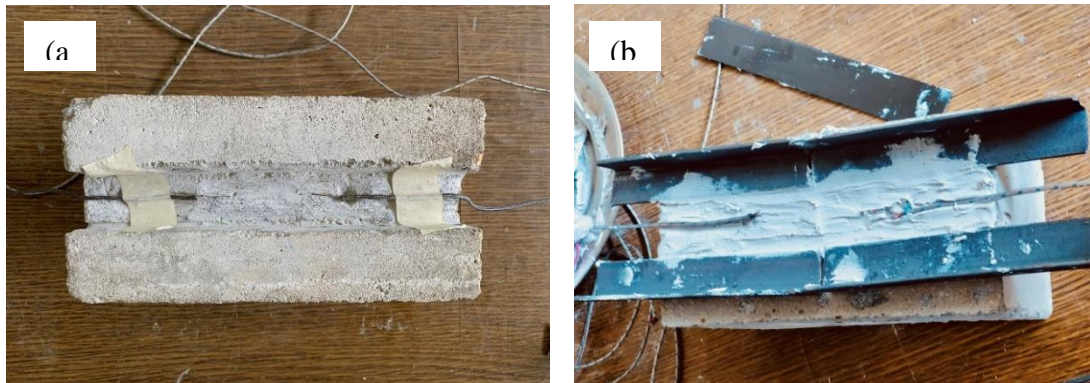


Figure 29. (a) Fixing the thermo couples; (b) Applying the adhesive layer



Figure 30. (a) Prepared B0_0 samples; (b) Prepared B20_0 samples

3.2.2.4. Applying Insulation layer

Dried vermiculite was mixed with the required amount of water using a mortar mixer according to manufacturer guidelines (Figure 31(a)). The target density of the mix proportion was $600 - 700 \text{ kg/m}^3$. The well-mixed insulation material was firmly applied on top of CFRP laminates according to the beam specifications mentioned above (Figure 31(b-c)). Timber formwork was used to apply the insulation layer to the required thickness. The insulated samples were again kept for dry curing for about 14 days (Figure 32).

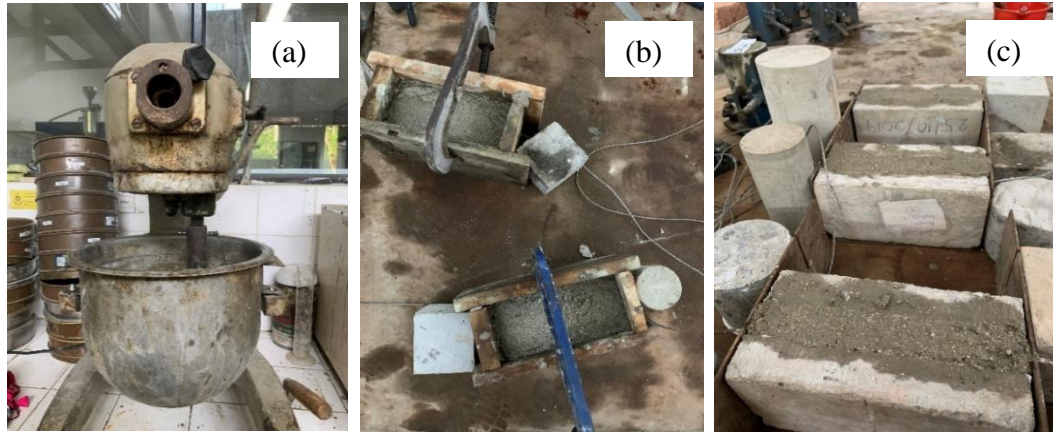


Figure 31. (a) Mixing the vermiculite-cement mortar; (b) Applying insulation for B0_20 specimen; (c) Applying insulation for B20_0 specimen

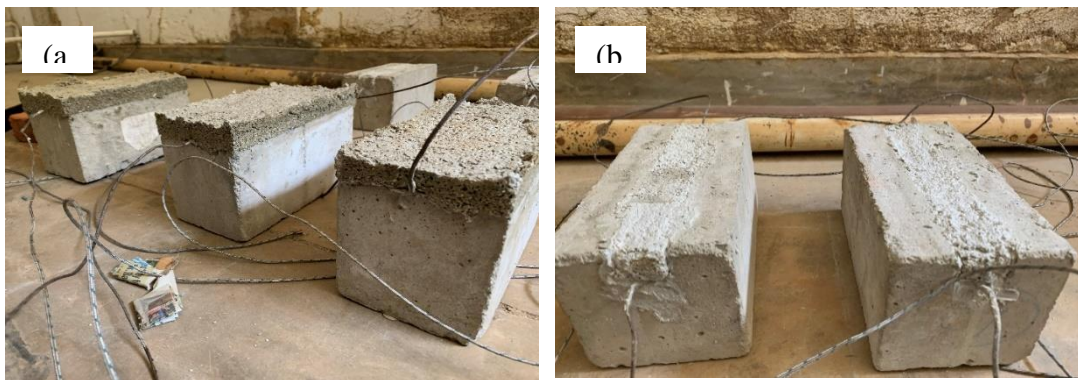


Figure 32. (a) B_20 specimen after applying the insulation; (b) B20_0 specimen after applying

3.2.3. Testing of material properties

A series of tests were carried out to obtain the thermal properties of the selected insulation material.

3.2.3.1. Thermal conductivity

Three samples with 5 mm thickness and 60 mm diameter were cast and their thermal conductivities were tested using the Lee's disk method, in accordance with ASTM D7340. (2018). The average of all three samples was taken as its thermal conductivity. The samples prepared and the testing instrument are shown in Figure 33(a) and Figure 33(b), respectively. A detailed testing and calculation procedure are described in Section 4.2.7 and the curves are attached to Annex B. The tested results and

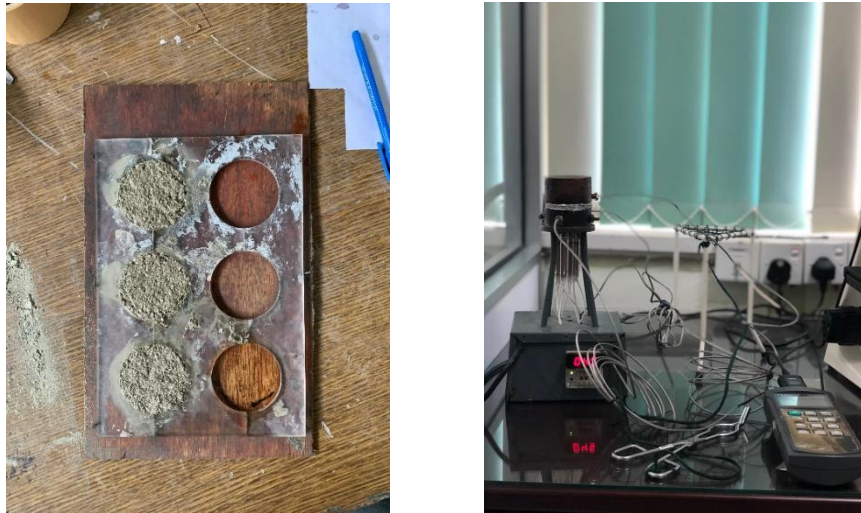


Figure 33. (a) Specimen preparation; (b) Testing of thermal conductivity

manufacturer provided results are shown in Table 4. The deviation in the results shows testing of material property is essential rather using the manufacturer provided properties (Monokote ® Z-146PC, 2018).

Table 4. Comparison of thermal conductivity

Test value	Manufacturer value	% deviation
0.12 W/m.K	0.14 W/m.K	17%

3.2.3.2. Specific heat

Specific heat is defined as the amount of energy required to raise the temperature of 1kg of a material by one unit of temperature. This is an important property as it will give an indication of how much energy will be required to heat or cool an object of a given mass by a given amount.

An experimental program was conducted to determine the specific heat capacity of the vermiculite cubes (Figure 34). The sample was heated initially up to 95°C temperature and dropped into an insulated flask bottle containing water at room temperature. The final peak temperature rise of the water inside the jar was measured using thermocouples.

Heat loss of the specimen = Heat gain by the water

$$mc\theta = MS(\Delta\theta) \quad (8)$$

where

m = mass of the aerated concrete sample

c = specific heat capacity of the prepared sample

θ = temperature reduction in the prepared sample

M = mass of the water

S = specific heat capacity of water at 30°C

$\Delta\theta$ = temperature increase in water



Figure 34. (a) Specimen preparation; (b) Testing of specific heat

Three samples were tested for specific heat to get more accurate results. The observations and results are listed in Table 5. The room temperature during the experiment was 28°C. The specific heat of the water (S) was assumed as 4186 J/kg.K.

Table 5: Measurements for specific heat calculations

Measurements	Sample 1	Sample 2	Sample 3
M (g)	629.8	632.7	647.9
$\Delta\theta$	2.8	1.3	0.8
m (g)	21.13	18.1	20.9
θ	58.9	64.8	63.9
C (J/kg.K)	3321.6	2935.5	1624.6

From the results obtained from all 3 samples, the average specific heat was calculated as **2600 J/kg.K**.

3.2.3.3. Density

The weights and volume of all the samples prepared were measured to calculate the average bulk density of the prepared vermiculite-cement mortar. The calculated densities are listed in Table 6.

Table 6: Measurements and density calculations

Sample	Weight (g)	Volume (cm ³)	Density (g/cm ³)
1	6.1	14.14	0.431
2	7	14.14	0.495
3	5.2	14.14	0.367
4	113.2	249.6	0.453

From the results obtained for density, the average density was calculated as 0.4375 g/cm³. However, since the volumes were smaller than the expected dimensions, a higher density than the experimentally obtained density is expected.

3.2.3. Testing

The selected data logger was calibrated for the temperature range from -20°C to 630°C by defining the voltage respected to the temperature. To ensure the accuracy of the data logger and the thermocouple, the thermocouples were placed into ice and boiling water and the noted readings were 1°C, and 98°C, respectively.

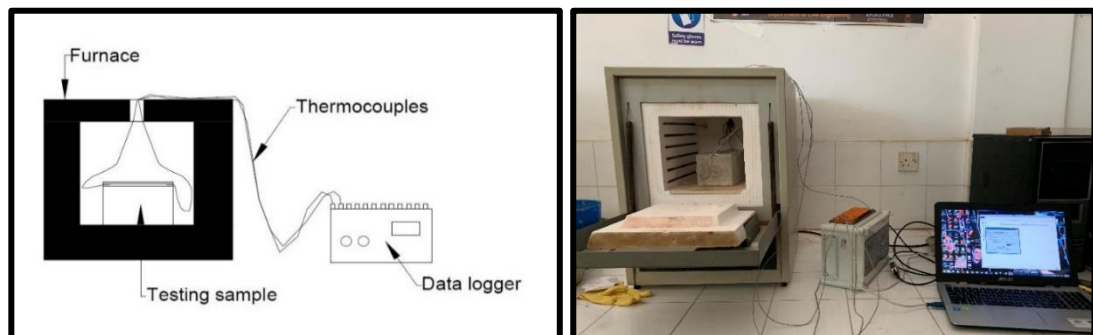


Figure 35. Test set-up

As shown in Figure 35, the specimen was kept in the furnace and the thermocouples were connected to a data logger to retrieve the temperature measurements. The thermocouple readings were recorded in 10 s intervals in the data logger and then it was sent to the computer. The temperature profile of the testing furnace without any samples was recorded prior to the testing. The temperature profile of an empty oven is shown in Figure 36.

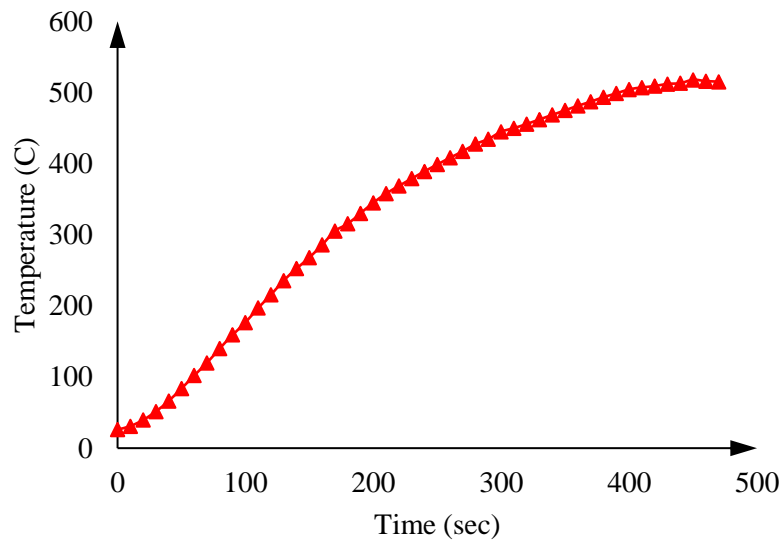
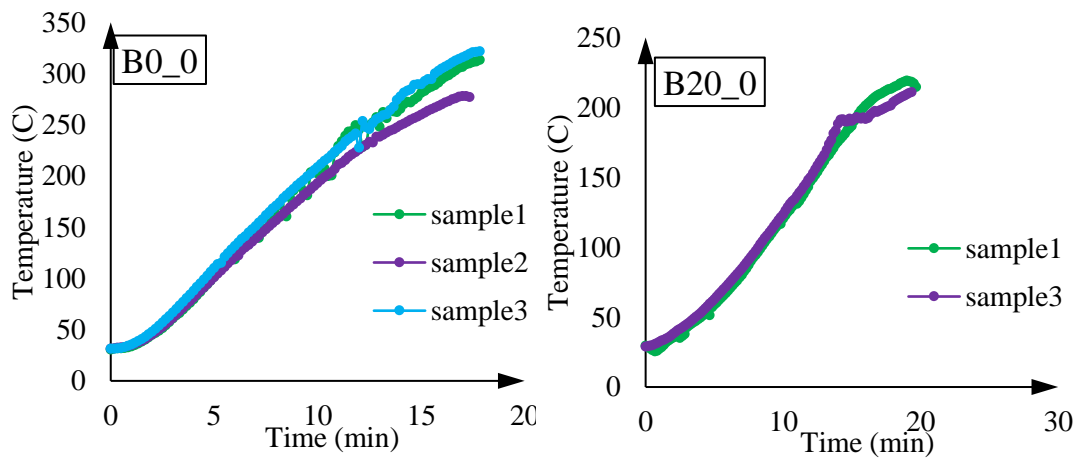


Figure 36. Temperature profile of the oven

3.2.4. Results

Three samples were tested from each specimen to increase the accuracy of the results. The average temperature variation within the adhesive layer of each three samples obtained from two thermocouples is plotted in Figure 37 for all five specimens. And



the compared results of all five specimens were plotted in Figure 38 and the corresponded temperature where the adhesive reaches its glass transient temperature (assumed as 70° C) is also shown in the graph.

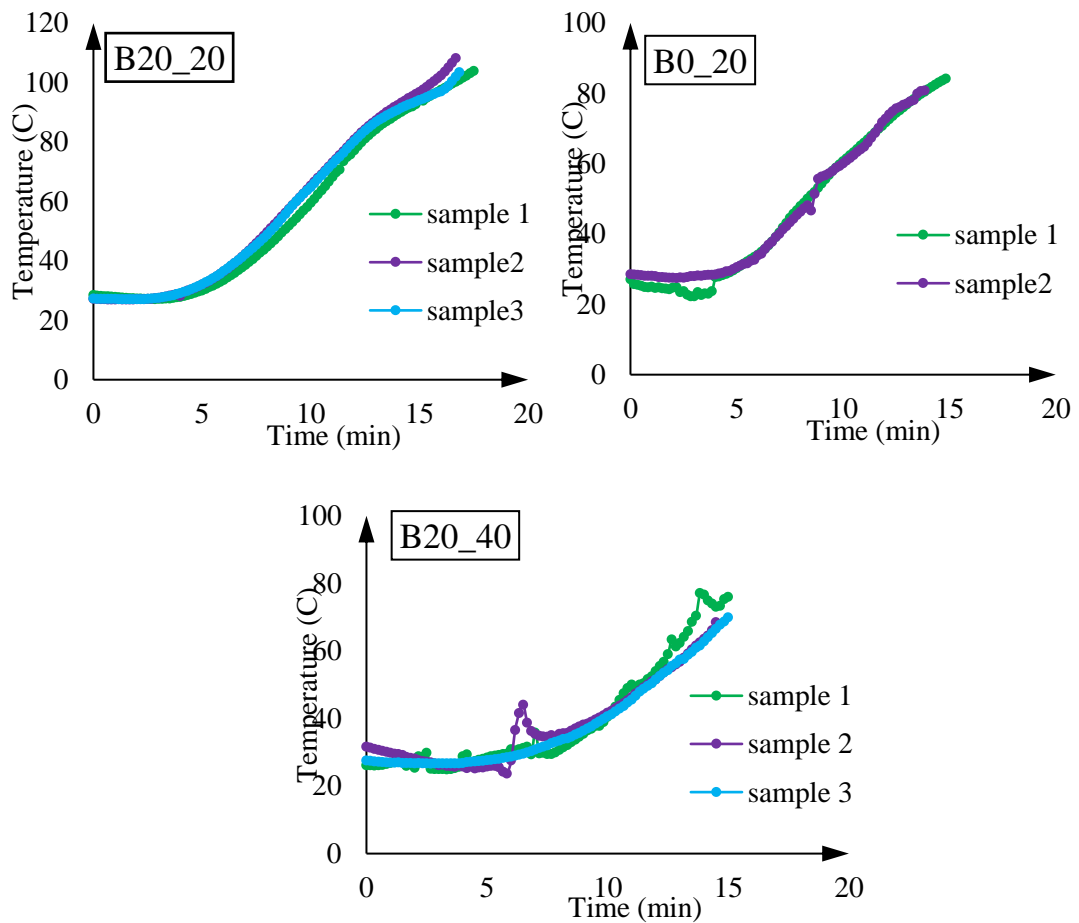


Figure 37. Average temperature variation with time within the adhesive layer

From the results obtained in the test program, the time taken to reach its glass transient temperature (70°C) was 3.3 min, 5.6 min, 10.2 min, 10.5 min, and 14.7 min, for B0_0, B20_0, B20_20, B0_20, and B20_40, respectively. This shows that the thermal resistance to the elevated temperature of the samples with 20 mm grooves has increased 1.7 times than the samples without grooves. It was also noted that the samples with groove-filled insulation have almost a similar effect the samples with 20 mm insulation layer without groves. And with an additional insulation layer, the thermal resistance further increases.

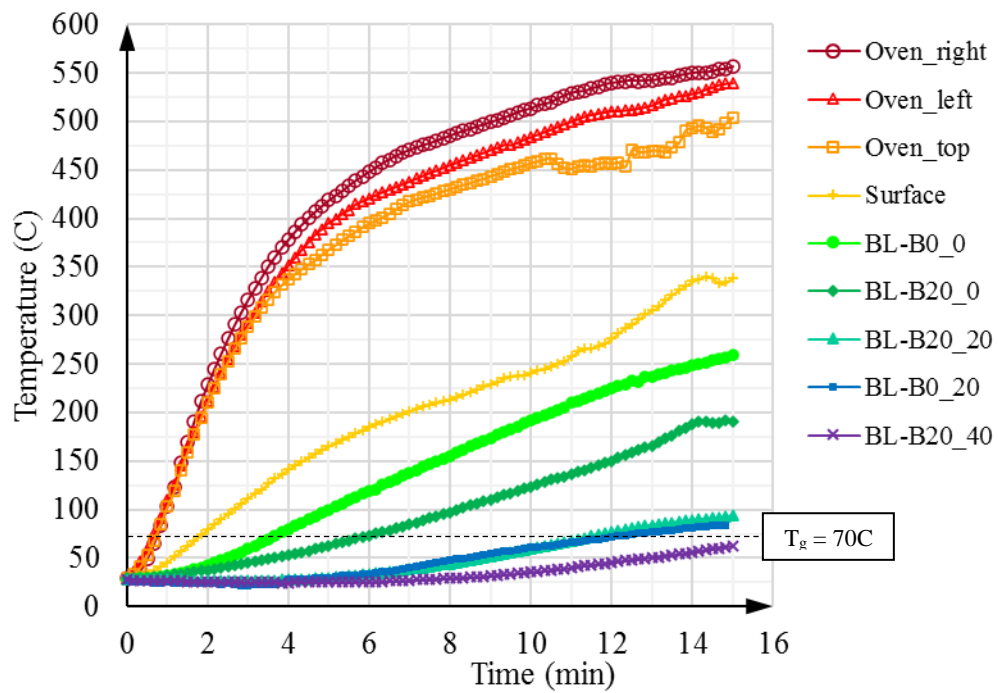


Figure 38. Comparison of the specimens

3.3. Theoretical Analysis of flexural performance prediction

The manufacturer provided mechanical properties (Table 7) were used to compare the moment capacities of both bonding types EBT & GBT (Figure 39) composite structures. The flexural strength of the section with FRP bonded reinforced concrete can be computed from Equations 9-11 (ACI committee 440, 1996).

Table 7. Mechanical properties

Material Properties	Elastic Modulus (GPa)	Compressive strength (MPa)	Tensile strength (MPa)	Rupture strain
Concrete	23.5	24.7	2.9	-
CFRP	170	-	2800	0.016
Adhesive	7.1	70	3	-

The selected bond types for flexural calculations are shown in Figure 39. And the selected beam dimensions for corresponded bond arrangements are shown in Table

A1. Grade 25 concrete with 2 no of 12 mm steel bars were used for this retrofitting calculations. A nominal cover of 35 mm was used, and half-width CFRP laminates

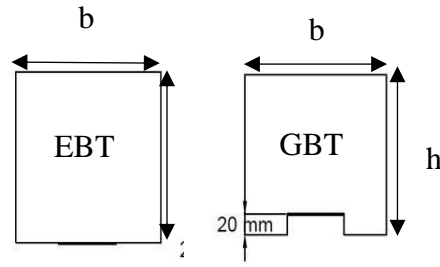


Figure 39. Bond arrangements

were used for bonding.

$$M_n = \phi[M_{ns} + \phi_f M_{nf}] \quad (9)$$

$$M_{ns}(\text{Contribution of steel}) = A_s f_s (d - \frac{\beta c}{2}) \quad (10)$$

$$M_{nf}(\text{Contribution of FRP}) = A_f f_f (d_f - \frac{\beta c}{2}) \quad (11)$$

Where, A_s , A_f , f_s , f_f , d , d_f , β , and c , are steel area, FRP area, the stress in steel, stress in FRP, depth to steel, depth to FRP, concrete stress block factor (*ACI 318-14*, 2014), and depth to the neutral axis. The moment carrying capacities of CFRP strengthened reinforced concrete beams using both bond types EBT & GBT were calculated separately. In this regard, the beam configurations are tabulated in Table 8. The obtained moment capacities for selected specimens are tabulated in Table 9. However, this value will vary depending on the section & mechanical properties and a slight increment can be further expected after filling the grooves. Though the flexural enhancement due to GBT is slightly lower than the EBT bonding technique, an

Table 8. Beam configurations

Beam ID	Bond Type	Dimensions
EBT-1	EBT	200 mm x 350 mm x 1 m
EBT-2	EBT	300 mm x 600 mm x 1 m
GBT-1	GBT	200 mm x 350 mm x 1 m
GBT-2	GBT	300 mm x 600 mm x 1 m

improved fire rating is expected in GBT which is described in the following sections. The detailed calculations are attached in Annex A.

Table 9. Moment capacity results

Specimen Id	Moment capacity (kNm)	Specimen ID	Moment capacity (kNm)	% reduction in moment capacity due to deep grooves
EBT-1	461.4	GBT-1	453.4	1.7%
EBT-1	175.8	GBT-2	168.2	4.3%

3.4. Numerical Modelling

A three dimensional (3D) transient heat transfer analysis was conducted using a commercially available finite element software ABAQUS. Five models were simulated to predict the fire performance of the CFRP-concrete member with and without insulation. 100 mm x 100 mm x 300 mm concrete blocks and 30 mm width CFRP laminate strips with adhesive as a bonding agent was used for this study. A computer with 8 GB RAM, 2 core processor, and 2 GB VGA was used for this analysis.

3.4.1. Thermal properties

The thermal properties of concrete, CFRP laminates, and Adhesive were obtained from the available literature and they are explained in the sections below. The thermal properties of vermiculite were tested in the laboratory at a temperature less than 100°C. And the properties at the elevated temperature were derived from the models available in the literature.

3.4.1.1. Concrete

Since the tested average compressive strength after 28 days was 24 MPa, the thermal properties of a normal strength concrete were obtained from Eurocode 2 (*EN 1992-1-2 (2004): Eurocode 2: Design of Concrete Structures - Part 1-2, 2004*). And the density was assumed as 2400 kg/m³. The equation for the specific heat at elevated temperature is given in equations 12-15. And the upper limit for the thermal conductivity and the

lower limit for the thermal conductivity is given by equation 16, and 17, respectively. The average thermal conductivity was used in the finite element model.

$$c = 900 \frac{J}{kgK} \quad 20^{\circ}C \leq \theta \leq 100^{\circ}C \quad (12)$$

$$c = 900 + (\theta - 100) \frac{J}{kgK} \quad 100^{\circ}C \leq \theta \leq 200^{\circ}C \quad (13)$$

$$c = 1000 + \frac{(\theta - 200)}{2} \frac{J}{kgK} \quad 200^{\circ}C \leq \theta \leq 400^{\circ}C \quad (14)$$

$$c = 1100 \frac{J}{kgK} \quad 400^{\circ}C \leq \theta \leq 1200^{\circ}C \quad (15)$$

$$k = 2 - 0.2451 \left(\frac{\theta}{100} \right) + 0.0107 \left(\frac{\theta}{100} \right)^2 \frac{W}{mK} \quad 20^{\circ}C \leq \theta \leq 1200^{\circ}C \quad (16)$$

$$k = 1.36 - 0.136 \left(\frac{\theta}{100} \right) + 0.0057 \left(\frac{\theta}{100} \right)^2 W/mK \quad 20^{\circ}C \leq \theta \leq 1200^{\circ}C \quad (17)$$

Where Θ is the atmosphere temperature.

3.4.1.1. CFRP

The thermal properties of CFRP laminates were obtained from the study conducted by Kodur et al. (2005) and it is illustrated in Figure 40. The drastic change in the specific heat in between 400 °C and 600°C and the gradual reduction in the thermal

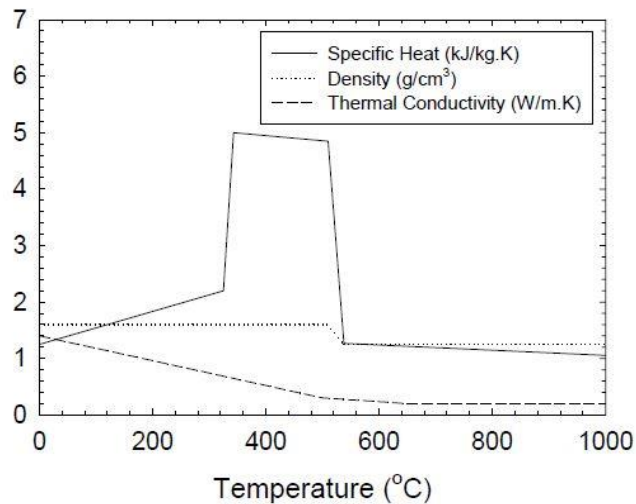


Figure 40. Thermal properties of CFRP

conductivity till 600 °C are notable. no significant variation was noted in the density of CFRP materials.

3.4.1.3. Epoxy adhesive

The thermal properties of the epoxy resin were obtained from the available literature and the thermal conductivity variation and the specific heat variation are illustrated in Figures 41, and 42, respectively (Evseeva & Tanaeva, 1995). It can be seen that the thermal conductivity and specific heat both increases with temperature.

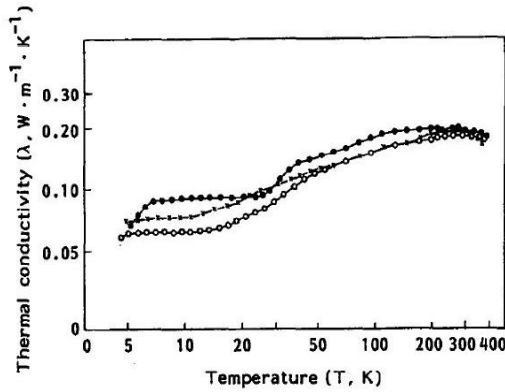


Figure 41. Thermal conductivity variations of Epoxy resin

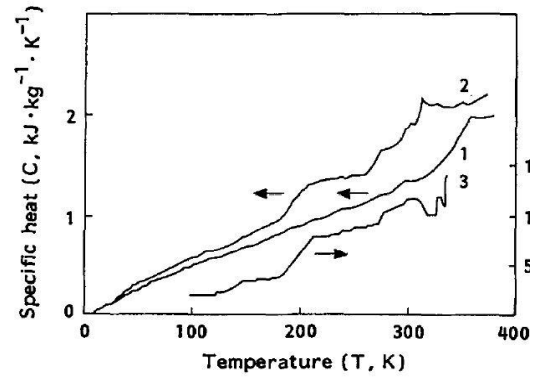


Figure 42. Specific heat variations of Epoxy resin

3.4.1.4. Vermiculite

The thermal properties of the vermiculite were tested in the laboratory at room temperature and the thermal properties of elevated temperature were derived from the model developed by Sadiq et al (Sadiq et al., 2014). The developed model for thermal conductivity, density, and specific heat is given in equations 18-20, 21-23, and 24-27, respectively.

Thermal conductivity:

$$k' = k(1 + 6\phi) \quad 20^\circ\text{C} \leq \theta \leq 90^\circ\text{C} \quad (18)$$

$$k' = k \left(1 + 6\phi \frac{\theta_2 - \theta}{\theta_2 - \theta_1} \right) \quad 90^\circ\text{C} \leq \theta \leq 120^\circ\text{C} \quad (19)$$

$$k' = k \quad \theta > 120^\circ\text{C} \quad (20)$$

Density:

$$\rho' = \rho(1 + \emptyset) \quad 20^\circ\text{C} \leq \theta \leq 90^\circ\text{C} \quad (21)$$

$$\rho' = \rho \left(1 + 6\emptyset \frac{\theta_2 - \theta}{\theta_2 - \theta_1} \right) \quad 90^\circ\text{C} \leq \theta \leq 120^\circ\text{C} \quad (22)$$

$$\rho = \rho \quad \theta > 120^\circ\text{C} \quad (23)$$

Specific heat:

$$\rho' c' = \rho c (c + c_w \emptyset) \quad 20^\circ\text{C} \leq \theta \leq 90^\circ\text{C} \quad (24)$$

$$\rho' c' = \rho \left(c + \frac{\emptyset}{\theta_2 - \theta_1} \left((\theta_2 - \theta) c_w + \frac{d\zeta}{d\theta} \cdot L_w \right) \right) \quad 90^\circ\text{C} \leq \theta \leq 120^\circ\text{C} \quad (25)$$

$$\rho' c' = \rho \left(c + \frac{d\zeta}{d\theta} \cdot \frac{L_w}{\theta_4 - \theta_3} \right) \quad 120^\circ\text{C} \leq \theta \leq 500^\circ\text{C} \quad (26)$$

$$\rho' c' = \rho c \quad \theta > 540^\circ\text{C} \quad (27)$$

Where \emptyset is the moisture content which was assumed as 25%; temperatures Θ_1 and Θ_2 are the evaporation temperatures at the start and end, respectively ($\Theta_1 = 90^\circ\text{C}$ and $\Theta_2 = 120^\circ\text{C}$). The latent heat required to evaporate the moisture was incorporated in the specific heat computation in the range of 90°C to 120°C . A bell curve function for the apparent specific heat of the water was assumed in this temperature range by using the dimensionless function, $d\zeta/d\theta$, from Harmathy's model (Babrauskas & Science, 2018).

3.4.2. Finite element mesh and interactions

An 8-node linear heat transfer brick elements (DC3D8) were used to model the concrete, adhesive, CFRP, and insulation elements. Appropriate mesh sizes were used to each element after conducting a mesh sensitivity analysis. The concrete and insulation layers were discretized into 10 mm mesh size elements. 5 mm mesh size was used to CFRP and adhesive layers to get more precise results in the adhesive temperature. A tie constraint was used to represent the bond between concrete-

adhesive, adhesive-CFRP, and CFRP-insulation. The Finite element mesh of the model is shown in Figure 43.

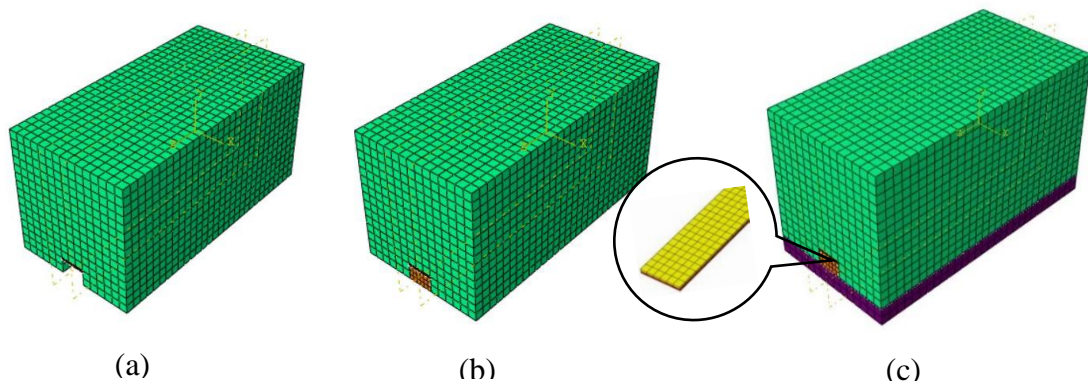


Figure 43. Finite element mesh of (a) B20-0; (b) B20-20; (c) B20-40

3.4.3. Transient Heat transfer Analysis

The heat transfer was assumed through conduction, convection, and radiation. And the model was assumed exposed to a flow shown in Figure 36 (Oven profile) with convection and radiation. The film coefficient of convection was assumed as $35 \text{ J}/(\text{s kg C})$ at room temperature and reducing with increasing temperature. The emissivity of the medium was assumed as 1. The initial temperature of the specimen was assumed as $27 \text{ }^\circ\text{C}$.

3.4.4. Preliminary Analysis for ensuring the heat transfer parameters

In order to select the suitable heat transfer coefficients for the particular inputs, A CFRP-concrete from the past studies was simulated using ABAQUS software for non-insulated, and insulated conditions exposed to the elevated temperature using a furnace (J. Gamage et al., 2005). The experimental sample and the finite element model simulated by Gamage et al. is shown in Figure 44. And the numerical model simulated using ABAQUS software in this study is shown in Figure 44. Further, the model was subjected to the ASTM standard fire and the temperature variation within the adhesive layer was observed.

The temperature variation within the adhesive layer was compared to the results obtained by Gamage et al., and the heat transfer coefficients were ensured during subjected to the elevated temperature using a furnace. Further, the model was subjected to the ASTM standard fire and again the temperature variation within the adhesive layer was compared to the literature and the coefficients during the standard fire were ensured. The temperature variation at both conditions is illustrated in Figure 45.

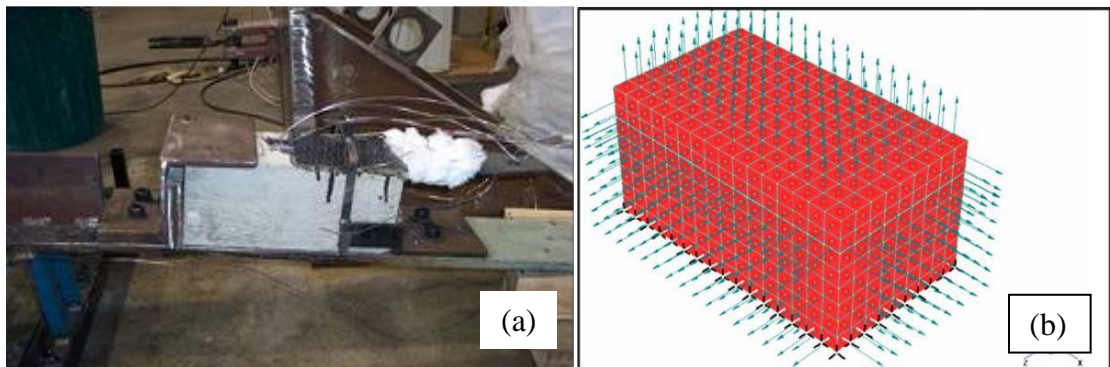


Figure 44. (a) Experiment sample; (b) Finite element model.

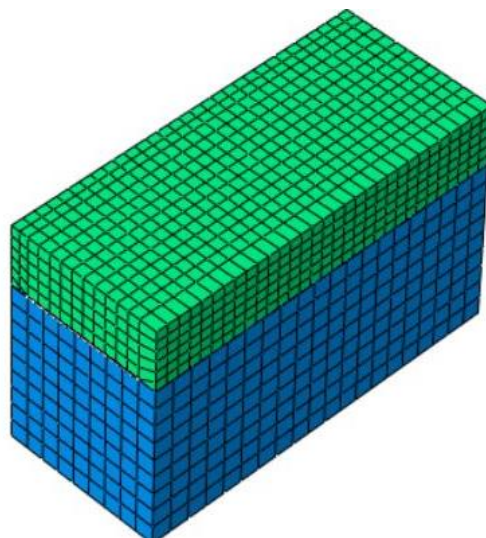


Figure 45. CFRP concrete-member simulated using ABAQUS with 50 mm thick vermiculite layer

From the results obtained (Figure 46) for the test conducted using a furnace, it can be confirmed that the selected heat transfer parameters are suitable for the following problem. By changing the heat transfer parameters, the model was analyzed under

ASTM standard fire and the most suitable parameters were concluded for convective coefficient and emissivity. From the available results in the literature and the compatibility in the FE model by Gamage et al. the convective coefficient was selected as $5 \text{ J}/(\text{s kg C})$ (J. C. P. H. Gamage et al., 2006; Qunitiere & Veloo, 2011; C. Zhang & Usmani, 2015) and the average emissivity during the standard fire was selected as 0.2 (Sudheer & Prabhu, 2010).

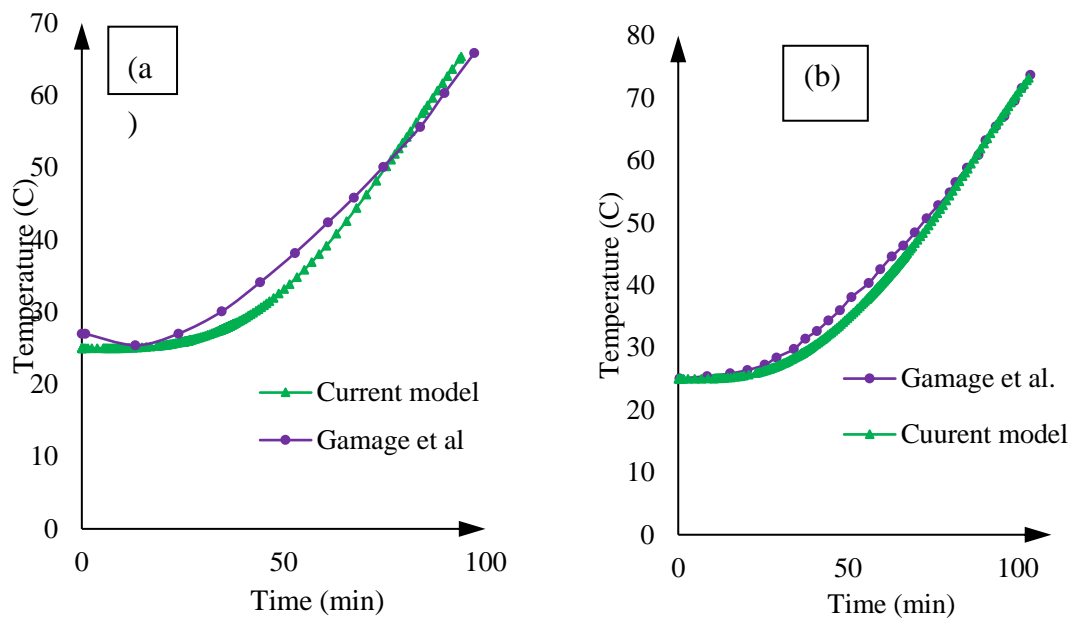


Figure 46. Temperature variation within the adhesive layer when (a) subjected to elevated temperature in the furnace: (b) subjected to ASTM standard fire

3.4.6. Results & Validation

The temperature variation at the bond line and concrete surface (B20_0) were noted and plotted in Figure 47 against their experimental results. The temperatures in the adhesive layer and concrete surface respect to $t = 10 \text{ min}$ are tabulated in Table 11. Since the glass transition temperature (T_g) of the adhesive varies from $60^\circ\text{C} - 80^\circ\text{C}$, the temperature variations were observed when the furnace reached the maximum temperature. The temperature variation across the specimen cross-section for all 5 specimens are shown in Table 9. A high-temperature profile can be noted in the insulation layer due to its thermal properties. It can be also noted, with the addition of

the insulation layer, the temperature contours moved further away from the adhesive layer, the adhesive can be protected from fire.

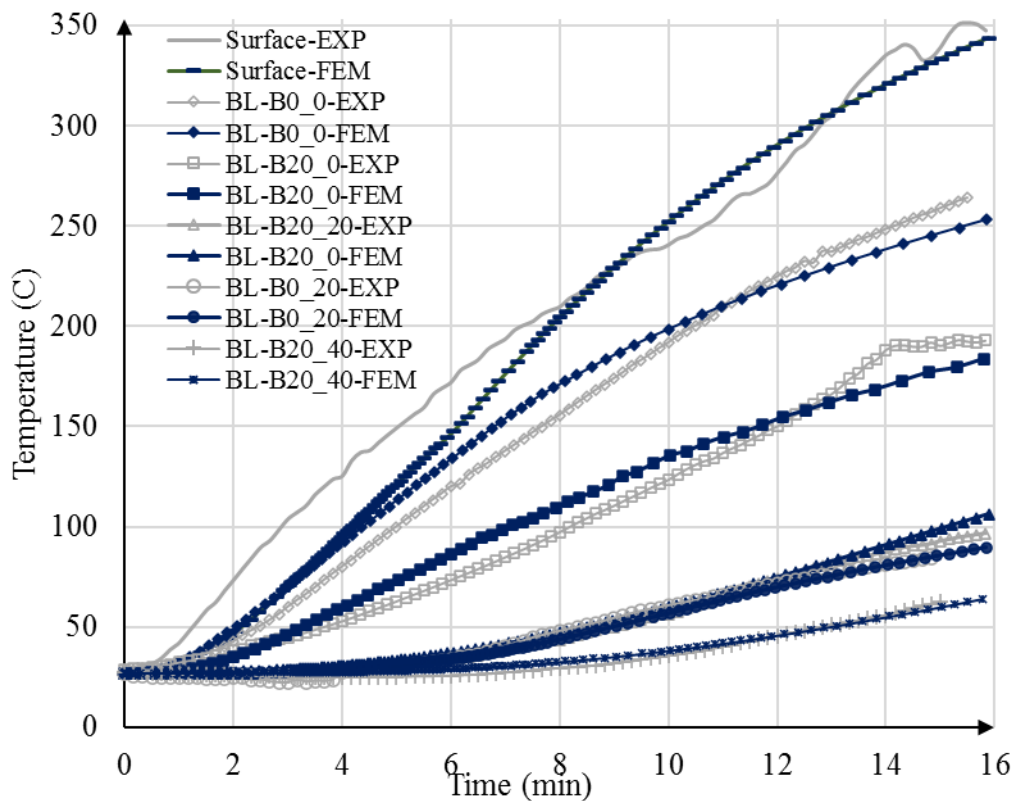


Figure 47. Comparison of experimental results (Exp) and numerically predicted results

The temperature profile within the adhesive layer is also shown in Table 10. A very high temperature was noted at the edges of the adhesive layer where it is directly exposed to the fire. The mean temperature of the mid-region was used to study the temperature-time behavior of the adhesive. With the addition of the insulation layer, the contours move towards the middle which shows the additional prevention of the adhesive layer.

The model predicted and tested temperature variation in the bond line were compared and tabulated in Table 11. It can be noted that the maximum deviation is less than 5% in insulated samples and less than 10% in non-insulated samples. The reason behind a slight higher deviation in the non-insulated sample may be the direct exposure of the CFRP bond to the elevated temperature. The accuracy of the model allows for further

simulations to find out the effects of different thermal properties and geometrical properties.

Table 10. Temperature variations predicted using FE model

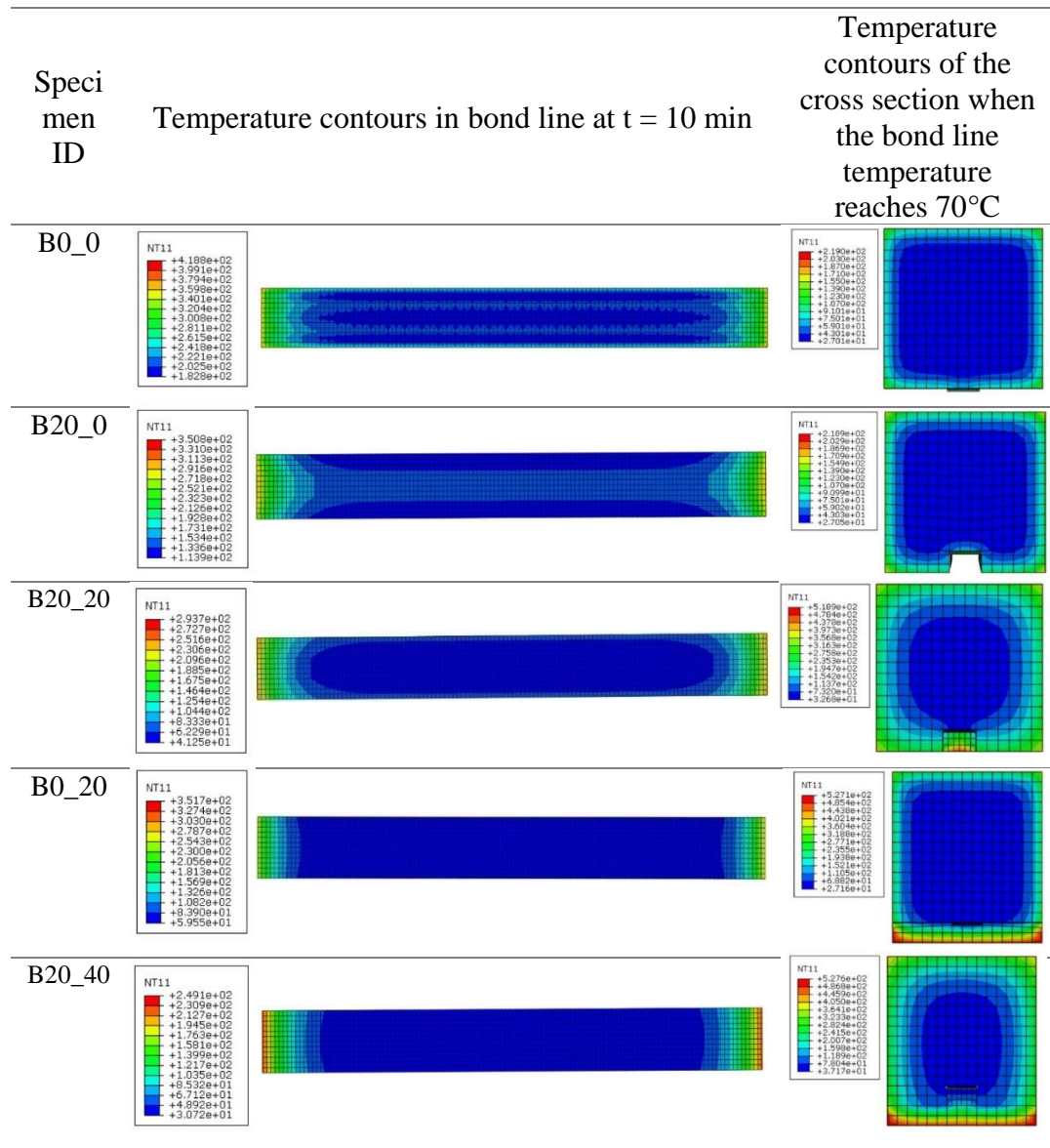


Table 11. Comparison of temperatures at t = 10 min

Temperature Location	Test Results (°C)	FEM results (°C)	% difference
Adhesive of B0_0	191.7	199.5	4.06%
Adhesive of B20_0	124.5	137.7	10.6%

Adhesive of B20_20	56.4	58.1	3.01%
Adhesive of B0_20	60.6	62.5	3.1%
Adhesive of B20_40	38.4	40.1	4.43%
Concrete surface	240.6	251.5	4.5%

3.5. Heat transient analysis under ISO standard fire

The validated models were further analyzed under ISO 834 standard fire curve (*ISO-834. Fire-Resistance Tests - Elements of Building Construction - Part 1: General Requirements.*, 1999). The standard fire curve is given in equation 28 and the curve is shown in Figure 48. The heat transfer was assumed through conduction, convection, and radiation as in previous analysis. The convection coefficient and emissivity for the standard fire were obtained from the literature (Sudheer & Prabhu, 2010). A preliminary analysis was carried out to validate the appropriate usage of coefficients

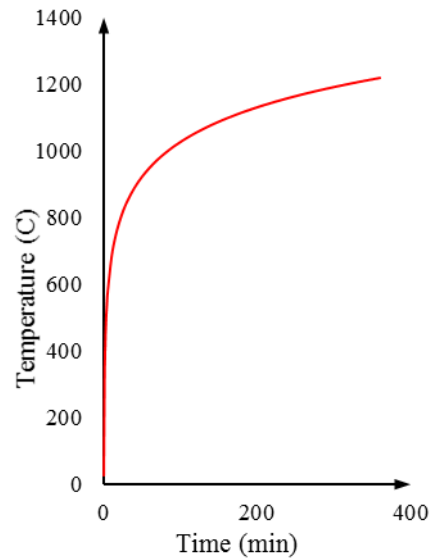


Figure 48 Standard fire curve – ISO 834

with experimental results in the literature (J. C. P. H. Gamage et al., 2006). The simulations were carried out under two conditions; (i) four sides exposed to the fire; and (ii) only the bottom side exposed to the fire. The temperature variations at the bond line were observed and illustrated in Figure 49. (see Annex A2 for model results)

$$T_{(t)} = T_{(t_0)} + 345 \log(8t - 1) \quad (28)$$

Time taken for the adhesive layer to reach the glass transition temperature (70°C) of each specimen under both fire conditions are listed in Table 12 along with the Insulation volume used. In the insulated specimens, a high fire resistance was noted

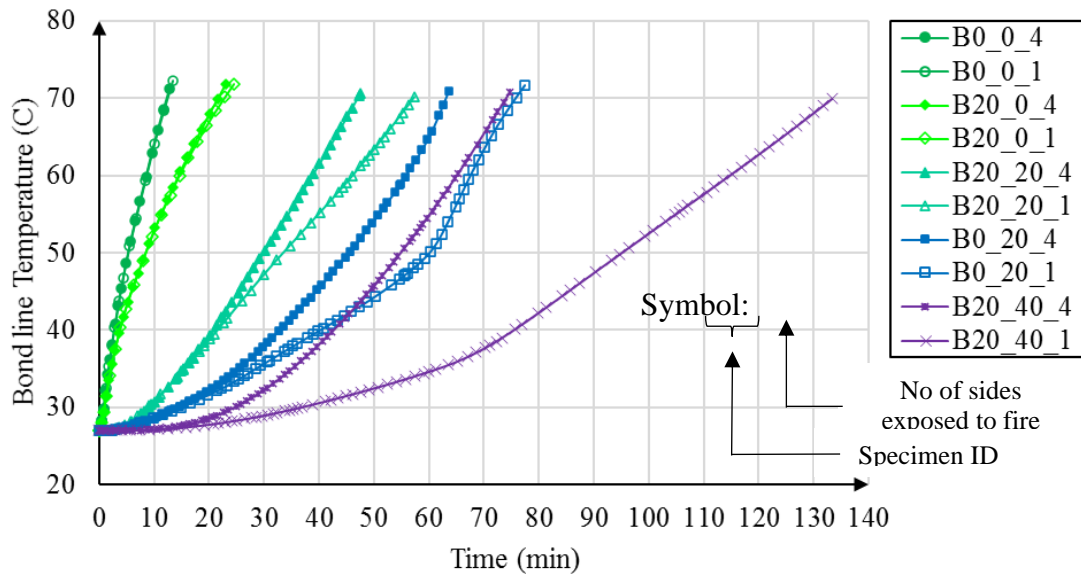


Figure 49. Bond line Temperature under ISO 834 fire curve

when only the bottom side of the specimen is exposed to the fire while similar performance in non-insulated specimens was noted in both exposure conditions. The noted percentage increments when the insulated specimens were exposed to the fire from the bottom side only are 21.7%, 20.5%, and 77.5% in B20_20, B0_20, and B20_40, respectively. And nearly 2 times of fire resistance was noted in the B20_40 specimen than in B0_20 during the exposure condition (ii). These results revealed the selected CRRP bonding technique in this study is more effective when only the bottom surface is exposed to the fire compared to the structures in which all sides are exposed to the environment.

Table 12. Fire resistance durations under ISO 834 standard fire curve

No of sides exposed	B0_0	B20_0	B20_20	B0_20	B20_40
4	12.3 min	21.5 min	47.2 min	63.1 min	75.1 min
1	12.3 min	22.8 min	57.3 min	75.8 min	133.3 min
Insulation volume (cm³)	0	0	180	600	780

3.5 Parametric study

Since the thermal and geometrical properties significantly affect the thermal performance of structural elements, a detailed parametric study was carried out by changing the sensible parameters on the fire performance of the composites. The grooved specimen with an additional insulation layer (B20_40) was used in this study in both exposure conditions: case (i) four sides exposed and case (ii) only the bottom exposed.

3.5.1. Effect of the geometry of the concrete specimen

It was found that the ratio of the overall height to the breadth of a beam has a significant effect on the temperature within the beam (Saafi, 2002). Therefore, it is essential to investigate the effect of geometry on the thermal performance of CFRP-strengthened concrete specimens. In such a case, a range of aspect ratios (h/b) from 1.0 to 2.0 was used. The noted bond line temperature variations in the specimens with different aspect ratio is plotted in Figure 50 under the condition when four sides of the specimen are exposed, and CFRP is attached in 20 mm deep grooves. From the results obtained, though there is an effect of specimen geometry on the thermal performance, the noted effects are less.

However, based on the temperature contours across the cross-section (Figure 50), it was revealed that the location of the minimum temperature line is the key factor that decides the temperature of the bond line. In the specimen with aspect ratio 2.0, two minimum temperature locations were observed, while only one was noted in the specimen with aspect ratio 1.0. Therefore, when increasing insulation at the bottom of the specimen with

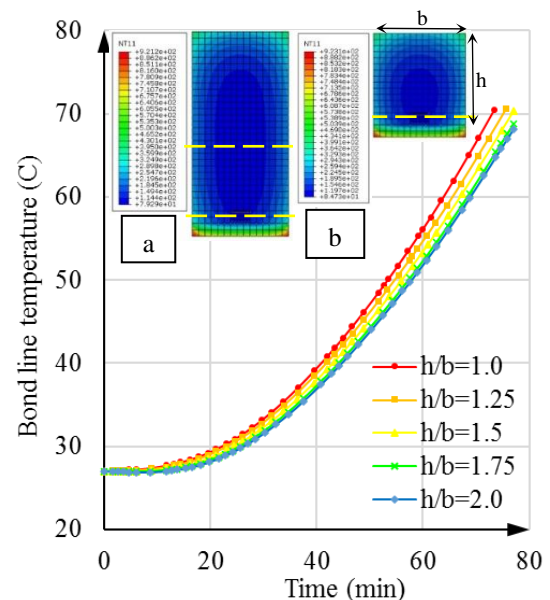


Figure 50. Effect of concrete geometry on Bond line Temperature (a) 2.0; (b) 1.0

aspect ratio 1.0, the minimum temperature line will move downward, and the bond line temperature will increase beyond an increment in insulation due to the heat transfer from the top part. Hence, it is expected that the specimens with different insulation parameters may get influenced more by the geometry of the specimen which is discussed in the next sections.

3.5.2. Effect of insulation layer thickness

The thickness of insulation (T_k) was found as a key parameter in the fire performance in EBR-CFRP-Concrete composites in past studies (J. C. P. H. Gamage et al., 2006). From the temperature contours observed it was revealed, a requirement of an extra insulation layer at the bottom is required to achieve the minimum fire resistance period when the bottom surface of the structure is exposed to the fire.

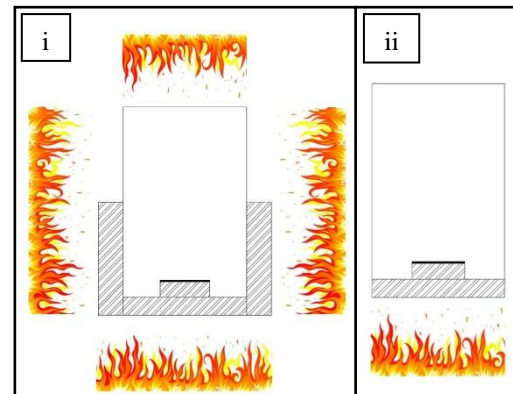


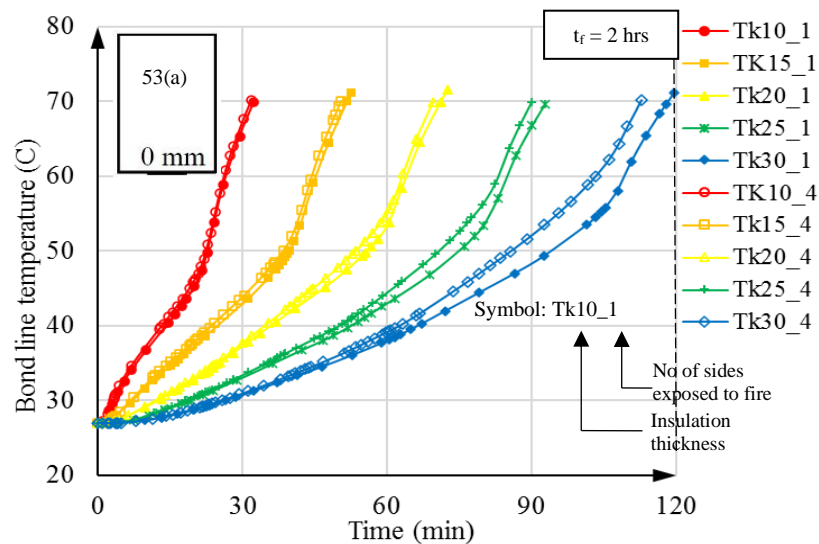
Figure 51. Schematic diagram (i) Insulation application (3 sides) when all sides are exposed; (ii) Insulation application (1 side) when only bottom surface is exposed

Further, the results obtained in this study suggests to provide an additional insulation on both sides of the specimen to achieve adequate fire resistance for the composites in situations when all four sides are exposed. In such a case, a range of 10 mm to 30 mm thick insulation layer applied onto the bottom surface was simulated to study the fire resistance period (t_f) when only the bottom surface is exposed. The provision of the same thickness range of insulation to the three faces of the beam was considered in the case when four sides of the beam are exposed to the fire as shown in Figure 51. Vermiculite insulation ($K = 0.12 \text{ W/mK}$) was used for this study. The bond line temperature variations in both exposure conditions are shown in Figure 52. From the results predicted, it was found that a 17 mm thick insulation application at the bottom surface is required to provide 2 hours of fire resistance when only the bottom side of the specimen is exposed (Exposure condition (ii)). However, the exposure condition

(i) requires a 23.4 mm thick insulation application to three surfaces to ensure 2 hours of fire rating.

3.5.3. Effect of groove depth

Since this is a newly introduced technique, the effect of groove depth needs to be investigated in order to find out the optimum parameters. A range of groove depths between 0 mm and 30 mm was used in this study to minimize the negative effects as structural performance. This study was also conducted under both exposure conditions as mentioned in the above sections. The model predicted bond line temperature variation with time is illustrated in Figure 53 (a) -(c). It was noted that the fire resistance period increases with the increasing groove depth in both exposure conditions. Thus, the required additional insulation thickness for fire endurance reduces with an increment of the groove depth. Using the above-mentioned insulation material ($K = 0.12 \text{ W/mK}$), 2 hours of fire resistance can be achieved in the following ways listed in Table 13. However, the effect of groove depth is less for the specimens with complete exposure compared to the specimen only exposed at the bottom. This shows the possibility of effective application of GBT in retrofitted slabs than in the beams.



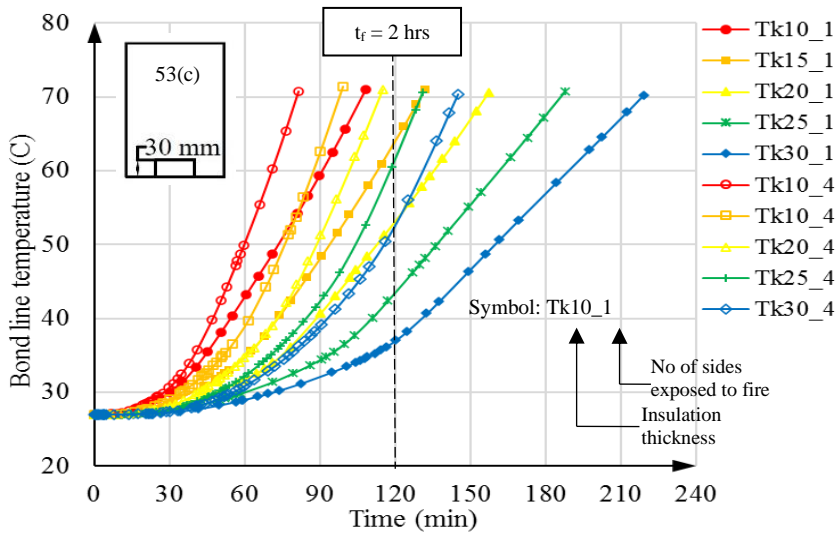
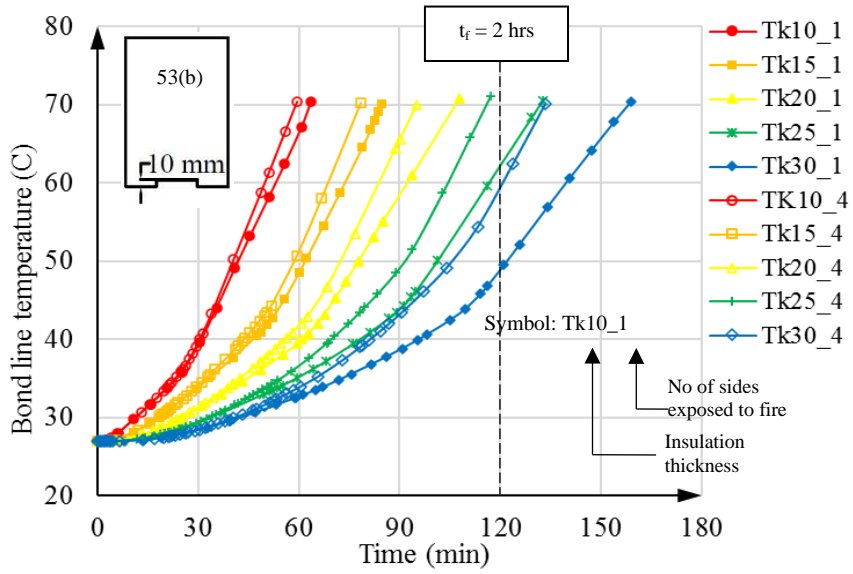


Figure 53. Effect of groove depth on bond line temperature (a) 0 mm; (b) 10 mm; (c) 30 mm

Table 13. Required insulation thicknesses to achieve 2 hours of fire resistance (t_f)

No of sides exposed	Groove depth			
	0 mm	10 mm	20 mm	30 mm
1	30.5 mm	22.6 mm	17.0 mm	12.7 mm
4	31.7 mm	26.1 mm	23.4 mm	21.9 mm

3.5.4. Effect of thermal conductivity

Conductivity (K) is the most sensitive parameter which represents the thermal behavior of insulation material. The effect of thermal conductivities of the materials influences the heat transfer performance. The specimens with 20 mm groove depth and 20 mm thick additional insulation layers were used for this study. A range from 0.04 W/mK to 0.2 W/mK of thermal conductivities were used to predict the fire performance. Similar to other retrofitting techniques, fire resistance increases with the increasing thermal conductivity (Figure 54). Use of 0.08 W/mK thermal conductivity material with a 20 mm thick layer of insulation in three surfaces will results in 2 hours of fire resistance during the exposure condition (i). To achieve the same performance in exposure condition (ii), the conductivity of the insulation to be doubled.

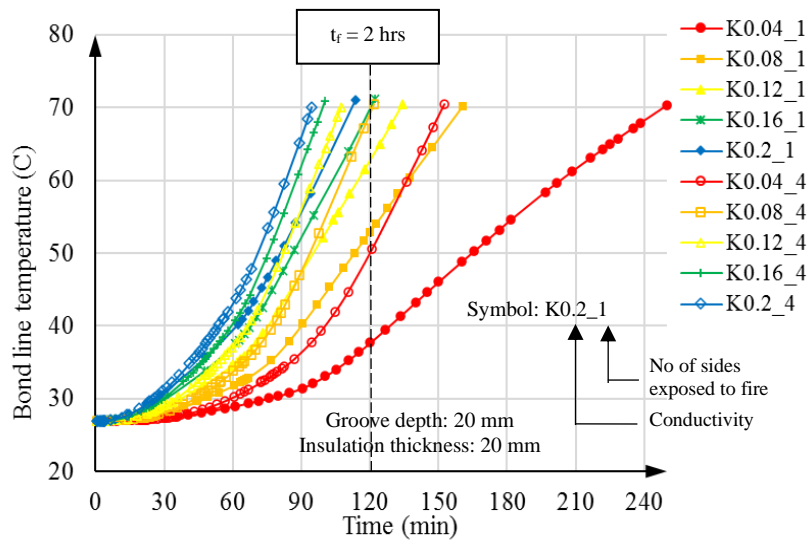
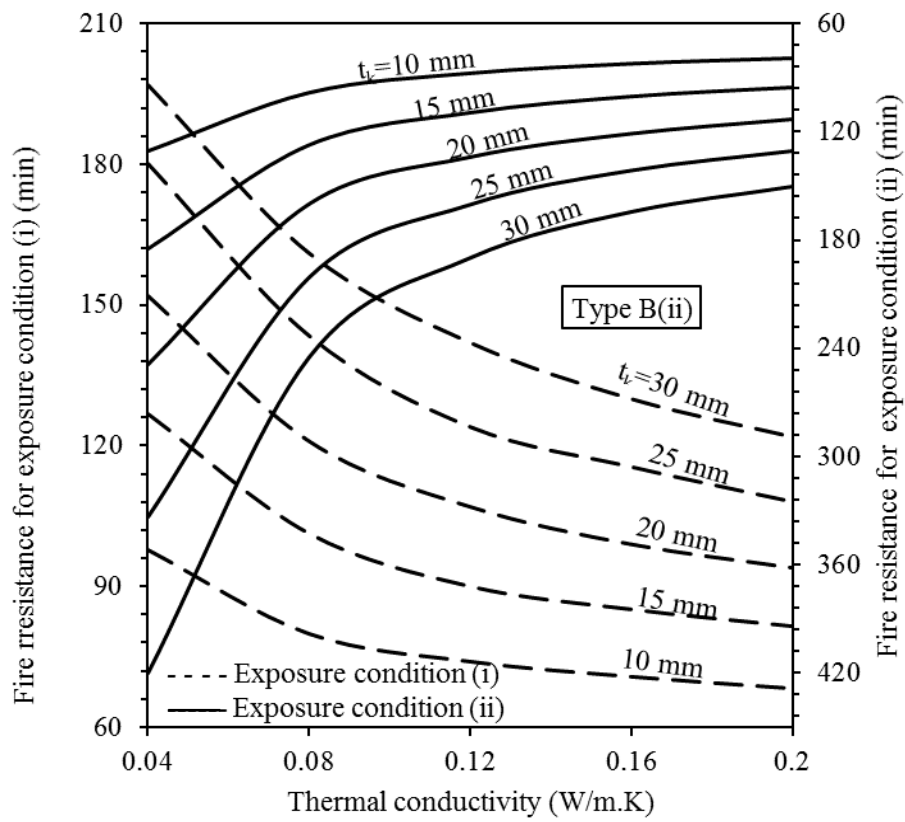
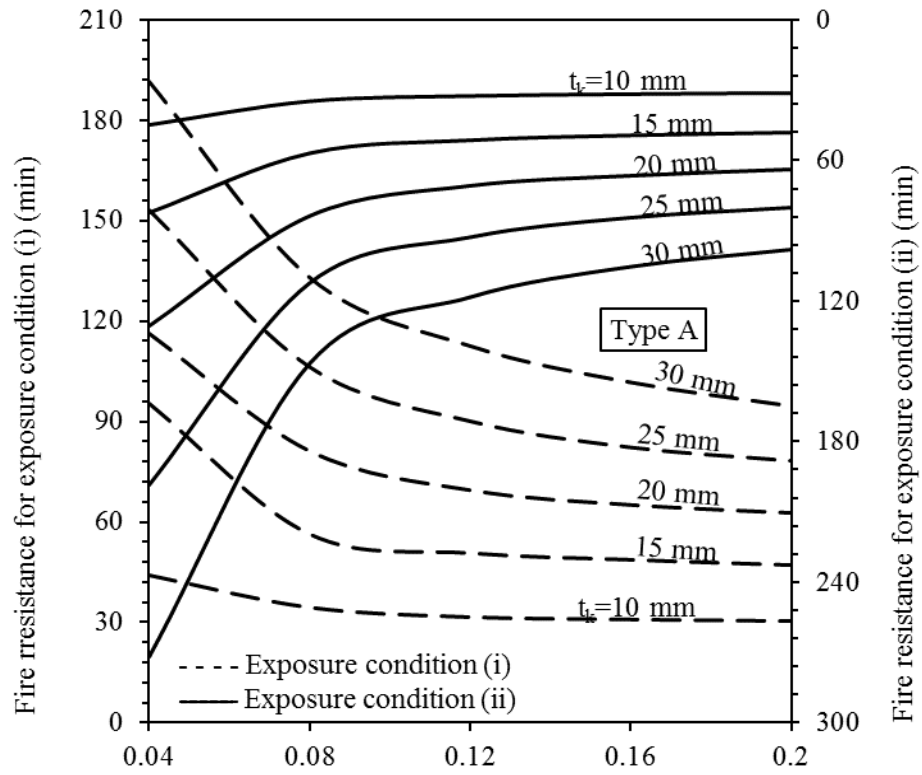


Figure 54. Effect of thermal conductivity on bond line temperature

3.6. Design Recommendations



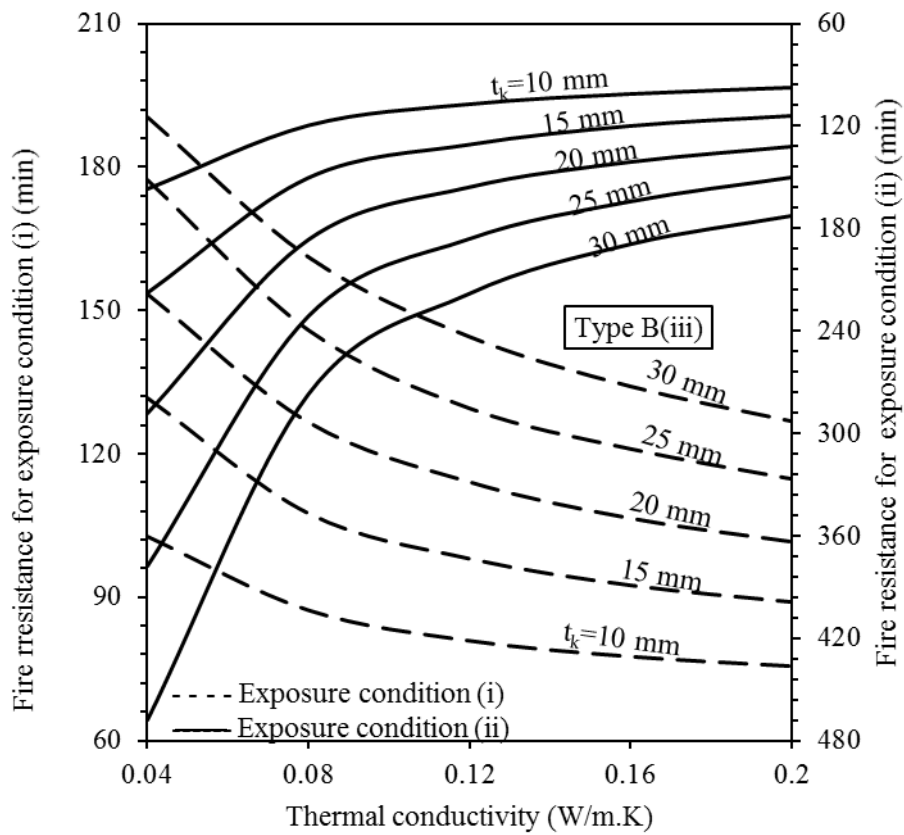
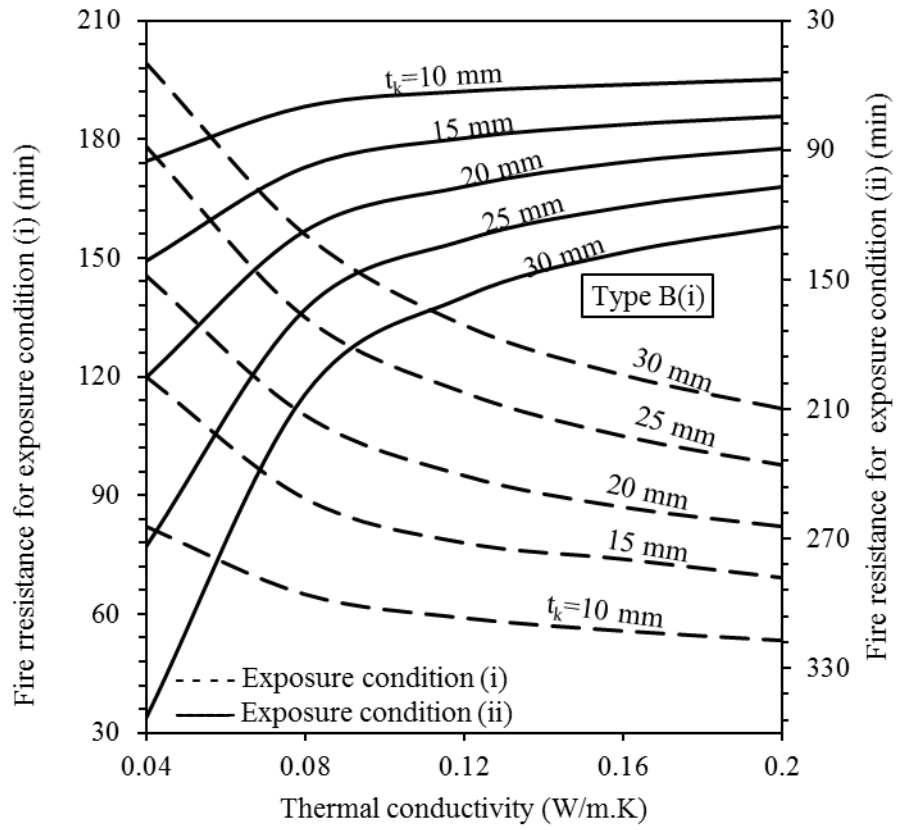
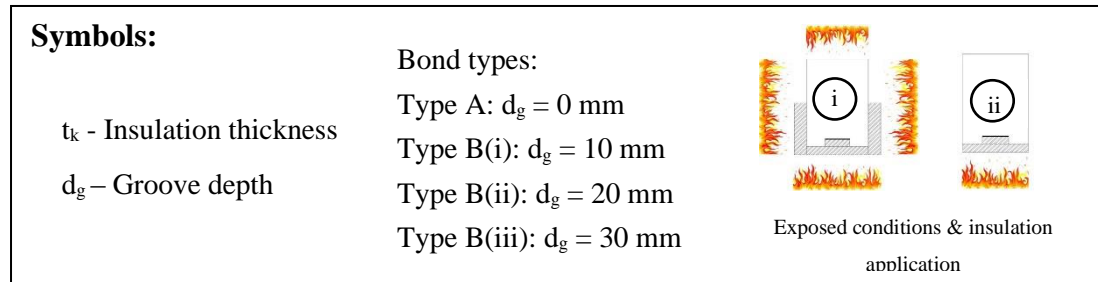


Figure 55. Design Fire resistances for different bond types and different exposure conditions

From the results obtained in this study, the following design charts (Figure 55) can be recommended for the application of CFRP for flexural strengthening in an effective manner. These charts provide quick guidance to select a suitable bonding technique and insulation material depending on possible fire scenarios. In addition to that, these charts help to predetermine the amount of insulation material required.



3.7. Summary

1. The Groove Bonding Technique (GBT) used to install the CFRP composites in flexural members enhances the fire performance than the External Bonding Technique (EBT), irrespective from the exposure condition. The loss of flexural capacity due to groove bonding CFRP application within the nominal cover of the member is less than 4% with respect to EBT even though it enhances the fire performance up to 68% while saving more than 36% of the required volume of the insulation material.
2. Both bonding techniques (GBT & EBT) cannot provide sufficient fire rating to the CFRP-strengthened members in the absence of insulation.
3. The aspect ratio of the beam influences on the fire performance of CFRP strengthened flexural members when all sides of the beam are exposed to the fire.
4. The heat transfer from the sides of CFRP is considerably high in the GBT than EBT. Hence, it is recommended to apply insulation material on the bottom and also at least 60 mm from the bottom at both sides to minimize the heat penetration from the side faces in GBT. However, it may be necessary to apply

insulation in similar manner for all exposed sides to preserve the aesthetic appearance of the beam.

5. The bonding technique, groove depth, Insulation thickness, and thermal conductivity are the key parameters which affect the fire rating of CFRP strengthened members.
6. Since the slabs are planar elements, GBT ensures better fire performance in applications of slabs than in the beams due to the restricted heat transfer from the vertical sides of retrofitted members.
7. It is important to optimize the project cost while ensuring the safety of strengthened structures. Design recommendations are provided in forms of charts to guide the design and construction engineers for their decision-making process on CFRP strengthening in building construction projects. These charts help to minimize the insulation usage while ensuring the structural integrity in case of fire.

CHAPTER 4: DEVELOPMENT OF A COST-EFFECTIVE CEMENTITIOUS INSULATION MATERIAL USING LOCALLY AVAILABLE MATERIALS

The objective of this study is to develop an insulation material which is cost-effective and sustainable than the materials available in the market. An insulation material was developed using EPS as the base material. EPS particles were used as a partial replacement to fine aggregate in this study.

4.1. Test Program

4.1.1. Overview

The scope of this study was categorized into several stages and they are described below.

Stage 1: By using different mix proportions, obtaining the optimum mix of this mortar which has better thermal and mechanical performance as well. In order to ensure the optimum thermo-mechanical performance, compressive strength, flow, thermal conductivity, and density were used for material selection.

Stage 2: The suitability of the developed mortar in building walls for improved thermal comfort was assessed. Optimum mix accordance with ASTM requirements for N-type mortar was selected for this assessment. (Chapter 5)

Stage 3: A thermal analysis has to be carried out for CFRP-concrete specimen with the mortar developed in this study, and commercially available insulation material. This test is to find out the equivalent thickness of developed mortar respect to commercially available insulation materials. Then, the bond performance of CFRP composites with developed Insulation is supposed to be tested using double-lap-shear test. The optimum mix should be used for this test and the test to be carried out at room temperature and elevated temperature as well.

4.2. Development of EPS-cement blend mortar (Stage 1)

4.2.1. Materials

Ordinary Portland Cement (OPC) with a 28-day compressive strength of more than 42.5MPa was used as the basic component for all the mixtures. River sand passing through 800 um sieve and EPS dust passing through 3.35 mm sieve was used at the initial stage. The EPS blend was obtained from the waste EPS produced EPS factory. The development of the mortar was carried out in 2 phases and they are followed.



Figure 56. Materials (a) Cement; (b) River sand; (c) EPS dust

4.2.2. Sample preparation & testing (Phase 1)

In phase 1 development, 5 different mix proportions were considered by replacing the sand by EPS blend in 1: 3 cement sand (weight ratio) mortar (1: 2.25 volume ratio). The typical w/c ratio of 0.4 was used for phase 1 development. 70.1 mm x 70.1 mm x 70.1 mm cubes were cast (Figure 58) cast to test the compressive strength of the mixes

Table 14: Mix proportions for phase 1

Mix ID	% of EPS replacement	Cement (cm ³)	Sand (cm ³)	EPS (cm ³)
EPS-0	0	1000	2250	0
EPS-30	30	1000	1575	673
EPS-50	50	1000	1125	1124
EPS-70	70	1000	675	1572
EPS-90	90	1000	225	2020

in accordance with ASTM C109 (ASTM C109/C109M-02, 2002). 6 cubes were cast from each mix to test 3 cubes for 7 days strength and 3 cubes for 28 days strength. Samples with 5 mm thickness and 60 mm diameter were cast (Figure 57) to test the thermal conductivity using Lee's Disk method, in accordance with ASTM D7340 (2018). The sample preparation for thermal conductivity tests are shown in Figure 57. All the prepared samples were kept for curing for 28 days prior testing. A flow table test was also carried out in accordance with ASTM C 1437-07 (2009). The testing apparatuses used for thermal conductivity and compressive strength are shown in Figure 59. The mix proportions used in phase 1 are listed in Table 14. The volumetric percentage of replacement of sand by EPS blend was increased from 0% to 90% in the following mixes.



Figure 57. Sample preparation for thermal conductivity testing



Figure 58. Sample preparation for compressive strength testing

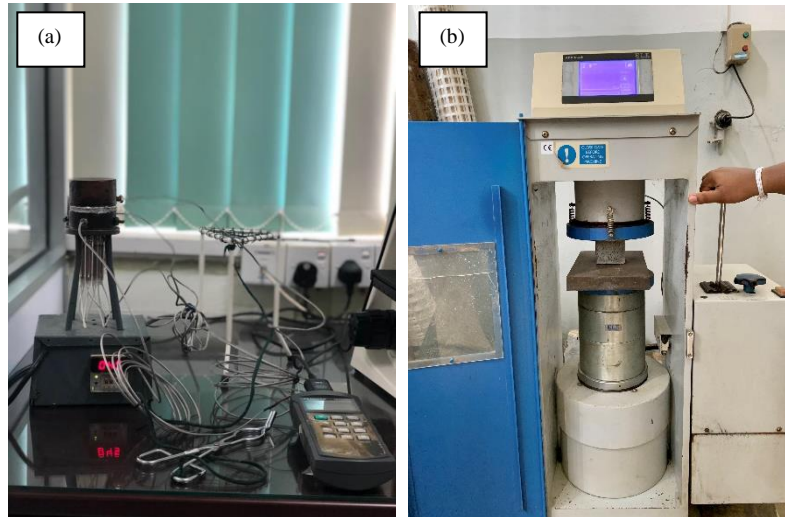


Figure 59. Testing apparatus (a) Thermal conductivity; (b) Compressive strength.

4.2.3. Test results (Phase 1)

The test results obtained for compressive strength, flow, and density are listed in Table 15. The percentage of EPS fraction in the mix varied from 0% to 54% in the testing phase 1. Each of these results was obtained by testing three identical samples in order to get precise results. The variation in the flow, compressive strength, and density of each mix are illustrated in Figure 60-62.

Table 15: Test results - phase 1

Mix ID	Flow (%)	Density (kg/m ³)	7 days Compressive strength (N/mm ²)	% EPS in total Volume
EPS-0	14	2075	22.29	0%
EPS-30	54	2049	11.3	17%
EPS-50	65	1976	19.74	29%
EPS-70	97	1690	9.9	41%
EPS-90	128	1453	6.7	54%

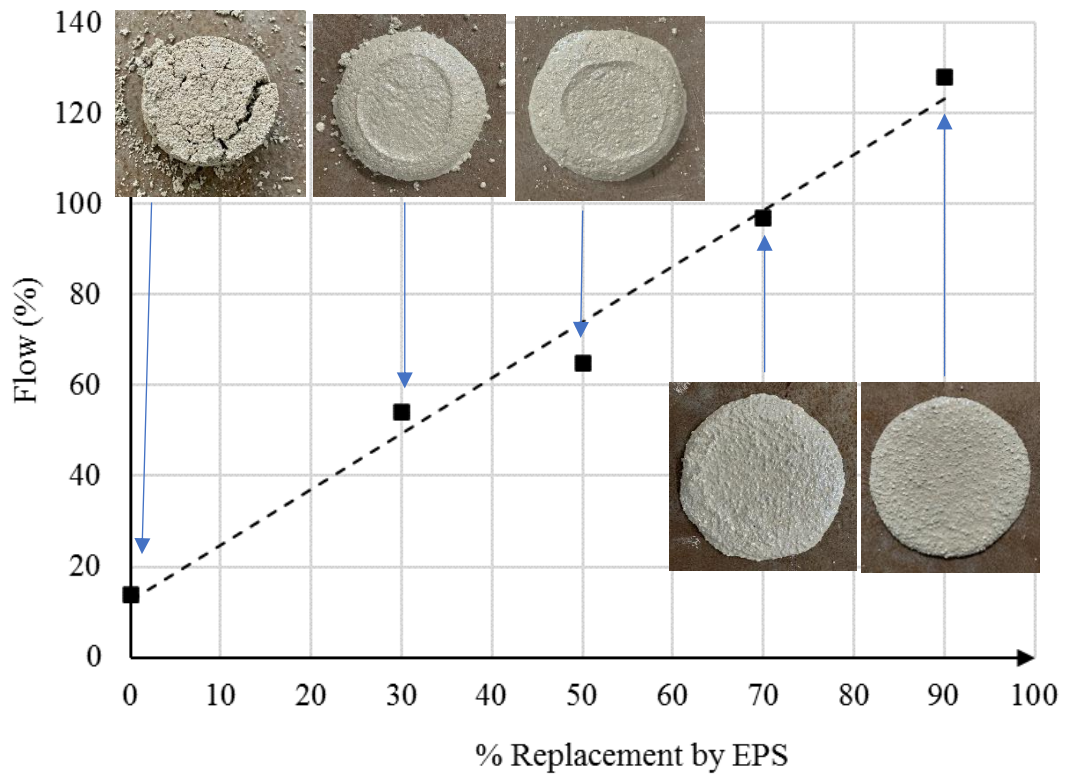


Figure 60. Variation of the flow – phase 1

From the Figure 60, it can be seen that replacing sand with EPS particles results in higher workability of the mortar. This can be due to the low water absorption of EPS

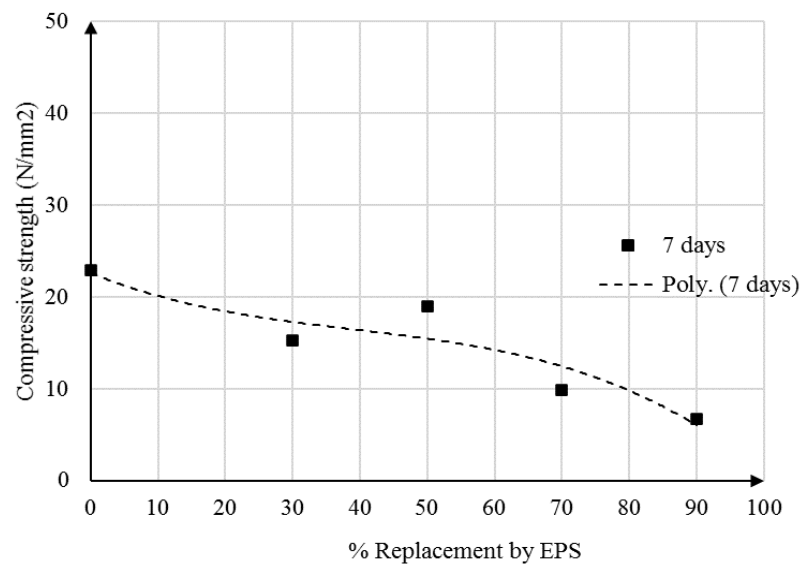


Figure 61. Compressive strength variation – Phase 1

particles than the sand particles. Further, it was noted that the compressive strength and density of the mortar decreases with EPS replacement which is due to the low weight and low strength of the EPS particles.

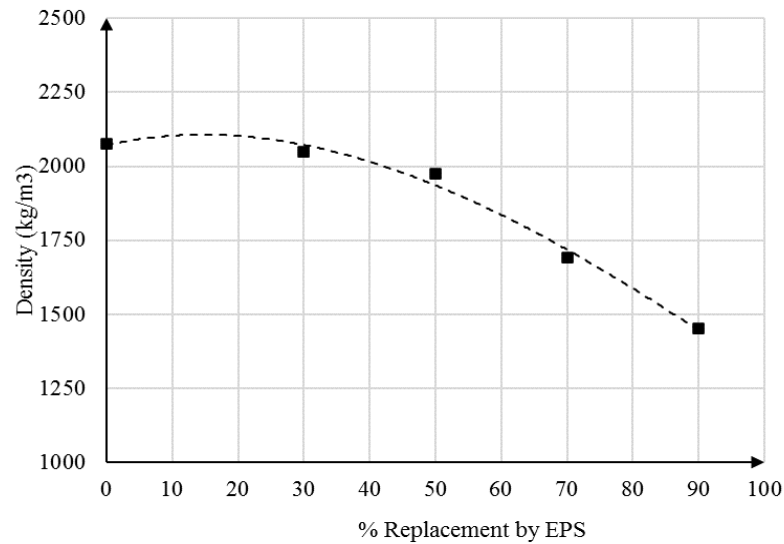


Figure 62. Density variation – Phase 1

From the results obtained for mechanical properties, it is clear that with the increasing replacement of EPS, the flow increases. The compressive strength and density of the mix reduce with the increasing replacement of EPS in the mixes. From the studies conducted on lightweight concrete using EPS, it was found that with increasing EPS amount, the thermal conductivity will reduce (Schackow et al., 2014). Therefore, it is expected with increasing replacement EPS, the thermal conductivity will reduce. Therefore, the mixes EPS-70 and EPS-90 were used for further development in phase



Figure 63. Mix samples – Phase 1

2 with different cement: fine aggregate ratio. The prepared samples of selected mixes are shown in Figure 63.

4.2.4. Sample preparation & results (Phase 2)

In phase 2, different control mixes were used with 1: 2 cement: fine aggregates weight ratio (1: 1.5 volume ratio) and 1: 4 cement: fine aggregates weight ratio (1: 3 volume ratio). 70% and 90% Replacement of sand by EPS method was used to study the effect of cement: aggregates ratio. A water/ cement ratio of 0.4 was used in this phase as well. The mix proportions used are listed in Table 16 and the tested results are tabulated in Table 17.

Table 16: Mix proportions for phase 2

Mix ID	% of EPS replacement	Cement (cm³)	Sand (cm³)	EPS (cm³)
1.5-EPS-70	70	1000	515	1195
3-EPS-70	70	1000	900	2095
3-EPS-90	90	1000	300	2694

Table 17: Test results - phase 2

Mix ID	Flow (%)	Density (kg/m³)	7 days Compressive strength (N/mm²)	% EPS in total Volume
1.5-EPS-70	120	1738	11.1	36%
3.0-EPS-70	55	1652	6.9	46%
3.0-EPS-90	72	1381	6.3	59%

The effect of aggregate/cement ratio on flow, compressive strength, and density is illustrated in Figure 64-66. It is clear that higher the ratio lesser the 7 days strength becomes since the % of cement reduces. And there is a drastic change in the flow with the change in ratio. It is also clear that the lesser aggregate/cement contributes to the higher flow in the mortar mix. Henceforth, it is clear that higher cement can provide higher compressive strength and flow and it does not affect the density significantly.

However, the guidelines suggest the minimum compressive strength after 28 days for N-type mortar as 5.2 MPa (required 7 days strength – 3-3.5 MPa) and the flow as $110 \pm 5\%$ (ASTM International, 2010). Therefore, it was revealed further EPS can be added to the sample to enhance its thermal performance till the 28 days compressive strength reaches 5.2 MPa. Since sand is more durable at elevated temperature than EPS, EPS-90 was used for further development rather than replacing 100% sand by EPS.

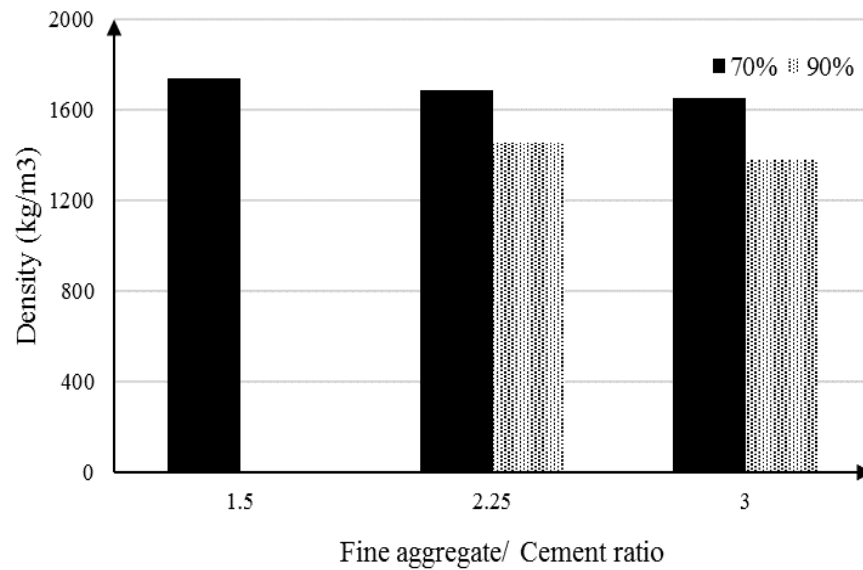


Figure 64. Effect of aggregates/cement volume ratio in the Density

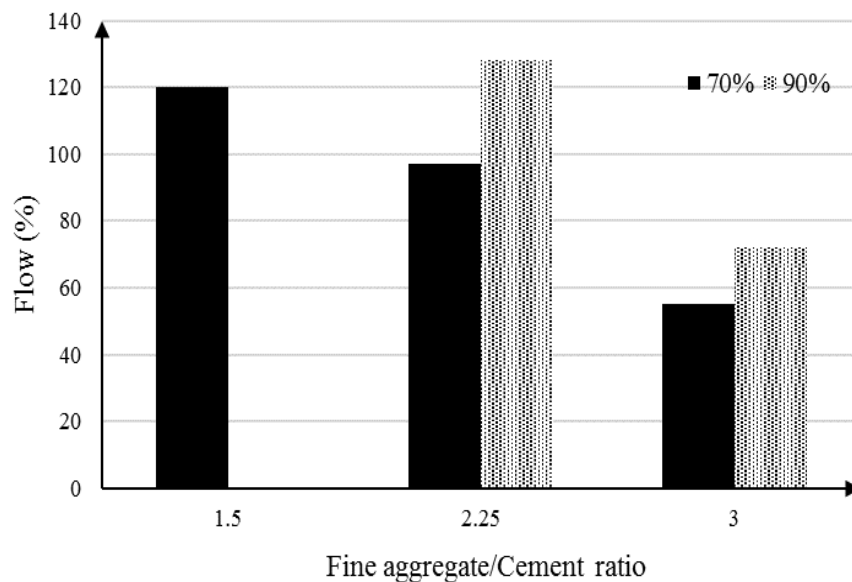


Figure 65. Effect of aggregates/cement volume ratio in the flow

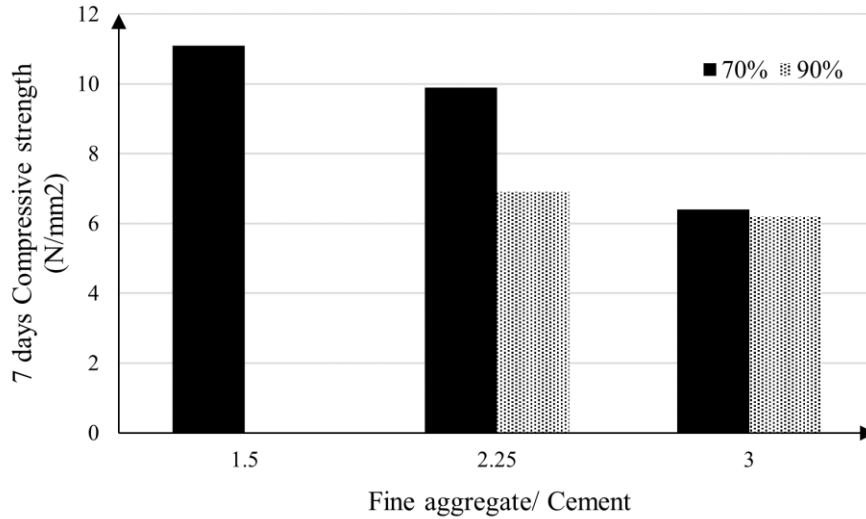


Figure 66. Effect of aggregates/cement volume ratio in the Compressive strength

4.2.4. Sample preparation & results (Phase 3)

The percentage of EPS in EPS-90 is further increased up to 200% by keeping other volumes as it is. A water/cement ratio of 0.4 was used again. In such case, the mix specifications are listed in Table 18 and the test results are listed in Table 19.

Table 18: Mix proportions for phase 3

Mix ID	% of EPS addition	Cement (cm ³)	Sand (cm ³)	EPS (cm ³)
EPS-125	125	1000	225	2809
EPS-150	150	1000	225	3375
EPS-172	172	1000	225	3866
EPS-200	200	1000	225	4500



Figure 67. Mix samples – Phase 3

Table 19: Test results - phase 3

Mix ID	Flow (%)	Density (kg/m ³)	7 days Compressive strength (N/mm ²)	% EPS in total Volume
EPS-125	65%	1282	4.30	61%
EPS-150	19.1%	1176	4.16	65.2%
EPS-172	33%	1148	2.93	68.2%
EPS-200	10.3%	968	2.24	70.9%

The prepared samples of the selected mixes are shown in Figure 67. The variations in the flow, compressive strength, and density are illustrated in Figure 68-70. From the flow variation diagram (Figure 68), it is clear that the selected w/c ratio is optimum for the EPS-90 mix and w/c needs to be increased for the mix with higher EPS mixes. Similar to the test results obtained in phase 1, here also the compressive strength and

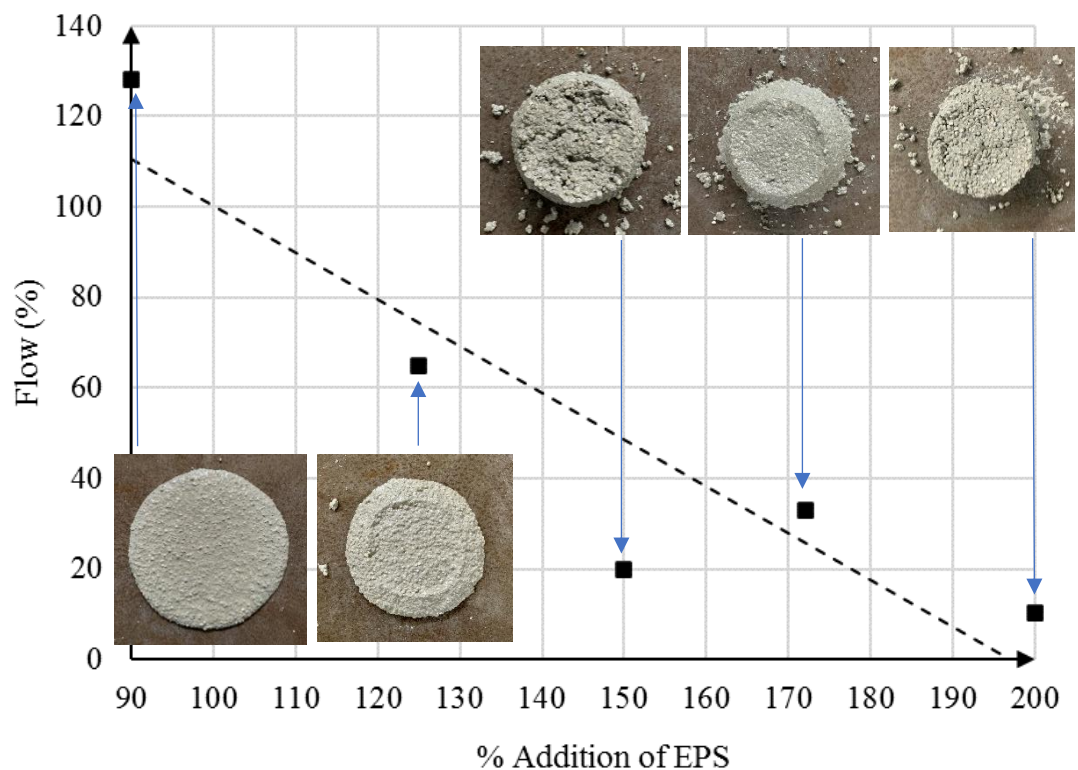


Figure 68. Variation of the flow – Phase 3

density reduces with higher EPS fractions. To maintain the strength, super plasticizers can be added to the water which is described in the phase 4.

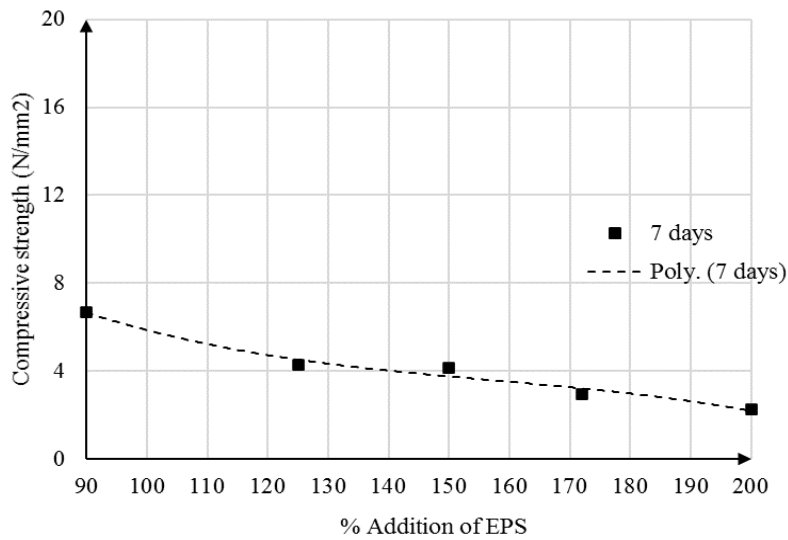


Figure 69. Compressive strength variation – Phase 3

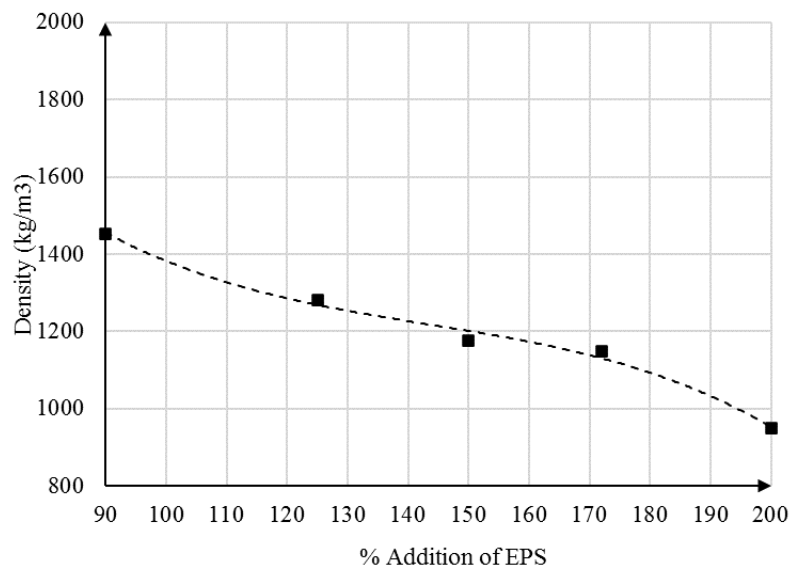


Figure 70. Density variation – Phase 3

4.2.6. Sample preparation & results (Phase 4)

Different grades of EPS particles were used to the mix. In this study, EPS resin was used as fine aggregates (less than 1.18 mm) to improve the mechanical properties of



Figure 71. EPS resin particles



Figure 72. Mix using EPS resin

the mix. Two mix proportions from phase 4 have been selected to further study in order to satisfy the N-type mortar plaster and fireproofing plaster. A w/c cement ratio of 0.65 was used in this phase due to the less workability of the EPS resin particles. The mixed consistency with EPS resin particles is shown in Figure 72. The selected mix proportions are tabulated in Table 20 and the test results for mechanical properties are listed in Table 21. And the flow of selected mixes is shown in Figure 73. The loose density of coarse and finer EPS is 10 kg/m^3 and 32 kg/m^3 , respectively.

Table 20: Mix proportions for phase 4

Mix ID	% of EPS addition	Cement (cm^3)	Sand (cm^3)	EPS (cm^3)
EPS-125-F	125	1000	225	2809
EPS-200-F	200	1000	225	4500

Table 21: Test results - phase 4

Mix ID	Flow (%)	Density (kg/m^3)	7 days Compressive strength (N/mm^2)	% EPS in total Volume
EPS-125-F	55%	1500	5.04	61%
EPS-200-F	14%	1325	2.90	70.9%

Similar to the test results obtained using coarser particles, use of higher amount of EPS finer particles results in lesser strength and density as well.



Figure 73. Variation of the flow – Phase 3 (a) EPS-125-F; (b) EPS-200-F

The comparison of the mechanical properties using coarser particles and finer particles are shown in Figure 74-75. Though 0.65 w/c ratio was used in Finer EPS mix, while 0.4 in coarser EPS mix, the finer EPS has gained higher compressive strength after 7 days curing. Since the density of finer EPS particles is higher, its mortar mix is also higher than the coarse EPS mix (Figure 75).

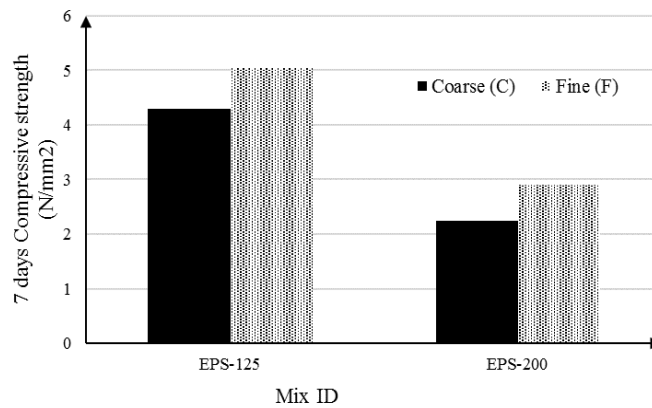


Figure 74. Effect of particle size in compressive strength

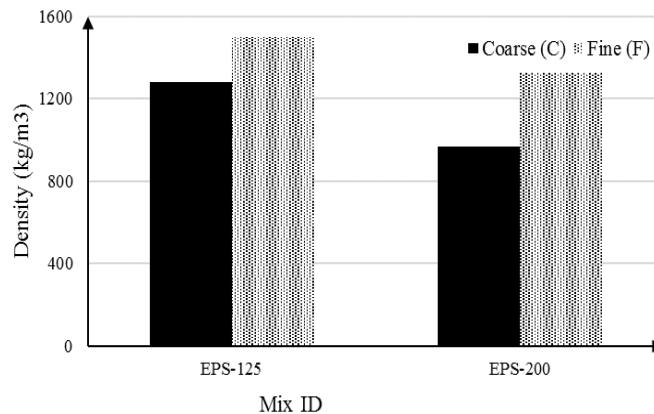


Figure 75. Effect of particle size in density

4.2.7. Testing thermal conductivity

The thermal conductivity of the selected mixes was tested to study the thermal effect of EPS in cement mortar. The test procedure consists of 2 stages: (i) heating stage of disk C and (ii) cooling stage of disk D. When the heat flows from disk B to disk C through the sample (G), the temperature T1 and T2 will be recorded. The T2 will almost remain steady with the temperature the user set. Based on the thermal performance of the sample T1 will increase and reach a steady state. Once it has reached the steady state, it will be separated from the heater and kept for cooling. The cooling curve of the disk is always irrespective of the sample and only varies with the environmental conditions. Then, the thermal conductivity was calculated by equalizing the heat flow equations of two stages as given in Equation 29.

$$Q = k.A.(T_1 - T_2) = m.c.\frac{dT}{dt} \quad (29)$$

The assumptions made:

- The environmental conditions were assumed constant throughout the experiment.
- There is no convection from the sides of the sample while heating. Only one-dimensional conduction was assumed.
- In the cooling stage, convection from the other three sides was assumed as the only heat loss.

The T1 curve in the heating and cooling stage is shown in Figure 76. From the cooling curve, the dT/dt at the steady-state temperature can be obtained as shown. A sample calculation is given below.

$$T1 = 74.0 \text{ }^\circ\text{C}$$

$$T2 = 129 \text{ }^\circ\text{C}$$

Measured diameter of the sample $d = 58 \text{ mm}$

$$\text{Area } A = 0.0025 \text{ m}^2$$

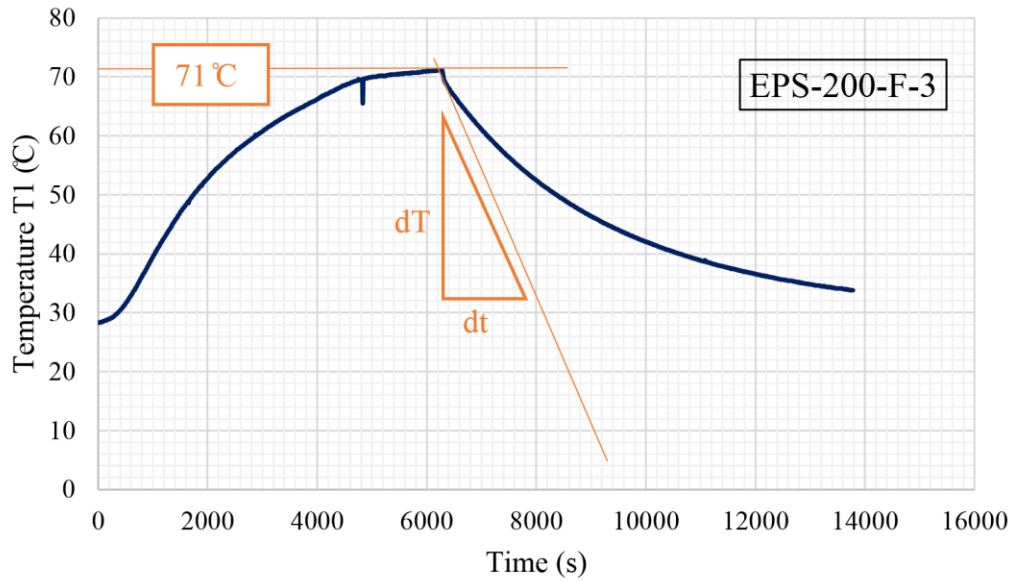


Figure 76. Temperature of Lee's disk (T1) vs time for EPS-0

Thickness of the sample (x) = 5 mm

Gradient at 74 °C (dT/dt) = 0.018 °Cs⁻¹

Specific heat of the disk (c) = 0.385 J/kg.°C⁻¹

Mass of the disk (m) = 880 g

From equation 1,

$$k = \frac{(m \cdot c \cdot \frac{dT}{dt})}{A \cdot (T_1 - T_2)}$$

$$k = 0.394 \text{ W/m.K}$$

To precise results, two other samples were tested, and the average was taken as the average thermal conductivity of the sample.

Sample 2 – 0.402 W/m.K

Sample 3 – 0.197 W/m.K

Average thermal conductivity of EPS-0 = 0.331 W/m.K

The average thermal conductivities for the selected samples are listed in Table 22. And the variation in the thermal conductivity with % replacement of cement is shown in Figure 77.

Table 22: Measured thermal conductivities

Sample ID	Thermal conductivity (W/mK)
EPS-0	0.685
EPS-90	0.349
EPS-200	0.216
EPS-125-F	0.411
EPS-200-F	0.336

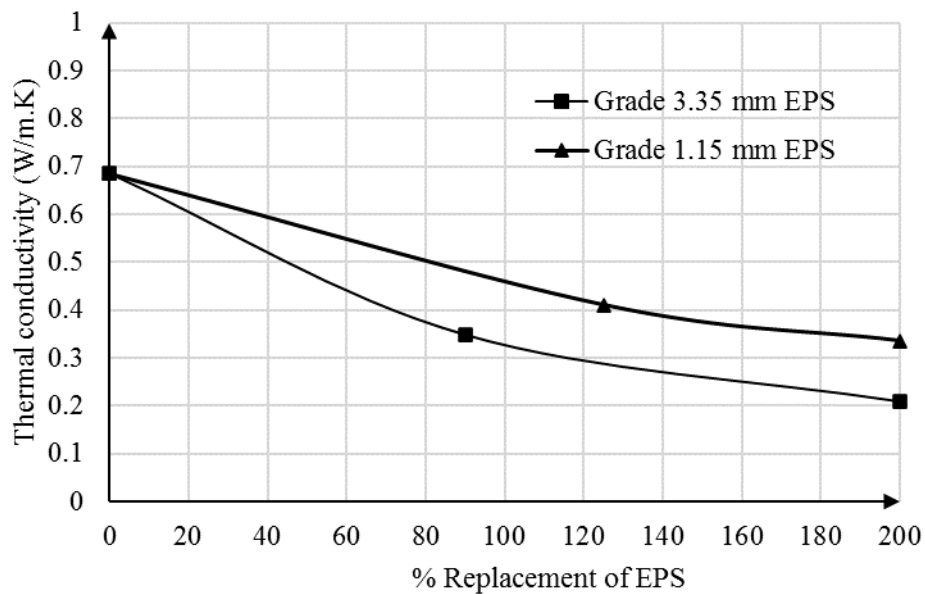


Figure 77. Thermal conductivity variation

From Figure 77, it can be seen that the thermal conductivity of the mix reduces with an increasing amount of EPS particles in the mix. In addition, the coarser particles have a greater influence in the thermal conductivity reduction than the finer particles. From the results obtained for thermal and mechanical behavior of the trial mixes up to phase 4, the following mixes were selected for further studies.

1. EPS-125-F: Insulated plaster for masonry walls

2. EPS-200 & EPS-200-F: Insulation material for CFRP composites

Further, development was carried out for the selected samples for the above mentioned two purposes.

4.2.7. Modification of insulated plaster for masonry walls (Phase 5)

Mix EPS-125-F was selected to modify the wall plaster material. The specification for N-type mortar was used to modify the mortar according to ASTM C270-10. In such a case, though the compressive strength is adequate to use as an N-type mortar, the flow is inadequate. Therefore, the water/cement ratio has increased to 0.75. In addition, a superplasticizer was used 10 ml per 1 kg cement. The mix proportions are listed in Table 23 and the test results are listed in Table 24.

Table 23: Mix proportions for phase 5

Mix ID	Cement (cm ³)	Sand (cm ³)	EPS (cm ³)	Super plasticizer (ml)	Water (cm ³)
EPS-125-F	1000	225	2809	0	1080
EPS-125-F-S	1000	225	2809	14.4	1080

Table 24: Test results - phase 5

Mix ID	Flow (%)	Density (kg/m ³)	7 days Compressive strength (N/mm ²)	Water/cement ratio
EPS-125-F	95%	1466	3.24	0.75
EPS-125-F-S	98%	1418	3.72	0.75

It is noted, there is no significant difference in the flow and density with the use of a selected superplasticizer. However, there is a slight enhancement in the compressive strength after 7 days. Though the effect of superplasticizer is low in the selected mix, the mix without admixtures was selected as the final product for insulated plaster for masonry walls. Despite, the use of different superplasticizers or additives the properties may be able to enhance. Therefore, further study on improving the product is recommended. The significant drop in the thermal conductivity in the selected mix

compared to the conventional mortar shows the suitability as an insulated plaster for masonry structures to improve the thermal comforts in the buildings. The effect of the water/cement ratio in mechanical properties is shown in Figure 78 for the selected Mix (EPS-125-F).

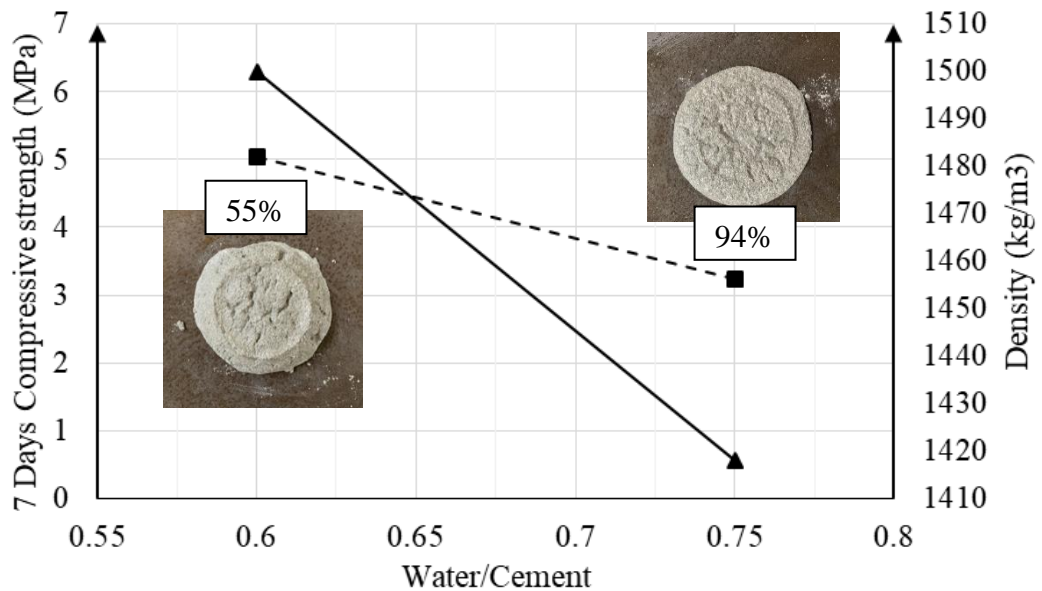


Figure 78. Effect of water/cement ratio in EPS-125-F

4.2.8. Modification of insulated plaster for CFRP composites (Phase 6)

Since the purpose of this development is to protect the CFRP composites from the fire, a higher insulated plaster is required. Therefore, the mixes with 200 % EPS was used for further study. However, the sample tested in phases 3 & 4 does not give enough workability to apply on CFRP composites. The selected mix proportions for this application are listed in Table 25. The test results are listed in Table 26 and compared with commercially available fireproofing material for CFRP composites (Vermiculite-cement blend-VC).

Table 25: Mix proportions for phase 6

Mix ID	Cement (cm ³)	Sand (cm ³)	EPS (cm ³)	Super plasticizer (ml)	Water (cm ³)

EPS-200	1000	225	4500	0	1095
EPS-200-F	1000	225	4500	0	1095

Table 26: Test results - phase 6

Mix ID	Flow (%)	Density (kg/m³)	7 days Compressive strength (N/mm²)	Water/cement ratio
EPS-200	121	847	0.81	0.725
EPS-200-F	60	1227	1.38	0.95

The effect of water/cement ratio in both type mortars is shown in Figure 79 & 80. Though the strength reduces with increasing w/c ratio, a significant flow is required to apply on CFRP composites. However, reducing density adds some advantage to the material as well. Therefore, the plasters should be mixed as the flow becomes between 100% and 120% for easy application.

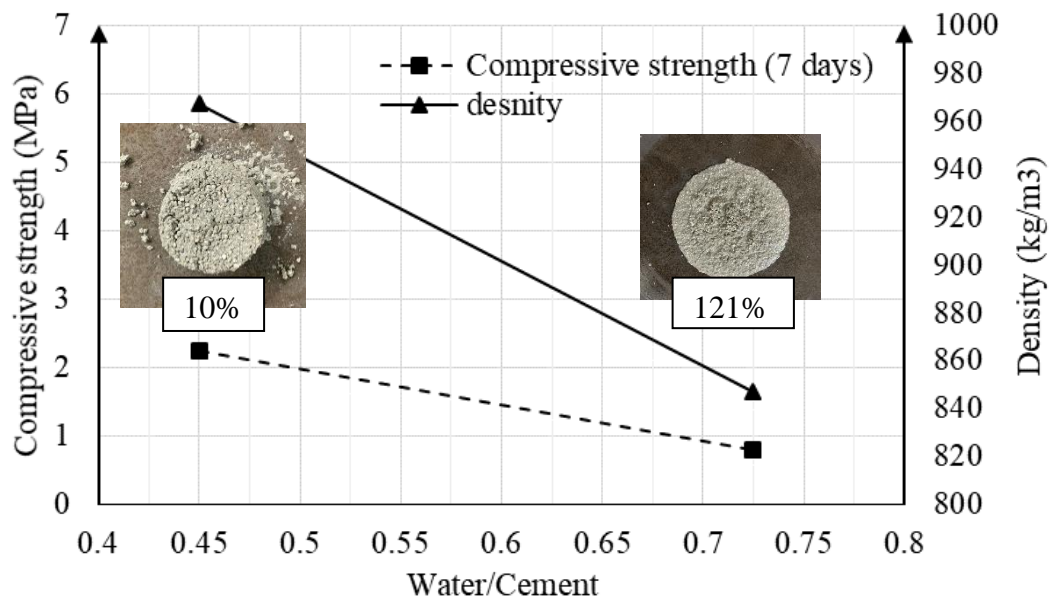


Figure 79. Effect of water/cement ratio in EPS-200

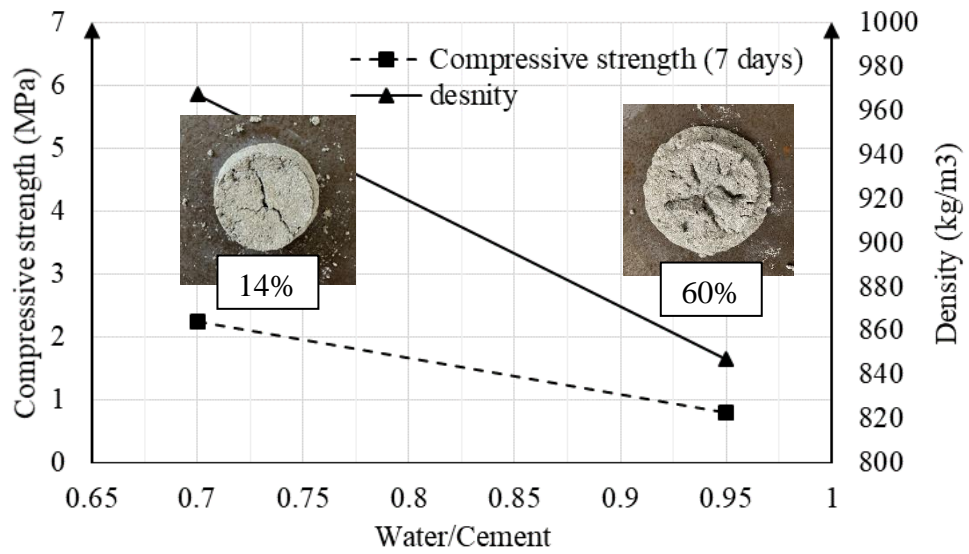


Figure 80. Effect of water/cement ratio in EPS-200-F

4.3. Applications of the selected mortar mixes

As mentioned in section 4.2.7, three mix proportions have been selected for different applications. To assess the suitability and the adhesion of the mortar, the selected mortar has been applied on the recommended surfaces. The mix EPS-125-F was applied on a masonry wall construction and the mixes EPS-200 and EPS-200-F have been applied on top of CFRP-concrete composites. (Figure 81 and 82).



Figure 81. Application of EPS plaster as external wall plaster

Since, the adhesion of the plaster on the masonry wall was good enough, this plaster can be recommended to use as an external wall plaster to enhance the thermal comfort in the buildings.



Figure 82. Application of EPS plaster as insulation for CFRP composites

To assess the suitability as an insulation material for CFRP/concrete composites, CFRP sheets were bonded to the Concrete members using adhesive. And then, on top of CFRP-epoxy, the developed insulation materials (EPS-200 and EPS-200-F) were applied. From this application, the adhesion between the insulation and CFRP found good enough to recommend this material for CFRP insulation.

4.4. Exposure to the Fire

Preliminary testing for fire performance was carried out for the selected mortar types (EPS-200, EPS-200-F). Figures 83 & 84 show the effect of fire on the selected mortar types. The effect of fire can be clearly seen in the mortar mix with coarser EPS particles. However, there was no notable contribution to the fire from the developed mix.



Figure 83. Testing for fire



Figure 84. Effect of fire

4.5. Summary

In this chapter, a series of test programs were carried out to develop a multi-purpose cement-based plaster using EPS particles. A conventional mortar mix of 1: 3 cement: sand (weight ratio) was used for this study by replacing the sand by EPS particles by 30%, 50%, 70%, 90%, 125%, 150%, 175%, and 200%. The compressive strength, flow, density, and thermal conductivity of the trial mixes were tested in the laboratory. From the trial mixes, 125% and 200% replacement plasters were selected for further development. The EPS particles were replaced by finer particles in the next stage of development and three mixes were selected for further study and they are listed in Table 27. The complete product specifications of all three specimens are listed in Table 28-30.

Table 27: Selected Products

Product ID	Description	Mix ID
LIP-F	Low Insulated plaster with fine particles	EPS-125-F
MIP-F	Medium Insulated plaster with fine particles	EPS-200-F
HIP-C	Highly Insulated plaster with coarse particles	EPS-200-NS

Table 28: Product specification of LIP-F

Material property	Values	Testing Standard
Loose density	1195 kg/m ³	-
Bulk density	1466 kg/m ³	-
Dry density	1046 kg/m ³	-
Thermal conductivity	0.411 W/m.K	ASTM D7340-07
Compressive strength (7 days)	3.24 MPa	ASTM C109
Mixing ratio	1.35 L for 2 kg	-
Grade	1.15 mm	-
Workability	95%	ASTM C1437-07
% volume fraction of EPS	61%	-

Table 29: Product specification of MIP-F

Material property	Values	Testing Standard
Loose density	833 kg/m ³	-
Bulk density	1227 kg/m ³	-
Dry density	825 kg/m ³	-
Thermal conductivity	0.336 W/m.K	ASTM D7340-07
Compressive strength (7 days)	0.81 MPa	ASTM C109
Mixing ratio	1.25 L for 2 kg	-
Grade	1.15 mm	-
Workability	110%	ASTM C1437-07
% volume fraction of EPS	71%	-

Table 30: Product specification of HIP-C

Material property	Values	Testing Standard
Loose density	647 kg/m ³	-
Bulk density	847 kg/m ³	-
Dry density	626 kg/m ³	-
Thermal conductivity	0.216 W/m.K	ASTM D7340-07
Compressive strength (7 days)	1.38 MPa	ASTM C109
Mixing ratio	1.1 L for 2 kg	-
Grade	1.15 mm	-
Workability	120%	ASTM C1437-07
% volume fraction of EPS	71%	-

CHAPTER 5: PREDICTING THE THERMAL PERFORMANCE OF CFRP/CONCRETE COMPOSITES WITH EPS-CEMENT INSULATION

5.1 Overview

Based on the development process explained in chapter 4, two types of insulations were selected for CFRP/Concrete composites. The morphology of the developed materials was studied and compared with the commercially available insulation materials. As the next step, the developed insulation materials were applied to the CFRP/Concrete composites to study the thermal performance of the composite system.

5.2. Morphology

To study the molecular structure of the developed plaster, a SEM imaging was conducted and compared with the images obtained for conventional plaster. Figure 85(a) and 85(b) show the SEM image of developed mix while Figure 85(c) shows the

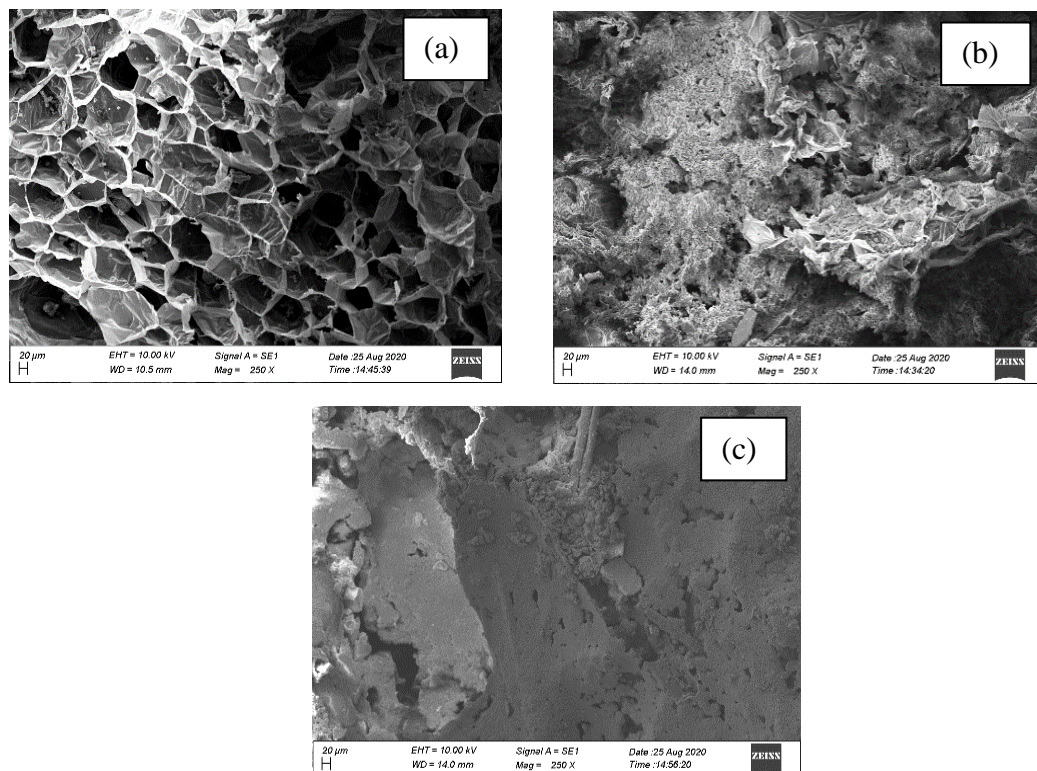


Figure 85. SEM images of (a)HIP; (b) MIP; (c) Vermiculite-cement mix

SEM image of vermiculite-cement mix which is already commercially available for CFRP insulation. It can be seen that the air-entrainment in the developed insulation materials are higher than the commercially available material which makes the developed material suitable as an insulation material. Further, the HIP (EPS-200) can be found more porous than the MIP (EPS-200-F) which has shown lesser thermal conductivity as well.

5.3. Experimental program

5.3.1. Material properties and specimen preparation

In situ concrete with 28 days compressive strength was used to prepare 100 mm x 100 mm x 200 mm concrete blocks. 0.116 mm thick CFRP fabrics (*Technical Data Sheet, CFRP*) were used to retrofit the concrete members using two-part epoxy adhesive (*Technical Data Sheet, Adhesive*). To insulate the CFRP/Concrete members, insulation materials developed in this study (HIP & LIP) and commercially available fire proofing material (Vermiculite-cement) were used in 20 mm thickness. Though higher thickness insulation layer can provide more thermal resistance to the composite specimen, due to the laboratory restraints a 20 mm thickness was selected. The obtained thermal and mechanical properties of insulation materials are listed in Table 31 and the material properties of other materials were obtained from the available literature.

Table 31. Thermal and mechanical properties at ambient temperature

Material Properties	Density (kg/m ³)	Thermal conductivity (W/mK)	Specific heat (W/m ² /C)	Compressive strength (MPa)
Concrete	2400	0.8	700	24.7
CFRP	1800	1.5	800	-
Adhesive	1400	1.5	700	70
Vermiculite-cement	730	0.118	2050	0.21
HIP	845	0.259	1442	1.51
MIP	862	0.308	1475	1.23

Table 32. Specimen Configurations

Specimen ID	Description
CC-N	CFRP/Concrete member without insulation
CC-VC	CFRP/Concrete member with commercially available insulation (Vermiculite-cement blend)
CC-EPSC	CFRP/Concrete member with coarse EPS insulation developed in this study (EPS-200-C-3)
CC-EPSF	CFRP/Concrete member with fine EPS insulation developed in this study (EPS-200-F-3)

Four distinct CFRP/Concrete members (Table 32) with and without insulation materials were cast to determine the heat transfer effect through the composite member. Two samples under each category were tested and the test specimens are shown in Figure 86. A total number of eight concrete blocks were cast and kept for curing for 28 days. CFRP fabrics were applied to the concrete surface using Wet-lay-up method and kept for curing for another 7 days. To measure the bond line temperature, K-type thermo couples were installed within the adhesive layer. At the top of the CFRP layers, above mentioned (Table 1) insulation layers were applied to protect the bond from elevated temperature.



Figure 86. (a) CFRP application; (b) Prepared specimens

5.3.2. Testing & results

The specimens were heated to elevated temperature within the Muffle furnace as explained in 3.2.3 (Figure 87). The obtained oven profile and average bond line temperatures for each configuration are shown in Figure 88(a). Several studies have shown that due the degradation of bond near its T_g , the debonding of CFRP turns as the major failure mode of CFRP/Concrete composite structures at the elevated

temperature. Thereby in this study, the time taken to reach the T_g (70°C) in the bond line is assumed as the “Thermal resistance period” of the composite structures when it is exposed to the elevated temperature. From the test results obtained, the time taken to reach the glass transition temperature of bond line were 2.7 min, 13.2 min, 14.3 min, 15.0 min for CC-N, CC-VC, CC-EPSC, and CC-EPSF, respectively.

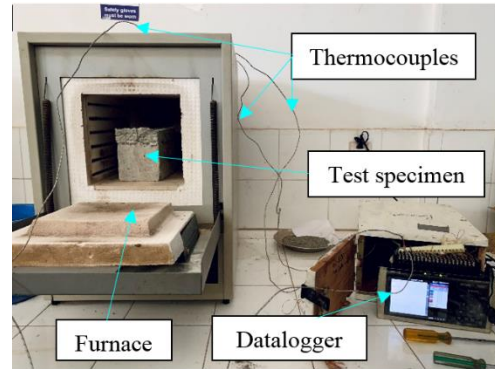


Figure 87. Testing under elevated temperature

A drastic increment in the thermal resistance can be noted in the specimens with the insulation. The reason behind the less thermal resistance of CC-VC may be due to the spalling of Vermiculite material during heating which can be noted in Figure 88(b). Compared to the Vermiculite/CFRP/Concrete composites, EPS/CFRP/Concrete maintained the integrity between the composite materials during the heating process (Figure 88(c) and 88(d)). Thereby, the developed insulation can be recommended for

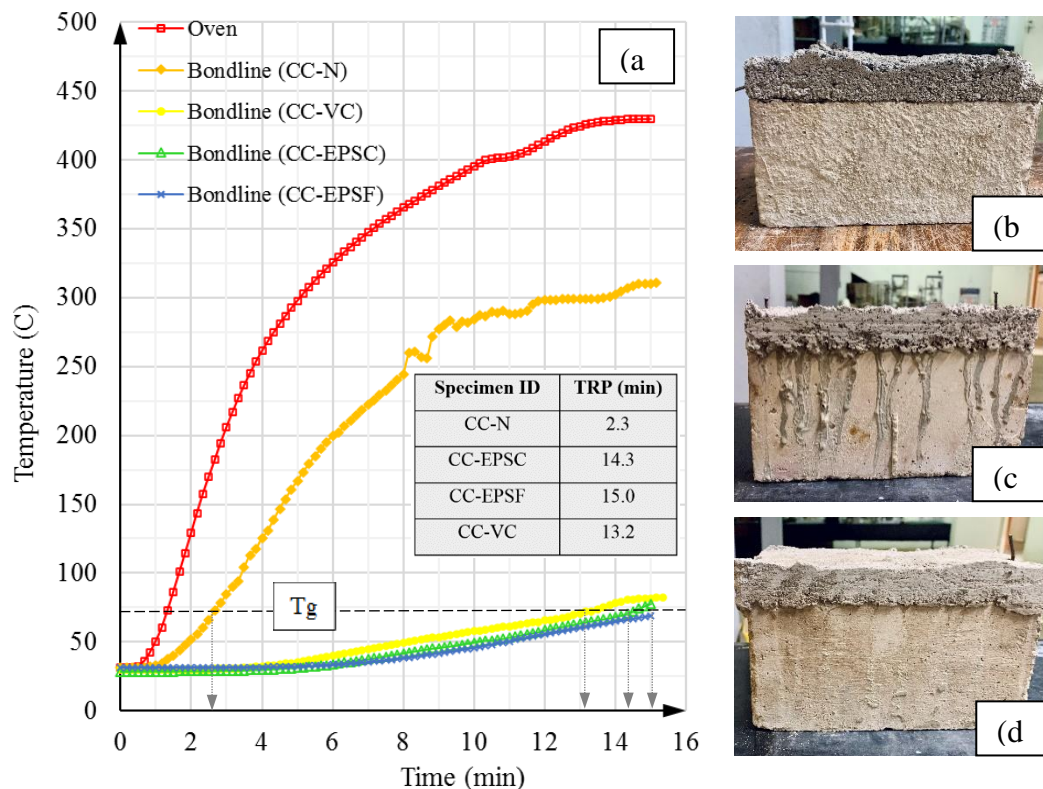


Figure 88. Test results (a) Temperature variation with time; and specimens after testing (b) CC-VC; (c) CC-EPSC; (d) CC-EPSF

CFRP/Concrete composites as an alternative to commercially available materials with less cost and recycling benefits.

5.4. Finite Element Modelling to understand the heat transfer behaviour of CFRP/Concrete composites with developed insulation

A three dimensional (3D) numerical model was developed using commercially available finite element software. Four models (Table 4) were simulated to predict the bond line temperature of CFRP/Concrete specimens with and without insulations under elevated temperature. The finite element models are shown in Figure 89. The geometrical modeling was followed by a similar procedure mentioned in the section 3.4. A mesh sensitivity analysis was carried out to select the appropriate mesh size and the results are shown in Figure 90. Considering the time restraint and computer capacity, 2.5 mm mesh size for CFRP & Epoxy and 5 mm for the concrete and insulation were selected.

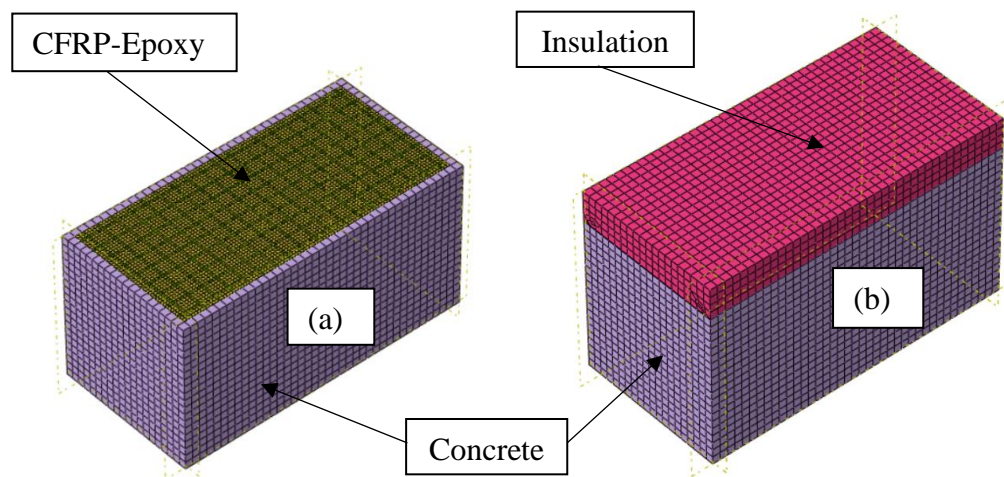


Figure 89. Finite element model of (a) non-insulated specimen; (b) insulated specimen

The heat transfer analysis of the developed models was carried out at two different temperature conditions as follows:

1. Experimental temperature conditions - Oven profile
2. Standard fire curve as specified in ISO-834

The temperature condition 1 was used to validate the heat transfer models developed in this study. The validated models were used for further studies under temperature condition 2.

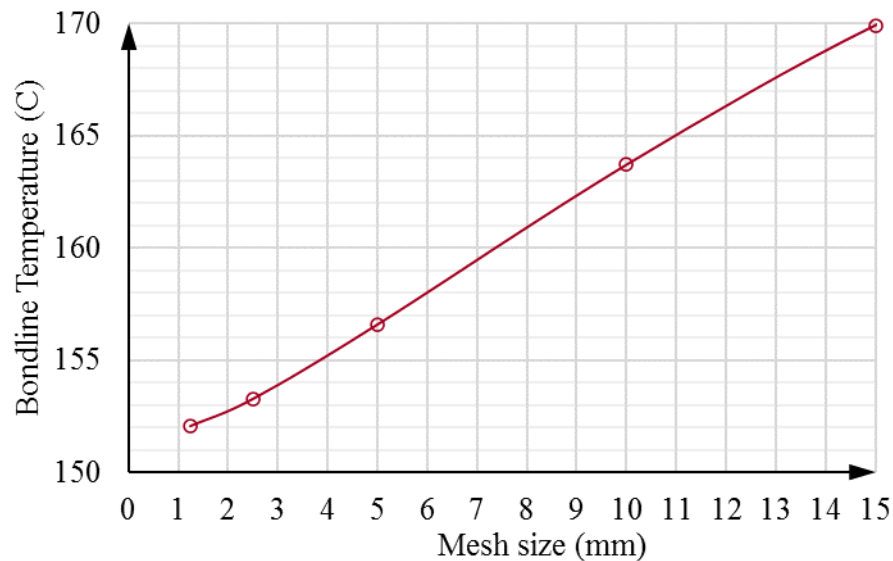


Figure 90. Mesh sensitivity analysis results

5.5 Model results & validation

The bond line temperature was predicted from the mean nodal temperature in the adhesive layer. The bond line temperature variation is plotted in Figure 91 (a) against the test results. The percentage difference in the thermal resistance period (TRP) has been calculated and less than 10% deviation was noted in the specimens except the model insulated with Vermiculite-Cement blend (CC-VC). This can be due to the poor workmanship and spalling effects of Vermiculite-cement during the experimental program as shown in the Figure 9(b). However, it is clear that with the proper application of vermiculite-cement blend, its thermal resistance period can be extended. The bond line temperature contours at $t=10$ min is shown in Figures 91 (b-e). The elements in the grey represents the degraded material which has exceeded the T_g of the adhesive.

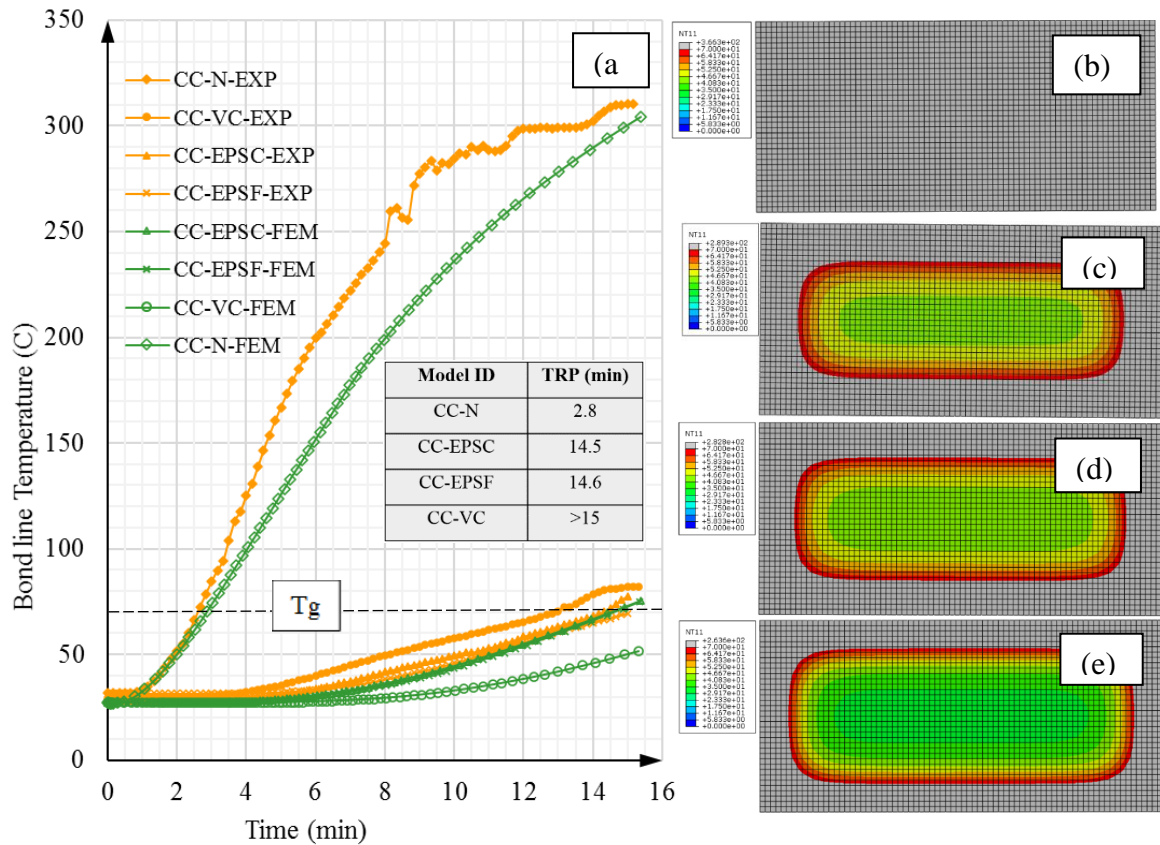


Figure 91. Model results and validation

5.6. Heat transfer Analysis of CFRP/Concrete composites under ISO Standard fire

The validated models were further analyzed under ISO 834 standard fire curve [35]. The procedure of this analysis was also very similar to the analysis in the section 3.4. From the observations made in previous simulations, it was decided to provide a U-wrap insulation layer to avoid the heat transfer from both sides of the specimen which significantly affects the bond line temperature. The temperature variations at the bond line were observed and illustrated in Figure 92. The predicted fire resistances for CFRP/Concrete composites with Vermiculite-cement (VC), HIP, and MIP were 43.6 min, 40.7 min, and 41.3 min, respectively. This indicates that the developed insulation in this study has achieved 93% to 95% fire resistance respect to the commercially available (Vermiculite-Cement) insulation material using 20 mm thickness layer application. However, based on the temperature contours shown in Figure 91(c-e), it

is clear that the heat transfer from the sides of the member are significantly high. Therefore, providing insulations in both sides as a U-wrap is recommended. In addition, the appropriate thickness for the required fire resistances has to be determined.

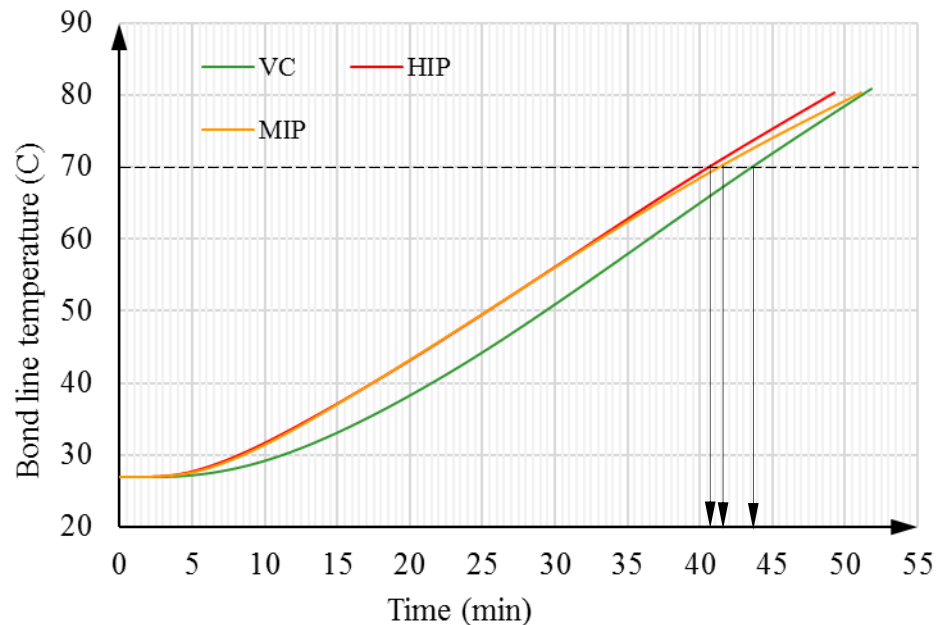


Figure 92. Model results under standard fire

5.7 Summary

The application of the developed products for the CFRP/composites has been assessed in this chapter. An experimental program was conducted to evaluate the thermal performance of Concrete/CFRP/Insulation composites under elevated temperature. It was noted that by using the insulation material developed in this study, spalling effects can be significantly reduced compared to the currently used materials.

A finite element analysis was followed, and the developed numerical model was validated by the experimental results. The finite element model was analysed under the ISO standard fire and the CFRP/Concrete composite with the developed insulation in this study has achieved 93% to 95% fire resistance respect to the commercially available (Vermiculite-Cement) insulation material.

CHAPTER 6: NUMERICAL MODELLING TO PREDICT THE THERMAL COMFORT OF BUILDINGS WITH EPS-BASED INSULATIVE PLASTER

6.1. Heat transfer modeling

On the process of developing an insulation material, it was revealed that some mix proportions undergo with the requirements of N-type mortar mix. In such a case, the mortar mix with 125% replacement of sand by fine EPS particles was selected (Low insulated plaster with fine particles, “LIP”; EPS-125-F). Compressive strength of 5.2 MPa (28 days) is required for any N-type mortar for masonry units and the flow should be 110+/-10% (ASTM C 270-07, 2010). Therefore, a study on the application of the selected mortar on the masonry wall was carried out.

A three-dimensional finite element model was simulated using an advanced finite element software. A 3 m x 4 m x 0.1 m dimension of masonry wall panel was developed for this study, and it is assumed that the wall panel is constructed using cement-sand blocks. From the results obtained from the experimental program in Chapter 4 EPS-125-F (LIP) was selected since it performed well in both thermal and mechanical assessment (Table 12). Hence, it was chosen to analyze the heat transfer behavior through a wall panel.

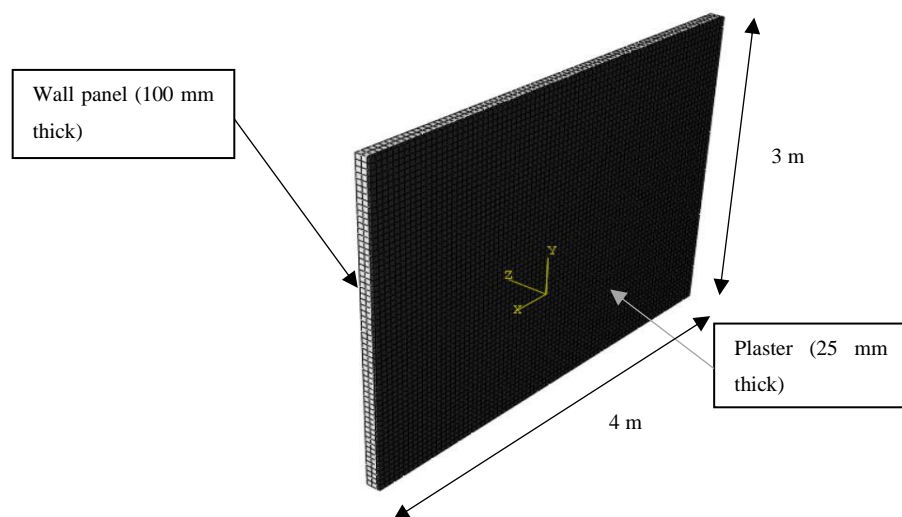


Figure 93. Finite element mesh of the wall panel with plaster

8-node linear heat transfer brick elements (DC3D8) were used to model both wall and plaster elements. From a mesh sensitivity analysis, the mesh size was decided as 50 mm and the selected aspect ratios for the wall and the plaster were 1:1, and 1:2, respectively. Since the plaster and the wall panel are assumed as perfectly bonded, a tie constraint was used to represent its bond. The finite element mesh of the wall panel with plaster is shown in Figure 93.

The thermal performance of the masonry wall is to be evaluated based on two parameters which are “decrement factor” and “time lag”, respectively. The decrement factor is defined as the ratio between the amplitude of the temperature wave at the indoor wall surface and the amplitude at outer wall surface. And the time takes for the maximum temperature to propagate from the outer surface to the inner surface in referred as time lag. The decrement factor (f) and the time lag (t_{ϕ}) can be computed using equations 32 & 33, respectively.

$$t_{\phi} = t_{o-max} - t_{i-max} \quad (32)$$

$$f = \frac{T_{I-max} - T_{I-min}}{T_{O-max} - T_{O-min}} \quad (33)$$

Where t_{o-max} and t_{i-max} represent the time when the outside surface temperature and inside surface temperature reaches the maximum, respectively. And T_{I-max} , T_{I-min} , T_{O-max} , and T_{O-min} represent the inside maximum, inside minimum, outside maximum, and outside minimum surface temperatures, respectively.

6.1.1. Wall Panel specification

Three distinct wall panels were simulated to compare the heat transfer effect of plaster using EPS-cement plaster and conventional plaster. The model descriptions are listed in Table 33.

Table 33: Wall panel specifications

Model ID	Description
WP_0	Wall panel (WP) without plaster
WP_CS	Wall panel (WP) with cement-sand plaster
WP_EPS125	Wall plaster (WP) with EPS-cement plaster (EPS125)

6.1.2. Material properties

The thermal properties of the concrete block wall panel were obtained from the available literature (Irsyad et al., 2017). And the properties obtained from this experimental program mentioned above were used to simulate the thermal behavior of the plaster. All the material properties used in this numerical model are listed in Table 34.

Table 34: Thermal properties

Material	Thermal conductivity (W/m.K)	Specific heat (J/kg.K)	Density (kg/m ³)
Concrete block wall	1.37	840	2778
CS	0.8	1500	2000
EPS125	0.41	1450	1400

6.2. Theoretical prediction & Validation

6.2.1. Steady-state analysis

The simulated heat transfer model was validated by applying the Fourier law to the plastered wall panel at steady-state heat transfer condition. The heat transfer through conduction based on the Fourier law is given in Equation 34.

$$Q_x = -KA \frac{dT}{dx} \quad (34)$$

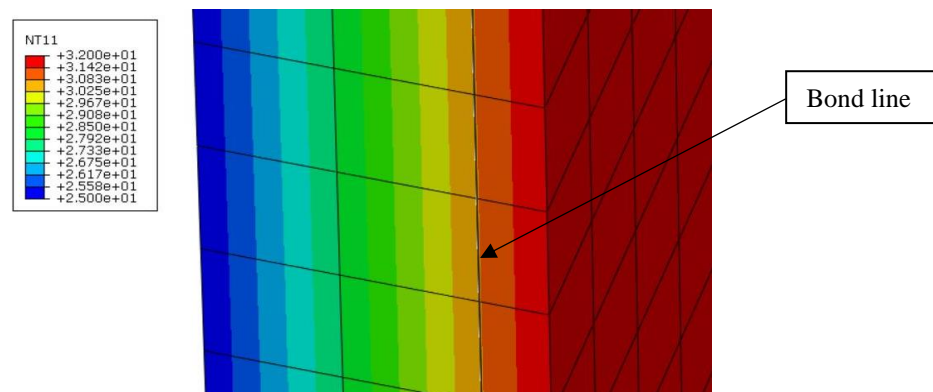
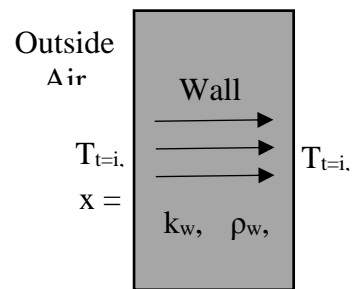


Figure 94. Temperature profile across the wall panel

Where Q_x , K , A , T , and x are the heat transferred through conduction in x -direction, thermal conductivity, cross-section, temperature, and the distance respectively. The plaster surface and the external surface of the wall were kept at 32°C , and 25°C , respectively, and the temperature at the bond line between the wall and the plaster was calculated as 30.8°C by applying the Fourier law across the plastered wall. The obtained temperature from the numerical model was 30.83°C as shown in Figure 94.

6.2.2. Transient Analysis

The simulated heat transfer model was validated through the theoretical solution of the transient one-dimensional heat transfer problem (Figure 95). The governing equation for the heat flow through a wall can be expressed as



equation 35. Where α is the thermal diffusivity $k/\rho c_p$ and k , ρ , c_p , and T are thermal conductivity, density, specific heat, and temperature, respectively. Let's assume an equal distance of the points x_i in one dimension with intervals of $\Delta x = x_{i+1} - x_i$, and equal timesteps t_n at intervals of $\Delta t = t_{n+1} - t_n$. Based on the described discretization, the following derivatives can be written (Equation 36 & 37). From equations 35, 36, and 37, the general solution for $T_{x_i, t_{n+1}}$ can be written by equation 38.

$$\frac{\partial T}{\partial t} - \alpha \nabla^2 T = \frac{\dot{q}}{\rho c_p} \quad (35)$$

$$\frac{\partial T}{\partial t} \Big|_{x_i, t_{n+1/2}} \cong \frac{T_{i,n+1} - T_{i,n}}{\Delta t} \quad (36)$$

$$\frac{\partial T}{\partial x} \Big|_{x_{i+1/2}, t_n} \cong \frac{T_{i,n+1} - T_{i,n}}{\Delta x} \quad (37)$$

$$T_{i,n+1} = T_{i,n} + \Delta t \left[\alpha \frac{T_{i-1,n} - 2T_{i,n} + T_{i+1,n}}{(\Delta x)^2} + \frac{\dot{q}}{\rho c_p} \right] \quad (38)$$

The initial temperature of the wall specimen without plaster (WP_0) was assumed as 25°C and the external surface of the wall was subjected to 32°C (T_{out}). The model

predicted temperature variation across the wall is shown in Figure 96. The nodal temperature with time at $x = 25$ mm, 50 mm, and 100 mm was computed using equation 6 and compared with the results predicted from the finite element model (Figure 97). The acceptable agreement between the theoretical results and the FE model predicted results show the accuracy of the developed model. The detailed calculations are attached in Annex B.

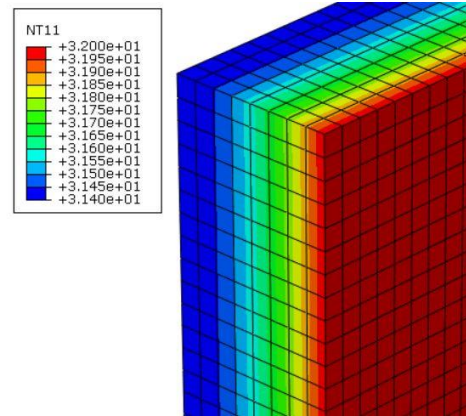


Figure 96. Temperature contours through the wall cross section (WP_0)

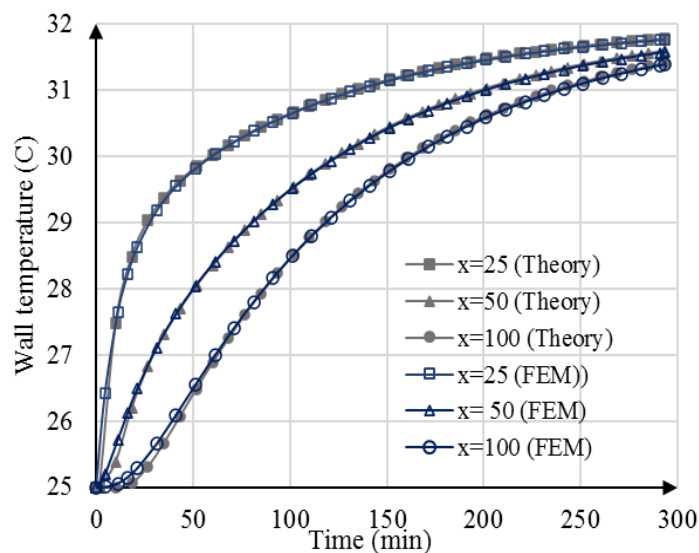


Figure 97. Comparison of theoretical results and FE model predicted results

6.3. Model results & experimental validation

To validate the numerical model, a small-scale building prototype with external wall plaster was built (Figure 98) and an EPS roof was fixed to avoid the heat transfer from the top of the building. The wall surface temperatures inside and outside were monitored for 6 consecutive hours and compared with the results predicted from the numerical model. Figure 99 shows a comparison of measured surface temperatures and numerically predicted temperatures and it indicates fairly good agreement between the experimental and numerical results. Moreover, the internal wall surface

temperature with the developed plaster (WP_EPS125) seems less compared to the wall with conventional plaster (WP_CS).



Figure 98. Building prototype (a) Construction of building prototype; (b) preparation of mortar mix; (c) External plaster application; (d) Completed prototype; (e) Placing EPS roof panel (f) Monitoring wall temperature

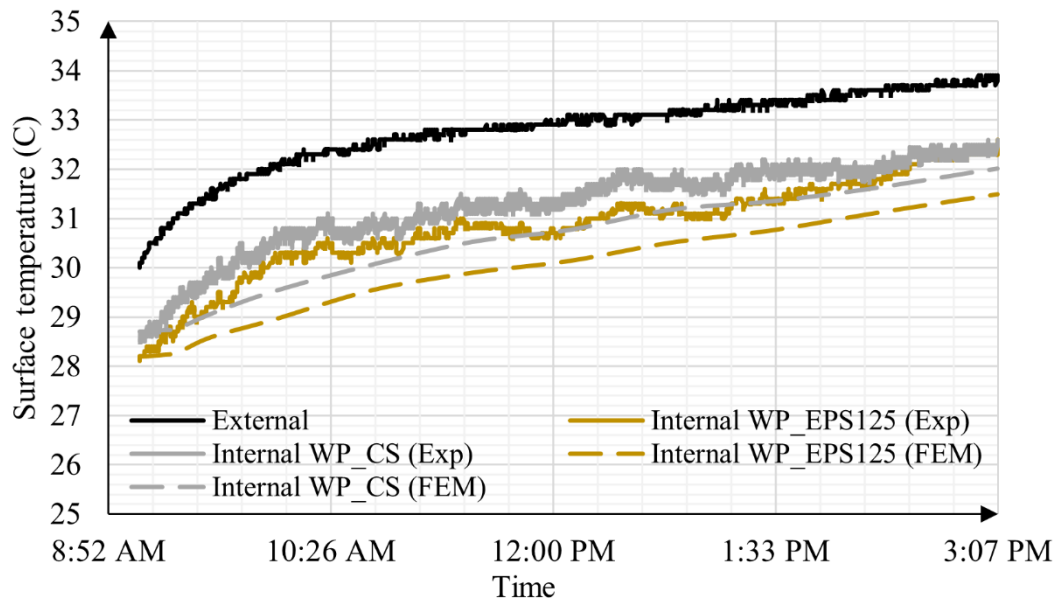


Figure 99. Comparison of measured temperature and predicted temperature

In order to predict the thermal performance throughout a day, the measured environmental temperature profile of a random day was selected (*Time and Date*, 2020) at the external wall surface as shown in Figure 99. An initial temperature at the internal wall surface was assumed as 25°C and the model was running for a cyclic temperature for 6 days to ensure the convergence of the internal temperature variation. The applied temperature at the external surface and the obtained temperature for the internal surface with Conventional plaster are plotted in Figure 100 for 6 consecutive days. Then, the temperature variation within the 24 hours was extracted from the model results after the convergence of the internal variation (Figure 100).

Figure 101 shows the internal and external temperature of walls for different conditions for period of a 24 hours. According to the graphs, the wall with the innovative plaster shows better thermal performance. The decrement factor of the wall was observed as 0.85 without any application of the plaster (WP_0). The time lag in the wall panel model without plaster was noted as 2 hours and 27 min. Shaik et al. have also investigated the heat transfer behavior of building walls exposed to the periodic temperature profile and the noted decrement factor for 100 mm thick concrete block walls was 0.86 and 2 hours 30 min (Shaik et al., 2016). The similarity of these

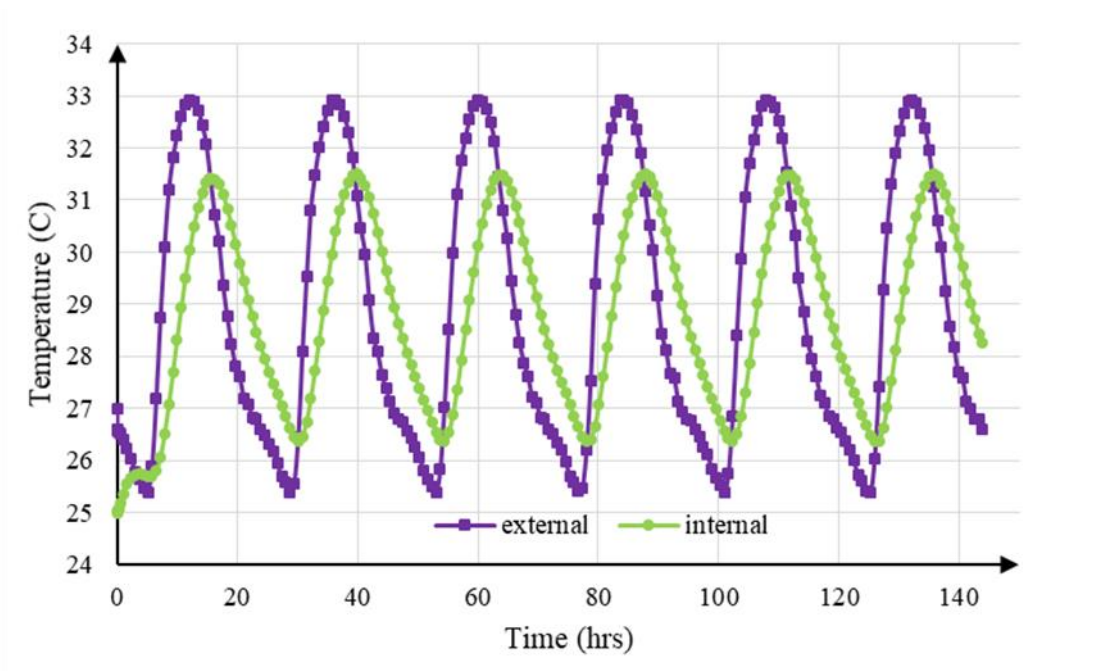


Figure 100. Temperature variation in the outside surface and inside surface for 6 days period in model WP_CS

results also shows the accuracy of the heat transfer model developed in this study. By applying the conventional plaster (WP_CS), the decrement factor of the composite wall reduced by 20%. In addition, 18% reduction was noted in the composite wall with the application of the plaster developed in this study (WP_EPS125) which shows the improved thermal performance. The time lags in the models with plaster increased by 55.1%, and 85.7% of the wall panels WP_CS, and WP_EPS125, respectively. The time lags and decrement factors are listed in Table 35.

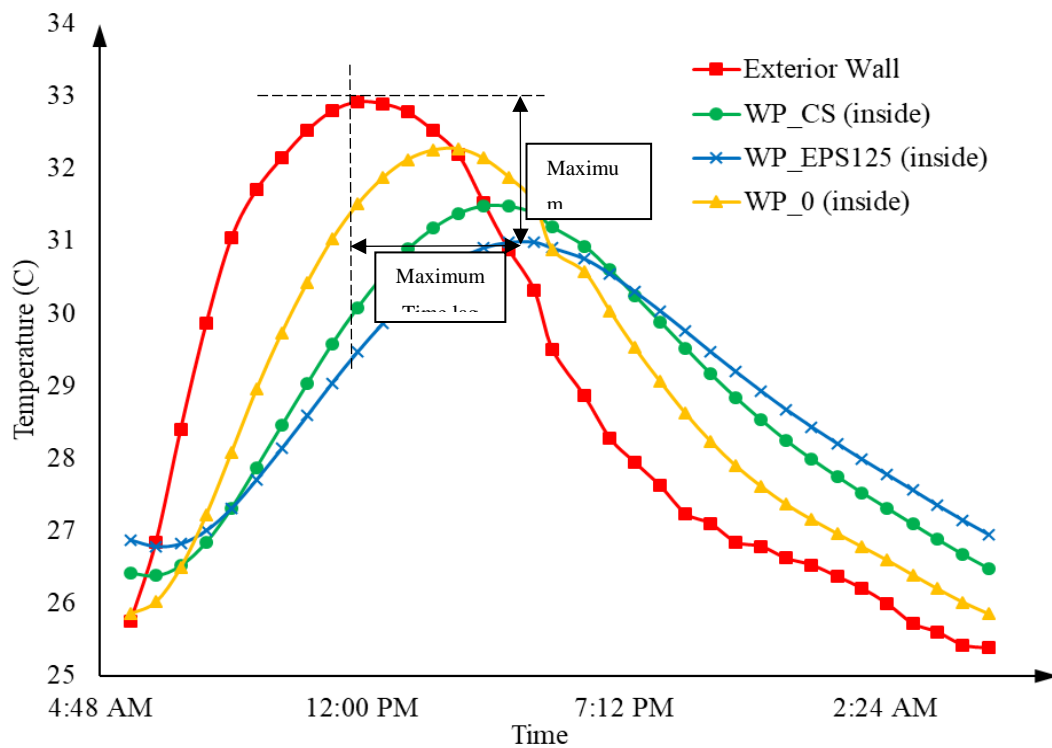


Figure 101. Temperature variation in the outside surface and inside surface for 24 hours period

Table 35: Computed decrement factors & time lags

Model ID	Time lag	Decrement factor
WP_0	2 hours 27 min	0.85
WP_CS	3 hours 48 min	0.68
WP_EPS125	4 hours 33 min	0.56

6.4. Parametric study

6.4.1. Effect of thickness of plaster

The selection of the optimum thickness of a thermal insulation layer is an important parameter that needs to be studied for an economical construction project. Different thicknesses were used in the heat transfer analysis in the possible range of 10 mm to 30 mm and the internal wall temperature of WP_EPS125 was observed and plotted in Figure 102. It was noted that the decrement factor gradually reduces with the

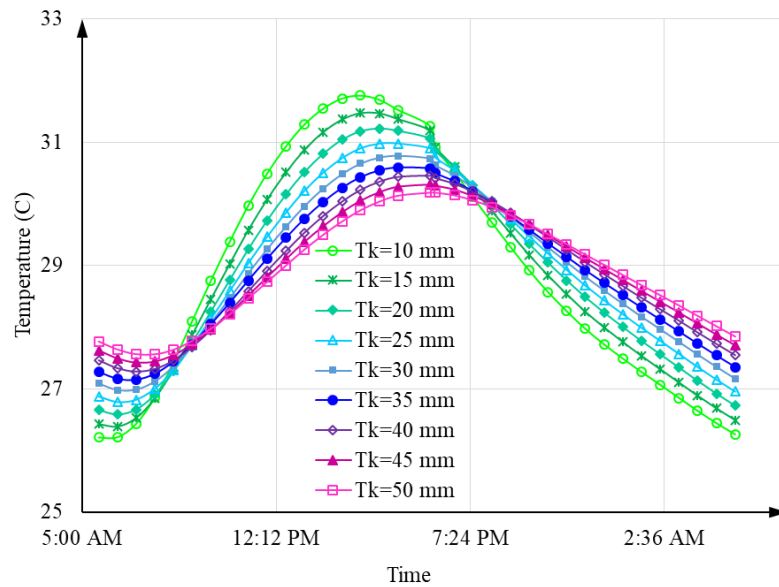


Figure 102. Effect of plaster thickness on thermal performance of developed composite wall

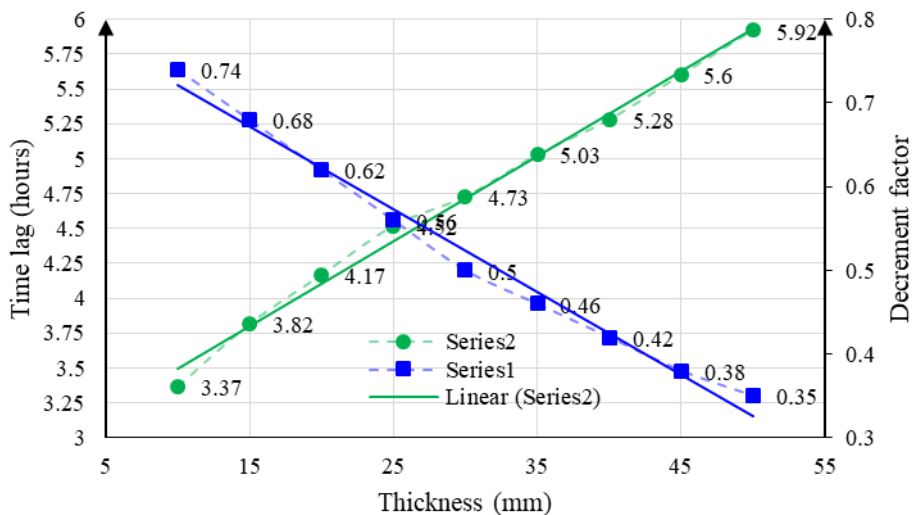


Figure 103. Effect of plaster thickness on decrement factor and time lag

increment of the thickness of the plaster and the time lag nearly gradually increases respectively. The obtained decrement factors and the time lags were illustrated in Figure 103. From the values obtained for decrement factor and time lag, it can be concluded that plasters with higher thickness can provide greater thermal insulation for the masonry walls.

6.4.2. Effect of thermal conductivity of the plaster

The thermal conductivity of plaster has a significant effect on the thermal insulation of the building elements. The conductivity of the innovative plaster and was compared with the conventional cement plaster (0.7-1.1 W/m.K), vermiculite-cement plaster (0.15 W/m.K) which is a commercially available fireproofing material, bottom-ash based cement plaster (0.5-0.8 W/m.K; developed by Kahandawa Arachchi *et al.* (2020) in the University of Moratuwa), and rice-husk based cement plaster (0.2-0.4 W/m.K; developed by Kajanan *et al.*(2020) in the University of Moratuwa). The conductivities of these materials are experimentally obtained in this study and listed in Table 36.

Table 36: Thermal conductivities of the control materials selected for this study

Plaster description	Thermal conductivity (W/s.K)
Vermiculite-cement plaster (VC)	0.12
EPS-cement plaster (EPS125)	0.41
Rice husk ash-cement plaster (RHA50)	0.33
Bottom ash-cement plaster (BA60)	0.7
Conventional cement plaster (CS)	0.8

The heat transfer behavior of WP_EPS125 was further carried out with different conductivities in the range which covers the above-mentioned conductivities. The temperature profiles in the internal wall with varying conductivities is illustrated in Figure 104. The decrement factors and the time lag were calculated from the results obtained from the numerical model and plotted in Figure 105 for corresponded conductivities. It can be seen that the decrement factor increases, and the time lag reduce with increasing thermal conductivity which shows the improved thermal performance using low thermal conductivity materials. Further, it was also noted, the

effect of low thermal conductivity material is high on thermal performance compared to high thermal conductivity materials.

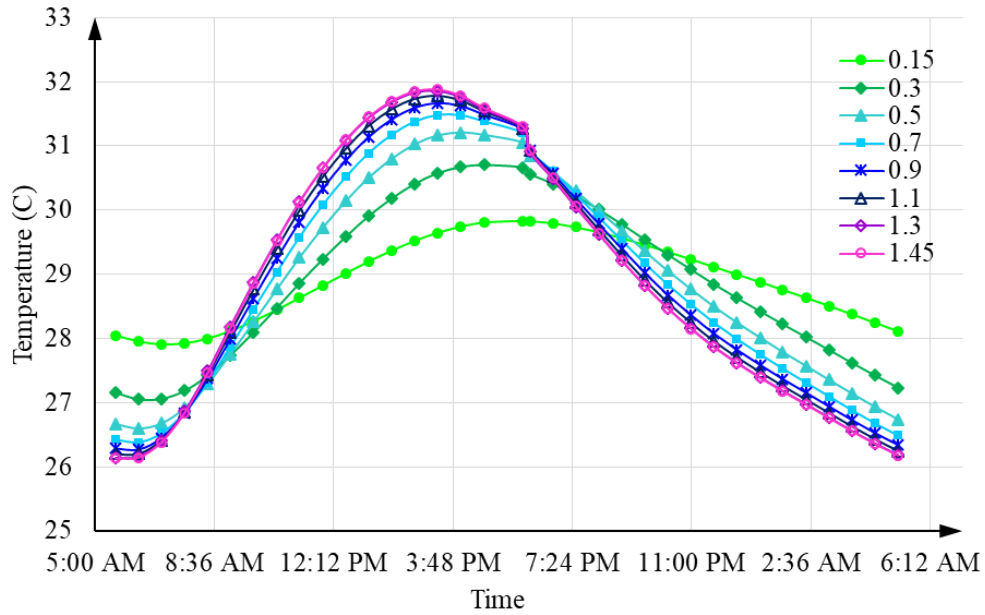


Figure 104. Effect of thermal conductivity on thermal performance of developed composite wall

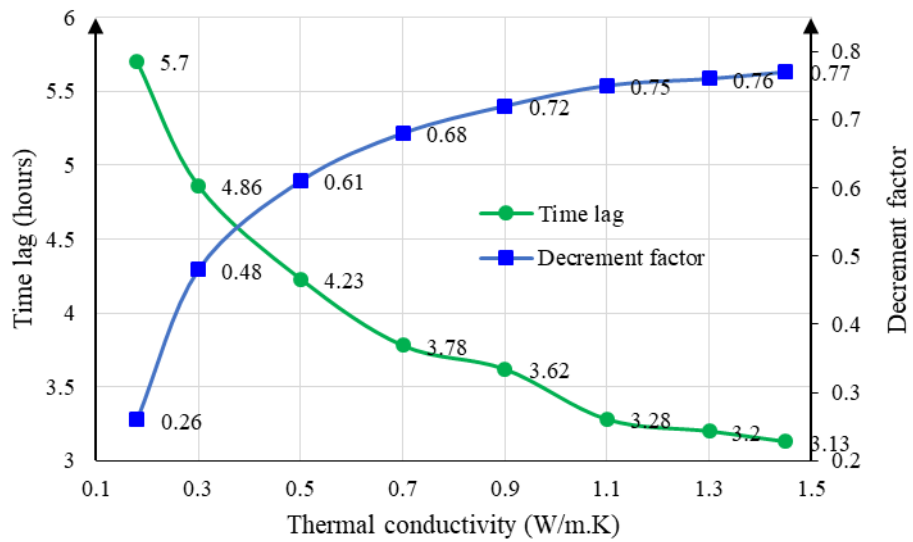


Figure 105. Effect of thermal conductivity on decrement factor and time lag

6.4.3. Effect of specific heat of the plaster

An investigation on specific heat is to be carried out in any heat transfer analysis because it is the heat energy required to raise the temperature of the substance. Various specific heat was selected in this analysis, similar to the study conducted on the effect of conductivity. The specific heats of the above-mentioned materials are listed in Table 37.

Table 37: Specific heats of the control materials selected for this study

Plaster description	Specific heat (J/kg.K)
Vermiculite-cement plaster (VC)	2300
Bottom ash-cement plaster (BA60)	900
Rice husk ash-cement plaster (RHA60)	1080
Conventional cement plaster (BA0)	1085
EPS-cement plaster (EPS125)	1450

A specific heat range of 500 J/kg.K to 3500 J/kg.K was selected for this study. The temperature variation in the internal wall surface for the given specific heat is plotted in Figure 106. It was noted that the effect of specific heat of the insulation material on

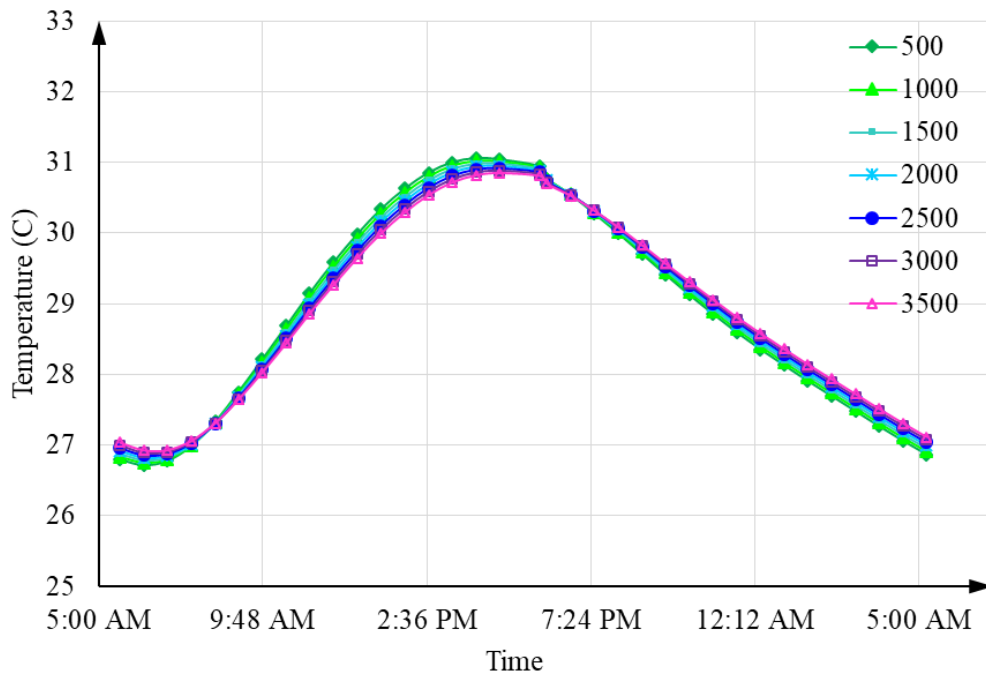


Figure 106. Effect of specific heat on thermal performance of developed composite wall

thermal performance is small compared to other parameters. However, the decrement factors and the time lags were calculated for different specific heats and are plotted in Figure 107. The relationship between specific heat vs decrement factor and time lag were noted to be linear in the selected range.

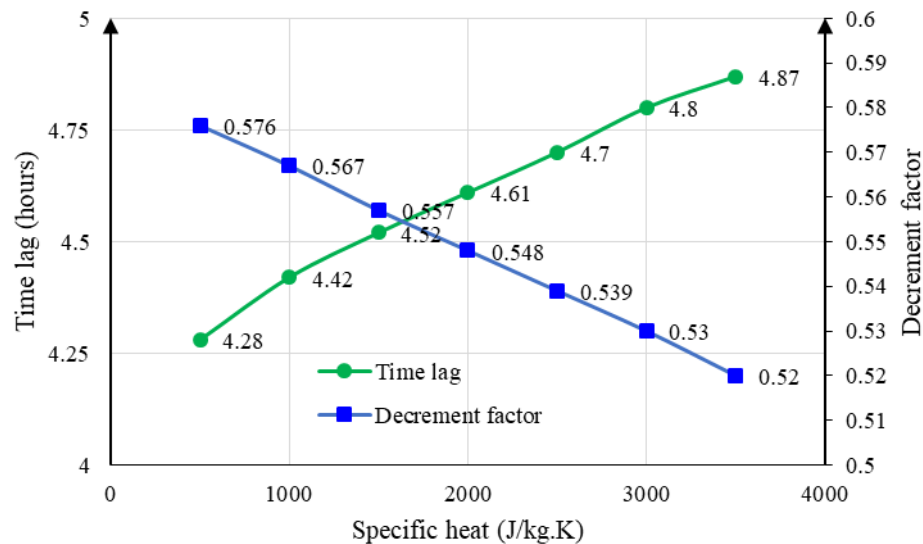


Figure 107. Effect of specific heat on decrement factor and time lag

6.6. Summary

A numerical model of the wall panel with cement-based plaster was developed in this study in order to predict the thermal performance of insulated cement-based plasters. From the trial mixes in Chapter 4, The LIP (EPS-125-F) was selected for this study. A small-scale building prototype has built and tested to validate the numerical model and comparison indicated the acceptance of the developed model.

Further, the effect of thickness, conductivity, and the specific heat of the plasters was studied, and the results were interpreted using the decrement factor and time lag. It was noted that there is no significant effect of varying the specific heat of the materials. And a small change in the thermal conductivity in low thermal conductivity materials can make a larger change in the thermal comfort of the buildings.

From the parametric analysis, it was noted that a decrement factor increments of 7% to 70%, and a time lag reduction of 28% to 133% can be achieved by providing an appropriate plaster with good thermal properties.

CHAPTER 7: COST ANALYSIS

7.1. Bill of Quantities

A preliminary cost analysis was carried out to the developed materials to compare with commercially available products. The initial cost of the developed materials can be computed using bills of quantities. The market prices according to January 2020 was used to prepare the bill of quantities. The Bill of quantities was prepared for all three selected materials and the conventional mortar as well. The market price of the materials is listed in Table 38.

Since EPS is being reused, it can be found in several places in the country, it does not have any initial cost during the manufacturing process. For this particular project, it was obtained from factories located in Ja-Ela and Horana free of charge. But for the mass manufacturing process, it may have few charges from for the dealers. Therefore, a transportation cost to the University of Moratuwa was considered in this estimation. A transportation cost for cement and sand was also considered from plants in Ratmalana and Mount Lavaniya, respectively. Since transportation costs can be varied with time and transport ways, more attention should be paid for the material cost. The storage cost was assumed as zero in this analysis.

The bills of quantities for 5 litre of Conventional cement – sand mortar, LIP, MIP, and HIP are given in Table 39. The material cost and transportation cost have been calculated separately.

Table 38: Market prices of materials

Material	Quantity	Material cost (LKR)	Transportation cost (LKR)
Cement	50 kg	950	90
Sand	1500	11500	1500
EPS	5 m ³	0	5000

Table 39: Bill of Quantities

Material	Unit	Unit Price (LKR)	Conventional Plaster		LIP		MIP		HIP	
			Quantity	Cost (kg)	Quantity	Cost (kg)	Quantity	Cost (kg)	Quantity	Cost (kg)
Cement	kg	19	2.22	42.09	1.78	33.91	1.26	23.89	1.26	23.89
Sand	kg	8	6.64	53.17	0.53	4.28	0.38	3.02	0.38	3.02
EPS	m ³ x 1000	0	0	0	3.48	0	3.02	0	3.02	0
Total Material cost for 5 liter mix			95.26		38.19		26.91		26.91	
Cement	kg	1.8	2.22	3.99	1.78	3.21	1.26	2.26	1.26	2.26
Sand	kg	1	6.64	6.64	0.53	0.53	0.38	0.38	0.38	0.38
EPS	m ³ (/1000)	1	0	0	3.48	3.48	3.02	3.02	3.02	3.02
Total Transport cost for 5 liter mix			10.63		7.22		6.06		6.06	

The conventionally used fireproofing material for CFRP composites in Sri Lanka is the Vermiculite-cement blend which is being imported. The cost was the Vermiculite-blend mix for 50 liters is 1,020,000 + vat according to the year 2019. Since LIP is recommended as a wall plaster material, a comparison between the conventional plaster and LIP is shown in Figure 108. And a comparison between MIP, HIP, and Vermiculite-cement (VC) mix is shown in Figure 109.

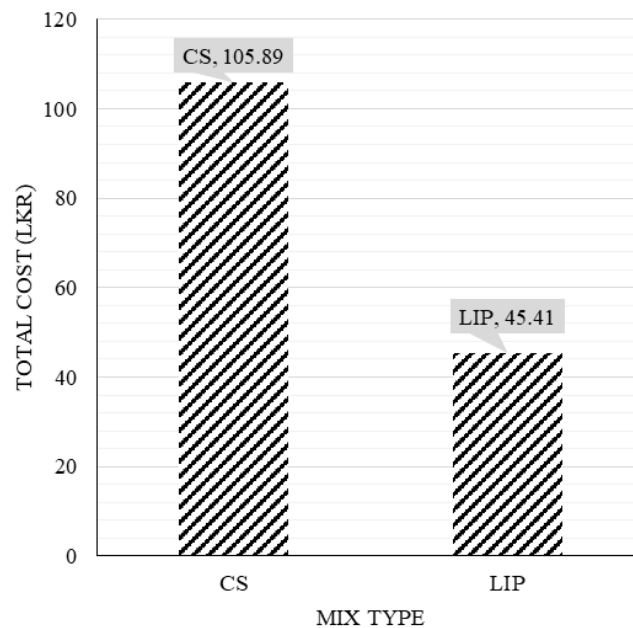


Figure 108. Cost comparison for wall plasters

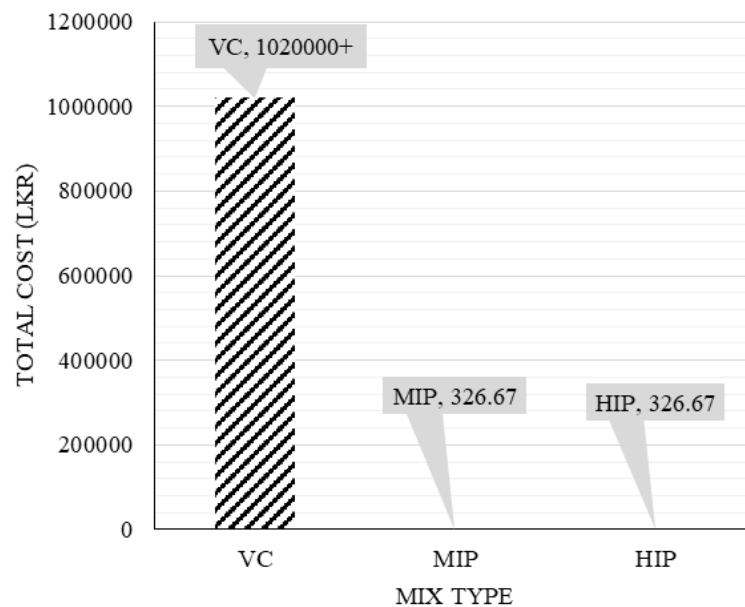


Figure 109. Cost comparison for CFRP insulation materials

7.2. Summary

From the preliminary cost analysis performed in this chapter, it is clear that using the Low insulated plaster (LIP) developed in this study would be cost-effective while providing additional thermal comfort to the buildings. The noted cost reduction when using the LIP is 57% of the conventional plaster.

Further, the cost of the insulation system for CFRP composites can be reduced almost by 100% when using the products developed in this study. But this cost value will vary if the manufacturer uses virgin EPS or produce it themselves.

CHAPTER 8: CONCLUSIONS

This study explored the CFRP retrofitting technique in reinforced concrete infrastructures and identified the fire resistance of CFRP composites still remains unsolved. Due to the low glass transition temperature of epoxy adhesive, the CFRP bond degrades when the composite is exposed to the fire or elevated temperature. Hence, providing solutions to overcome the drawback in CFRP retrofitting projects due to the effect of fire was the aim of this study. In that case as the early solution, a new bonding technique has been identified for CFRP-concrete flexural members which was referred as “Groove bonding technique” (GBT). By using this technique, the required quantity of Insulation material can be reduced up to 36% hence the cost of insulation project can be also reduced by 36%. And it was noted only a slight reduction less than 4% can be encountered using this technique than the External bonding technique.

It was revealed this technique is more efficient for slabs than beams since this prevents the heat transfer from the bottom side. Despite as the other beam retrofitting techniques, here also insulations should be provided at least for 3 sides when the beams are fully exposed to the environment. From the results obtained in the parametric study, design charts have been developed for engineers which can be easily referred prior to application using this method.

As the next phase of this study, an EPS mixed Cement based Insulation material was developed in order to reduce the cost of Insulation material. Since a huge amount of used EPS are available in the Country, this application would help to contribute reuse the EPS materials. Trial mixes were prepared with different mix proportions and the thermal and mechanical properties of the mixes were tested in the Laboratory. Thermal conductivity variation from 0.2 W/m.K to 0.7 W/m.K, compressive strength (7 days) variation from 20 MPa to 1 MPa, and density variation from 2100 Kg/m³ to 900 Kg/m³ were noted from the test results. The aggregate size and water/cement ratio were identified as a key parameter in thermal and mechanical properties of the EPS-cement mix. From several trial mixes, some optimum mixes were identified for multi-purpose in Civil Engineering Industry.

The mix with 200% replacement of fine aggregates by EPS was identified as the ideal mix for the CFRP composites. The selected mix was indicated 93-95% fire resistance respect to the commercially available product which shows the effectiveness of the developed plaster in this study.

A mix proportion with 125% replacement of fine aggregates by EPS, which also satisfy the N-type mortar requirement was identified and its application on masonry wall has been assessed. A heat transfer model of a plastered wall was developed and validated with the experimental results. Based on the decrement factor and the time lag the effect of this plaster was analyzed using the developed numerical model. On average, 0.5 C reduction in the maximum & minimum temperature was noted with a 25 mm thick EPS plaster compared to the conventional plaster. Moreover, from the parametric study, it was revealed that, by using 15 mm of the innovative wall plaster (LIP), a similar thermal comfort to the 25 mm conventional plaster can be achieved. Hence, it can be concluded that this innovative plaster will significantly improve the thermal comfort in the buildings than the conventional plaster.

In addition, a preliminary cost analysis was carried out to compare the developed products with the currently used products for various applications such as wall plastering and insulating CFRP composites. And the results indicated the cost saving in the developed products at the highest quality requirements.

CHAPTER 9: RECOMMENDATIONS

9.1 Groove bonding technique

Though this technique is almost similar to the External bonding technique, further study on the flexural performance of Groove bonded CFRP-concrete members is essential. Since the CFRP laminates are proposed to attach within the nominal cover of reinforced concrete members, the width of the CFRP strips/grooves may be limited than the external bonding technique. Therefore, the sensible parameters on bond patterns should be investigated. In addition, the bond and cover of steel members should be taken into care when selecting the groove locations.

9.2 Application of Insulation material on CFRP composites

From the trial mixes prepared in this study two types of plasters (MIP and HIP) can be recommended to use for CFRP composites for fire prevention. In that case, the bond strength between the CFRP and Insulation should be tested as the first recommendation. To study the bond strength between CFRP and the developed Insulation at elevated temperature, a shear-lap test should be performed, and the bond slip should be assessed. The application of the developed insulation should be extended with U-wrap coating and different thicknesses to develop the precise guidelines on the fire resistance periods

9.3. Application of Insulation material on wall panels

The Low insulated plaster (LIP) developed in this study can be used as a wall plaster in buildings to enhance the thermal comfort. Though, a numerical model has been developed to study the effect in thermal comfort, a detailed test program should be conducted to study the practical challenges in the application of Material in the wall panels. The plaster should be monitored for cracking, spalling, and rain. In addition, the energy reduction due to this plaster should be computed and compared with the conventional plaster.

REFERENCES

- Aaruga, S. (2019). Finite Element Modelling on Flexural Performance of CFRP Strengthened Reinforced Concrete Curved Beams. *2019 Moratuwa Engineering Research Conference (MERCOn)*, 662–667.
- ACI 318-14. (2014). <https://doi.org/10.2748/tmj/1232376167>
- ACI committee 440. (1996). Guide for the design and construction of externally bonded FRP systems for strengthening existing structures. In *ACI committee 440*.
- Ahmad, M. M., Ahmad, F., Azmi, M., Zulham, M., & Mohd, A. (2015). Properties of Cement Mortar Consisting Raw Rice Husk. *Applied Mechanics and Materials Vol., 802*, 267–271. <https://doi.org/10.4028/www.scientific.net/AMM.802.267>
- Al-homoud, M. S. (2005). Performance characteristics and practical applications of common building thermal insulation materials. *Building and Environment*, 40, 353–366. <https://doi.org/10.1016/j.buildenv.2004.05.013>
- ASTM C 1437-07. (2009). Standard Test Method for Flow of Hydraulic Cement Mortar. In *ASTM Standards* (pp. 6–7).
- ASTM C 270-07. (2010). Standard Specification for Mortar for Unit Masonry. In *ASTM International* (pp. 2–13). <https://doi.org/10.1520/C0270-10>.
- ASTM C109/C109M-02. (2002). Standard Test Method for Compressive Strength of Hydraulic Cement Mortars. In *ASTM International* (Vol. 04, pp. 1–6). <https://doi.org/10.1520/C0109>
- ASTM D7340. (2018). Standard Practice for thermal conductivity of Leather. In *ASTM International*. ASTM International2018.
- ASTM International. (2010). *ASTM C 270-10, Standard Specification for Mortar for Unit Masonry* (pp. 1–14). West Conshohocken. <https://doi.org/10.1520/C0270-10>.

- Babrauskas, V., & Science, F. (2018). Fire safety design and concrete. *Fire Safety Journal*, 7112(August). [https://doi.org/10.1016/0379-7112\(94\)90007-8](https://doi.org/10.1016/0379-7112(94)90007-8)
- Bentz, D. P., Peltz, M. A., & Valdez, P. (2009). Thermal Properties of High-Volume Fly Ash Mortars and Concretes. *Waste Management*, 1–19.
- Blontrock, H. (2003). *Analysis and modeling of the fire resistance of concrete elements with externally bonded FRP reinforcement*. Ghent University.
- Borhan, T. M., & Janna, H. (2016). *Thermal properties of cement mortar containing waste aluminium fine aggregate*. January.
- Chandra Das, S., & Haque Nizam, E. (2014). Applications of Fibber Reinforced Polymer Composites (FRP) in Civil Engineering. *International Journal of Advanced Structures and Geotechnical Engineering ISSN*, 03(03), 2319–5347. https://www.researchgate.net/profile/Subrata_Das30/publication/305305006_Applications_of_Fiber_Reinforced_Polymer_Composites_FRP_in_Civil_Engineering/links/5787609d08aea50b6b1901a8/Applications-of-Fiber-Reinforced-Polymer-Composites-FRP-in-Civil-Engineeri
- Chandrathilaka, E. R. K., Gamage, J. C. P. H., & Fawzia, S. (2018). Mechanical characterization of CFRP / Steel bond cured and tested at elevated temperature. *Composite Structures*. <https://doi.org/10.1016/j.compstruct.2018.09.048>
- Chowdhury, E. U., Bisby, L. A., & Green, M. (2011). *Mechanical Characterization of Fibre Reinforced Polymers Materials at High NRCC-50851*. May 2014. <https://doi.org/10.1007/s10694-009-0116-6>
- Chowdhury, E. U., Green, M., & Bisby, L. A. (2007). Thermal and mechanical characterization of Fibre Reinforced Polymers , Concrete , Steel , and Insulation materials for use in numerical fire endurance modeling. *Structures under Extreme Loading, Proceedings of Protect, August*, 1–10.
- Das, S. C., & Enamul, H. N. (2014). *Applications of Fibber Reinforced Polymer Composites (FRP) in Civil Engineering*. 03(03).
- Dong, K., Hu, K., & Gao, W. (2018). *Fire Behavior of Full-Scale CFRP-Strengthened*

- RC Beams Protected with Different Insulation Systems*. 7581.
<https://doi.org/10.3130/jaabe.15.581>
- EN 1992-1-2 (2004): Eurocode 2: Design of concrete structures - Part 1-2 (Vol. 2, Issue 2004)*. (2004).
- Evseeva, L. E., & Tanaeva, S. A. (1995). Thermophysical properties of epoxy composite materials at low temperatures. *Cryogenics*, 35(4), 277–279.
- Ferrándiz, V., Huesca, J. A., & García, E. (2014). *Normalized cement mortar with expanded polystyrene*. *Normalized cement mortar with expanded polystyrene*. October. <https://doi.org/10.13140/2.1.5013.2484>
- Firmo, P., Correia, R., & Bisby, L. A. (2015). *Fire behaviour of FRP-strengthened reinforced concrete structural elements : A state-of-the-art review*. 80, 198–216. <https://doi.org/10.1016/j.compositesb.2015.05.045>
- Gamage, J. C. P. H., Wong, M. B., & Al-mahaidi, R. (2006). Bond characteristics of CFRP plated concrete members under elevated temperatures. *Composites*, 75, 199–205. <https://doi.org/10.1016/j.compstruct.2006.04.068>
- Gamage, J., Wong, B., & Al-mahaidi, R. (2005). Performance of CFRP strengthened concrete members under elevated temperatures. *Proceedings of the International Symposium on Bond Behaviour of FRP in Structures, January*, 113–118.
- Ghosh, A., Ghosh, A., & Neogi, S. (2018). Reuse of fly ash and bottom ash in mortars with improved thermal conductivity performance for buildings. *Heliyon*, 4(July), 1–32. <https://doi.org/10.1016/j.heliyon.2018.e00934>
- González, A. S., Merino, M. R., Martínez, R. M., & Sáez, P. V. (2014). *Properties of Lightweight Plaster Materials Made With Expanded Polystyrene Foam (EPS)*. 413–417. <https://doi.org/10.1007/978-94-007-7790-3>
- Habeeb, G. A., & Mahmud, H. Bin. (2010). Study on Properties of Rice Husk Ash and Its Use as Cement Replacement Material 3 . Experimental Work 2 . Scope of Work. *Material Research*, 13(2), 185–190.
- Hu, K., He, G., & Lu, F. (2007). Experimental study on fire protection methods of

- reinforced concrete beams strengthened with carbon fiber reinforced polymer. *Frontiers of Architecture and Civil Engineering in China*, 1(4), 399–404. <https://doi.org/10.1007/s11709-007-0054-7>
- Irsyad, M., Pasek, A. D., Indartono, Y. S., & Pratomo, A. W. (2017). Heat transfer characteristics of building walls using phase change material. *1st International Symposium on Green Technology for Value Chains*, 60(1). <https://doi.org/10.1088/1755-1315/60/1/012028>
- Islam, G. M. S. (2014). *Application of FRP materials for strengthening of RC Structural Members. October 2017.*
- ISO-834. *Fire-resistance tests - Elements of building construction - Part 1: General requirements.* (1999).
- Johnson, B., Soltero, S., Stomski, D., & Teliska, A. (2017). *Investigation of the Thermal Properties of Rice Husk Ash in Cement.* Worcester Polytechnic Institute Submitted.
- Kami, A., Szoldra, P., & Fra, M. (2019). *Lightweight Cement Mortars with Granulated Foam Glass and Waste Perlite Addition Waldemar Pich or. 2019.*
- Karuppiyah, P. L., Angeline Prabhavathy, R., & Anantha Babu, R. (2016). A study on the behaviour of RC beams retrofitted using CFRP laminates under single point loading. *International Journal of Chemical Sciences*, 14, 302–310.
- Klamer, E. L., Horrdijk, D, A., & Janssen, H, J, M. (2015). The influence of temperature on the debonding of externally bonded CFRP. *Proceedings of 7th International Symposium on Fiber Reinforced Polymer Reinforcement for Concrete Structures 7*, 1–19.
- Kodur, V. R., Bisby, L. A., Green, M., & Chowdhury, E. U. (2005). *Fire Performance of FRP Systems for Infrastructure: A State-of-the-Art Report* (Issue National Research council, Ottawa). National Research council. <https://doi.org/10.4224/20377587>
- L, A. L. M., Jose, Y. S., & Jose, J. P. A. (2020). Experimental on Improving Thermal

- Comfort of Building using Locally Available Biomass Wastes. *International Journal of Recent Technology and Engineering*, 8(5), 145–150. <https://doi.org/10.35940/ijrte.E5091.018520>
- Leung, C. K. Y., & Lin, M. S. W. (2012). *HIGH PERFORMANCE CEMENTITIOUS MATERIALS WITH THERMAL*. 2012(June), 236–241.
- Li, L., Zhou, W., Dao, V., Ozbakkaloglu, T., & Liu, X. (n.d.). *Properties of cement-based materials containing fly ash. c*, 1543–1554.
- Maraveas, C., Miamis, K., Vrakas, A. A., & Partnership, C. M. (2014). *Fiber-Reinforced Polymer-Strengthened / Reinforced Concrete Structures Exposed to Fire: A Review*. November 2012. <https://doi.org/10.2749/101686612X13363929517613>
- Monokote ® Z-146PC. (2018). *Product Data sheet*. GCP applied technologies.
- Morsy, A., & Mahmoud, E. T. (2013). Bonding techniques for flexural strengthening of R.C. beams using CFRP laminates. *Ain Shams Engineering Journal*, 4(3), 369–374. <https://doi.org/10.1016/j.asej.2012.11.004>
- Palmieri, A., Matthys, S., & Taerwe, L. (2011). Bond behavior of NSM FRP bars at elevated temperatures. *First Middle East Conference on Smart Monitoring Assessment and Rehabilitation of Civil Structures (SMAR 2011)*.
- Petrella, A., Mundo, R. Di, & Notarnicola, M. (2020). *Recycled Expanded Polystyrene as Lightweight Aggregate for Environmentally Sustainable Cement Conglomerates*.
- Piyarathne, R. M. I. E., & Udamulla, K. M. L. A. (2016). Use of Bottom Ash in Replacement of River Sand in Making Cement Mortar. *ACEP Proceeding*, 191–197.
- Putra Jaya, R., Nor, M, M., Ahmad, Z, A., & Amin, Z, M. (2013). Properties of Mortar Containing Rice Husk Ash at Different Temperature and Properties of Mortar Containing Rice Husk Ash at Different Temperature and Exposed to Aggressive Environment. *Advanced Materials Research Vol., April 2014*.

<https://doi.org/10.4028/www.scientific.net/AMR.620.87>

- Qunitiere, J. G., & Veloo, P. S. (2011). *CONVECTIVE HEAT TRANSFER COEFFICIENT IN COMPARTMENT FIRES*.
- Rafi, M. M. (2010). *Analytical Behaviors of Steel and CFRP Reinforced Concrete Beams in Fire Analytical Behaviors of Steel and CFRP Reinforced Concrete. February 2015*. <https://doi.org/10.1520/JAI102641>
- Rafi, M. M., & Nadjai, A. (2014). *Analytical Method of Temperature Prediction in Reinforced Concrete Beams*. 5(4), 367–380.
- Saafi, M. (2002). Effect of fire on FRP reinforced concrete members. *Composite Structures*, 58, 11–20.
- Sadiq, H., Wong, M. B., Al-Mahaidi, R., & Zhao, X. L. (2014). *Heat transfer model for a cementitious-based insulation with moisture. July 2013*, 550–558. <https://doi.org/10.1002/fam>
- Salama, A. ., Ghanem, G. ., & S.F, A.-E. (2012). Behaviour of thermally protected RC beams strengthened with CFRP under dual effect of elevated temperature and loading. *HBRC Journal*, 8, 26–35.
- Salama, A. E., Ghanem, G. M., Abd-Elnaby, S. F., El-Hefnawy, A. A., & Abd-Elghaffar, M. (2012). Behavior of thermally protected RC beams strengthened with CFRP under dual effect of elevated temperature and loading. *HBRC Journal*, 8(1), 26–35. <https://doi.org/10.1016/j.hbrcj.2012.08.005>
- Schackow, A., Effting, C., Folgueras, M. V, Güths, S., & Mendes, G. A. (2014). Mechanical and thermal properties of lightweight concretes with vermiculite and EPS using air-entraining agent. *Construction and Building Materials*, 57, 190–197. <https://doi.org/10.1016/j.conbuildmat.2014.02.009>
- Shaik, S., Gorantla, K. K., & Setty, A. B. T. P. (2016). Investigation of Building Walls Exposed to Periodic Heat Transfer Conditions for Green and Energy Efficient Building Construction. *Procedia Technology*, 23, 496–503. <https://doi.org/10.1016/j.protecy.2016.03.055>

- Shon, C., Mukashev, T., Lee, D., Zhang, D., & Kim, J. R. (2019). *Can Common Reed Fiber Become an Effective Construction Material ? Physical , Mechanical , and Thermal Properties of Mortar Mixture Containing Common Reed Fiber*. <https://doi.org/10.3390/su11030903>
- Stoner, J. G. (2015). *Finite Element Modelling of GFRP Reinforced*.
- Sudheer, S., & Prabhu, S. V. (2010). Measurement of flame emissivity of gasoline pool fires. *Nuclear Engineering and Design*, 240(10), 3474–3480. <https://doi.org/10.1016/j.nucengdes.2010.04.043>
- Technical data sheet, S & P Resin 220 HP, High performance epoxy adhesive, (2004). *Technical data sheet (Adhesive)*. (n.d.).
- Technical data sheet (CFRP)*. (n.d.).
- Time and date*. (2020). <https://www.timeanddate.com/weather/sri-lanka/sri-jayawardenapura-kotte/hourly>
- Zeitler, M., & Munchen, F. (2010). *Thermal insulation material for building equipment* (pp. 274–304). <https://doi.org/10.1033/9781845699277.2.274>
- Zhang, C., & Usmani, A. (2015). Heat transfer principles in thermal calculation of structures in fire. *Fire Safety Journal*, 78, 85–95. <https://doi.org/10.1016/j.firesaf.2015.08.006>
- Zhang, J., Chen, B., Ph, D., & Yu, F. (2019). *Preparation of EPS-Based Thermal Insulation Mortar with Improved Thermal and Mechanical Properties*. 31(9), 1–9. [https://doi.org/10.1061/\(ASCE\)MT.1943-5533.0002825](https://doi.org/10.1061/(ASCE)MT.1943-5533.0002825).

ANNEXES

ANNEX A

A1. Sample Calculation of flexural performances

EBT-2

Table 40: Moment Capacity- Sample calculation

Reference	Calculations	Output
440.2R-08 Table 9.1	Design strength $f_{fu} = 0.95 \times 2800 = 2660 \text{ N/mm}^2$ Design strain $\epsilon_{fu} = 0.95 \times 0.016 = 0.019$	
ACI 318-05 Section 10.2.7.3	ratio of depth of equivalent rectangular stress block to depth of the neutral axis $\beta_1 = 1.05 - 0.05 \frac{f_c'}{6.9}$ $= 1.05 - 0.05 \frac{25}{6.9} = 0.868$	
440.2R-08	Area of FRP $A_f = n t_f w_f = 1.2 \times 150 = 180 \text{ mm}^2$ Dead load (DL) = beam weight = 240 N/m Corresponding moment $M_{DL} = \frac{0.24 \times 6^2}{8} = 1.08 \text{ kNm}$	$A_f = 180 \text{ mm}^2$
ACI 318-05	Cracked moment of inertia $I_{cr} = \frac{b k^3 d^3}{3}$ Where, $K = 0.334$; $I_{cr} = 1,356,919 \text{ mm}^4$ strain level in concrete substrate at time of FRP installation $\epsilon_{bi} = \frac{M_{DL}(d_f - kd)}{I_{cr} E_c} = \frac{1.08 \times 10^6 \times (100 - 0.344 \times 100)}{1356919 \times 23500}$	

Eq. (10-2)	$\varepsilon_{bi} = 6.1 \times 10^{-3}$ <p>design strain of FRP accounting for debonding failure mode $\varepsilon_{fd} = 0.41 \sqrt{\frac{25}{170000 \times 1.2}}$</p> $\varepsilon_{fd} = 0.0045 < 0.9 \times 0.016 = 0.0114$ <p style="text-align: center;">\Rightarrow Debonding failure will occur before FRP rupture</p> <p>Assume $c = 0.20d = 0.2 \times 545 = 109$ mm</p>	Ok
Eq. (10-3)	<p>Effective strain level in FRP $\varepsilon_{fe} = 0.003 \left(\frac{d_f - c}{c} \right) - \varepsilon_{bi}$</p> $\varepsilon_{fe} = 0.003 \left(\frac{600 - 109}{109} \right) - 0.00061 = 0.0131 > 0.0045$	$\varepsilon_{fe} = \varepsilon_{fd} = 0.0045$
Eq. (10-10)	<p>Concrete strain $\varepsilon_c = (\varepsilon_{fe} + \varepsilon_{bi}) \left(\frac{c}{d_f - c} \right)$</p> $\varepsilon_c = (0.0144 + 0.00061) \left(\frac{109}{609 - 109} \right) = 2.6 \times 10^{-3}$ <p>Stress in the FRP $f_{fe} = E_f \varepsilon_{fe} = 170000 \times 0.00114 = 1938 \text{ N/mm}^2$</p> $\varepsilon_c^1 = \frac{1.7 \times 25}{23500} = 0.0018$	$\varepsilon_c = 0.0026$

A2. FEM results for Bond line temperature

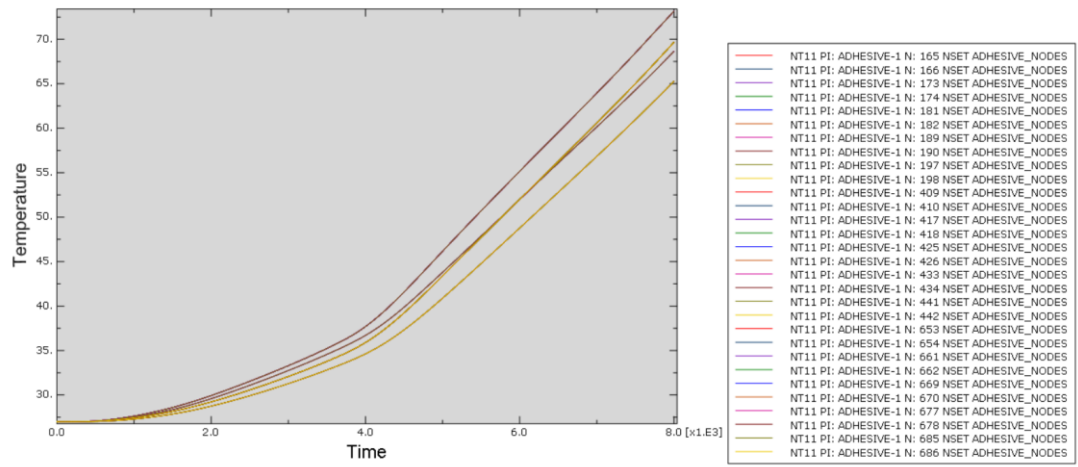


Figure 110. Bond line temperature for different nodes of B20_40 specimen when one side is exposed to ISO standard fire

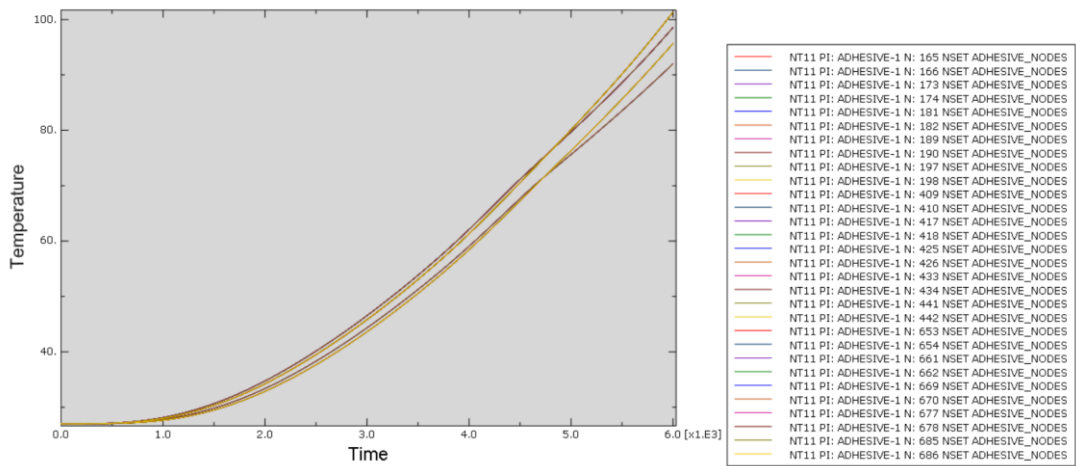


Figure 111. Bond line temperature for different nodes of B20_40 specimen when four sides are exposed to ISO standard fire

ANNEX B

B1. Heating and cooling curves obtained during thermal conductivity test

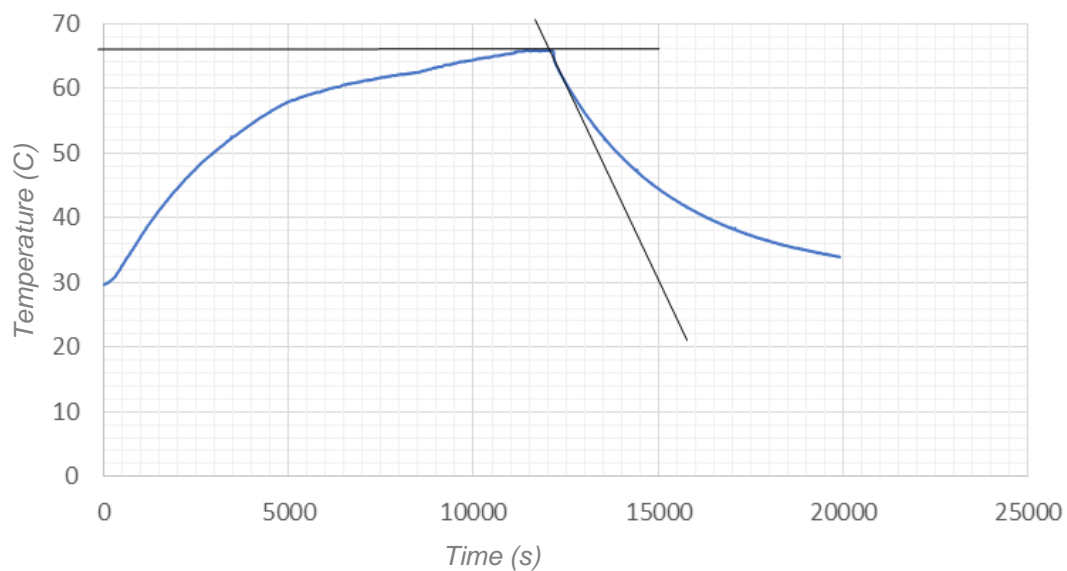


Figure 112. Heating & cooling curve of Vermiculite sample

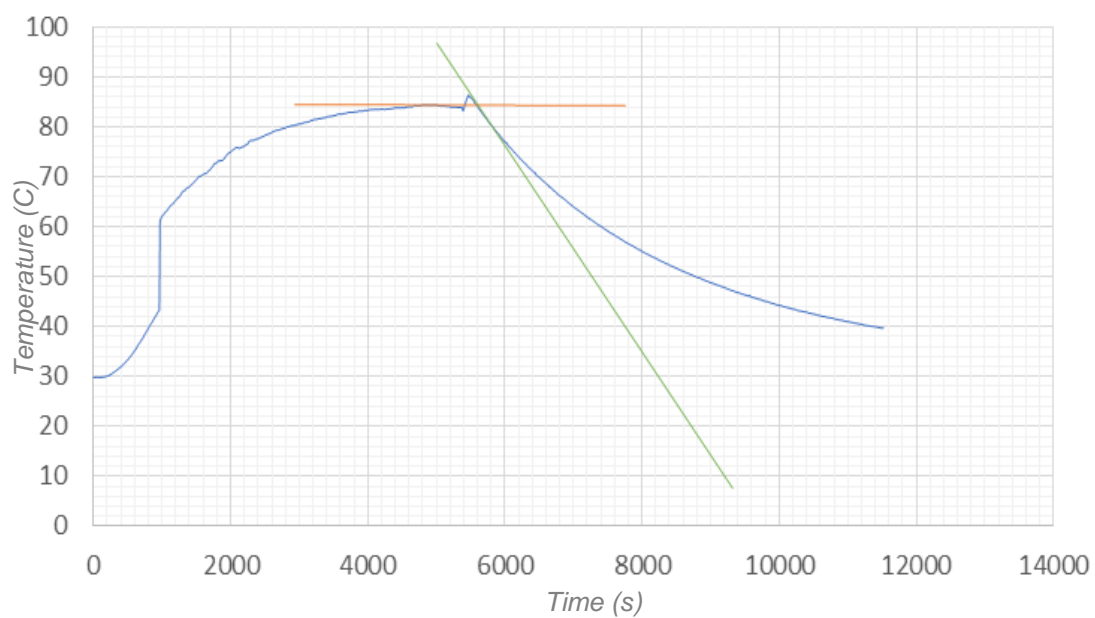


Figure 113. Heating & cooling curve of EPS-0-3 sample

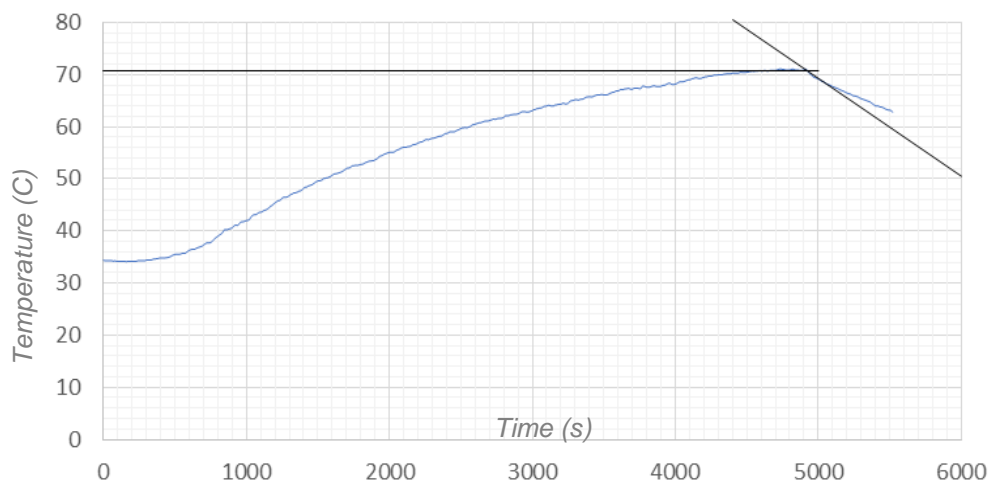


Figure 114. Heating & cooling curve of EPS-200 sample

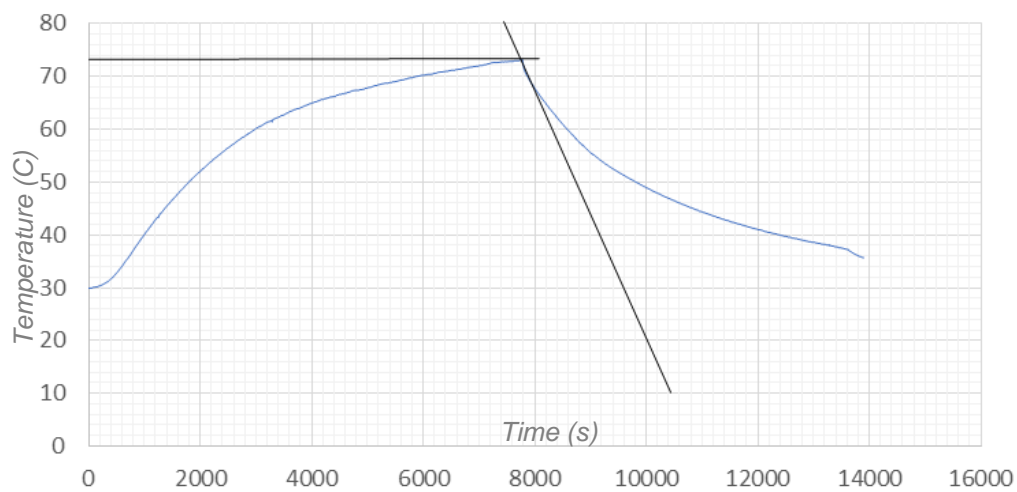


Figure 115. Heating & cooling curve of EPS-200-F sample

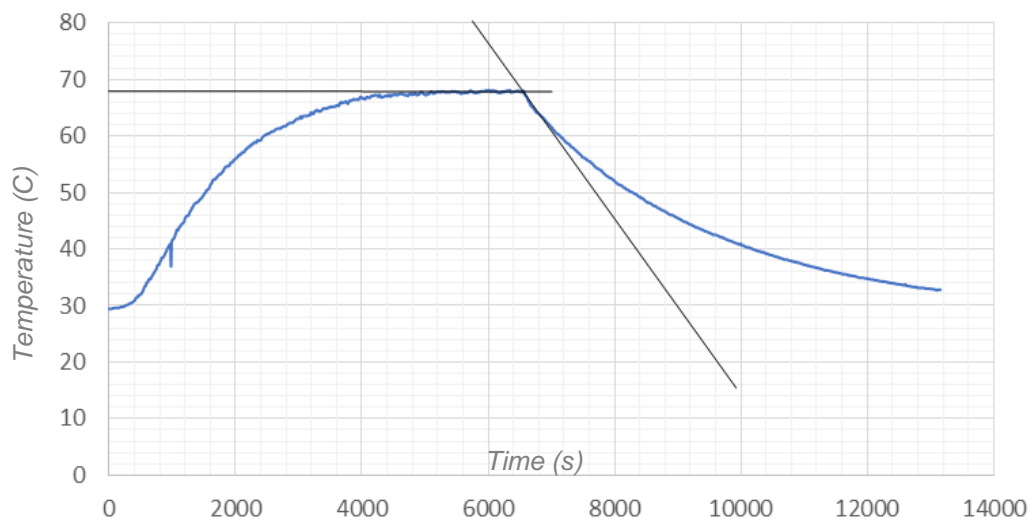


Figure 116. Heating & cooling curve of EPS-125-F sample

ANNEX C

C1. Theoretical analysis for transient heat transfer

Table 41: Finite difference method for temperature prediction

T _{m,j}	25	25	25	25	25	25	25	25	25
j+1	20	20	20	20	20	20	20	20	20
delta t	20	20	20	20	20	20	20	20	20
desnity,c,m	1800	1800	1800	1800	1800	1800	1800	1800	1800
specific,m,j	1065	1065	1065	1065	1065	1065	1065	1065	1065
m	0	0.0125	0.025	0.0375	0.05	0.0625	0.075	0.0875	0.1
delta y	0.0125	0.0125	0.0125	0.0125	0.0125	0.0125	0.0125	0.0125	0.0125
conductivity,m-1,j		1.2	1.2	1.2	1.2	1.2	1.2	1.2	1.2
conductivity,m,j	1.2	1.2	1.2	1.2	1.2	1.2	1.2	1.2	1.2
conductivity,m+1,j	1.2	1.2	1.2	1.2	1.2	1.2	1.2	1.2	1.2
temp,m-1,j	32	25	25	25	25	25	25	25	25
temp,m,j	25	25	25	25	25	25	25	25	25
temp,m+1,j	25	25	25	25	25	25	25	25	25
1	25	25	25	25	25	25	25	25	25
2	0.134	0.067	0.067	0.067	0.067	0.067	0.067	0.067	0.134
3	2.625	0	0	0	0	0	0	0	0
4	0	0	0	0	0	0	0	0	0
T _{m,j+1}	29	25	25	25	25	25	25	25	25

T _{m,j}	29	25	25	25	25	25	25	25	25
j+1	100	100	100	100	100	100	100	100	100
delta t	80	80	80	80	80	80	80	80	80
desnity,c,m	1800	1800	1800	1800	1800	1800	1800	1800	1800
specific,m,j	1065	1065	1065	1065	1065	1065	1065	1065	1065
m	0	0.0125	0.025	0.0375	0.05	0.0625	0.075	0.0875	0.1
delta y	0.0125	0.0125	0.0125	0.0125	0.0125	0.0125	0.0125	0.0125	0.0125
conductivity,m-1,j		1.2	1.2	1.2	1.2	1.2	1.2	1.2	1.2
conductivity,m,j	1.2	1.2	1.2	1.2	1.2	1.2	1.2	1.2	1.2
conductivity,m+1,j	1.2	1.2	1.2	1.2	1.2	1.2	1.2	1.2	1.2
temp,m-1,j	32	29	25	25	25	25	25	25	25
temp,m,j	29	25	25	25	25	25	25	25	25
temp,m+1,j	25	25	25	25	25	25	25	25	25
1	29	25	25	25	25	25	25	25	25
2	0.534	0.267	0.267	0.267	0.267	0.267	0.267	0.267	0.534
3	1.125	4.8	0	0	0	0	0	0	0
4	4.8	0	0	0	0	0	0	0	0
T _{m,j+1}	31	26.282	25	25	25	25	25	25	25

T _{m,j}	31	26.282	25	25	25	25	25	25	25
j=200; j+1=400	200	200	200	200	200	200	200	200	200
delta t	100	100	100	100	100	100	100	100	100
desnity,c,m	1800	1800	1800	1800	1800	1800	1800	1800	1800
specific,m,j	1065	1065	1065	1065	1065	1065	1065	1065	1065
m	0	0.0125	0.025	0.0375	0.05	0.0625	0.075	0.0875	0.1
delta y	0.0125	0.0125	0.0125	0.0125	0.0125	0.0125	0.0125	0.0125	0.0125
conductivity,m-1,j		1.2	1.2	1.2	1.2	1.2	1.2	1.2	1.2
conductivity,m,j	1.2	1.2	1.2	1.2	1.2	1.2	1.2	1.2	1.2
conductivity,m+1,j	1.2	1.2	1.2	1.2	1.2	1.2	1.2	1.2	1.2
temp,m-1,j	32	31	26.282	25	25	25	25	25	25
temp,m,j	31	26.282	25	25	25	25	25	25	25
temp,m+1,j	25	25	25	25	25	25	25	25	25
1	31	26.282	25	25	25	25	25	25	25
2	0.668	0.334	0.334	0.334	0.334	0.334	0.334	0.334	0.668
3	0.375	5.662	1.538	0	0	0	0	0	0
4	7.2	1.538	0.000	0	0	0	0	0	0
T _{m,j+1}	32	27.659	25.514	25	25	25	25	25	25

ANNEX D

D1. Copy of Publications

1. Selvaratnam, A., Gamage, J.C.P.H. (2020) ‘A Review on Thermo-mechanical behaviour of CFRP-Concrete composites at elevated temperature and available insulation systems’, *Lecture Notes in Civil Engineering*, Volume 94. pp. 9.
http://doi.org/10.1107/978-981-15-7222-7_43
2. Aaruga, S., Chandrathilaka, E.R.K. and Gamage, J.C.P.H. (2019), ‘Finite element Modelling on Flexural Performance of CFRP strengthened reinforced concrete curved beams’, *5th International multidisciplinary engineering research conference*, Moratuwa, Sri Lanka.
<http://doi.org/10.1109/MERCon.2019.8818797>
3. Selvaratnam, A. and Gamage, J.C.P.H. (2019), ‘Effect of steel reinforcement ratio on flexural enhancement in CFRP-strengthened concrete curved beams’, *10th International Conference on Sustainable Built Environment*, Kandy, Sri Lanka, 12-14 December.
4. Aaruga, S. and Gamage, J.C.P.H. (2019), ‘Numerical modelling of effect of anchorages on flexural behaviour of CFRP-strengthened reinforced concrete curved beams’, *75th Annual session of Sri Lanka Association for the advancement of Science*, Sri Lanka, 2 – 6 December.
5. Selvaratnam, A., Gamage, J.C.P.H. and De Silva, G.I.P. (2020) ‘EPS blended cementitious plaster for improved thermal comfort in buildings’ *11th International Conference on Sustainable Built Environment*, Kandy, Sri Lanka, 10-12 December 2020. (Submitted)

A Review on Thermo-mechanical Behaviour of CFRP-Concrete Composites at Elevated Temperature and Available Insulation Systems



A. Selvaratnam and J. C. P. H. Gamage

Abstract The use of Carbon Fibre Reinforced Polymer (CFRP) composites have become a prominent solution for retrofitting the concrete structures. Though CFRP composites have superior mechanical properties, resistance of CFRP/Concrete composites to fire remains unsolved. The degradation of the epoxy resin at elevated temperature makes the FRP composites weaker due to the low glass transition temperature of epoxy resin. A review on CFRP-concrete composites at elevated temperature and available insulation systems are presented in this paper. The paper summarises the results obtained from experimental and numerical studies on the fire performance of CFRP-concrete composites. Hence, it was concluded that by providing appropriate insulation system, the CFRP-concrete members can be protected from fire. However, there are several drawbacks with available insulation systems, such as high cost, addition of dead load, and less aesthetic appearance which are also discussed in this paper.

Keywords CFRP/Concrete composites · Insulation system · Fire resistance · Elevated temperature

1 Introduction

Investigation on application of Fibre Reinforced Polymer (FRP) materials was started in 1980s due to its rapid use in the Construction industry [10]. FRP composites are produced by embedding high strength fibres into the polymer matrix and hence, they achieve excellent properties such as high strength to weight ratio, low conductivity, and flexibility [3]. Generally, the fibres have high strength and the matrix helps to protect the fibres from degradation and to transfer the stresses between fibres [22]. Though FRP composites have excellent mechanical and thermal behaviour at service temperature, it's properties get drastically affected at elevated temperature due to the low glass transition temperature (T_g) of epoxy resin [13].

A. Selvaratnam (✉) · J. C. P. H. Gamage
Department of Civil Engineering, University of Moratuwa, Moratuwa, Sri Lanka
e-mail: aaruga93@gmail.com

When the FRP composites are heated to high temperature, the consistency of the resin will change from brittle to viscous [11, 17]. This process is called as “Glass transitioning” and glass transition temperature for epoxy resin varies from 50 °C to 100 °C [5, 6]. Beyond the T_g , all polymer resins will soften and eventually ignite and makes the resin matrix weaker. Therefore, the mechanical properties such as bond strength, tensile strength, and elastic modulus of the FRP composites drastically reduces [7, 11, 13, 17].

Fire resistance is a key property for construction materials and typically varies from 30 to 240 minutes depending on the requirements [9]. Several researches have been focused on the behaviour of FRP strengthened concrete members subjected to fire and it was found that the epoxy layer reaches the T_g within 5–6 min under exposure to the standard fire [13]. Therefore, it is required to provide adequate fire resistance for CFRP strengthened members to ensure the integrity between FRP and concrete at elevated temperature. The suitability of several insulation systems for CFRP-concrete members such as calcium silicate board, ultra-thin coating, Vermiculite, Vermitex, and perlite have been investigated in recent times [12, 16, 21].

2 The Behaviour of FRP-Concrete Members Under Elevated Temperatures

Strengthening the concrete structures using FRP composites was found as a successive solution over the last two decades. The two widely used techniques are the Externally bonded reinforcement (EBR) technique and Near-surface mounted (NSM) technique where NSM technique has many advantages such as larger bond surface, high resistance to peeling-off, and less installation time [1]. Szabo et al. have shown that using the same amount of laminate, a higher flexural performance can be achieved in the NSM technique compared to EBR technique [23].

Many researchers have investigated the bond performance of CFRP strengthened concrete members at elevated temperature. Blontrock et al. conducted a double-lap shear test on concrete member strengthened with CFRP laminates using EBR technique and the noted bond strength percentages were 141%, 124%, and 82% at 40 °C, 55 °C, and 70 °C, respectively [4]. And a concrete cohesive failure was observed at ambient temperature and concrete-adhesive interface failure was observed at elevated temperature. Gamage et al. performed a single-lap shear test on CFRP sheet bonded concrete blocks and they have also observed strength reduction with increasing temperature. A combination of bond failure and concrete rupture was noted in low temperatures less than 50 °C. And peeling-off of the CFRP sheet was the recorded failure pattern for the samples tested at high temperatures greater than 60 °C [14]. The proposed relative strength variation of CFRP-epoxy-concrete bond obtained by Gamage et al. is shown in Fig. 1.

Palmieri et al. have investigated the concrete members strengthened with CFRP strips and rods using NSM technique at a temperature between 20 °C and 100 °C.

Fig. 1 Proposed relative strength variation of CFRP/epoxy/concrete bond [14]

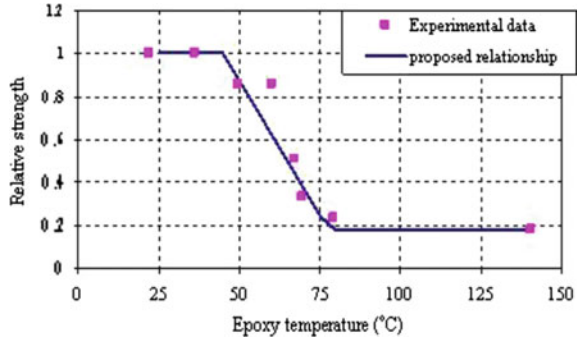
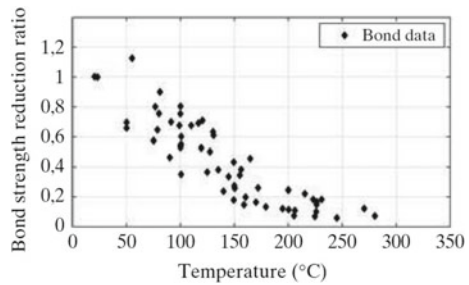


Fig. 2 Variation of bond strength with temperature [17]



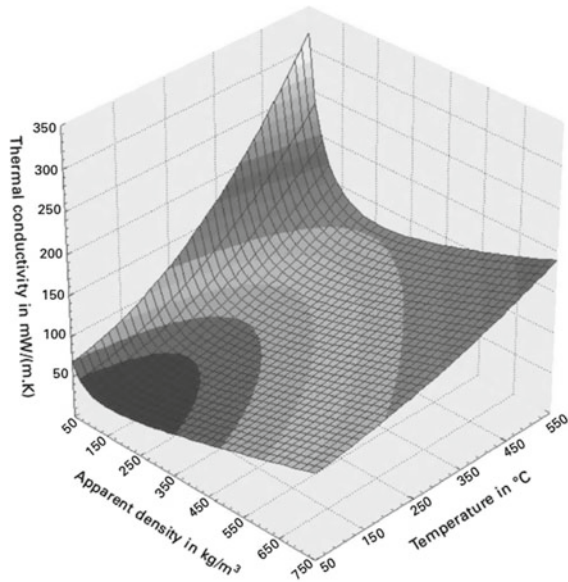
They also noted that the bond strength increases below the adhesive T_g and decreases above T_g . The failure mode changed from a combined failure of debonding and splitting of resin to combined failure of debonding at CFRP-epoxy interface and pull-out of the CFRP strips/bars [18]. Maraveas et al. have reviewed the CFRP-Concrete structures exposed to fire and suggested that the temperature can compromise the bond between the concrete and FRP [17]. The variation in the bond strength obtained by Maraveas et al. is shown in Fig. 2.

The tensile strength of FRP composites plays also an important role when determining the load carrying capacity of FRP strengthened concrete members. The effect of temperature on the tensile strength and elastic modulus have investigated by several researchers [11, 17]. It was noted that the tensile strength of FRP materials reduces similarly with increasing temperature. However, the tensile strength of epoxy reduces suddenly when the temperature reaches the T_g . Similar behaviour was observed in the tensile modulus also, with increasing temperature.

3 Thermal Insulation Materials

The major parameters affecting the performance of thermal insulation materials are thermal conductivity, temperature, specific heat, thermal resistance, density, open joints, convection, moisture, ageing, and permeability [19, 24]. However, thermal

Fig. 3 Thermal conductivity of insulation materials depending on apparent density and temperature [24]



conductivity is the key property of thermal insulation materials in the general strategy [20]. The thermal conductivity of a material is depended on the temperature and the apparent density [20]. The interdependence of the conductivity on temperature and apparent density is shown in Fig. 3. It was noted that the effect of thickness on thermal conductivity is small compared to the effect of temperature [24].

Most widely used thermal insulation materials for building constructions are Mineral fibre (0.03–0.04 W/m K), Cellulose (0.04–0.05 W/m K), Expanded polystyrene (EPS) (0.036 W/m K), Polyurethane (0.03–0.04 W/m/K), Vermiculite (0.06–0.12 W/m K), Aerogel (0.013 W/m K) [15, 20]. Among various thermal insulation materials, the appropriate material should be selected depending on the cost, durability, strength, fire resistance, airtightness, availability, environmental impact, and ease of application [2].

4 Thermal Insulation Systems for FRP-Concrete Members

Many researchers have investigated the insulation systems to provide protection for the CFRP-concrete composites during the fire. Dong et al. have investigated the fire behaviour of CFRP-bonded reinforced concrete beams with various insulation systems [8]. Four similar CFRP strengthened reinforced beams were cast and insulated completely using 50 mm thick coating (L1), partially using 50 mm thick coating (L2), completely using 40 mm thick calcium silicate board (L3), and completely using 1.5 mm thick ultrathin coating (L4). The anchorage zone of the beams was in the fire

except the beams insulated using the thick coating. In this study, the main intention of fire protection materials was to delay the adhesive failure and hence reduce the degradation of CFRP-concrete beams. The cross sections of CFRP-strengthened beams with the insulation scheme are shown in Fig. 4.

Gamage et al. have studied the bond characteristics of CFRP plated concrete members during the fire [13]. A three-dimensional numerical model has been simulated to investigate the heat effects and validated using experimental results. Concrete with compressive strength 55 MPa was used to this study. 0.176 mm thickness CFRP laminates were bonded to the surface of the concrete member with the use of epoxy adhesive. After revealing the need of insulation, Vermitex-TX was used as an insulation material for fire protection, which thermal conductivity is 0.127 W/m K. The finite element model of CFRP-concrete specimen with insulation is shown in Fig. 5. It was noted that the thermal conductivity and the thickness of the insulation layer affect the fire resistance of the CFRP-concrete specimen significantly. It was also observed that the bond length does not have considerable effects on the fire resistance [12]. Fire resistance of 1.76 h was able to achieve using a 50 mm thick Vermitex layer.

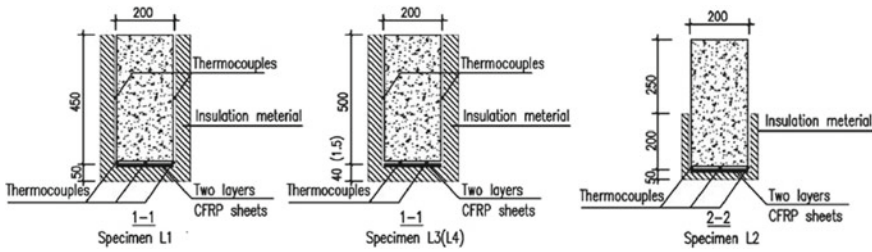
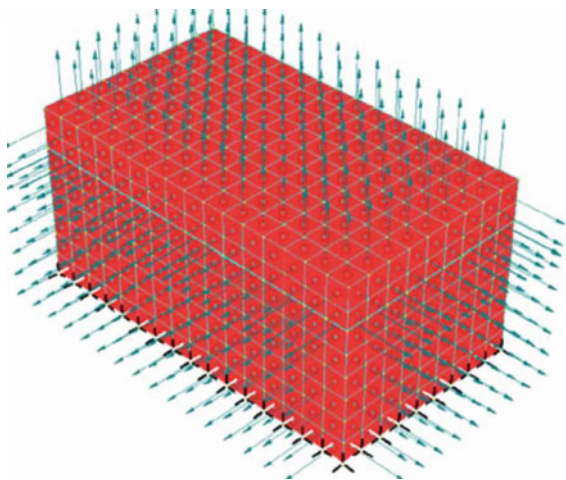


Fig. 4 Insulation and thermocouple details for specimens [8]

Fig. 5 Finite element model of insulated CFRP-concrete specimen [13]



Salama et al. investigated the behaviour of CFRP strengthened RC beams subjected to the dual effect of elevated temperature [21]. Six distinct cement-based mixes using Perlite and Vermiculite were developed to obtain the most appropriate mix which gives both, low thermal conductivity, and adequate strength. The thermal conductivities were tested according to ASTM C177-07 and the obtained thermal conductivities for Perlite, and Vermiculite mortar were in the range of 0.158–0.277 W/m K, and 0.329–0.396 W/m K, respectively. The developed mixes were applied on reinforced concrete beams as cement rendering up to 5 cm thickness. All the beams covered by thermal insulation layer showed no loss in the capacity up to 500 °C temperature.

Firno and Correira also investigated the performance of flexural strengthened reinforced concrete beams with EBR CFRP strips and NSM CFRP strips [10]. The focus of this study was understanding the structural effectiveness of CFRP retrofitting systems during the fire and evaluating the efficiency of fire protection. Calcium silicate (CS) boards were used as the insulation material at the bottom surface of the beam. The EBR-CFRP and NSM-CFRP strengthened beams insulated with CS boards are shown in Fig. 6a, b, respectively.

The thickness of the insulation layer ranged from 0 to 50 mm. A numerical model was simulated to analyse the fire performance using an advanced finite element software. A two-point loading was applied to investigate the structural performance of the beams subjected to ISO 834 fire. The results confirmed that the NSM technique has a better fire resistance compared to EBR technique irrespective from the insulation thickness. It was also noted that the higher the thickness of the insulation layer, higher the fire resistance. The comparison of fire resistance of NSM and EBR strengthening system with different thickness insulation layer is shown in Fig. 7.

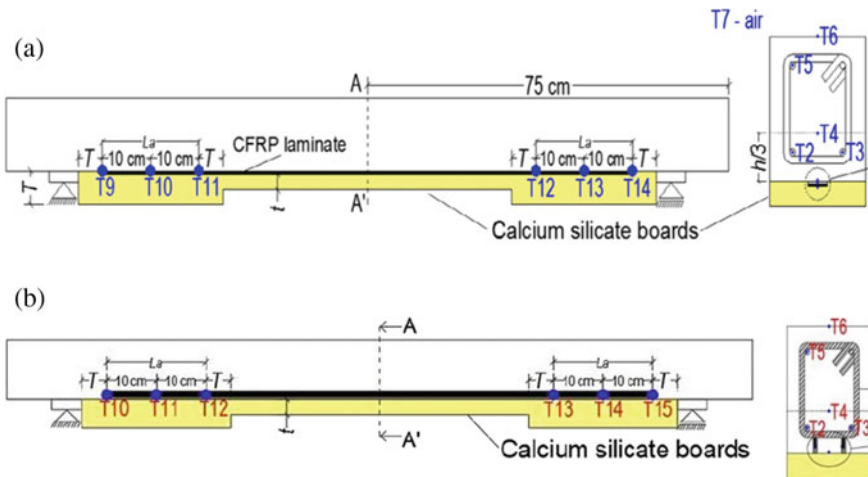
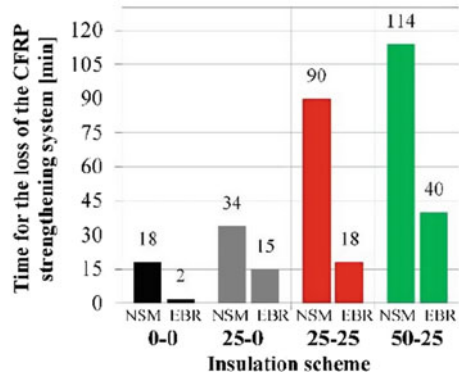


Fig. 6 a EBR-CFRP-strengthened RC beams with CS boards [10]. b NSM-CFRP-strengthened RC beams with CS boards [10]

Fig. 7 Comparison between the fire performance of EBR and NSM strengthening systems [10]



5 Conclusions

This paper discussed the behaviour of CFRP-strengthened beams during the fire and the effect of available insulation systems. In order to predict the thermo-mechanical behaviour of CFRP-concrete members at elevated temperature, bond tests and flexural tests could be conducted. Generally, the single-lap shear tests, double-lap shear test, and pull-out tests were the most widely used bond tests to predict the bond performance between CFRP-epoxy-concrete. Many researchers have concluded that by using appropriate insulation to CFRP-concrete member, the required fire resistance can be achieved. The adhesive temperature, insulation thickness, thermal conductivity, rate of heating, and CFRP amount were noted as the key factors affecting the thermal resistance of the insulation system. And the bond length, insulation density, and the specific heat capacity of insulation material were found as less susceptible parameters.

Further, several investigations have concluded that the NSM-CFRP concrete members have relatively high fire resistance compared to the EBR-CFRP concrete members. However, majority of the researchers have shown that, in order to achieve a fire resistance of 2 h, more than 50 mm thickness of insulation is required if the thermal conductivity of insulation is greater than 0.12 W/mK result in high cost. This will cause for additional dead load transfer to the structural members. Therefore, further investigations are required to overcome such problems in the fire performance of CFRP-strengthened members.

Acknowledgements The authors would like to express their sincere gratitude to all the staff in Building materials Laboratory of Department of Civil Engineering, University of Moratuwa. The financial support provided by National Research Council, Sri Lanka; grant number PPP 18-01 is greatly appreciated.

References

1. Aaruga S (2019) Finite element modelling on flexural performance of CFRP strengthened reinforced concrete curved beams. In: Moratuwa engineering research conference (MERCCon). IEEE, pp 662–667. Available at: <https://doi.org/10.1109/MERCCon.2019.8818797>
2. Al-homoud MS (2005) Performance characteristics and practical applications of common building thermal insulation materials. *Build Environ* 40:353–366. <https://doi.org/10.1016/j.buildenv.2004.05.013>
3. Arunothayan R, Gamage JCPH (2016) Modelling of CFRP strengthened concrete beam to quantify the effects of bond parameters in flexure. In: 7th international conference on sustainable built environment, p 8
4. Blontrock H (2003) Analysis and modeling of the fire resistance of concrete elements with externally bonded FRP reinforcement. Ghent University, Ghent, Belgium
5. Blontrock H, Taerwe L, Vandeveldel P (2017) Fire testing of concrete slabs strengthened with fibre composite laminates, thermal and external effects
6. Chandrathilaka ERK, Gamage JCPH, Fawzia S (2018) Mechanical characterization of CFRP/Steel bond cured and tested at elevated temperature. *Compos Struct*. <https://doi.org/10.1016/j.compstruct.2018.09.048>
7. Chowdhury EU, Bisby LA, Green M (2011) Mechanical characterization of fibre reinforced polymers materials at high NRCC-50851 (May 2014). <https://doi.org/10.1007/s10694-009-0116-6>
8. Dong K, Hu K, Gao W (2018) Fire Behavior of full-scale CFRP-strengthened RC beams protected with different insulation systems. *J Asian Archit Build Eng* 7581:9. <https://doi.org/10.3130/jaabe.15.581>
9. EN 1992-1-2 (2004): Eurocode 2: Design of concrete structures—Part 1-2 (2004)
10. Firmo JP, Correia JR (2015) ‘Fire behaviour of thermally insulated RC beams strengthened with NSM-CFRP strips: experimental study. *Compos B Eng* 76:112–121. <https://doi.org/10.1016/j.compositesb.2015.02.018>
11. Firmo P, Correia R, Bisby LA (2015) Fire behaviour of FRP-strengthened reinforced concrete structural elements: a state-of-the-art review. *Compos B* 80:198–216. <https://doi.org/10.1016/j.compositesb.2015.05.045>
12. Gamage JCP, Al-mahaidi R, Wong B (2005) Effect of insulation on the bond behaviour of CFRP-plated concrete elements. In: Proceedings of the international symposium on bond behaviour of FRP in structures, pp 119–123
13. Gamage JCPH, Wong MB, Al-mahaidi R (2006) Bond characteristics of CFRP plated concrete members under elevated temperatures. *Compos struct* 75:199–205. <https://doi.org/10.1016/j.compstruct.2006.04.068>
14. Gamage J, Wong B, Al-mahaidi R (2005) Performance of CFRP strengthened concrete members under elevated temperatures. In: Proceedings of the International Symposium on Bond behaviour of FRP in Structures, pp 113–118
15. Hawileh RA (2014) Heat transfer analysis of reinforced concrete beams reinforced with GFRP bars (October 2011), pp 299–314. <https://doi.org/10.5772/22236>
16. Hu K, He G, Lu F (2007) Experimental study on fire protection methods of reinforced concrete beams strengthened with carbon fiber reinforced polymer. *Front Archit Civil Eng China* 1(4):399–404. <https://doi.org/10.1007/s11709-007-0054-7>
17. Maraveas C et al (2012) Fiber-reinforced polymer-strengthened/reinforced concrete structures exposed to fire: a review. *Struct Eng Int* 4(November 2012):500–513. <https://doi.org/10.2749/101686612X13363929517613>
18. Palmieri A, Matthys S, Taerwe L (2011) Bond behavior of NSM FRP bars at elevated temperatures. In: First Middle East conference on smart monitoring assessment and rehabilitation of civil structures, Dubai, p 8
19. Papadopoulos AM (2005) State of the art in thermal insulation materials and aims for future developments. *Energy Build* 37:77–86. <https://doi.org/10.1016/j.enbuild.2004.05.006>

20. Petter B (2011) Traditional, state-of-the-art and future thermal building insulation materials and solutions—properties, requirements and possibilities. *Energy Build J* 43(7465):2549–2563. <https://doi.org/10.1016/j.enbuild.2011.05.015>
21. Salama AE et al (2012) Behavior of thermally protected RC beams strengthened with CFRP under dual effect of elevated temperature and loading. *HBRC J* 8(1):26–35. <https://doi.org/10.1016/j.hbrcj.2012.08.005>
22. Stoner JG (2015) Finite element modelling of GFRP reinforced concrete beams
23. Szabo Z, Balazs G (2007) Near surface mounted FRP reinforcement for strengthening of concrete structures. *Periodica polytechnica; Civil Eng* 51(1):33–38. Available at: <https://doi.org/10.3311/pp.ci.2007-1.05>
24. Zeitler M, Munchen F (2010) Thermal insulation material for building equipment, pp 274–304. <https://doi.org/10.1033/9781845699277.2.274>

Finite Element Modelling on Flexural Performance of CFRP Strengthened Reinforced Concrete Curved Beams

S.Aaruga

Department of Civil Engineering
University of Moratuwa
Moratuwa, Sri Lanka
aaruga93@gmail.com

E.R.K. Chandrathilaka

Department of Civil Engineering
University of Moratuwa
Moratuwa, Sri Lanka
kanishkachandrathilaka@gmail.com

J.C.P.H.Gamage

Department of Civil Engineering
University of Moratuwa
Moratuwa, Sri Lanka
kgamage@gmail.com

Abstract—A numerical model was developed to investigate the flexural performance of Carbon Fibre Reinforced Polymer (CFRP) strengthened concrete curved beams subjected to out-of-plane bending. In this study, near surface mounted (NSM) technique has been used to strengthen the curved beams due to easy of application in curved beams subjected to out-of-plane bending. A commercially available finite element analysis software was used to simulate a numerical model and a non-linear analysis was carried out. Alternative bonding arrangements were considered. The results indicate the highest strength performance in the curved beams with CFRP strip bonded in the radial direction of the beams. Further, it was revealed that the CFRP thickness, Elastic Modulus of CFRP, Concrete Grade, and the beam curvature affect the strength enhancement.

Keywords— CFRP, FEM, NSM, Curved beams, out-of-plane bending

I. INTRODUCTION

In recent years, Fibre Reinforced Polymer (FRP) application in the Civil Engineering industry has been significantly increased due to their superior properties. FRP materials were initially introduced in the aerospace and automotive industries due to their high strength to weight ratio. Later, due to the shortcomings in Civil engineering industry, FRPs have been started utilizing and it was found an excellent solution for retrofitting the structures.

Several researchers have investigated the behaviour of CFRP strengthened Concrete straight beams [1] – [5]. The behaviour of CFRP strengthened Reinforced Concrete (RC) straight beams have been investigated by Arunothayan et al. [3]. This study revealed that the load carrying capacity of RC beams can be increased in the range between 80%-110% with CFRP laminates and the flexural capacity can be further enhanced by providing end anchorages. Another experimental investigation was carried out by Hosen et al and it was found that the ultimate load capacity can be increased by 92% using NSM CFRP retrofitting technique [4]. Various failure modes were observed in FRP strengthened straight beams [6], [7] and the major failure modes were found as Pre-mature (Debonding) failure modes and classical failure modes [3]. Comparing to the Plate bonding technique, near surface mounted technique has many advantages [7]. The larger bond surface induces better anchorage capacity. It provides higher

resistance against peeling-off, so it has a higher percentage of the tensile strength, and less installation time [7]. Further, Szabo et al. have found that the same amount of NSM reinforcement provides a higher load carrying capacity compared to the EBR technique [7].

There are many applications of Concrete curved beams in Civil Engineering infrastructures in recent times. However, strengthening the reinforced concrete curved beams with out-of-plane bending have not been investigated according to available research data. Therefore, the attention was given to see the possibilities of application of CFRP strengthening technology in concrete curved beams. Conducting experiments on CFRP strengthened curved beams have many drawbacks such as cost, time, and technical feasibility. Therefore, developing a finite element model is more reliable and productive in parametric studies. Several FEM models have been simulated to analyze the FRP strengthened RC straight beams using external bonding technique and as well as a near-surface mounted technique [1], [2], [9]. In this research, a numerical model was developed to evaluate the flexural performance of CFRP strengthened concrete curved. The outcome of this research can be used for retrofitting the reinforced concrete curved beams subjected to out of plane bending using CFRP technology.

II. FINITE ELEMENT MODELLING

Finite element method is the widely used discretization technique in structural analysis and other engineering

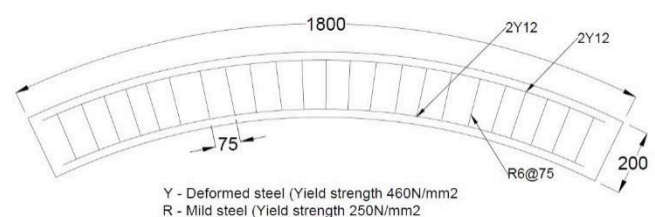


Fig. 1. Reinforcement details (Plan view)

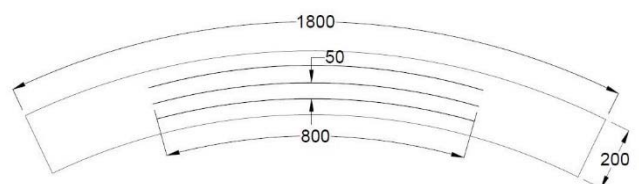


Fig. 2. Schematic diagram of the arrangement of Grooves (Plan view – bottom surface)

applications. This simulation can be conducted either two dimensional (2D) or three dimensional (3D) models, depending on their suitability. Though 2D models are less complicated and have less running time, its results are always less accurate. Therefore, a 3D numerical model was chosen for this study.

TABLE I. MECHANICAL PROPERTIES OF GRADE 30 CONCRETE [9]

Density	2400kg/m ³
Elastic modulus	25 GPa
Poisson ratio	0.2
Initial equibiaxial compressive yield stress/ initial uniaxial compressive yield stress	1.16
Eccentricity	0.1
Stress invariant	0.667
Dilation angle	36°
Viscosity	0

Reinforced Concrete curved beams with 2000 mm radius were modelled using Abaqus/Explicit 6.14. 200 mm x 200 mm cross-sections were used for the beam. Reinforcement details of the beam are shown below in Fig. 1.

The reinforced concrete beam was grooved at 3 locations along the beam with a 15 mm deep and 10mm wide channel for 800 mm length. 10 mm wide CFRP strips were embedded into the grooves with epoxy adhesive. The groove arrangement is shown in Fig. 2 and the cross-section of CFRP strengthened curved beam is shown in Fig. 3.

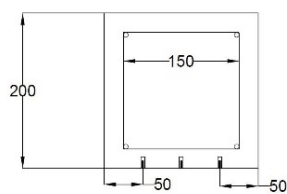


Fig. 3. Cross section of the strengthened beam

Note: All the dimensions are in millimeters

A. Element Types and Interactions

According to the available elements in Abaqus/Explicit package eight-node brick (C3D8) element was used to model the concrete beam and adhesive layer. Two-node linear beam (B31) elements, and four-node doubly curved thin or thick shell (S8R5) were used for steel reinforcement, and CFRP plates respectively. A mesh sensitivity analysis was carried out to obtain the appropriate mesh size.

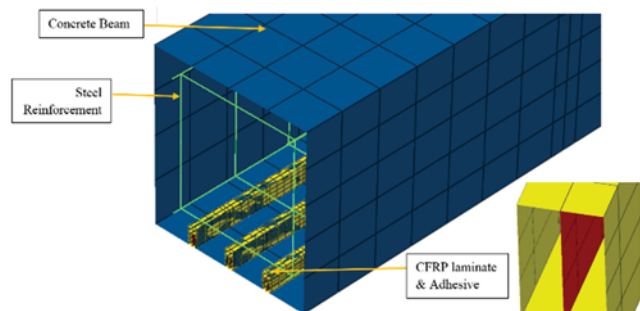


Fig. 4. Finite element mesh

The interaction between steel bars and the concrete beam was assumed as embedded constraint where the nodes of steel

bars are slave nodes and nodes of concrete are host nodes. Similarly, the interaction between the CFRP plate and epoxy resin was also modelled. A surface-surface tie constraint was assumed modelling the interaction between concrete and adhesive.

B. Material Properties

1) Concrete

Grade 30 concrete was used, and a non-linear analysis was carried out to predict the flexural performance of the beams. A concrete damaged plasticity model was used which can represent the complete inelastic behaviour of concrete in tension and compression including the damage parameters. All the elastic and plastic properties of the concrete are listed below in table I [9].

The concrete damaged plasticity model considers two main failure mechanisms and they are compressive crushing and tensile cracking [10]. Hence, it is applicable in this modelling, as it has been successfully used in several past studies [10], [12].

To define the compressive stress-strain relationship, stresses (σ_c), inelastic strains (ϵ_c^{in}) and corresponding damage properties are required to input. Damage parameter (d_c) is the ratio between the inelastic strain and the total strain. To obtain the compressive behaviour a verified numerical method by Hsu and Hsu [11], Wahalathantri's model [12], and Abaqus Manual [10] were used.

Stresses (σ_t), cracking strains (ϵ_t^{ck}) and corresponding damage properties (d_t) are required to define the complete tensile stress-strain behaviour of concrete. The damage parameter is the ratio between the cracking strain and total strain. Wahalathantri's model [12], and ABAQUS Manual [10] were used to develop the tension stiffening relationship of the concrete.

2) Steel

Linear elastic behaviour of steel was assumed. Deformed steel bars were used to model the top & bottom reinforcement and the stirrups. Two numbers of 12 mm diameter deformed steel bars were used for the top and bottom reinforcements. 6 mm diameter rebars were used for stirrups in 75 mm spacing. Tensile strength of deformed steel and plain steel was 460 N/mm² and 250 N/mm², respectively. Elastic modulus and Poisson ratio were taken as 200 GPa and 0.3 respectively [13].

3) CFRP

Mechanical properties of 1.5 mm thick CFRP Laminates were used for strengthening. Linear elastic behaviour of CFRP plate was assumed. Manufacturer provided [15] tensile strength, Elastic Modulus, and Density 2800 N/mm², 190 GPa, and 1600 kg/m³, respectively. The Poisson ratio was assumed as 0.3

4) Adhesive

The two-part epoxy adhesive was used as a bonding agent. The brittle cracking behaviour was assumed to model the adhesive layer. The manufacturer provided [16] material properties; Tensile strength – 23 N/mm² and Tensile modulus – 10 GPa were used. Density and Poisson ratio were assumed as 1300 kg/m³ and 0.3, respectively.

C. Beam Specifications

Two models were developed where one was the control beam (C1) and the other one was the CFRP strengthened beam (CF1).

D. Boundary Conditions and Loading

Both ends of the beams were partially fixed (Fig. 5). i.e. Lateral horizontal rotation and longitudinal displacement were released to obtain this boundary condition. To test under four-point bending, uniform transient displacements were applied at one-third of the beam.

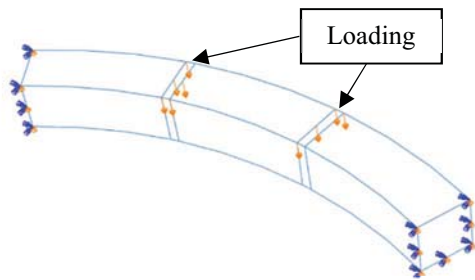


Fig. 5. Loading and boundary conditions

III. RESULTS AND VALIDATION

A. Non-strengthened Beams

The deformed shape of the control beam (C1) is shown below in Fig. 6. A larger magnitude of deflection has been observed at the outside of the mid-span, and it has been proved by Tamura & Murata [17]. It was also observed that the curved beam has been displaced vertically as well as laterally. The control beam failed in flexure. The crack propagation of C1 beam is shown in Fig. 7.

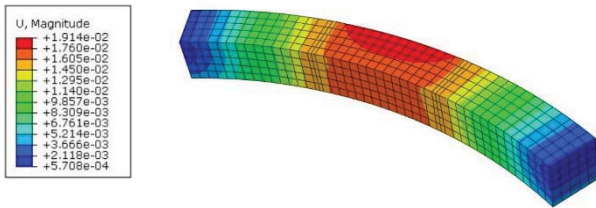


Fig. 6. Deformation of C1 model at Ultimate failure



Fig. 7. Strain contours related to crack profile of C1 model

Curved beam C1 with fixed support was validated using existing literature [17]. Grade 30 concrete with shear span to depth ratios (a/d) 3.2 (S1) and 2.5 (S2) were modelled with an axial bar according to the experimental program by Tamura & Murata [17]. All the parameters were modelled similar to the literature and its load vs deflection was compared (Fig. 8). Comparison of model predicted results with test results done by Tamura & Murata [17] is listed in table II.

TABLE II. FAILURE LOADS

Analysis	S1	S2
Experiment [17]	135.3 kN	169.8 kN
FEM	131.5 kN	162.9 kN
% difference	2.8%	4.1%

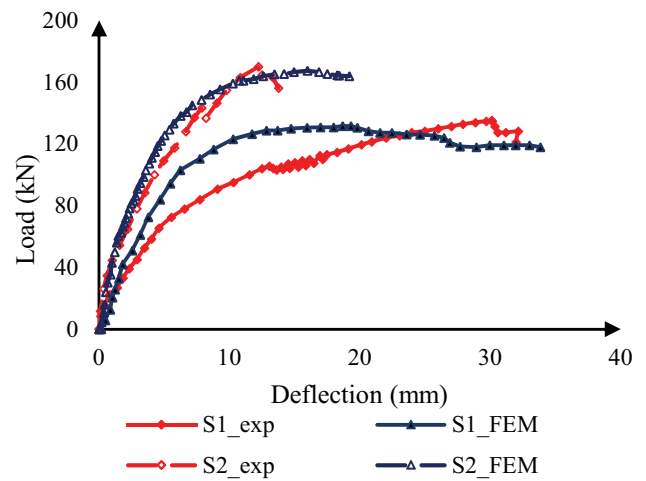


Fig. 8. Comparison of Load vs vertical deflection at mid span

Initially, both experiment and numerical models indicate similar behaviour within its elastic region in both shear span-depth ratios. With load increment, the numerical model shows stiffer behaviour than the experiment one in both cases. This might be due to the theoretically obtained stress-strain behaviour of Grade 30 Concrete. However, the percentage difference in ultimate load becomes less than 5% for both shear span-depth ratios. Hence, the predicted results indicate the accuracy of the model developed to predict the performance of non-strengthened beams.

B. CFRP-strengthened Beams

The deformed shape of the CF1 beam model is shown in Fig. 9. A large magnitude of the deflection can be seen at the mid-span. The stress contours in steel and CFRP at failure is shown in Fig. 10. It can be seen that high stresses had concentrated in the CFRP plates. The adhesive failure was followed by the concrete failure at the ends of CFRP strips.

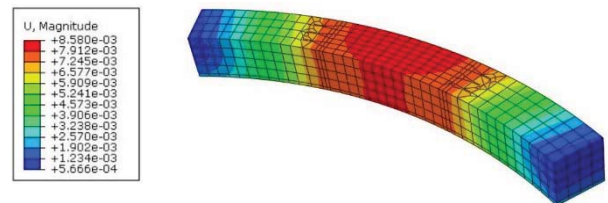


Fig. 9. Deformation of CF1 model at Ultimate failure

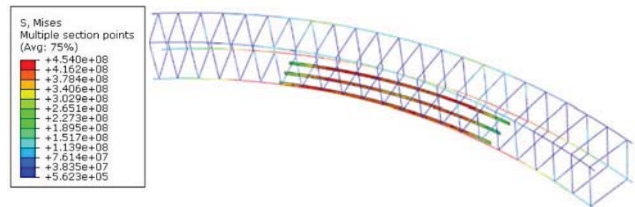


Fig. 10. Stress distribution in CF1 model



Fig. 11. Strain contours related to crack profile of CF1 model

The crack propagation of CFRP strengthened beam is shown below in Fig. 11. It can be seen that the cracks are concentrated at the ends of CFRP plates. The cracks in the mid-span have been significantly reduced after strengthening.

The load vs vertical deflection at midspan of the non-strengthened beam (C1) and CFRP strengthened beams (CF1) are shown in Fig. 12. The ultimate loads and the maximum deflection of C1 beam were 55.8 kN, and 19.1 mm respectively. Those for CF1 type beam were 60.6 kN, and 8.6 mm, respectively.

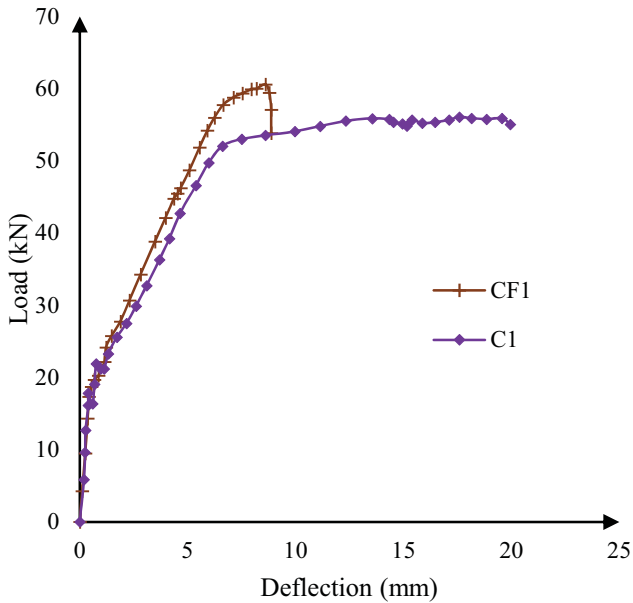


Fig. 12. FEM results of C1 and CF1 on load – deflection behaviour

From the results obtained from FE analysis, the ultimate load can be increased by 9% in the beam with 2000 mm curvature by strengthening. Further, the deflection reduction of 55% was observed with the application of NSM CFRP. This is mainly due to the premature bond failure in strengthened beam and yielding of reinforcement was dominant in the non-strengthened beam. Similar behaviour has also been noted in NSM CFRP strengthened reinforced concrete straight beams in previous literature [18,3]. Further, 25% - 50% of ductility reduction was noted in NSM CFRP strengthened beams[18] very similar to the ductility reduction observed in this study. To avoid premature failure, CFRP end anchors can be introduced which can improve the ductility of the beam. Since this is a continuation of the on-going project, authors did not include its results in the current paper.

IV. PARAMETRIC STUDY

A. Curvature Effect of RC Beam

The load capacity enhancement of beam with 2000 mm curvature was 8.6% while the beam with 4000 mm got only 6.7%. However, the deflection reduction was found higher in the larger curvature beam which is about 60% where the smaller curvature beam got 55%. The influence of curvature on load-deflection behaviour is shown in Fig. 13.

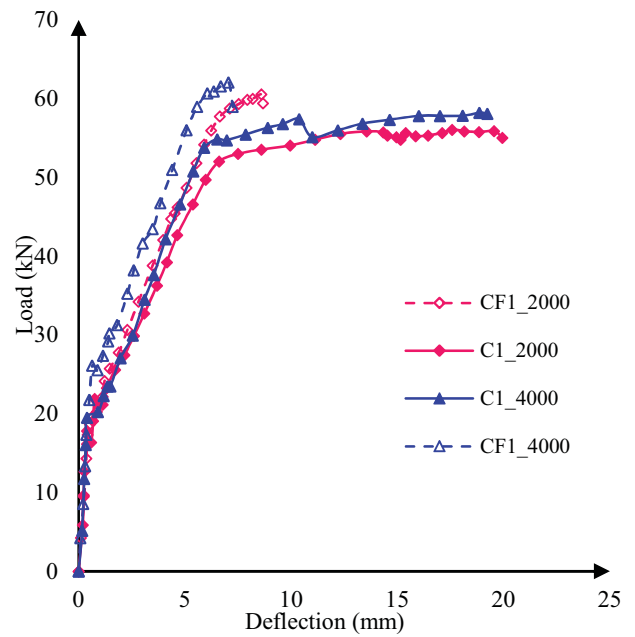


Fig. 13. Effect of curvature on load – deflection behaviour

B. Effect of Grade of Concrete

Significant variation can be observed in the ultimate loads and deflection with the change in grade of concrete (Fig. 14). Different stress-strain models for each grade were used in concrete damage plasticity model to carry out this study. The load increment in CFRP retrofitted beams with grade 25, 30, and 35 concrete substrates were observed as 6.4%, 9.0%, and 9.7%, respectively. This indicates a higher flexural enhancement with increased mechanical properties of the substrate. Further, a higher deflection reduction of 57.8% was found in the beam with grade 35 concrete.

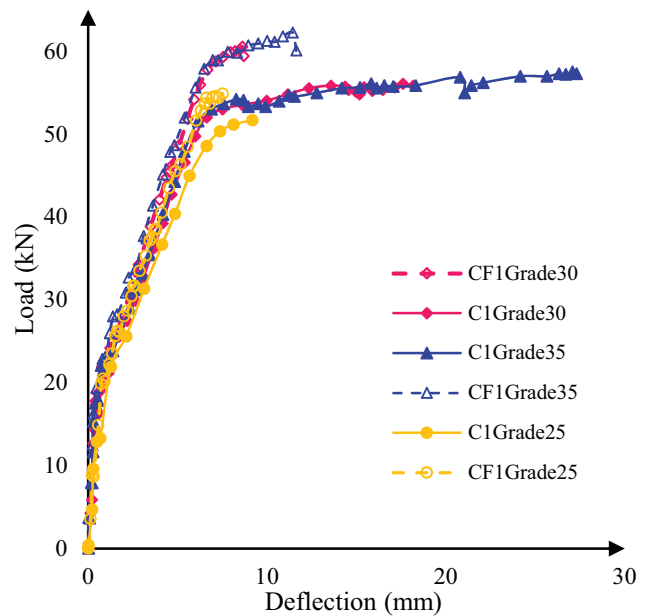


Fig. 14. Effect of concrete grade on load – deflection behaviour

C. Effect of Thickness of CFRP Plates

With the change of CFRP thickness, a significant variation in ultimate load and corresponding deflection can be observed. The influence of CFRP thickness was studied using Grade 35 RC curved beam retrofitted using CFRP plates which thicknesses varied from 0.5 mm to 2.5 mm in 1 mm steps. The capacity enhancement using 0.5 mm, 1.5 mm, and 2.5 mm thickness were noted as 26.3%, 9%, and 7.1%, respectively. This shows an increase in the flexural performance with the use of lower thickness of CFRP plates. However, with higher thickness of CFRP plates, higher deflection reduction was observed which was 70% in the beam with 2.5 mm CFRP plates. And using 0.5 mm thick CFRP, 50% of deflection increment was noted. This shows the evidence for a possible increase in ductility of the beam with lesser thickness of CFRP plates. Hence, using a low thickness of CFRP can increase the load capacity, and the ductility of

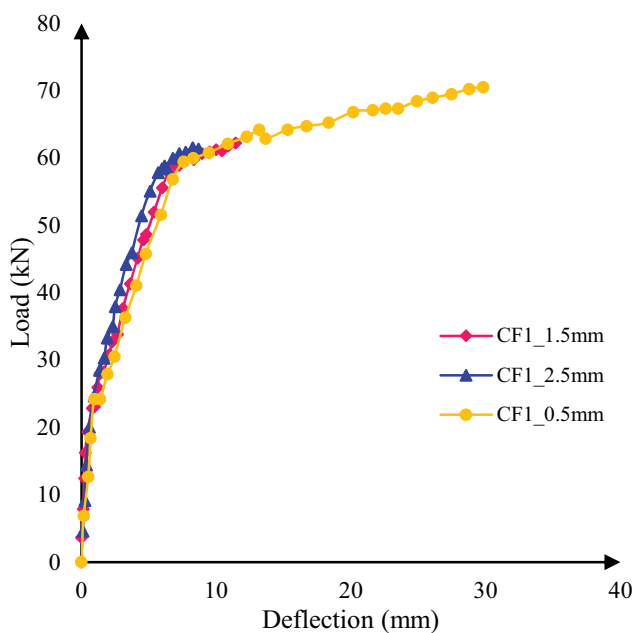


Fig. 15. Effect of thickness of CFRP plates on load – deflection behaviour

the concrete curved beams subjected to out of plane bending. The effects on the behaviour of beams with the variation of CFRP thickness is shown in Fig. 15.

D. Effect of Young's modulus of CFRP Plates

A CFRP plate with lower Young's modulus makes a large variation in load increment. Grade 35 RC curved beam with 150 GPa Elastic modulus of CFRP plate gained 25% load increment which is much larger than the 190 GPa CFRP plates. The beams with 240 GPa gained 10% load increment which is almost similar to the beam with 190 GPa CFRP plates. In the beams with lower Young's modulus of CFRP, increment in maximum deflection was noted while the maximum deflection reduced in the beams with higher Young's modulus of CFRPs. Hence, using a lower Young's modulus of CFRP within the acceptable range will result in higher flexural enhancement and higher ductility of NSM CFRP retrofitted concrete curved beams.

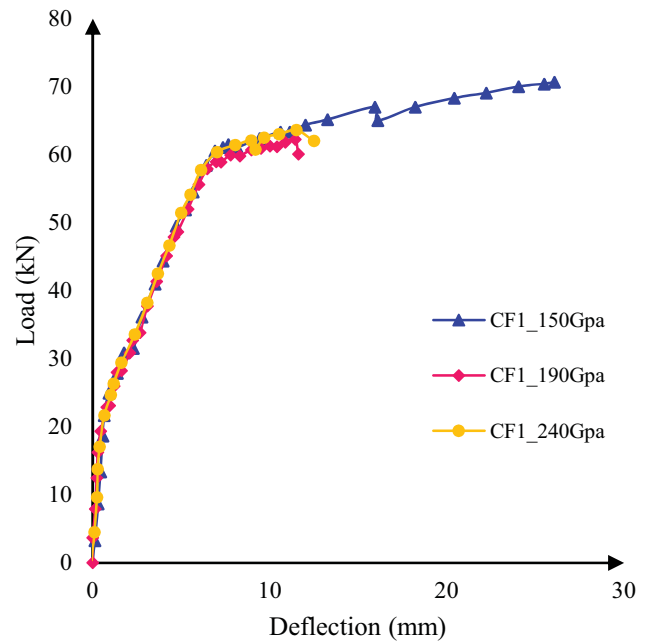


Fig. 16. Effect of young's modulus of CFRP plates on load – deflection behaviour

V. CONCLUSIONS

This paper presented a non-linear finite element model developed to predict the flexural performance of CFRP strengthened RC curved beams. The control beam model result was well agreed with the experimental results. According to the results obtained from the FE model, 5% - 27% of load capacity can be increased in a partially fixed curved beam under flexure by strengthening the beam using three CFRP strips. The load carrying capacity increases considerably with increasing the Concrete Grade. Using CFRP with low Young's modulus, and less thickness also, a high strength enhancement can be expected.

Further, a deflection reduction up to 70% and increment up to 50% were noted depending on the beam type. Therefore, the NSM technique with the application of NSM CFRP can be recommended in deflection sensitive structures as well. By strengthening the beam, the crack propagation in the strengthened region has been significantly reduced.

Further study of different strengthening patterns should be carried out to predict the optimum flexural enhancement. With the introduction of end anchorages, further flexural enhancement can be expected of retrofitted beams.

ACKNOWLEDGMENT

We extend our gratitude to the staff of Computer Laboratory, Department of Civil Engineering for their support. The financial support provided to the undergraduate research projects and SRC grant (SRC/ST/2018/15) is greatly appreciated.

REFERENCES

- [1] J. C. P. H. Gamage and E. Ariyachandra, "Investigation on Enhancing Flexural Performance of CFRP Strengthened Concrete Beams," *Int. J. Civ. Struct. Eng.*, vol. 2, no. 2, pp. 263–267, 2015.
- [2] R. Arunothayan and J. C. P. H. Gamage, "Modelling of CFRP strengthened Concrete Beam to quantify the effects of Bond parameters in flexure," in *7th International Conference on Sustainable Built Environment*, p. 1-8, 2016.
- [3] A. Hosen, M. Z. Jumaat, and U. J. Alengaram, "Near Surface Mounted Composites for Flexural Strengthening of Reinforced Concrete Beams," *Polymers (Basel)*, vol. 8, no. 67, pp. 1–18, 2016.
- [4] N. A. Amarasinghe and J. C. P. H. Gamage, "Investigation on Effectiveness of NSM CFRP Vs EBR CFRP for Strengthening Concrete Members," in *5th International Conference on Sustainable Built Environment*, pp. 184–188, 2014.
- [5] N. Wijerathne, D. M and J. C. P. H. Gamage, "Investigation on effective use of CFRP laminates for flexural performance," in *Special session on Sustainable Design, 4th International Conference on structural engineering*, pp. 99–106, 2013.
- [6] B. Gao, C. K. Y. Leung, and J. Kim, "Failure diagrams of FRP strengthened RC beams," *Composite Struct.*, vol. 77, pp. 493–508, 2007.
- [7] N. Attari, S. Amziane, and M. Chemrouk, "Flexural strengthening of concrete beams using CFRP , GFRP and hybrid FRP sheets," *Construction and Building Materials*, vol. 37, pp. 746–757, 2012.
- [8] Z. Kálmán and S. György, "Near surface mounted FRP reinforcement for strengthening of concrete structures," *Periodica Polytechnica*, vol. 1, pp. 33–38, 2007.
- [9] H. Y. Omran and R. El-hacha, "Finite Element Modeling of RC Beams Strengthened in Flexure with Prestressed NSM CFRP Strips," in *5th International Conference on FRP Composites in Civil Engineering*, 2010.
- [10] P. Kmiecik and M. Kaminski, "Modelling of reinforced concrete structures and composite structures with concrete strength degradation taken into consideration," *Arch. Civ. Mech. Eng.*, vol. XI, no. 3, pp. 623–636, 2011.
- [11] Abaqus 6.14-1, "Analysis user manual, "Dassault Systems Simula Corp., Providence, Rhode, 2014.
- [12] L. S. Hsu and T. Hsu, C, T, "Complete stress - strain behaviour of high-strength concrete under compression," *Mag. Concr. Res.*, vol. 46, no. 169, pp. 301–312, 1994.
- [13] B. L. Wahalathantri, D. Thambiratnam, T. Chan, and S. Fawzia, "A Material Model for Flexural Crack Simulation in Reinforced Concrete Elements Using ABAQUS," in *First International Conference on Engineering, Designing and Developing the Built Environment for Sustainable Wellbeing*, pp. 260–264, 2011.
- [14] R. Muralidharan, T. M. Jeyashree, and C. Krishnaveni, "Analytical Investiagtion on RC Curved Beams," *Jr. Ind. Pollut. Control*, vol. 33, no. S3, pp. 1387–1392, 2017.
- [15] SP-Reinforcement, S & P C-Laminate, Carbon fibre polymer plates for structural reinforcement, Laminate.TDS.CH-EV.V1 technical datasheet.
- [16] X-Calibur, X-Wrap Plate Adhesive, High performance epoxy adhesive for carbon fiber strengthening systems, 80050213 technical datasheet.
- [17] T. Tamura and H. Murata, "Experimental study on the ultimate strength of R / C curved beam," in *Fracture Mechanics of Concrete and Concrete Structures-High Performance, Fiber Reinforced Concrete, Special Loadings and Structural Applications*, pp. 1783–1788, 2010.
- [18] W. Jung, J. Park, J. Kang, and M. Keum, "Flexural Behavior of Concrete Beam Strengthened by Near-Surface Mounted CFRP Reinforcement Using Equivalent Section Model," *Adv. Mater. Sci. Eng.*, vol. 2017, p. 16, 2017.

EFFECT OF STEEL REINFORCEMENT RATIO ON FLEXURAL ENHANCEMENT IN CFRP-STRENGTHENED CONCRETE CURVED BEAMS

A.Selvaratnam^{1*} and J.C.P.H.Gamage¹

¹Department of Civil Engineering, University of Moratuwa, Moratuwa, Sri Lanka

*Correspondence E-mail: aaruga93@gmail.com, TP: +94775751783

Abstract: Rehabilitation of concrete infrastructures remains as a challenge in the construction industry. The introduction of Carbon Fibre Reinforced Polymer (CFRP) materials has become a prominent solution for retrofitting the deteriorated concrete structure. In this study, a finite element model is simulated to predict the behaviour of near surface mounted (NSM) CFRP retrofitted reinforced concrete curved beams. Two different curvature of 2000 mm and 4000 mm radius beams were used to this study. A commercially available finite element software was used to develop the finite element models. The results indicated that the 4000 mm radius reinforced concrete curved beams has a higher flexural capacity comparing to the 2000 mm beam. However, the effect of NSM-CFRP strengthening was observed to be higher in 2000 mm beams. Further, it was noted that the effect of CFRP retrofitting reduces with the increment of steel reinforcement area to concrete area ratio.

Keywords: CFRP; Curved beams; NSM; Numerical modelling; Steel reinforcement

1. Introduction

The retrofitting of the concrete members using high-strength FRP materials has become popular in recent years especially in rehabilitation of buildings and bridges. Application of FRP retrofitting is most widely used in strengthening the old bridges due to the deterioration from corrosion and increment in the traffic volume by time (Żyjewski, Chróścielewski and Pyrzowski, 2017). Apart from rehabilitation, this retrofitting processes are being used in new structures as well, due to additional design requirements. The high tensile strength, light weight, and resistance to chemical harm of FRP composites make them more effective in retrofitting applications (Gamage and Ariyachandra, 2015).

Most commonly used FRP materials in construction industry are Carbon, Glass, Aramid, and Basalt fibre reinforced polymers. Though the external bonding technique has initiated with steel plates, due to the drawbacks in the steel, the adoption of FRP plates has been increased. Later, the near surface mounted technique has been introduced as a more productive solution for retrofitting due to its high resistance to debonding failures (Attari, Amziane and Chemrouk, 2012; Szabo and Balazs, 2007).

Several investigations have been conducted on CFRP strengthened concrete beams, slabs, and columns as well (Silva and Gamage, 2018). Up to 114 % flexural strength enhancement has been documented in the reinforced concrete straight beams using CFRP laminates (Arunothayan and Gamage, 2016; Önal, 2014). Since there are several

applications of reinforced concrete curved beams in construction of highway bridges, and interchanges, the retrofitting of the concrete curved beams have to be investigated. However, the behaviour of CFRP strengthened reinforced concrete curved beams have not been widely investigated (Aaruga, Chandrathilaka and Gamage, 2019).

Aaruga et al. have simulated a numerical model to predict the flexural performance of NSM-CFRP strengthened reinforced concrete curved beams under out-of-plane bending. It was shown that flexural enhancement of 5% - 27 % can be achieved using three NSM-CFRP strips in reinforced concrete curved beams at partially fixed condition (Aaruga *et al.*, 2019). The amount of steel reinforcement is a significant parameter in FRP retrofitting which affects the flexural and shear enhancement of FRP strengthening. Several researchers have investigated the effect of reinforcement ratio on flexural and shear enhancement of CFRP strengthened concrete beams (Almusallam and Elsanadedy, 2015; Osman *et al.*, 2019). However, the effect of steel reinforcement ratio in CFRP strengthened concrete curved beams has not been widely studied which may have a great influence in the strengthening process of curved beams as well. This paper focuses the effect of primary steel reinforcement on the CFRP strengthening of concrete curved beams.

2. Numerical modelling

2.1 Numerical modelling of reinforced concrete curved beams

A three-dimensional (3D) non-linear model was simulated to predict the flexural performance of the non-strengthened and CFRP-strengthened reinforced concrete curved beams. Reinforced concrete curved beams with 2000 mm radius (C2) and 4000 mm radius (C4) were modelled using Abaqus/Explicit 6.14. The length of the beam was 1800 mm and the cross section was 200 mm x 200 mm. 13 mm diameter deformed bars were used for top and bottom reinforcements and 6 mm bars were

used for stirrups. The plan view of the concrete curved beam with the reinforcement details is shown in Figure 1.

Grade 30 concrete was used to simulate the curved beam and the non-linear behaviour of concrete was used to increase the accuracy of the results. A concrete damaged plasticity model which is a successful

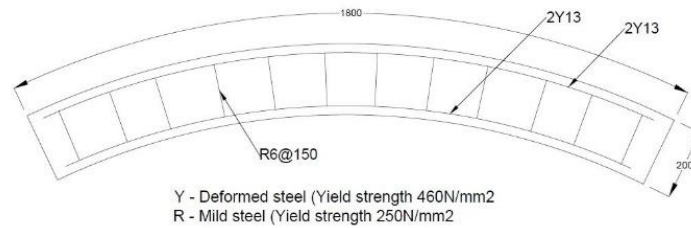


Figure 1: Reinforcement details of concrete curved beam

representation of stress-strain behaviour of concrete was used in this model (*ABAQUS Analysis User's Guide*, 2013). The elastic properties of concrete are listed in Table 1 and the non-linear properties were obtained based of Wahalathantri and Hsu & Hsu's model (Wahalathantri *et al.*, 2011)(Hsu and Hsu, 1994). A poisson ratio of 0.2 and 0.3 were assumed for concrete and steel respectively.

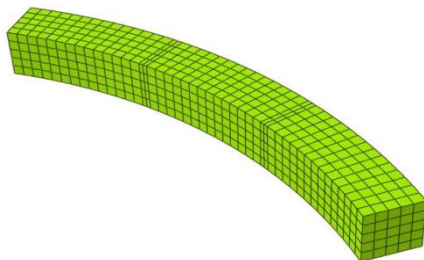


Figure 2. Finite element mesh of reinforced concrete curved beam

Based on the availability of the elements in explicit package, eight-node brick (C3D8) element was used to represent the concrete curved beam and two-node linear beam (B31) elements were used for steel reinforcements. From a mesh sensitivity analysis, appropriate mesh sizes were selected for each element. The finite element mesh of the reinforced concrete curved beam is shown in Figure 2. An embedded constraint was assumed between the steel reinforcement and concrete to represent the bond between those two elements. Both ends of the beams were fixed and the beams were tested under four-point bending as shown in Figure 3.

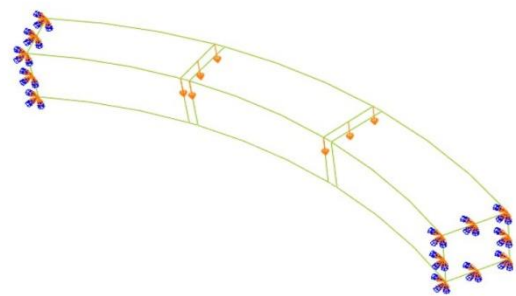


Figure 3. Boundary conditions and loading

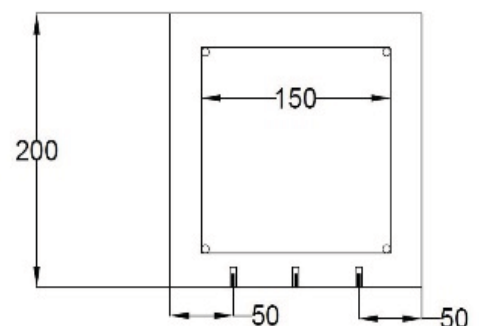


Figure 4. Cross section of NSM-CFRP strengthened beam

2.2 Numerical modelling of CFRP-strengthened reinforced concrete curved beams

1.5 mm thick NSM-CFRP laminates were used for retrofitting the curved beams. The cross-section of the CFRP-strengthened beam is shown in Figure 4. A linear-elastic behaviour of CFRP plate was used. The material properties were obtained from the manufacturing data sheet (2018, p. 2; 2019, p. 7). A tensile strength of 2800 N/mm², elastic modulus of 190 GPa, and density of 1600 kg/m³ were used. The two-part epoxy adhesive was used to bond the CFRP to the concrete substrate. The material

properties obtained from manufacturer for tensile strength, tensile modulus, and density were 23 N/mm², 10 GPa, and 1300 kg/m³, respectively. The spacing of steel stirrups has been reduced to 75 mm to avoid the shear failure of the beams.

The adhesive elements were modelled using eight-node brick elements (C3D8) and the CFRP plates were modelled using four-node doubly curved shell elements (S8R5). The finite element mesh of the CFRP-strengthened beam is shown in Figure 5. A tie constraint was used to represent the bond between CFRP-adhesive and adhesive-concrete.



Figure 5. Finite element mesh of NSM-CFRP strengthened beams

3. Results and validation

3.1 Analysis of Reinforced concrete curved

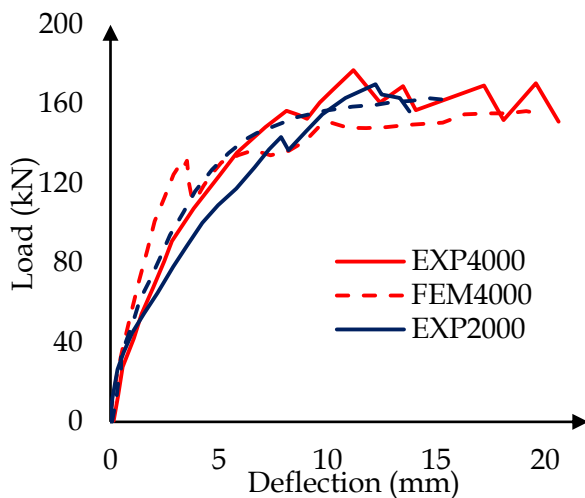


Figure 6. Comparison of Load-deflection behavior at mid-span

beams

The beams were loaded under four-point bending with a shear span-depth ratio of 2.5 in order to validate the experimental results (EXP4000,

EXP2000) with available literature (Tamura and Murata, 2010). A combined failure of bending and shear was noted in both curvatures beams similar to the available experimental results. The load-deflection behaviour obtained from the finite element model was compared with the available experimental results and is shown in Figure 6. It was noted that, both experimental and the FEM results show a similar behaviour. The percentage deviation in the ultimate loads were less than 10% in both beams.

3.2 Analysis of CFRP-strengthened reinforced concrete curved beams on the effect of steel reinforcement ratios

Five numbers of 2000 mm radius beams and five numbers of 4000 mm radius beams were used to analyse the effect of NSM-CFRP strengthening with different steel reinforcement ratios ranging from 0.001 -0.005 using 8 mm, 10 mm, 12 mm, 13 mm, and 16 mm rebars. All the beams were fixed at both ends and tested under four-point bending with a shear-span depth ratio of 3.0 (1/3 of span).

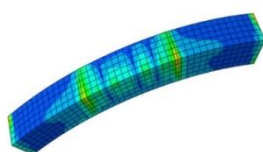


Figure 7(a). Crack pattern of control beam (CO) with 2000 mm radius

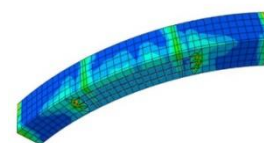


Figure 7(b). Crack pattern of CFRP-strengthened beam (FS) with 2000 mm radius

The crack patterns of 2000 mm radius and 12 mm reinforcement bars are shown Figure 7(a) and 7(b). It was noted that, after retrofitting the beams using NSM-CFRP, the concentration of flexural cracks has been reduced at failure. And the premature debonding failure can be noted at the end of the CFRP strips. The load-deflection behaviour of the beams is shown in Figure 8(a) and 8(b). It has been noted that, the ductile behaviour of the beams is reducing with high steel reinforcement ratios in 2000 mm radius beams and is increasing with high steel reinforcement ratio in 4000 mm radius. This is because, the 4000 mm radius beams have high ductile capacity itself compared to 2000 mm radius beams according to the results obtained (Figure 4). Therefore, it leads in the delay of premature debonding failure due to the CFRP strips. But, by bonding the CFRP strips in 2000 mm curved beams with high steel ratios, it was not able to provide increment in capacity due to its immediate premature failures. Therefore, better ductile performance can be observed in the beams with less reinforcement in 2000 mm beams and high reinforcement in 4000 mm beams after strengthening. For further increment of the ductile performance of CFRP-strengthened beams, end

anchorage can be introduced (Kahandawaarachchi *et al.*, 2019).

The noted ultimate loads of 2000 mm control beams (CO) were 78.4 kN, 96 kN, 116.3 kN, 125.1 kN, and 160.7 kN for corresponding steel ratios 0.001, 0.002, 0.003, 0.0035, and 0.005, respectively. And the corresponding ultimate loads of CFRP-strengthened (FS) 2000 mm radius beams were 110.9 kN, 125.1 kN, 137.5 kN, 147.5 kN, and 162.7 kN. Hence, 41.5%, 30.1%, 18.2%, 17.6%, and 1.2% flexural capacity enhancement was achieved using NSM-CFRP retrofitting technique in 2000 mm radius beams. Similarly, 22.6%, 20.5%, 18.6%, 18.4%, and 10.2% enhancement was obtained in 4000 mm radius beams for corresponding steel ratios 0.001, 0.002, 0.003, 0.0035, 0.005 respectively.

The noted ultimate loads of 2000 mm control beams (CO) were 78.4 kN, 96 kN, 116.3 kN, 125.1 kN, and 160.7 kN for corresponding steel ratios 0.001, 0.002, 0.003, 0.0035, and 0.005, respectively. And the corresponding ultimate loads of CFRP-strengthened (FS) 2000 mm radius beams were 110.9 kN, 125.1 kN, 137.5 kN, 147.5 kN, and 162.7 kN. Hence, 41.5%, 30.1%,

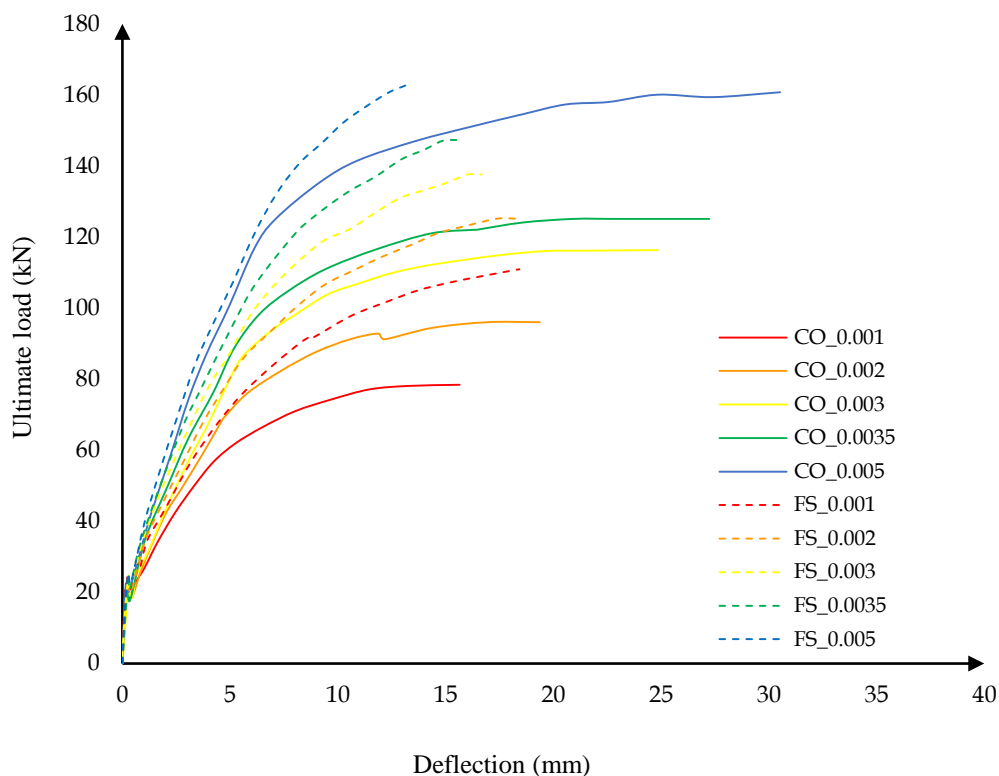


Figure 8(a). Load-deflection behaviour of 2000 mm radius beams

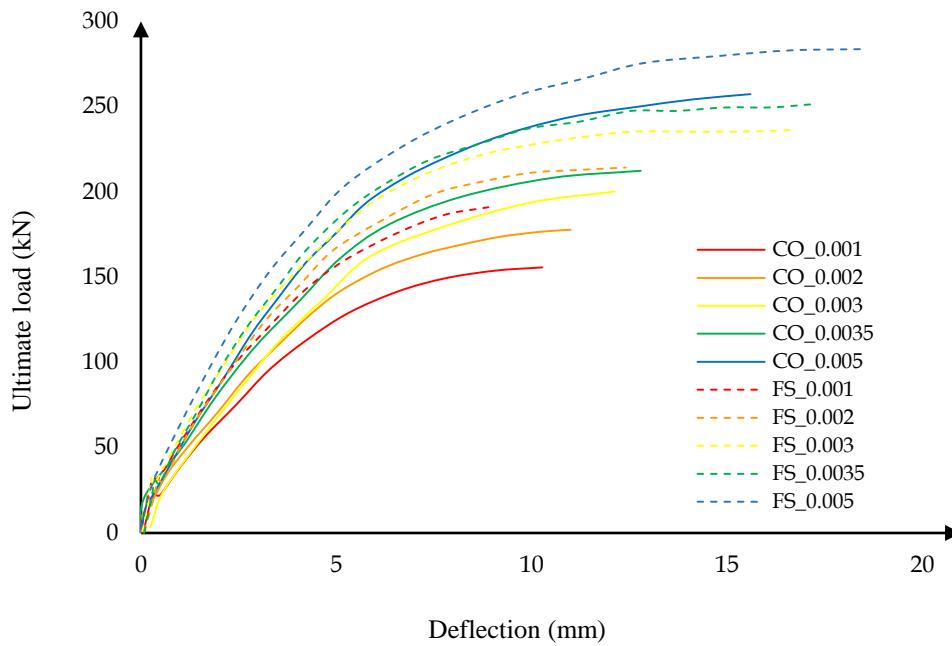


Figure 8(b). Load-deflection behaviour of 4000 mm radius beams

18.2%, 17.6%, and 1.2% flexural capacity enhancement was achieved using NSM-CFRP retrofitting technique in 2000 mm radius beams. Similarly, 22.6%, 20.5%, 18.6%, 18.4%, and

10.2% enhancement was obtained in 4000 mm radius beams for corresponding steel ratios 0.001, 0.002, 0.003, 0.0035, 0.005 respectively.

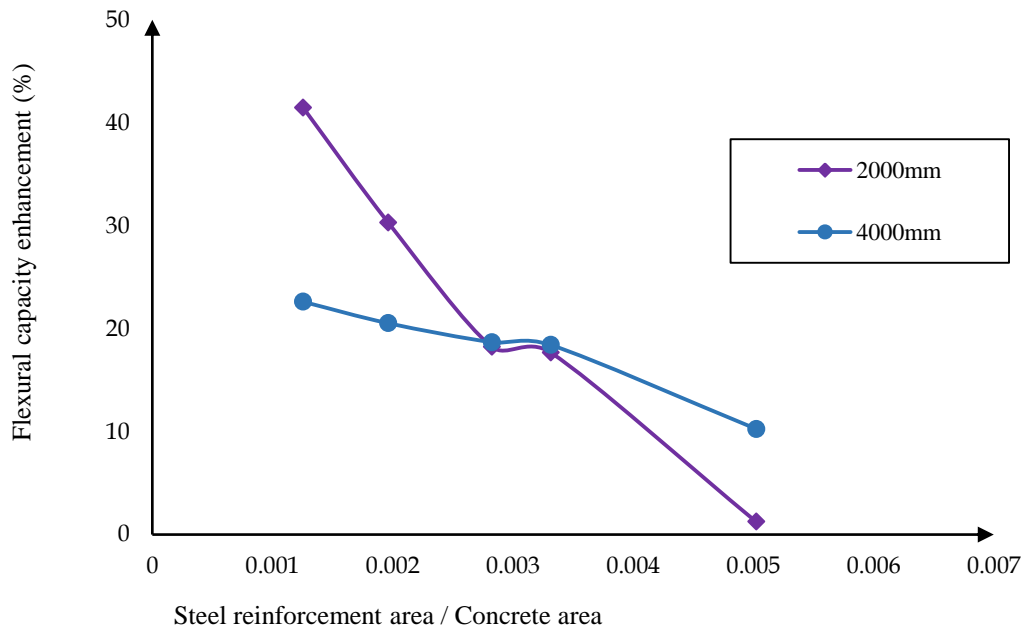


Figure 9. Flexural capacity enhancement vs steel reinforcement-concrete ratio

The variation of flexural enhancement with steel reinforcement ratios is plotted in Figure 9. It can be observed that, the effect of NSM-CFRP strengthening is reducing with increment of steel reinforcement ratio at both curvature beams. Further, this strengthening technique is more effective in 2000 mm radius beams than the 4000 mm beams with less steel reinforcement ratio. And this method is less effective in 2000 mm radius beams beyond 0.0035 steel reinforcement/concrete area

The variation of flexural enhancement with steel reinforcement ratios is plotted in Figure 9. It can be observed that, the effect of NSM-CFRP strengthening is reducing with increment of steel reinforcement ratio at both curvature beams. Further, this strengthening technique is more effective in 2000 mm radius beams than the 4000 mm beams with less steel reinforcement ratio. And this method is less effective in 2000 mm radius beams beyond 0.0035 steel reinforcement/concrete area.

4. Conclusion

A non-linear numerical model has been simulated to predict the effect of primary steel reinforcement of concrete curved beams and the beams were in good agreement with the experimental results available in the literature. It was noted that the flexural capacity of the curved beam with 2000 mm is lesser than the beam with 4000mm radius. After strengthening the beams using NSM-CFRP strips, 1% - 42% increment in the flexural performance was noted. Using this NSM-CFRP retrofitting, a higher effect was obtained in the beams with 2000 mm radius. It was observed that with the increment of existing steel reinforcement, the effect of strengthening reduces. Further, in 2000 mm beams the ductile performance of the beams reduces with the increment of steel reinforcement while the effect starts to reverse for 4000 mm radius beams. This shows that, the premature debonding failure played a major role in 2000 mm beams with increasing steel ratios. Hence, there is a significant effect of primary steel reinforcement in retrofitting the concrete curved beams using NSM CFRP laminates. It also concludes that, using this technique at curved beams with less steel reinforcement can lead to higher flexural performance and higher ductile performance in larger curvature beams.

Acknowledgement

The authors would like to express their gratitude to the Staff of Computer laboratory, Department of Civil Engineering for their support.

References

- Aaruga, S., Chandrathilaka, E. R. K. and Gamage, J. C. P. H. (2019) 'Finite Element Modelling on Flexural Performance of CFRP Strengthened Reinforced Concrete Curved Beams', in *5th International Multidisciplinary Engineering Research Conference*, p. 6. doi: <https://doi.org/10.1109/MERCon.2019.8818797>.
- ABAQUS Analysis User's Guide* (2013).
- Almusallam, T. H. and Elsanadedy, H. M. (2015) 'Effect of Longitudinal Steel Ratio on Behavior of RC Beams Strengthened with FRP Composites: Experimental and FE Study', *Journal of composite structures*, 3(2002), pp. 1–18. doi: 10.1061/(ASCE)CC.1943-5614.0000486.
- Arunothayan, R. and Gamage, J. C. P. H. (2016) 'Modelling of CFRP strengthened Concrete Beam to quantify the effects of Bond parameters in flexure', in *7th International Conference on Sustainable Built Environment*, p. 8.
- Attari, N., Amziane, S. and Chemrouk, M. (2012) 'Flexural strengthening of concrete beams using CFRP, GFRP and hybrid FRP sheets', *Construction and Building Materials*. Elsevier Ltd, 37, pp. 746–757. doi: 10.1016/j.conbuildmat.2012.07.052.
- Gamage, J. C. P. H. and Ariyachandra, E. (2015) 'Investigation on Enhancing Flexural Performance of CFRP Strengthened Concrete Beams', *International Journal of Civil and Structural Engineering*, 2(2), pp. 263–267.
- Hsu, L. S. and Hsu, C. T. T. (1994) 'Complete stress - strain behaviour of high-strength concrete under compression', *Magazine of Concrete research*, 46(169), pp. 301–312.
- Kahandawaarachchi, T., Chandrathilaka, K. and Gamage, K. (2019) 'Bond Performance of Carbon Fiber Reinforced Polymer (CFRP) Strengthened Bond Performance of Carbon Fiber Reinforced Polymer (CFRP) Strengthened Reinforced Concrete Curved Beams', in *International Conference on Civil Engineering and Applications*, p. 6.

- Önal, M. M. (2014) 'Strengthening Reinforced Concrete Beams with CFRP and GFRP', *Advances in Materials Science and Engineering*, 2014, pp. 1–8.
- Osman, B. H. *et al.* (2019) 'Effect of reinforcement ratios on shear behavior of concrete beams strengthened with CFRP sheets Effect of reinforcement ratios on shear behavior of concrete beams strengthened with CFRP sheets', *HBRC Journal*. Housing and Building National Research Center, 14(1), pp. 29–36. doi: 10.1016/j.hbrcj.2016.04.002.
- Silva, A. and Gamage, J. C. P. H. (2018) 'Punching Shear Capacity Enhancement of Flat Slabs using End Anchored Externally Bonded CFRP Strips', *Research and Development Forum*, 28(02), pp. 16–21.
- Szabo, Z. and Balazs, G. (2007) 'Near surface mounted FRP reinforcement for strengthening of concrete structures', *Periodica polytechnica; Civil Engineering*, 51(1), pp. 33–38. Available at: doi: 10.3311/pp.ci.2007-1.05.
- Tamura, T. and Murata, H. (2010) 'Experimental study on the ultimate strength of R / C curved beam', in *Fracture Mechanics of Concrete and Concrete Structures-High Performance, Fiber Reinforced Concrete, Special Loadings and Structural Applications*, pp. 1783–1788.
- Technical data sheet, (2018) 'X-Wrap Plate Adhesive, High performance epoxy adhesive for carbon fibre strengthening systems, p. 2. Available at: <https://www.x-calibur.us>
- Technical data sheet, (2019) 'S & P C-Laminate, Carbon fibre polymer plates for structural reinforcement, p. 7. Available at: <https://www.sp-reinforcement.eu>
- Wahalathantri, B. L. *et al.* (2011) 'A Material Model for Flexural Crack Simulation in Reinforced Concrete Elements Using ABAQUS', in *First International Conference on Engineering, Designing and Developing the Built Environment for Sustainable Wellbeing*, pp. 260–264.
- Żyjewski, A., Chróścielewski, J. and Pyrzowski,



307/C

Effect of anchorages on flexural behaviour of carbon fibre reinforced polymer (CFRP) – strengthened reinforced concrete curved beams

S. Aaruga* and J. C. P. H. Gamage

Department of Civil Engineering, University of Moratuwa.

The use of Carbon Fibre Reinforced Polymer (CFRP) composites has become one of the prominent solutions for retrofitting the concrete structure in the construction industry. Among the other FRP materials, CFRP composites have the high tensile strength to the lightweight ratio which made it more effective in retrofitting applications. Several researchers have studied the applicability of CFRP composites in concrete elements such as beams, columns and slabs. It has been found that the load carrying capacity of the reinforced concrete straight beams can be increased up to 115% by retrofitting the beams using FRP materials. However, the use of CFRP composites in curved elements, especially the out-of-plane curvature has not been widely investigated. Though 27% of capacity increment can be achieved using high strength NSM-CFRP laminates according to the available results on reinforced concrete curved beams, the ductility of the beams gets affected due to the premature failure. A finite element model of Near-surface mounted (NSM) CFRP-strengthened concrete curved beam subjected to out-of-plane bending is developed in this study. The numerical model was validated with available test results in the literature. The model results showed a good agreement with the literature results. Since the premature debonding failure dominates in the CFRP-strengthened concrete beam models, an introduction of end-anchors has been investigated in this study to delay the premature failure. From the results obtained from the finite element model, it was noted that the ductility of the CFRP-strengthened concrete beams can be enhanced by providing the end anchors. The introduction of end-anchors can increase the flexural performance of the CFRP-strengthened beams up to 11%. This study also compares the alternative bonding arrangements with end-anchors on flexural performance of the CFRP-strengthened reinforced concrete curved beams. It was revealed that application of two end-anchors at appropriate locations would be sufficient.

Keywords: CFRP, NSM; End-anchor, FEM

aaruga93@gmail.com

1. Introduction

Repairing and rehabilitation of concrete infrastructures remain as a challenge in the Civil engineering industry due to various social and environmental impacts. The introduction of steel plate bonding technique has become popular by time to retrofit the concrete structures. However, due to the low corrosive resistance, rapid deterioration of the steel plate could not be eliminated. Therefore, using FRP composites for retrofitting the infrastructures has been invented as a new technology among the world to enhance the performance of reinforced concrete beams, slabs, columns, and bridges.

Several researchers have investigated the applicability of FRP composites in the straight beams [1-3]. However, the use of FRP composites in the curved beam retrofitting has not been widely investigated even though many possible applications are visible. An investigation was carried out by Aaruga et al [4] on the CFRP-strengthened reinforced concrete curved beams at it was found the flexural performance can be increased up to 27% using NSM CFRP retrofitting. However, due to the premature debonding failure, reduction in the ductile performance was observed. The focus of this study is to simulate a numerical model to predict the effect of end anchors in the NSM CFRP-strengthened reinforced concrete beams.

2. Methodology

2.1. Finite element modelling

A finite element model of reinforced concrete with 2000 mm was simulated using a commercially available finite element software [5]. Grade 30 concrete was used, and a concrete damaged plasticity model was used to present the non-linear behaviour of the concrete beam. The non-strengthened beam was validated with the available experimental results in the literature [6]. After validating the non-strengthened beam (N1), the reinforced concrete beam was strengthened using NSM CFRP strips (N2) and end-anchors were applied in addition, to delay the premature failure (N3). The Hashin damage model was used to represent the lamina behaviour of the CFRP end-anchors. Developed finite element mesh is shown in Fig 1. A partially fixed boundary conditions were applied throughout the simulation and four-point load bending test was conducted.

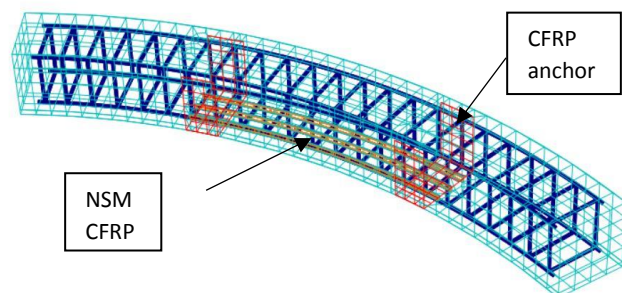


Fig 1. Finite element mesh

Table I. Material Properties

Material Property	Steel [4]	Adhesive [7]	CFRP plate [8]	CFRP fabrics [9]
Density (kg/m ³)	7800	1300	1600	240
Average Elastic Modulus (GPa)	200	10	170	176
Average Tensile strength (N/mm ²)	460	23	2800	1575

2.2. Alternative anchorage patterns

Different arrangements of end-anchors were used to study the effect of anchorages on the flexural enhancement of the NSM-CFRP strengthened reinforced concrete beams.

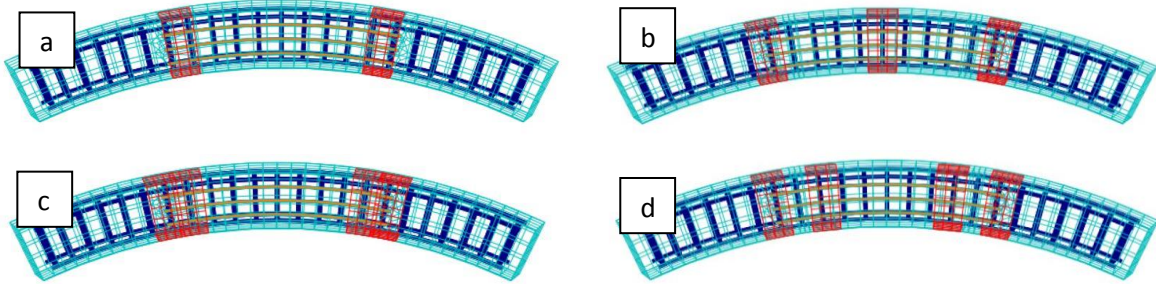


Fig 2. Alternative anchorage patterns (a) N3-1; (b) N3-2; (c) N3-3; (d) N3-4

As an alternative, an additional CFRP anchor was bonded to the mid-span of the beam (N3-2). Another alternative was also investigated with two additional anchors bonded next to end-anchors (N3-3) and bonded apart from the end-anchors (N3-4). The anchorage patterns are shown in Fig 2. The summary of the developed models is shown in Table II.

Table II. Material Properties

Model	Remarks	Model	Remarks
N3-1	CFRP strengthened beam with two CFRP anchors (N3)	N3-3	CFRP strengthened beam with two CFRP anchors at both ends
N3-2	CFRP strengthened beam with three CFRP anchors	N3-4	CFRP strengthened beam with two separated CFRP anchors at both ends

3. Results and discussion

The load-deflection behaviour observed experimentally [6] & numerically of the non-strengthened beam is shown in Fig 3. The fixed boundary condition was applied at ends, and the shear span-depth ratio was taken as 2.5 [6]. The percentage difference between the experimental results and the numerically predicted results was noted as 4.1 % which shows the accuracy of the developed numerical model.

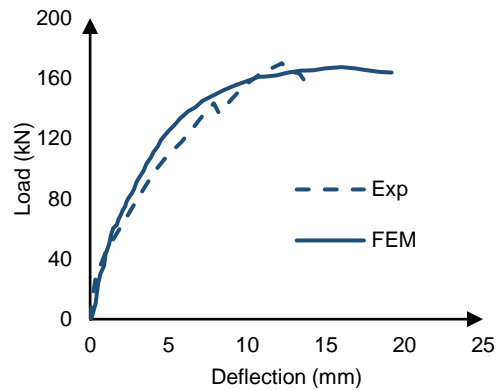


Fig 3. Comparison of Load-deflection behaviour

The load vs vertical deflection at midspan of all three specimens (N1, N2, N3) are shown in Fig 4. The ultimate loads of N1, N2, and N3 were noted as 55.8 kN, 60.6 kN, and 67.0 kN, respectively. An 8.6 % of flexural enhancement was observed with the NSM CFRP strip bonded beam (N2) with respect to the non-strengthened beam (N1). And 20.1% of total enhancement was observed in the end-anchored beam (N3) with respect to CFRP strengthened beam (N2). The failure modes in N1, N2, and N3 beams were concrete cracking, Adhesive failure, and Anchorage failure, respectively (Figure 5(b)). The introduction of end-anchors had caused to delay the pre-mature debonding failure and had enhanced the ductility of the beams as well.

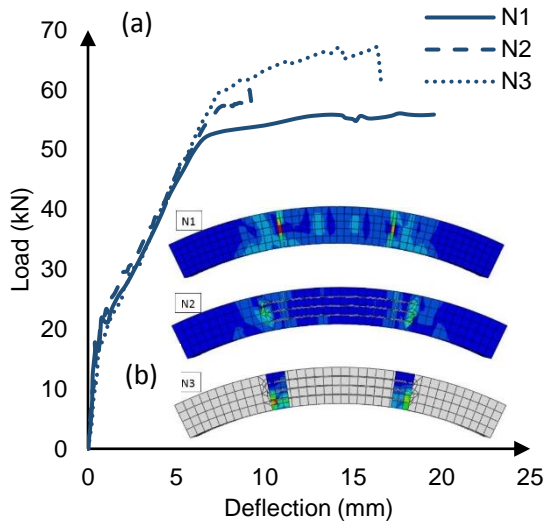


Fig 5. (a) Load-deflection behaviour of N1, N2, & N3; (b) Crack patterns of N1, N2, & N3

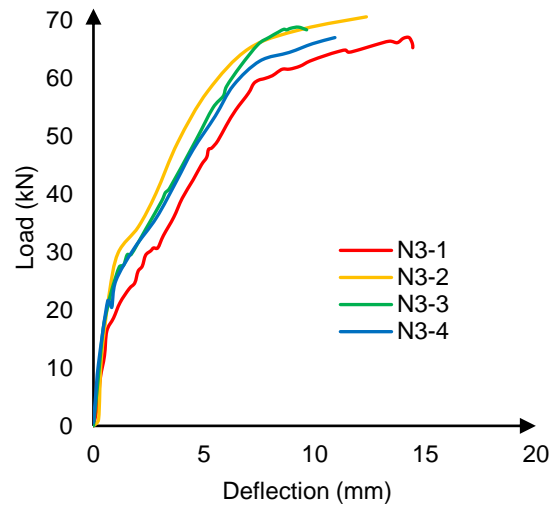


Fig 6. Load-deflection behaviour of N3-1,2,3,4

The load vs deflections of the beams with alternative anchorage patterns are shown in Fig 5. The ultimate loads of N3-1,2,3, and 4 were observed as 67 kN, 70.5 kN, 68.8 kN, and 67.1 kN, respectively. The maximum flexural enhancement of 26.3 % was noted in the N3-2 beam with respect to the non-strengthened beam. And the ductility of the N3-2 beam was also comparatively higher than the non-anchored beams.

4. Conclusions

Following conclusions were made from the study conducted to evaluate the CFRP-strengthened reinforced concrete curved beams.

- i. Addition of anchors at appropriate locations had caused for better performance of NSM CFRP-strengthened beams.
- ii. Maximum strength gain of 26% was noted from CFRP-strengthened beams with anchors at the ends and midspan.

5. References

- [1] Gamage, J. C. P. H., & Ariyachandra, E., (2015) *International Journal of Civil and Structural Engineering*, **2(2)**, 263–267.
- [2] Arunothayan, R., & Gamage, J. C. P. H., (2016) *7th International Conference on Sustainable Built Environment*, 8.
- [3] Wijerathne, D, M, N., & Gamage, J. C. P. H., (2013) *Special Session on Sustainable Design, 4th International Conference on Structural Engineering*, (December), 99–106.
- [4] Aaruga, S., Chandrathilaka, E. R. K., & Gamage, J. C. P. H., (2019) *5th International Multidisciplinary Engineering Research Conference*, 6.
- [5] ABAQUS 6.14, (2013) *Abaqus Analysis User's Guide*. Dassault Systems Simula Corp.
- [6] Tamura, T., & Murata, H., (2010) *Fracture Mechanics of Concrete and Concrete Structures-High Performance, Fiber Reinforced Concrete, Special Loadings and Structural Applications*, 1783–1788.
- [7] Technical data sheet, X-Wrap Plate adhesive, High Performance epoxy adhesive for carbon fiber strengthening systems.
- [8] Technical data sheet, S & P C-Laminate, Carbon fibre polymer plates for structural reinforcement.
- [9] Pederson, J. (2008) Thesis, 69

EPS BLENDED CEMENTITIOUS PLASTER FOR IMPROVED THERMAL COMFORT IN BUILDINGS

A. Selvaratnam^{1*}, J.C.P.H.Gamage¹, G.I.P. De Silva²

¹Department of Civil Engineering, University of Moratuwa, Sri Lanka

²Department of Material Science and Engineering, University of Moratuwa, Sri Lanka.

**Correspondence E-mail: aaruga93@gmail.com, TP: +94775751783*

Abstract: The use of green materials in building construction has become trendy to improve the thermal comfort within the buildings with minimized natural resources. This paper presents the development of a cementitious insulated plaster using Expanded Polystyrene (EPS) as partial replacement for fine aggregates. An experimental program was conducted by replacing the fine aggregates in the conventional plaster with EPS in the range of 0% to 200% by volume. A reduction up to 69% and 53% were noted in thermal conductivity and density, respectively due to the replacement of aggregates with EPS in the conventional mortar. From a trial and error process, the mix with 125% replacement by EPS was selected as the ideal mix for optimum thermo-mechanical performance. A numerical model was developed to examine the heat transfer behaviour through a Wall/Plaster composite and the predicted results were in satisfactory agreement with the experimental results. A reduction of 18% and an increment of 20% were noted in the decrement factor and time lag, respectively in the wall panels with the developed EPS-Cement plaster.

Keywords: EPS; Green insulation; Recycling; Thermal comfort; Wall plaster

1. Introduction

The production of EPS material has rapidly increased due to its frequent application in packaging, thermal insulation, and craft applications. The desire towards the EPS materials has risen because its superior properties such as lightweight, thermal insulation, impact resistance, airtightness, load-bearing capacity at a low weight, and long life (Ramli Sulong, Mustapa, and Abdul Rashid, 2019). However, EPS is bio-degradable (Ho, Roberts and Lucas, 2018) and hence tons of EPS are sent to the landfills every day. Since incorporating the waste materials into building construction has become attractive (Jayasinghe, Fonseka and Abeygunawardhene, 2016), utilization of the recycled EPS as a building construction material is an excellent solution towards a greener industry.

The research focus on the utilization of EPS in the civil engineering industry has become generic in the last few decades. In such a case, lightweight concrete (Schackow *et al.*, 2014), precast wall panels (Dissanayake, Jayasinghe and Jayasinghe, 2017), and sandwich panels (Fernando, Jayasinghe and Jayasinghe, 2017) are the extensive studies using EPS as a base material. Kaya and Kar (2016) have shown that a range of thermal conductivity from 0.048 – 0.390 W/mK can be obtained for the concrete containing waste EPS and natural resin. Schackow *et al.* (2014) have also investigated the mechanical and thermal properties of lightweight concrete with EPS and indicated that 7.7 MPa to 11.8 MPa of compressive strength and 0.50 – 0.56 W/mK of thermal conductivity can be achieved with 55-65 % of EPS volume fraction and 1% air-entraining agent by weight.

Thermal comfort is a key variable of indoor environment quality which is mainly influenced by the materials used in construction and the design strategies (Kahandawa Arachchi, Gamage and De Silva, 2019; Jannat *et al.*, 2020). Therefore, using insulating materials for the building walls or wall plasters could significantly reduce the heat transfer within the buildings. In such a case, addition of thermally insulative materials such as Rice husk ash, bottom ash, fly ash into the concrete and mortar mixes have been studied by many researchers (Gunawardhana and Gamage, 2015; Ghosh, Ghosh and Neogi, 2018; Selvaranjan, Gamage and Silva, 2020).

Few researchers have focused on the EPS-cement mortar and its thermal and mechanical properties. Ferrándiz-Mas *et al.* (2014) have investigated the cement mortar with EPS and paper sludge ash and discovered mortar mixes with a thermal conductivity range of 0.4 - 0.9 W/mK and compressive strength range of 0.5 - 8.5 MPa. Dylewski

and Adamczyk (2014) explored the ecological and economic performance of different types of thermal insulation plaster as EPS plaster one of them. This study has indicated that using EPS plaster is far more beneficial than conventional cement plaster for both economic and ecological reasons. Though few investigations have been made on EPS plaster, no studies have focused on the development and application of the EPS plaster to building walls to date, according to the authors' knowledge. This study focuses on the development of a thermally insulated cementitious wall plaster using EPS as a partial replacement for fine aggregates and on the application of the developed plaster to assess the heat transfer behaviour.

2. Test Program

2.1 Overview

A detailed experimental program was carried out to develop a light-weight cementitious insulated plaster with Expanded Polystyrene (EPS) as the base material. Figure 1 illustrates the test methodology followed in this experimental program. The conventional cement sand mortar with cement: sand weight ratio of 1: 3 (1:2.25 volume ratio) was selected as the control specimen for this study and it was modified by the replacement of sand by EPS particles. The thermal conductivity

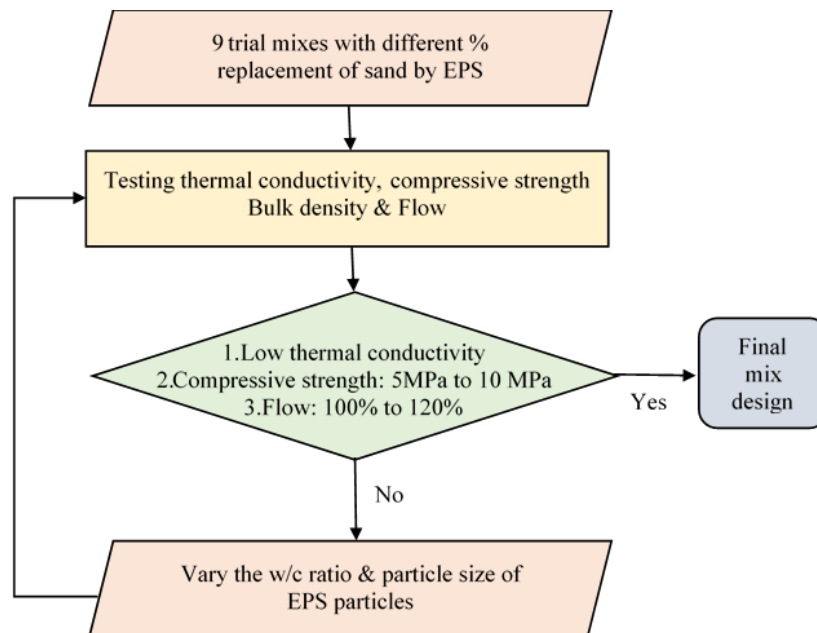


Figure 1. Methodology of the test program

and the compressive strength of the trial mixes were used for the selection criteria of the final product to match with the common industry practice for N-type mortar (ASTM C 270-07, 2010).

2.2 Materials & sample preparation



Figure 2. Materials (a) Cement (b) River sand (c) EPS – 3.35 mm (d) EPS – 1.15

Ordinary Portland cement with average 28 days strength of 42.5 MPa as the binding agent, river sand passing through 0.8 mm sieve, recycled EPS resin particles passing through 3.35 mm and 1.15 mm sieve as fine aggregates were used throughout the test program (Figure 2). A constant water/cement ratio of 0.45 was used at the first stage of the experimental program. 60 mm diameter and 5 mm thick specimens were prepared to test the thermal conductivities based on Lee's disk method in accordance with ASTM D7340-07 (2018). The compressive strength of the trial mixes was tested in accordance with SLS 107: Part 2 (1995). Figure 3 shows a few test samples and testing apparatus.



Figure 3. Specimen preparation & testing (a) Mixing mortar; (b) Compressive strength test samples; (c) Testing thermal conductivity

2.3 Test results

The obtained thermal and mechanical properties with 3.35 mm grade EPS are listed in Table 1. The test results show that replacing the sand particles with EPS drastically reduces the compressive strength, density, and thermal

Table 1: Test results

Sample	Replacement of sand by EPS (% volume)	Density (kg/m ³)	Compressive strength (MPa)	Thermal conductivity (W/m.K)	Flow (%)
E-0	0	2075	28.1	0.692	14
E-30	30	2049	23.9	-	54
E-50	50	1976	18.8	-	65
E-70	70	1690	12.5	-	97
E-90	90	1453	11.1	0.361	128
E-125	125	1282	5.5	0.281	65
E-150	150	1176	5.3	-	20
E-175	175	1145	3.6	-	33
E-200	200	968	2.9	0.216	10

conductivity where the reduction in compressive strength decrease the mechanical performance and reduction in the thermal conductivity enhance the thermal performance of the mixes. Figure 4 shows the variation in the compressive strength and thermal conductivity with respect to the volume replacement percentage. Though 62% replacement indicates the optimum performance, a lesser compressive strength value would be sufficient for an N-type mortar mix. Meanwhile, the introduction of EPS particles makes the mortar mix lightweight which adds more benefits to a green mortar mix. The flow table test results indicate that replacement of sand by EPS (E-0 to E-90) increases the flow of the mix and further addition of EPS particles (E-

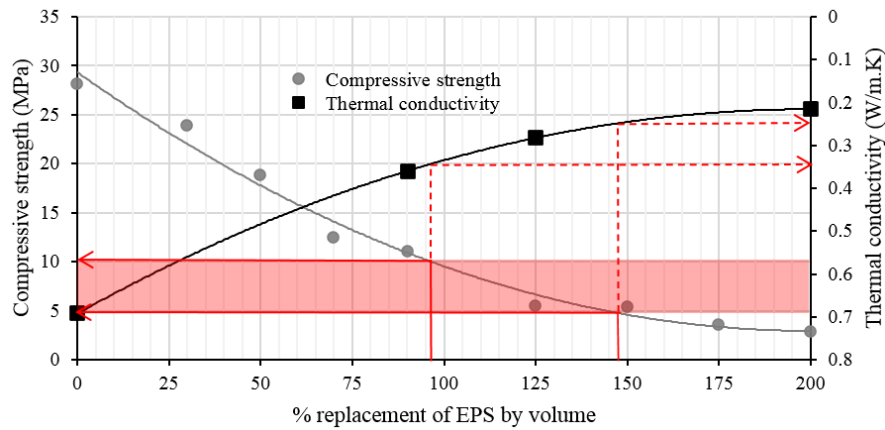


Figure 4. Thermal and mechanical properties variation with % replacement of sand by EPS

90 to E-200) decreases the flow back again due to the larger volume of aggregate particles.

Based on the values obtained for compressive strength, mixes between 100% and 150% replacement lie in the N-type mortar criteria. However, the respective flow table test results do not compile with the flow requirement specified in ASTM C 270-07, (2007). Hence, the E-125 mix was selected for further modification since it is the most ideal mix within the range.

2.4 Modification to the mortar

Two different particle sizes and a range of w/c ratios were used to modify the mortar in order to compile with the specifications. The selected mix proportions and the measured material properties are listed in Table 2. The test results show that finer EPS particles can enhance the mechanical performance of the mix. Nevertheless, thermal performance and lightweight behaviour reduce with the finer particles. However, to preserve the aesthetic appearance of the building walls, the mix with finer particles were further investigated with changing w/c ratios.

Table 2: Test results after modification

Mix ID	Grade of EPS	Water/Cement ratio	Density (kg/m ³)	Compressive strength (MPa)	Thermal conductivity (W/m.K)	Flow (%)
E-125-1	3.35	0.45	1282	5.50	0.281	65
E-125-2	1.15	0.55	1498	7.12	0.405	55
E-125-3	1.15	0.65	1436	5.43	-	63
E-125-4	1.15	0.75	1417	4.96	0.406	97

The effect of the w/c ratio was noted high in the compressive strength values compared to the thermal conductivity and density test results. The relationship between the w/c ratio and compressive strength is shown in Figure 5. From the three trial mixes, E-125-4 can be chosen as the ideal mix for an insulated wall plaster to enhance the thermal comfort in the buildings while ensuring the integrity of the masonry walls. Hence, a heat transfer analysis through the EPS plaster/wall composite was carried out in the next step of this study. Here onwards, the selected mortar mix will be referred to as EC.

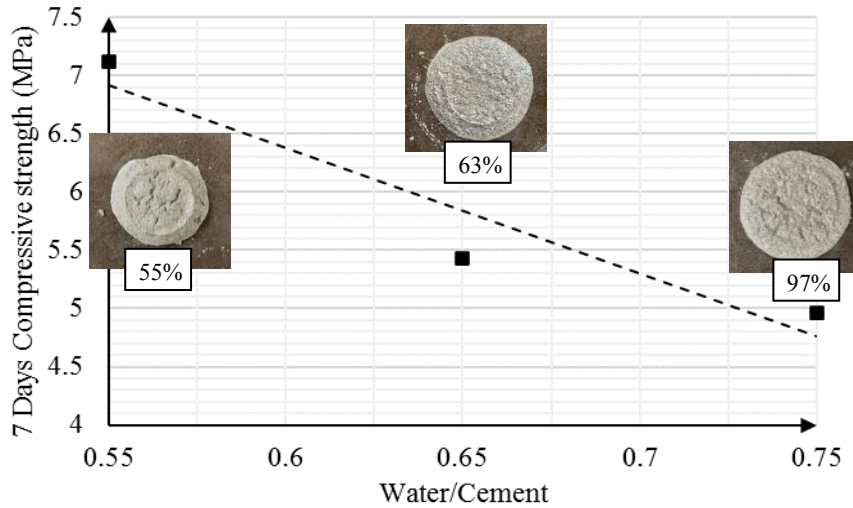


Figure 5. Relationship between compressive strength and w/c ratio

3. Heat transfer analysis

A three-dimensional finite element model of the composite wall was developed using an advanced finite element software (ABAQUS 6.13, 2013). A 3 m x 4 m x 0.1 m dimension wall panel with a 25 mm thick external plaster was developed for this study. 8-node linear heat transfer brick elements (DC3D8) were used to model both elements in the composite wall. From a mesh sensitivity analysis, the mesh size was determined as 50 mm. Since no sustained loads were applied, the plaster and the wall panel were assumed to be perfectly bonded, and hence a tie constraint was used to represent the bond. Figure 6 shows the finite element mesh of the composite wall.

The thermal performance of masonry walls can be assessed using “decrement factor” and “time lag” in common practice. The decrement factor is referred to as the ratio between the amplitude of temperature wave at the indoor wall surface and the outdoor wall surface (Toure *et al.*, 2019). And the time lag refers to the time taken

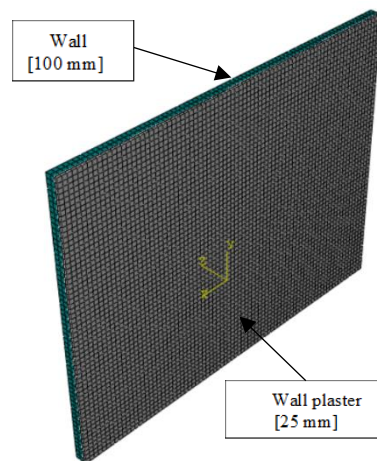


Figure 6. Discretized model

for the peak temperature to propagate from the outdoor surface to the indoor surface (Toure *et al.*, 2019). Wall panels with a low decrement factor and a higher time lag can act to enhance the thermal comfort within the buildings (Ozel and Ozel, 2012).

Two distinct wall panels were simulated to compare the thermal performances and they are (a) Wall panel with a conventional cement-sand plaster (WP_CS), and (b) Wall panel with the EPS-cement plaster developed in this study (WP_EC). The thermal properties of the selected plasters were tested in the laboratory and the properties of the concrete blocks were obtained from available literature (Irsyad *et al.*, 2017). Table 3 shows the material properties used for this simulation. It was assumed that the outdoor air temperature was transferred to the external wall surface through conduction and radiation.

Table 3: Thermal properties of the materials

Material	Thermal conductivity (W/m.K)	Specific heat (J/kg.K)	Density (kg/m ³)
Concrete blocks	1.263	1000	2000
CS	0.71	840	2011
EC	0.4	1094	1417

3.1. Model results & validation

To validate the numerical model, a small-scale building prototype with external wall plaster was built (Figure 7) and an EPS roof was fixed to avoid the heat transfer from the top of the building. The wall surface temperatures inside and outside were monitored for 6 consecutive hours and compared with the results predicted from the numerical model. Figure 8



Figure 7. Building prototypes

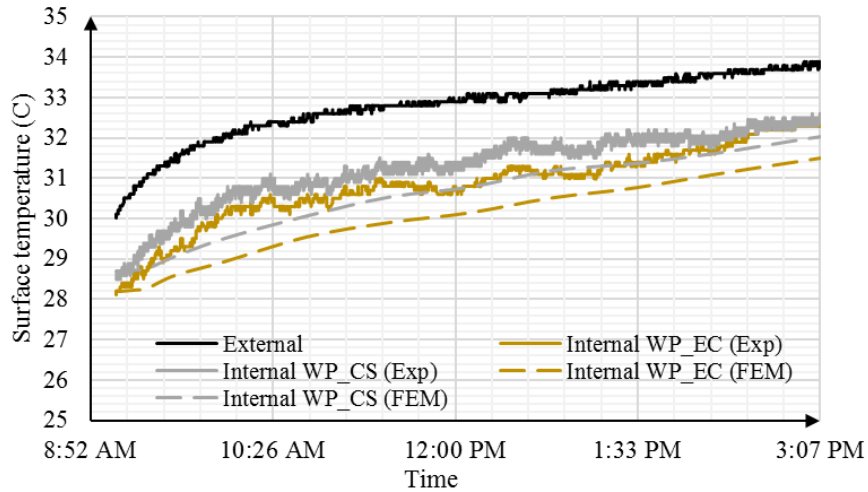


Figure 8. Comparison of measured temperature and predicted temperature

shows a comparison of measured surface temperatures and numerically predicted temperatures and it indicates fairly good agreement between the experimental and numerical results. Moreover, the internal wall surface temperature with the developed plaster (WP_EC) seems less compared to the wall with conventional plaster (WP_CS). To explore the thermal performance throughout a day, weather data of a random day in Colombo for 24

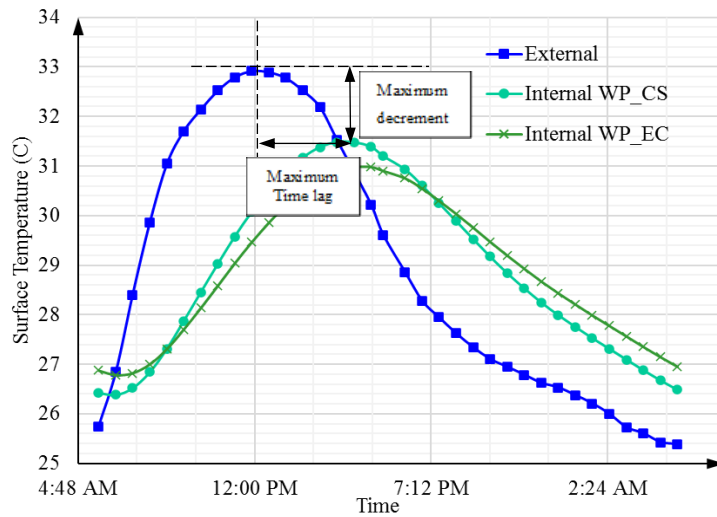


Figure 9. Predicted temperature profiles

hours (Time and date, 2020) was used. The model was simulated for consecutive 3 days to avoid the errors due to the initial boundary condition assumptions. The output for 24 hours was extracted beyond the convergence which is illustrated in Figure 9. The computed decrement factors and time lags for both models are listed in Table 4. The predicted results indicate that the buildings with WP_EC wall panels can enhance the thermal comfort compared to the buildings with WP_CS wall panels.

Table 4: Computed decrement factors and time lags

Model ID	Time lag	Decrement factor
WP_CS	3 hours 48 min	0.68
WP_EC	4 hours 33 min	0.56

3.2 Parametric study

3.2.1. Effect of plaster thickness

The selection of plaster thickness is a crucial aspect in terms of maintaining thermal comfort within the buildings. Therefore, a range of plaster thickness between 10 mm and 50 mm was selected in this study. The developed composite wall panel model (WP_EC) was re-analysed with changing plaster thicknesses and the indoor wall surface temperatures were monitored. From the results obtained, the decrement factors and time lags for respective plaster thicknesses were calculated and presented in Figure 10. The graph indicates that the decrement factor reduces with increasing plaster thickness and it reverses for the time lag. Moreover, it is noted that similar thermal perfor-

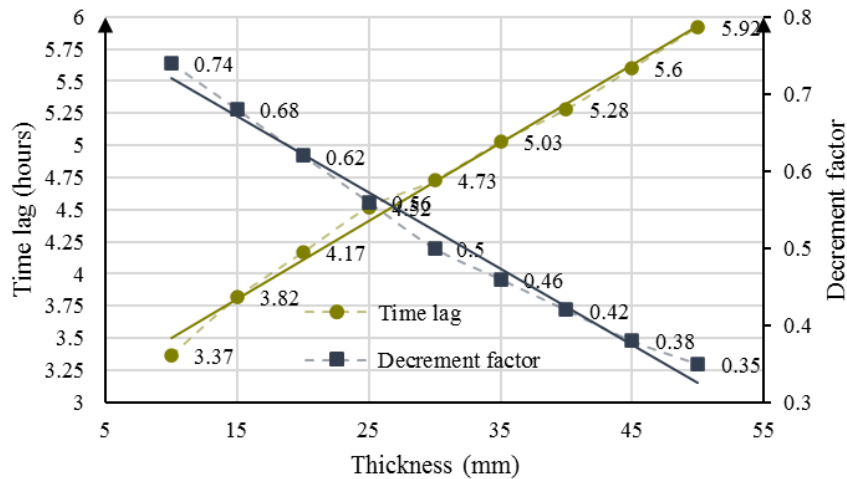


Figure 10. Effect of plaster thickness on heat transfer

mances can be achieved using 15 mm of EC plaster and 25 mm of CS plaster. This shows the reduced thickness requirement when using the plaster discovered in this study.

3.2.2. Effect of thermal conductivity

The thermal conductivity of a material is a key parameter in deciding the heat transfer process through any materials (Selvaratnam and Gamage, 2021). Since several mixes were developed in this study, assessing the effect of thermal conductivity of the plaster material on heat transfer analysis is essential. In such a case, a range of thermal conductivities between 0.15 W/m.K and 1.45 W/m.K were selected. By monitoring the indoor and outdoor wall surface temperatures, the relevant factors were calculated (Figure 11). The plot indicates that a range of decrement factors from 0.26 to 0.76 and a range of time lags from 3.1 hours to 5.7 hours can be achieved with the given range of thermal conductivity mixes. It is also noted that a small change in the thermal conductivity makes a huge change in the heat transfer analysis in the low thermal conductivity materials.

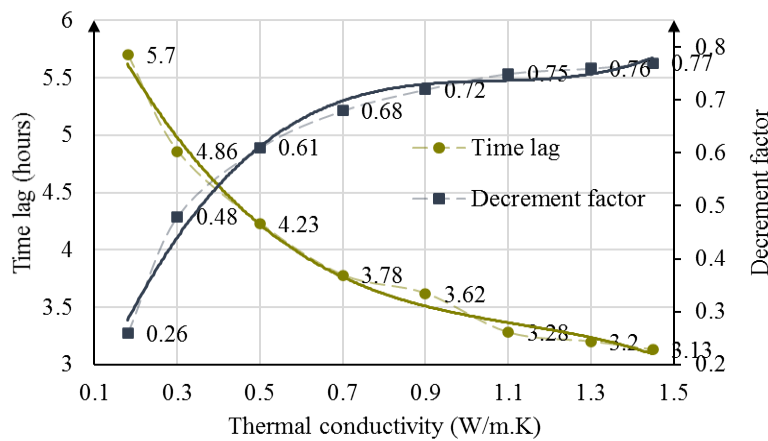


Figure 11. Effect of thermal conductivity of the plaster thickness on heat

4. Conclusions

An attempt has been made on developing a green insulation system for the building walls to enhance the thermal comfort within the buildings. The following conclusions were drawn:

1. Recycled Expanded Polystyrene (EPS) particles can be incorporated in the construction industry as a base material for the cementi-

tious plasters. On average of 95% to 145% of the sand can be replaced by coarse EPS particles to achieve a mortar mix match with N-type mortar requirements.

2. The thermal conductivity, compressive strength, and density drastically reduce with the replacement percentage. A thermal conductivity range of 0.22 W/m.k to 0.34 W/m.K can be obtained for the EPS-cement N-type plaster with 3.35 mm grade EPS.
3. The thermal conductivity of the mortar mixes significantly varies with the particle size distribution of the EPS particles. The mortar mix with 125% replacement by the 1.15 mm grade EPS has been identified as the ideal mix for the insulated wall plaster.
4. A numerical model of a composite wall panel was developed to study the heat transfer process through the wall panel with the developed plaster and the model results were in good agreement with the experimental results.
5. The heat sustains an additional 45 minutes within the composite wall with EPS plaster compared to the wall with the conventional plaster. The decrement factor of WP_ES is 18% less than the WP_CS which also adds value to the developed plaster in enhancing the thermal performance.
6. The parametric study shows that the plaster thickness and the thermal conductivity of the plaster have an adverse effect on the heat transfer through the composite wall. A similar thermal comfort to the buildings with a 25 mm thick conventional plaster can be expected in the buildings with a 15 mm thick developed plaster (EC).

Acknowledgments

The financial support provided by National Research Council; Sri Lanka (PPP 18-01) is greatly appreciated.

References

- ABAQUS 6.13 (2013) 'ABAQUS Analysis User's Guide'. Dassault Systems Simula Cooperation.
- ASTM C 270-07 (2010) 'Standard Specification for Mortar for Unit Masonry', *ASTM International*. West Conshohocken, pp. 2–13. doi: 10.1520/C0270-10.
- ASTM D7340 (2018) 'Standard Practice for thermal conductivity of Leather', *ASTM International*. West Conshohocken: ASTM International 2018.
- Dissanayake, D. M. K. W., Jayasinghe, C. and Jayasinghe, M. T. R. (2017) 'A comparative embodied energy analysis of a house with recycled expanded polystyrene (EPS) based foam concrete wall panels',

- Energy and Buildings*. Elsevier B.V., 135(November), pp. 85–94. doi: 10.1016/j.enbuild.2016.11.044.
- Dylewski, R. and Adamczyk, J. (2014) ‘The comparison of thermal insulation types of plaster with cement plaster’, *Journal of Cleaner Production*. Elsevier Ltd, 83, pp. 256–262. doi: 10.1016/j.jclepro.2014.07.042.
- Fernando, P. L. N., Jayasinghe, M. T. R. and Jayasinghe, C. (2017) ‘Structural feasibility of Expanded Polystyrene (EPS) based lightweight concrete sandwich wall panels’, *Construction and Building Materials*. Elsevier Ltd, 139, pp. 45–51. doi: 10.1016/j.conbuildmat.2017.02.027.
- Ferrándiz-Mas, V. *et al.* (2014) ‘Lightweight mortars containing expanded polystyrene and paper sludge ash’, *Construction and Building Materials*, 61, pp. 285–292. doi: 10.1016/j.conbuildmat.2014.03.028.
- Ghosh, Avijit, Ghosh, Arup and Neogi, S. (2018) ‘Reuse of fly ash and bottom ash in mortars with improved thermal conductivity performance for buildings’, *Heliyon*. Elsevier Ltd, 4(July), pp. 1–32. doi: 10.1016/j.heliyon.2018.e00934.
- Gunawardhana, D. S. R. S. S. and Gamage, J. C. P. H. (2015) ‘Performance of sand cement block produced with partial replacement of cement by rice husk ash’, in *6th International Conference on Structural Engineering and Construction Management 2015, Kandy, Sri Lanka*, pp. 172–175.
- Ho, B. T., Roberts, T. K. and Lucas, S. (2018) ‘An overview on biodegradation of polystyrene and modified polystyrene: the microbial approach’, *Critical Reviews in Biotechnology*. Informa Healthcare USA, Inc, 38(2), pp. 308–320. doi: 10.1080/07388551.2017.1355293.
- Irsyad, M. *et al.* (2017) ‘Heat transfer characteristics of building walls using phase change material’, in *1st International Symposium on Green Technology for Value Chains*. IOP Publishing. doi: 10.1088/1755-1315/60/1/012028.
- Jannat, N. *et al.* (2020) ‘A comparative simulation study of the thermal performances of the building envelope wall materials in the tropics’, *Sustainability*, 12, pp. 1–26. doi: 10.3390/SU12124892.
- Jayasinghe, C., Fonseka, W. M. C. D. J. and Abeygunawardhene, Y. M. (2016) ‘Load bearing properties of composite masonry constructed with recycled building demolition waste and cement stabilized rammed earth’, *Construction and Building Materials*. Elsevier Ltd, 102, pp. 471–477. doi: 10.1016/j.conbuildmat.2015.10.136.
- Kahandawa Arachchi, K. A. D. Y. T., Gamage, J. C. P. H. and De Silva, G.

- I. P. (2019) 'Thermal Insulation Systems for CFRP/Concrete Composites: A Review', in *International Conference on Structural Engineering and Construction Management*. Kandy, Sri Lanka.
- Kaya, A. and Kar, F. (2016) 'Properties of concrete containing waste expanded polystyrene and natural resin', *Construction and Building Materials*. Elsevier Ltd, 105, pp. 572–578. doi: 10.1016/j.conbuildmat.2015.12.177.
- Ozel, M. and Ozel, C. (2012) 'Effects of wall orientation and thermal insulation on time lag and decrement factor', in *9th International Conference on Heat transfer and Thermodynamics, Malta*, pp. 680–684.
- Ramli Sulong, N. H., Mustapa, S. A. S. and Abdul Rashid, M. K. (2019) 'Application of expanded polystyrene (EPS) in buildings and constructions: A review', *Journal of Applied Polymer Science*, 136(20), pp. 1–11. doi: 10.1002/app.47529.
- Schackow, A. *et al.* (2014) 'Mechanical and thermal properties of lightweight concretes with vermiculite and EPS using air-entraining agent', *Construction and Building Materials*. Elsevier Ltd, 57, pp. 190–197. doi: 10.1016/j.conbuildmat.2014.02.009.
- Selvaranjan, K., Gamage, J. C. P. H. and Silva, G. I. P. De (2020) 'Thermal performance of rice husk ash mixed mortar in concrete and masonry buildings', 19(4), pp. 43–52. doi: 10.35784/bud-arch.2121.
- Selvaratnam, A. and Gamage, J. C. P. H. (2021) 'A Review on Thermo-mechanical Behaviour of CFRP-Concrete Composites at Elevated Temperature and Available Insulation Systems', in *Lecture Note in Civil Engineering*, pp. 533–541. doi: 10.1007/978-981-15-7222-7_43.
- SLS 107 (1995) 'Specification for Ordinary Portland cement Part 2: Test methods', *Sri Lankan Standards*, p. 107.
- 'Time and date' (2020). Available at: <https://www.timeanddate.com/weather/sri-lanka/sri-jayawardenapura-kotte/hourly>.
- Toure, P. M. *et al.* (2019) 'Experimental determination of time lag and decrement factor', *Case Studies in Construction Materials*. Elsevier Ltd., 11, p. e00298. doi: 10.1016/j.cscm.2019.e00298.